SYNTHESIS AND CHARACTERIZATION OF ORGANO MODIFIED METAL CONTAINING MESOPOROUS MATERIALS FOR OXIDATION CATALYSIS

THESIS

SUBMITTED TO THE

UNIVERSITY OF PUNE

FOR THE DEGREE OF

DOCTOR OF PHILOSOPHY

IN CHEMISTRY

BY

SHYLESH S.

CATALYSIS DIVISION
NATIONAL CHEMICAL LABORATORY
PUNE 411008
INDIA

JULY 2006

CERTIFICATE

Certified that the work incorporated in the thesis

Synthesis and Characterization of Organo Modified Metal Containing Mesoporous Materials for Oxidation Catalysis

submitted by Mr. Shylesh S, for the Degree of Doctor of Philosophy was carried out by the candidate under my supervision at Catalysis Division, National Chemical Laboratory, Pune 411 008, India. Such material as has been obtained from other sources has been duly acknowledged in the thesis.

Dr. A. P. Singh
(Research Supervisor)

DECLARATION BY RESEARCH SCHOLAR

I hereby declare that the thesis entitled

Synthesis and Characterization of Organo Modified Metal Containing
Mesoporous Materials for Oxidation Catalysis

submitted for the Degree of Doctor of Philosophy to the University of Pune, has been carried out by me at Catalysis Division, National Chemical Laboratory, Pune 411 008, India, under the supervision of Dr. A. P. Singh. The work is original and has not been submitted in part or full by me for any other degree or diploma to this or any other University.

Shylesh S.

Dedicated

to my

Parents and Teachers

ACKNOWLEDGEMENTS

I find it difficult to write something in short to acknowledge my research supervisor, Dr. A. P. Singh. His constant inspiration, invaluable guidance and constructive criticism helped me a lot to focus my views in the proper perspective. I take this opportunity to express my intense reverence towards him for the extensive scientific discussions and for giving me the freedom in research. My deepest personal regards are due for him forever for his timely helps and for being a strong support, both scientific and personal, on all stages of my research period.

I am indebted to Dr. Rajeev Kumar, Head, Catalysis Division and Dr. A. V. Ramaswamy and Dr. S. Sivasankar, former Head of Catalysis Division, for allowing me to use all the available facilities in the division, for the stimulating discussions, valuable suggestions and for the constant encouragement and support. My heartfull thanks are due to Dr. D. Srinivas, Dr. C. V. V. Satyanarayana, Dr. N. M. Gupta, Dr. P. R. Rajmohanan, Dr. S. B. Halligudi, Dr. P. Manikandan, Dr. S. P. Mirajkar, Dr. P. A. Joy, Dr. Anil Kinage, Dr. K. R. Kamble, Dr. Nalini Jacob, Mr. R. K. Jha, Mrs. R. Parischa, Ms. Violet Samuel and all other scientific and non-scientific staff of the division and NCL for their valuable help and cooperation during my tenure as a research student.

I wish to convey my sincere gratitude to Dr. Bruce G. Anderson and Dr. Ch. Srilakshmi, Schuit Institute of Catalysis, Eindhoven Institute of Technology, The Netherlands and Dr. Mahendra P Kapoor, Taiyo Kagaku, Takaramachi, Japan, for rendering help, sharing knowledge and for fruitful discussions.

With much appreciation, I would like to mention the crucial role of my senior colleagues, Dr. Thomas Mathew, Dr. N. R. Shiju, Mr. Biju M. Devassy, Dr. Joly, Dr. Amit Dubey, Dr. Venkatesh, Dr. Sushama, Dr. Anirban Ghosh, Dr. Satyajyothi Senapthi and junior colleagues and labmates, Surendran, Prinson, Vandana, Chidambaram, Shrikant, Selvakumar, Bala, Jino and Neelu for their helping hands, splendid companionship and for making the lab feel like a family. Special thanks to Amit, Mahesh, Pranjal, Atul, Sahoo, Sachin, Pai, Rajendra, Satyanarayana Reddy, Vasudev Shetty and all other research scholars of catalysis division for such a friendly and cheerful working atmosphere, for their constant support, love and care throughout my stay in NCL.

It gives me immense pleasure to thank Raj Sankar, Sreeprasanth, Ajeesh, Harikrishna, Sanyo, Vivek and Vinod for their help, friendly attitude and compromising nature. I would like to confess *that, it is not possible for me to acknowledge and thank all those known and unknown faces individually for their direct and indirect contributions in my personal and professional life. I sincerely thank all of them for their incessant moral support, kind cooperation, love, respect, appreciation and for the scientific discussions.*

I take this opportunity to express my earnest respect to my school teachers, graduation tutors and Dr. Joby Thomas, Department of Chemistry, St. Thomas College, Thrissur and Prof. S. Sugunan, Department of Applied Chemistry, Cochin University of Science and Technology, for their way of teaching that build up my research career in science.

I am forever indebted to my parents and brother for their love, understanding and encouragement throughout my life. Their blessings and encouragement have always made me an optimist in any unknown areas I had ventured.

Finally, my thanks are due to Council of Scientific and Industrial Research, Government of India, for awarding the junior and senior research fellowships and Dr. S. Sivaram, Director, Dr. Paul Ratnasamy, former Director, and Dr. B. D. Kulkarni, Deputy Director, National Chemical Laboratory to carry out my research works, extending all infrastructural facilities and to submit this work in the form of a thesis for the award of Ph. D degree.

July 2006 *Shylesh S.*

“Research is the art of seeing what others see, but thinking what others don’t think”

- Ralph Waldo

CONTENTS

CHAPTER 1. INTRODUCTION AND LITERATURE SURVEY

CHAPTER 2. VANADIUM-CONTAINING PERIODIC MESOPOROUS SILICAS

CHAPTER 3. VANADIUM-CONTAINING PERIODIC MESOPOROUS ORGANOSILICAS

CHAPTER 4. CHROMIUM-CONTAINING PERIODIC MESOPOROUS SILICAS

CHAPTER 6. SUMMARY AND CONCLUSIONS

List of Figures

List of Tables

List of Schemes

List of Abbreviations

APTS	3-aminopropyl triethoxysilane
BE	Binding Energy
BET	Braunauer-Emmett-Teller
BJH	Barrett-Joyner-Halenda
BTEE	1,2-bis(triethoxysilyl)ethane
CMC	Critical Micelle Concentration
CP MAS	Cross Polarization Magic Angle Spinning
Cl-ES	3-chloropropyl triethoxysilane
CTAB	Cetyl trimethyl ammonium bromide
Cy-ane	Cyclohexane
Cy-ol	Cyclohexanol
Cy-one	Cyclohexanone
DFT	Density Functional Theory
DR UV-Vis	Diffuse Reflectance Ultraviolet-Visible
DTA	Differential Thermal Analysis
EPR	Electron Paramagnetic Resonance
FSM	Folded Sheet Materials
FTIR	Fourier Transform Infrared
GC	Gas Chromatography
GC-MS	Gas Chromatography-Mass Spectroscopy
HK	Horvath Kawazoe
HMM	Hybrid Mesoporous Material
HMS	Hexagonal Mesoporous Silica
HRTEM	High Resolution Transmission Electron Microscopy
ICP-OES	Inductively Coupled Plasma-Optical Emission Spectroscopy
LCT	Liquid Crystal Template

MCM	Mobil Crystalline Material
MAS NMR	Magic Angle Spinning Nuclear Magnetic Resonance
MeOH	Methanol
Me-MS	Methyl trimethoxysilane
1,4-NQ	1,4-Napthoquinone
OTAB	Octadecyl trimethyl ammonium bromide
PMO	Periodic Mesoporous Organosilica
PMS	Periodic Mesoporous Silica
PTA	Pthallic Anhydride
SBA	Santa Barbara Amorphous
SEM	Scanning Electron Microscopy
SG	Silica Gel
SLC	Silicatropic Liquid Crystal
TBHP	*tert*-Butyl Hydroperoxide
TEM	Transmission Electron Microscopy
TEOS	Tetraethyl Orthosilicate
TGA	Thermogravimetric Analysis
TMAOH	Tetramethyl Ammonium Hydroxide
TOF	Turnover Frequency
TON	Turnover Number
TPR	Temperature Programmed Reduction
TTAB	Tetradecyl trimethyl ammonium bromide
UOFMN	Unified Organically Functionalized Mesoporous Network
Vi-ES	Vinyl triethoxysilane
XPS	X-Ray Photoelectron Spectroscopy
XRD	X-Ray Diffraction

ABSTRACT

The surface modification of M41S type mesoporous materials by transition metals or reactive organic functional groups allows the preparation of multifunctional molecular sieves with desired catalytic properties.[1] The mesoporosity and very high surface area of the surface-functionalized mesoporous materials can also be exploited for the immobilization of different catalytically reactive species.[2] The principal aim of this thesis was to investigate the approach of heterogenization of various transition metals over solid mesoporous supports and organic-inorganic hybrid mesoporous materials for oxidation and epoxidation reactions, under different reaction conditions.

During the last few years, the catalytic transformations of bulky molecules over metal-containing and organo-modified metal-containing mesoporous materials constitute an interesting research area in fine chemical synthesis.[3] Hence, the incorporation of various heteroatoms in the framework or pore channels of different mesoporous materials had been systematically studied, characterized and also used as catalysts in various industrially relevant organic transformations. The high surface area, ordered pore channels and high-density silanol sites of the mesoporous molecular sieves were also exploited for the preparation of bifunctional molecular sieves for the heterogenization of catalytically reactive species.[4] Special attention was paid in the synthesis and use of silsesquioxane precursors for the development of periodic mesoporous organosilicas and their metal analogs.[5] Besides, throughout the thesis, much emphasis was placed on catalyst stability evaluations since this step is considered as a prime requirement for the successful development of metal-containing mesoporous materials. In-depth characterizations of all catalyst systems are highlighted to understand the mode of interaction of the active sites with the mesoporous silicate network and to evaluate the structure-catalytic activity relations and stability of the mesoporous solids.

Vanadium-containing mesoporous materials were found active in a number of liquid-phase oxidation reactions using H_2O_2 and TBHP as oxidants.[6] However, they show the leaching of active metal sites during oxidation reactions, in presence of *aqueous* oxidants. Recently, there has been an increasing demand in the synthesis of metal-

containing mesoporous materials with better catalytic activity and stability. Hence, it was thought interesting to study in detail the role of commonly used silica sources, *viz.*, fumed silica and tetraethyl orthosilicate in the structural stability and site isolation of vanadium sites in Si(V)-MCM-41 mesoporous materials. Further, the increased demand of organic-inorganic hybrid mesoporous materials and their unique hydrophobic features attracted attention in the development of heterogenized vanadium catalysts over various amino propyl modified mesoporous silica supports and in the development of vanadium-containing periodic mesoporous organosilicas having ethane groups in the mesoporous frame wall positions.

The design and synthesis of metal-containing mesoporous materials having pore size greater than 25 Å be the main area of research in the last decade, as their high surface area and pore size helps to overcome the limitations of the conventional small pore zeolite catalysts.[7] However, solid materials having pore sizes in between that of zeolites and mesoporous materials (super microporous region) received less attention and hence ordered porous silicas that effectively bridge the existing gap between the microporous and mesoporous materials are interesting in the field of heterogeneous catalysis.[8] Hence in search of new metal-containing porous materials, having pore size in the super microporous region, bifunctional mesoporous silicas having unprecedented organic groups in the pore channels as well as chromium in the frame wall positions was synthesized. Chromium-containing mesoporous materials having pore size in the super microporous region can be easily obtained by calcination of the bifunctional silicas and these materials are envisaged to exhibit high catalytic activity and better stability in various liquid phase oxidation reactions, than the conventional metal-containing mesoporous materials.

Selective oxidation reactions of relatively inert C-H bond of hydrocarbons is one of the most desirable and challenging reactions, since the products obtained are themselves important or act as valuable intermediates for industrial organic chemicals.[9] Among them, the oxidation of cyclohexane to cyclohexanol (A) and cyclohexanone (K) is important because they are the key intermediates in the production of adipic acid

(Nylon-66) and caprolactam (Nylon-6).[10] Chromium-containing mesoporous materials reported earlier for this reaction shows the facile leaching of chromium during liquid-phase reactions. In this context, in an attempt to improve the stability of chromium-containing mesoporous materials, ethane-silica hybrid periodic mesoporous organosilicas were synthesized and their catalytic performance were compared with other chromium-containing mesoporous molecular sieves, in the oxidation reaction of cyclohexane using peroxides and air as oxidants. In-depth characterization of all chromium catalysts are highlighted to understand the nature and location of active chromium sites in the porous network, the role of hydrophobic organic species in dispersing the active chromium sites and also to explore the origin of catalytic activity.

The specific problems chosen are:

(i) Synthesis of periodic mesoporous silica materials like Si-MCM-41, Si-MCM-48, Si-SBA-15 and their surface modification by organic functional groups *via.,* different routes.

(ii) Synthesis of periodic mesoporous organosilicas having organic groups like ethane ($-CH_2-CH_2-$) in the frame wall positions.

(iii) Synthesis of vanadium-containing mesoporous materials, by various preparation routes, over the periodic mesoporous silica and organosilica materials and application of these materials in the oxidation reaction of naphthalene and cyclohexane and in the epoxidation reaction of cyclooctene and styrene.

(iv) Synthesis of chromium-containing bifunctional mesoporous silicas, chromium-containing ethane-bridged hybrid mesoporous organosilicas and application of these samples in the selective oxidation reaction of cyclohexane using peroxides and air as oxidants.

(v) Detailed characterization of all the new organo-modified metal-containing mesoporous materials.

The thesis is presented in **SIX** chapters, a brief summary of which is given below.

Chapter 1. Introduction

Chapter 1 presents a general introduction about various physicochemical aspects of periodic mesoporous silica and periodic mesoporous organosilica materials. The different characteristic properties of these materials, their synthesis parameters, formation mechanisms, different approaches for surface-functionalization, characterization techniques and application as supports for different catalytically active transformations are discussed in brief. The scope and objectives of the present work have been outlined at the end of this chapter.

Chapter 2. Vanadium-containing periodic mesoporous silicas

Chapter 2 describes the synthesis of vanadium-containing mesoporous MCM-41 samples by the direct substitution method, grafting method and by the immobilization method. The synthesis procedures of the V-MCM-41 catalysts are probed in detail by using different silica sources in order to account the role of silica sources in the mesoporous structural ordering, stabilization of vanadium sites, catalytic activity and stability. The immobilization of vanadium was carried out over amino propyl modified mesoporous supports like SBA-15, MCM-41 and a silica gel, to probe the role of surface hydroxyl groups in the anchoring of organic groups as well as to attain information about the nature and coordination of vanadium over different modified supports. All samples were characterized by XRD, N_2 sorption technique, TEM, TG-DTG analysis, ICP analysis, solid state ^{13}C CP MAS NMR, ^{29}Si and ^{51}V MAS NMR, FT-IR, FT-Raman spectroscopy, UV-Vis, EPR and TPR. The catalytic activity and stability of vanadium catalysts was evaluated in the oxidation reaction of naphthalene and cyclohexane and in the epoxidation reaction of cyclooctene, using *aqueous* hydrogen peroxide (H_2O_2) as well as *tert*-butylhydrogenperoxide (TBHP) as oxidants and are discussed in detail.

Chapter 3. Vanadium-containing periodic mesoporous organosilicas

Chapter 3 describes the synthesis of vanadium-containing periodic mesoporous organosilica samples, having ethane groups in the frame wall positions, prepared by cationic surfactants of different chain lengths *viz.*, C18-, C16- and C14-. All the synthesized catalysts are characterized by XRD, N_2 sorption technique, SEM, TEM, TG-DTG analysis, ICP analysis, solid-state ^{13}C CP MAS NMR, ^{29}Si and ^{51}V MAS NMR, UV-Vis and FT-Raman spectroscopy. The catalytic activity and stability of hybrid vanadium catalysts was compared with V-MCM-41 catalyst in the epoxidation reaction of styrene, using *aqueous* hydrogen peroxide (H_2O_2) and *tert*-butylhydrogenperoxide (TBHP) as oxidants, under different reaction conditions, are discussed with intrinsic details.

Chapter 4. Chromium-containing periodic mesoporous silicas

Chapter 4 deals with the synthesis of bifunctional chromium-containing mesoporous materials, using various organo modifiers like chloro propyl, vinyl and methyl units and their further transformation to chromium-containing small pore silicas. The effect of different chain length organic groups in the percentage of chromium loading, structural shrinkage as well as the dispersion of chromium are discussed in detail by various characterization techniques including XRD, N_2 sorption technique, TEM, TG-DTA analysis, ICP analysis, solid-state ^{13}C CP MAS NMR, ^{29}Si MAS NMR, FT-Raman spectroscopy, UV-Vis, TPR and XPS. Further, the controlled transformation of these bifunctional mesoporous materials to small pore chromium silicas having pore size in the super microporous region is also discussed. The catalytic activities of the chromium catalysts were assessed in the oxidation reaction of cyclohexane to cyclohexanol and cyclohexanone using *non-aqueous tert*-butylhydrogenperoxide and air as oxidants under different reaction conditions. The stability as well as reusability of the catalysts were also carried out and are discussed.

Chapter 5. Chromium-containing periodic mesoporous organosilicas

Chapter 5 deals with the synthesis of chromium-containing periodic mesoporous organosilicas, having ethane groups in the frame wall positions, by two different synthesis routes, using 1,2-bis(triethoxysilyl)ethane as the silica source and 1,2-bis (triethoxysilyl)ethane and tetraethyl orthosilicate as a mixed silica source. The newly developed organo-modified mesoporous chromium samples are characterized by XRD, N_2 sorption technique, TEM, TG-DTA analysis, ICP analysis, solid-state ^{13}C CP MAS NMR, ^{29}Si MAS NMR, FT-IR spectroscopy, FT-Raman spectroscopy, UV-Vis and XPS. The catalytic activities and stability of the chromium catalysts were assessed in the oxidation reaction of cyclohexane to cyclohexanol and cyclohexanone using *aqueous* hydrogen peroxide, *non-aqueous tert*-butylhydrogenperoxide and air as oxidants under different reaction conditions and are compared with a conventional Cr-MCM-41 sample.

Chapter 6. Summary and Conclusions

Chapter 6 summarizes the results obtained and the basic findings of the present study.

References

1. J. Y. Ying, C. P. Mehnert, M. S. Wong, *Angew. Chem. Int. Ed*. **1999**, *38*, 56.
2. K. Moller, T. Bein, *Chem. Mater*. **1998**, *10*, 2950.
3. D. E. De Vos, M. Dams, B. F. Sels, P. A. Jacobs, *Chem. Rev.* **2002**, *102*, 3605.
4. A. Stein, B. J. Melde, R. C. Schroden, *Adv. Mater*. **2000**, *12*, 1403.
5. A. Sayari, S. Hamoudi, *Chem. Mater.* **2001**, *13*, 3151.
6. A. Taguchi, F. Schuth, *Microporous Mesoporous Mater*. **2004**, *77*, 1.
7. A. Sayari, *Chem. Mater*. **1996**, *8*, 1840.
8. M. Kruk, T. Asefa, M. Jaroniec, G. A. Ozin, *J. Am. Chem. Soc*. **2002**, *124*, 6383.
9. C. L. Hill, *Activation and Functionalization of Alkanes*, Wiley, New York, **1989**.
10. J. M. Thomas, R. Raja, *Chem. Commun*. **2001**, 675.

1.1 GENERAL BACKGROUND

Zeolites are crystalline aluminosilicates comprising corner sharing TO_4 tetrahedra (T = Si, Al) and consisting of a regular array of micropores of molecular dimensions (4-13 Å). The different valences of Si (tetravalent) and Al (trivalent) produce an overall negative charge for each incorporated aluminium atom. These negative charges can be balanced by protons (leading to Brönsted acids) or other cations. Substitution of trivalent atoms in the zeolite framework by tetravalent atoms like titanium produces metallosilicates with an electrically neutral, hydrophobic framework.[1]

Zeolites proved a substantial impact in the economics and sustainability of products and process in many sectors of industry and are the workhorses of petroleum refining operations, natural gas purification and organic synthesis in the production of fine and specialty chemicals.[2] Furthermore, microporous zeolitic materials have earned the reputation of environmentally benign catalysts due to several factors like waste minimization, simple operation, easy work-up and recyclability of the catalysts.[3] However, the main restriction of microporous materials is their low pore size and hence they are not suitable for catalytic transformations involving organic molecules having kinetic diameters above *ca.,* 7.5 Å, which are important precursors in the synthesis of fine chemicals. In view of the industrial relevance of porous materials and because of the intrinsic scientific interest in their structural complexity and diverse chemistry, considerable efforts has been directed in the synthesis of templated porous solids.[4] Thus, there has been an ever-growing interest in expanding the pore sizes of the materials from micropore to mesopore region, in response to the increasing demands in both industrial and fundamental studies.[3b]

The synthesis of surfactant-templated mesostructures is one of the most exciting discoveries in the field of materials synthesis in the last decade.[5] The excitement began with the discovery of hexagonally ordered mesoporous silicate structures by Mobil Corporation (M41S materials)[5c,b] and by Kuroda, Inagaki and coworkers (FSM-16 materials).[5c,d] In 1990, Yanagisawa *et al*. reported the synthesis of mesoporous solids, through the intercalation of long chain cetyl trimethyl ammonium cations into the layered silicate, kanemite. After calcination, to remove the organic species, a mesoporous material was obtained and the X-ray diffraction showed a broad peak centered in the low angle. Thus even though mesoporous materials of the first class were obtained, because of the lack of in depth characterization details their results are largely ignored.[5c] Further, it would be less appropriate to mention this synthesis as a templating pathway, since in its prototypic form, it resembles more a solid-state reaction in which a layered material is converted into a three-dimensional network material. It was therefore considered the synthesis procedures reported by Mobil researchers more realistic under the term surfactant templating for the development of ordered mesoporous materials. The ability of surfactants to self-assemble into well-defined structures has been, thereafter, taken advantage of for the design and synthesis of inorganic materials with nanosized dimensions.[6] More importantly, the pore size of these materials can be tuned in the nanometer range by choosing an appropriate surfactant templating system, sometimes with co-solvents or swelling agents. However, the original mesoporous silicates and aluminosilicates exhibited a number of limitations, including lower hydrothermal stability and lower reactivity than zeolites with comparable compositions.[5,7] Yet, the ability to manipulate structures of the porous solids in a controlled way having better thermal and hydrothermal stability proved to be so important to the research community.

The important members of the M41S mesoporous family are MCM-41, MCM-48 and MCM-50.[5a,b] MCM-41 posses honeycomb arrays of nonintersecting uniformly sized channels with diameters ranging from 15 to 100 Å depending on the template used, the addition of auxiliary organics and the synthesis parameters like synthesis time, synthesis temperature or post synthesis treatments. MCM-48 is a cubic phase with *Ia3d* symmetry consisting of an enantiomeric pair of nonintersecting three-dimensional channel systems that are mutually intertwined. Among the M41S materials, the hexagonally channel oriented MCM-41 receives much attention than the cubic three dimensionally channel oriented MCM-48, due to the simple synthesis protocols.[8] Moreover, the classical surfactants used in the synthesis of M41S related materials, like the alkyl trimethyl ammonium halides, preferentially form hexagonal or lamellar phases, which implies that the synthesis of high quality MCM-48 is subjected to a very narrow margin. However, the synthesis of MCM-48 with *Ia3d* symmetry is alluring as it has a more appealing structure and offers potential advantages than the MCM-41 material.[5a,b,9] MCM-50 posses lamellar phases and after surfactant removal the structure usually gets collapsed.

The demand for environmentally friendly and more efficient technology has enhanced considerable interest in the use and development of porous solids.[2d,10] Among the various methods opted for creating pore, the templating fabrication method created a variety of porous networks with a wide range of pore sizes, well defined morphologies on controllable length scales and various chemical functionalities to match the needs for different applications.[11] The word template or structure directing agent (SDA) suggests that the pore system is a direct replica of the template and are described on which how they are utilized in the fabrication of new porous materials *viz.,* as endotemplate or exotemplate.[12] The former term refers a template species, which is an isolated precursor and is included as an isolate entity into the growing solid material, while the later refer to a structure-producing scaffold with voids.

Endotemplating creates voids in a solid by inclusion of template species, which occupy the space around which the solid develops. If the template is removed by solvent extraction or by calcination the space becomes free and a pore develops. The size of the pores can be tailored by the judicious choice of the template molecules. However, during the templating process a favorable mechanism between the surfactant groups and the solid species has to occur otherwise the template will not be incorporated and may results in phase transformations or phase separations.[13] Exotemplates are extended structures that contain voids, which provides the necessary space in which a divided solid can form. This novel approach helps in the fabrication of new porous materials and had also been referred as *'confined space synthesis'* or *'compartment solidification'*.[14] Exo templating also refers to the process in which the structure of the template is essentially not affected during which the solid is formed so that a replica of the preformed structure can be produced by this procedure. Hence this replication process is ideal to be justified by the term '*nanocasting'*, since the template is actually used as a mold with characteristic dimensions in the nanometer range.[15] This method is widely used for the synthesis of mesoporous carbons using ordered mesoporous silicas as exotemplates. Mesoporous carbon, in turn, is an ideal template to create other ordered materials, since it can be easily removed by simple calcination.[16]

1.2. PERIODIC MESOPOROUS SILICAS (PMS): SYNTHESIS AND MECHANISM OF FORMATION

The M41S family of mesoporous materials are synthesized using a silica source and different organic structure directing agents, *e.g.*, cationic surfactants containing long alkyl chain quaternary ammonium compounds containing 10-20 carbons, often followed with addition of co-surfactants.[5b] Although, the synthesis conditions have some influence on the structure of the resulting mesoporous solids, the type of surfactant is certainly the dominating factor in directing the formation of a specific structure. The influence, which a certain surfactant exerts in the synthesis of a mesoporous material, can be rationalized by the packing parameter concept, introduced originally by Israelachvili *et al.*, who developed a microscopic model according to which the dimensionless packing parameter g plays a key role.[18] The packing parameter value is defined as, $g = V/a_o l$, where, V is the effective volume of the hydrophobic chain of the surfactant, a_o is the effective aggregate surface area of the hydrophilic head group and l is the effective hydrophobic chain length.

The dependence of surfactant/silica molar ratio in a ternary synthesis system containing tetraethylorthosilicate (TEOS, silica source), water and cetyltrimethylammonium cations (C_{16}-TMA, surfactant) at 100 °C on appearance of different phases of M41S family is summarized in Table 1.1. [17]

Table 1.1. Effect of surfactant/silica molar ratio on emergence of different mesophases

Surfactant/Silica ratio	Different phases of M41S type materials
<1.0	Hexagonal (*p6mm*, MCM-41)
1.0-1.5	Cubic (*Ia3d*, MCM-48)
1.2-2.0	Lamellar (*p2*, MCM-50)
2.0	Cubic octamer $[(C_{16}TMA)SiO_{2.5}]_8$

The most outstanding feature of M41S material synthesis, in contrast to the traditional single organic molecule or metal ion templating preparation, is that the templates used are surfactants, having an alky chain length greater than ten carbon atoms. The surfactants have a hydrophilic head group and a long chain hydrophobic tail group, within the same molecule, and in solution they will aggregate and self-organize in such a way so as to minimize the contact between the incompatible ends. Therefore, the mechanism responsible for the formation of M41S materials from its precursors had attracted much scientific attention. Moreover, an improved understanding about the self-organization of surfactant-silicate assembly can provide significant impact in the development of new application-oriented materials.[19] Hence, a number of models have been proposed to rationalize the mechanism of formation of mesoporous materials by various synthesis routes. All these models are based on the role of surfactants in solution to direct the formation of silicate mesostructure. Different synthesis mechanisms, different types of interaction between the surfactant and the inorganic precursor have been postulated in the literature to explain the formation mechanism of mesoporous materials and are briefly discussed in this section.

1.2.1. Liquid Crystal Templating (LCT) Mechanism

The researchers of Mobil Corporation proposed a ‘liquid crystal templating’ (LCT) mechanism to explain the formation of M41S type mesoporous materials.[5a,b] In a simple binary system of water-surfactant, surfactant molecules manifest themselves as very active components with variable structures.[20] At very low concentrations they energetically exist as monomoleules. With increasing concentration, surfactant molecules aggregate to form micelles in order to decrease the system entropy. The lowest concentration at which surfactant molecules aggregate to form spherical isotropic micelles is known as Critical Micelle Concentration (CMC_1). Increase in the surfactant concentration initiates the aggregation of spherical micelles into cylindrical or rod like micelle structure (CMC_2). In general, there are three main liquid crystalline phases with hexagonal, cubic and lamellar structures. The hexagonal phase results from the hexagonal packing of cylindrical micelles, cubic phase relates as a bicontinous structure and the lamellar phase corresponds to the formation of surfactant bilayers. The influence of alkyl chain length and the addition of organic swelling agents on the pore size of the final material have been taken as strong evidence for the LCT mechanism, since this phenomenon is consistent with the well-documented surfactant chemistry.

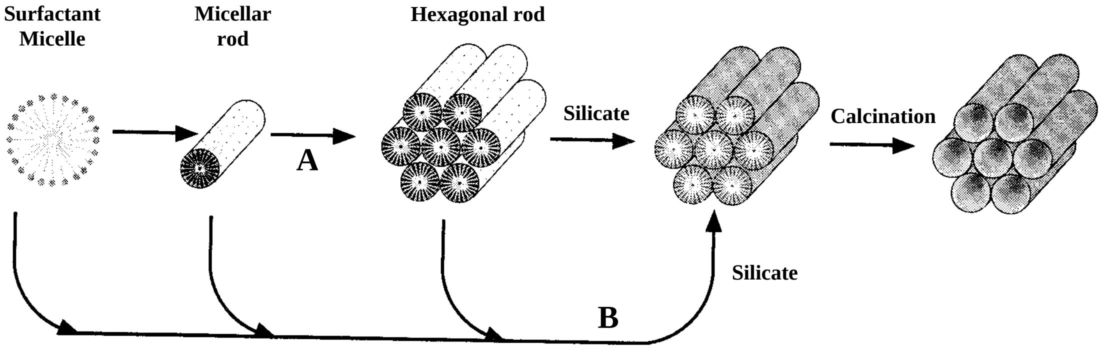

Scheme 1.1. Liquid Crystal Templating mechanism proposed for the formation of mesoporous MCM-41: (A) liquid crystal phase initiated and (B) silicate anion initiated. [*Source*: Ref. 5b]

The Mobil researchers proposed two synthesis mechanisms for the formation of ordered periodic mesoporous silica materials.[5a,b] In the first route, the cationic surfactant species organize into lyotropic liquid crystal phase, which can serve as template for the formation of hexagonal MCM-41 structure. For that, the surfactant micelles firstly aggregate into hexagonal array of rods, followed by the interaction of silicate anions present in the reaction mixture with the cationic head groups of the surfactant species. Thereafter, the condensation of the silicate species occurs leading to the formation of an inorganic polymeric species. After removing the template by calcination, hexagonally arranged inorganic hollow cylinders are produced (Scheme 1.1).

In the second route, the hexagonal ordering is presumed to initiate by the presence of silicate species in the reaction mixture.[5a,b] Chen *et al.* proposed that randomly distributed surfactant micelles with rod like morphologies form initially and their interaction with silicate oligomers by columbic interactions results in randomly oriented surfactant micelles surrounded by two or three silica monolayers. The presence of rod like micelles in solution was supported by isotropic *in situ* ^{15}N NMR studies.[21] These randomly ordered composite species spontaneously pack into a highly ordered mesoporous phase with an energetically favorable hexagonal arrangement, accompanied by silicate condensation. Further condensation between silicate species on adjacent rods occurs on heating and the inorganic wall continues to condense to form the stable hexagonal network (Scheme 1.2).

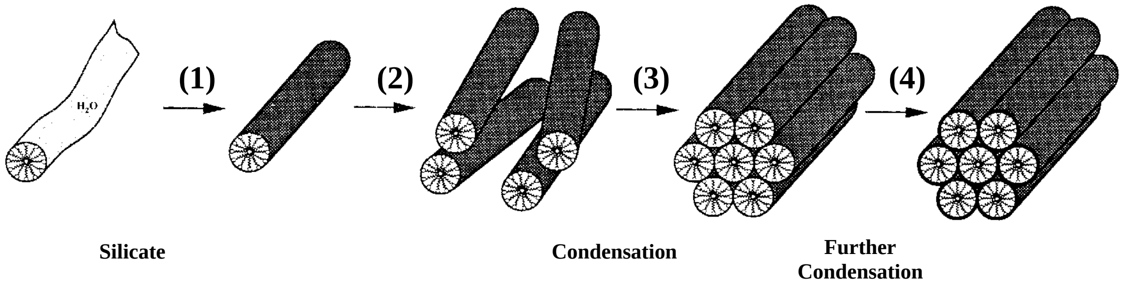

Scheme 1.2. Silicate rod assembly proposed for the formation of MCM-41: (1) random ordering of rod-like micelles, (2) interaction with silicate species, (3) spontaneous packing of the rods and (4) remaining condensation of silicate species on further heating. [*Source*: Ref. 21]

1.2.2. Charge Density Matching and Folded Sheet Mechanism

Both the charge density matching and folded sheet mechanistic models are based on the transformation of lamellar phase to hexagonal phases. The ‘charge density matching’ model proposed by Stucky *et al.* suggested that condensation occurs between initially formed silicate species by the electrostatic interactions between the anionic silicates and the cationic surfactant head groups.[22] This eventually reduces the charge density and therefore, curvature was introduced into the layers to maintain the charge density balance with the surfactant head groups, which leads to transformation of the lamellar mesostructure into the hexagonal one (Scheme 1.3.A).

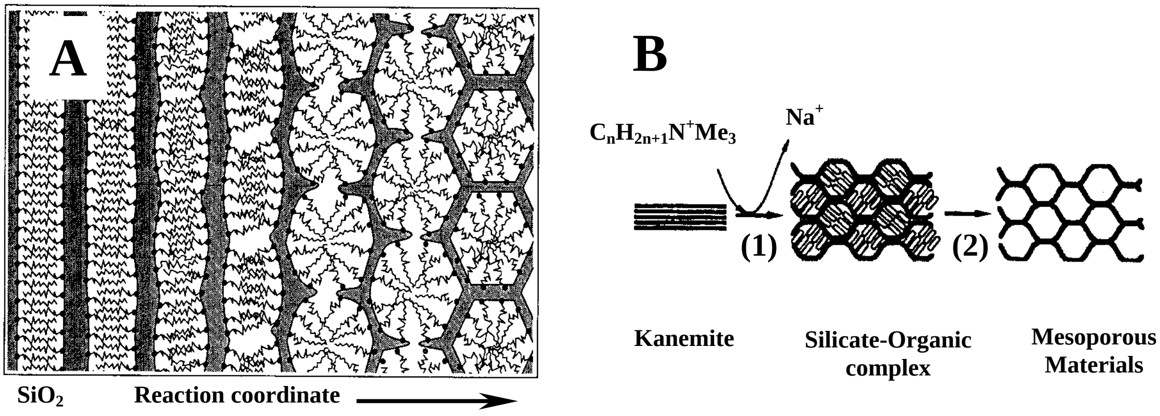

Scheme 1.3. Mechanisms proposed for the transformation of surfactant-silicate systems from lamellar to hexagonal mesophases: (A) Hexagonal mesophase obtained by charge density matching and (B) folding of kanemite silicate sheets around intercalated surfactant molecules. [*Source*: Ref. 22 and 5d]

The ‘folded-sheet mechanism’ postulated by Inagaki *et al.* indicated the presence of intercalated silicate phases in the synthesis medium of the reaction products.[5d] The flexible silicate layers of kanemite fold around the surfactant cations and cross-linking of the interlayer occurs by condensation of silanol groups on adjacent silicate sheets. This folding and cross-linking process is facilitated by the flexibility of the single-layered kanemite sheets. On increase of pH, the amount of occluded alkyltrimethylammonium cations in kanemite increases and as a result the interlayers of kanemite expand to form a regular hexagonal structure called FSM-16. The undissolved portion of kanemite converts to FSM-16 materials whereas the dissolved species yield amorphous silica (Scheme 1.3B).

1.2.3. Silicatropic Liquid Crystals

Firouzi *et al*. have developed a model based on cooperative organization of inorganic and organic molecular species into three-dimensional structured arrays.[23] According to this model, the physicochemical properties of a particular system were not determined by the organic arrays having long-range pre-organized order, but by the dynamic interplay among ion-pair inorganic and organic species, so that different phases can be readily obtained through small variation of controllable synthesis parameters. The silicate anions exchanged with the surfactant halide counter ions formed the 'silicatropic liquid crystal' (SLC) phase, which exhibited very similar behavior to that of typical lyotropic systems and finally condensed irreversibly into MCM-41 (Scheme 1.4).

1.2.4. Generalized Liquid Crystal Templating Mechanism

Many researchers have tired to explain the possible ways by which a surfactant species interacts with the silica species under various synthesis conditions for the development of mesoporous materials having interesting textual and structural properties. In all cases, a favorable interaction between the surfactant and silicate species is reported, unless results in disordered materials with any ordered pore structures. A brief summary of the possible interactions between surfactant and silicate species is discussed in this section and a summary of the various synthesis opted under different pathways are depicted in Table 1.2.

1.2.4.1. Ionic Route (Electrostatic Interaction)

Huo *et al*. proposed a generalized mechanism for the formation of mesostructures, which was based on specific types of electrostatic interaction between an inorganic precursor (I) and a surfactant head group (S). In this concept, four different approaches

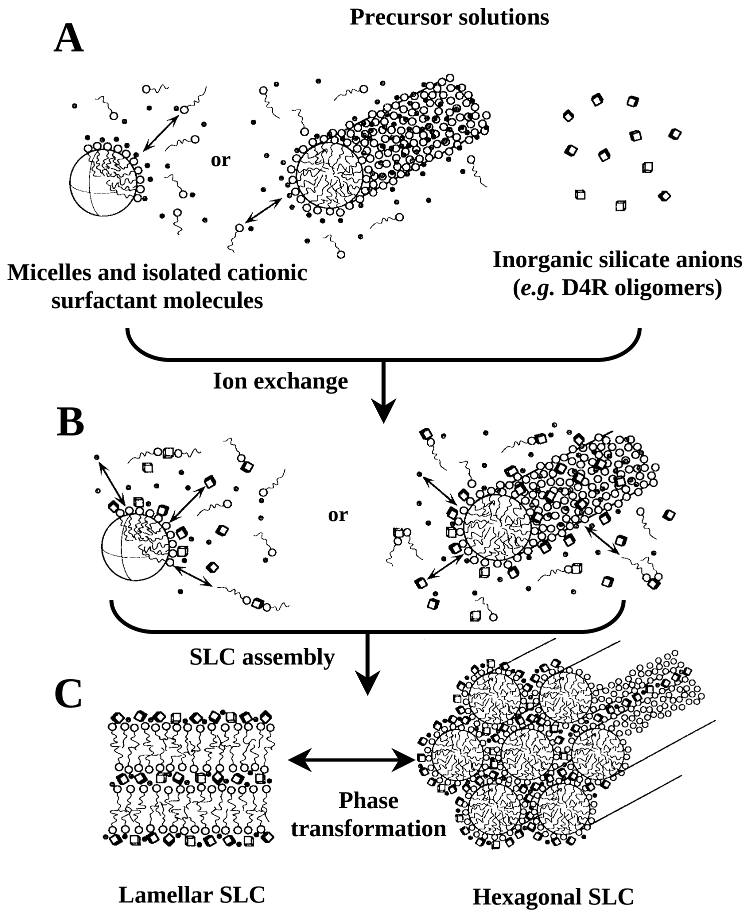

Scheme 1.4. Cooperative organization for the formation of silicatropic liquid crystal phase/silicate-surfactant mesophases: (A) organic and inorganic precursor solutions, (B) preliminary interaction of the two precursor solutions after mixing and (C) multidentate interaction of oligomeric silicate units with the surfactants. [*Source*: Ref. 23]

were proposed to synthesize transition metal oxide mesostructures.[24] The first route involves the charge density matching between surfactant cations and inorganic anions (S^+I^-). The second route deals with the charge-reversed situation, *i.e.*, anionic surfactant and cationic inorganic species (S^-I^+). Both the third and fourth routes are counter ion-mediated pathways. The third one demonstrates the assembly of cationic species *via.,* halide ions ($S^-X^+I^-$), while the fourth one depicts the assembly of anionic species *via.,* alkali metal ions ($S^+X^-I^+$). These synthesis strategies are acceptable for the formation of a wide variety of hexagonal, cubic or lamellar mesophases, but a common problem encountered was the instability of the inorganic framework after the removal of template.

1.2.4.2. Neutral Templating Route (Hydrogen Bonding Interaction)

Tanev and Pinnavaia proposed another route to synthesize hexagonal mesoporous silicas (HMS) having thicker pore wall, high thermal stability and smaller crystallite size.[6c,25] This route is essentially based on hydrogen bonding between neutral primary amines (S^o) and neutral inorganic precursors (I^o), wherein hydrolysis of tetraethyl orthosilicate (TEOS) in an aqueous solution of dodecylamine yields neutral inorganic precursor. However, these materials lacked long range ordering of pores and had broader pore size distribution and higher amounts of interparticle mesoporosity than MCM-41 materials.

Using the same approach, porous lamellar silicas with vesicular particle morphology (MSU-V) have been synthesized with the help of double headed alkyl amines linked by a hydrophobic alkyl chain (α,ω-dialkyl amine). Bagshaw *et al.* used nonionic polyethylene oxide surfactants (PEO) to prepare mesoporous materials (MSU) having pore size in the range 20-60 Å. An advantage of this method endows the low cost, non-toxic and biodegradable nature of surfactants and the facile recovery of the templates.[25c]

1.2.4.3. Ligand-Assisted Templating Route (Covalent Interaction)

Antonelli and Ying proposed a ligand-assisted templating mechanism for the synthesis of hexagonally packed mesoporous metal oxides.[6e] In a typical synthesis, the surfactant was dissolved in the metal alkoxide precursor, before addition of water, to form metal-ligated surfactants by nitrogen–metal covalent bond formation between the surfactant head group and the metal alkoxide precursor. The existence of this covalent interaction was confirmed by ^{15}N NMR spectroscopic studies. In this approach, the structure of the mesophases can be controlled by adjustment of the metal/surfactant ratio, which led to a new class of mesoporous transition metal oxides analogous to the M41S family.

Table 1.2. Synthesis of various mesoporous materials under different reaction conditions

Interaction	Template source	Pathway	Examples
Strong electrostatic interactions			
Direct interaction	Ammonium surfactants	S^+I^-	MCM-41, MCM-48, FSM-16, KIT-1
Anion mediated interaction	Ammonium surfactants	$S^+X^-I^+$	SBA-1,2,3
	Triblock copolymers	$(S^oH^+)X^-I^+$	SBA-15,16
	Ethylene oxides		SBA-11, 12,14
Weak van der Waals interactions			
Hydrogen bonding interaction	Amine surfactants	S^oI^o	HMS
Hydrogen bonding interaction	Non-ionic ethylene oxides	N^oI^o	MSU- *n*

1.3. SURFACE MODIFICATIONS OF MESOPOROUS SILICA

The applications of siliceous mesoporous materials itself is restricted because of the limitations in the active sites and have to be modified according to the requirements. Hence, in order to utilize the unique properties of the mesoporous material for specific applications in catalysis, sorption, sensing, ion exchange, *etc*, introduction of reactive organic functional groups, by the incorporation of organic components as part of the silicate walls or trapped within the channels to form organic-inorganic hybrid materials remains the key issues.[11b,c,26] The advantages of organic-inorganic hybrid materials arise from the fact that inorganic components can provide mechanical, thermal or structural stability, while the organic features can be readily modified for various specific applications.[27] Further, organic modification of the silicates permits precise control over the surface properties and pore sizes of the mesoporous sieves and at the same time stabilizing the materials towards hydrolysis.

Through the development of organic-inorganic hybrid mesoporous solids, much progress has been made in the last few years towards application of mesoporous solids in a variety of fields. Mesoporous solids have been functionalized at specific sites and were demonstrated to exhibit improved activity, selectivity, and stability in a large number of catalytic reactions and sorption processes.[28] The synthesis procedures developed so far effectively utilized the large amount of silanol groups resting in the surface of M41S related materials. Another advantage of these materials is that the hydrophilic-hydrophobic properties can be tailored by the judicious choice of the organo alkoxy silanes.[29] This section briefly highlights the possible ways of surface modifications over mesoporous materials for the formation of organic-inorganic hybrid mesoporous materials.

1.3.1. Grafting Methods

Grafting refers to post synthesis modification of the inner surface of a pre-fabricated mesoporous support, where the organic functional groups are introduced as the terminal groups of an organic monolayer, usually after surfactant removal (Scheme 1.5).[30] Mesoporous silicas possess surface silanol groups (Si-OH) in high concentration and, like in amorphous silica, it can act as convenient anchoring points for organic functionalization. Silylation generally occurs on free (≡Si–OH) and geminal silanol ($=Si(OH)_2$) groups, while hydrogen-bonded silanol groups are less accessible to modification because they form hydrophilic networks among themselves.[31] The original structure of the mesoporous support is usually maintained after grafting. However, if a high surface coverage of organic functional groups is required, it is important to maintain a large number of surface silanol groups, after the removal of surfactants. Surfactant removal is usually carried out either by calcination or by appropriate solvent extraction methods. Since calcinations at higher temperatures can lead to the condensation of silanol groups, a decrease in the density of silanol groups is often obtained than the solvent extraction process (*e.g.,* with acid/alcohol mixtures for cationic surfactants or with alcohols for neutral surfactants).

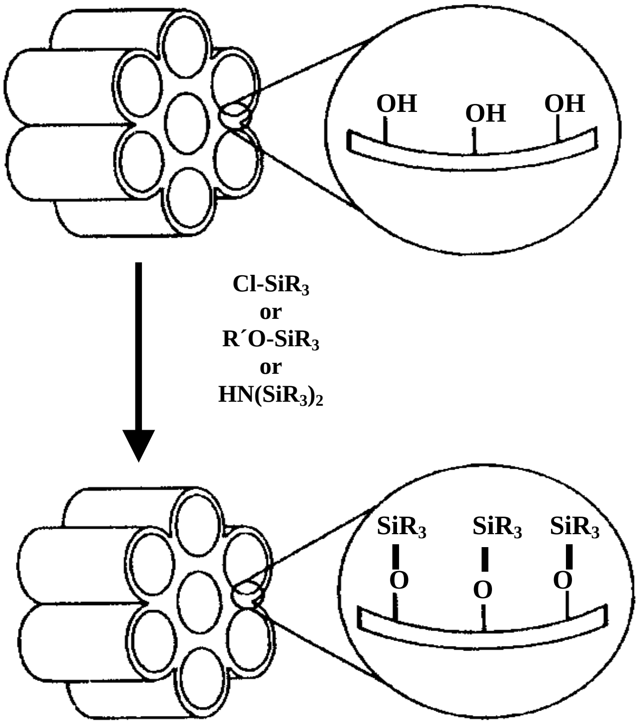

Scheme 1.5. Synthesis of organic-inorganic hybrid mesoporous silicates by grafting reactions. [*Source*: Ref. 28d]

In order to retain high-density silanol groups for the anchoring of large concentration of organic groups, the calcined mesoporous silica will be treated with boiling water[32] or steam[33] or by the acid hydrolysis.[34] Recently, supercritical fluids have been used as a reaction medium to anchor the siloxane to the mesopore channels. This method is particularly suitable for small pore materials due to the low density, viscosity, surface tension and the high diffusivity of the supercritical fluids like CO_2. It was also observed that when this technique was applied to mesoporous silica a high degree of cross-linking was observed, resulting in a higher hydrothermal stability for the materials.[35]

1.3.1.1. Grafting with Passive Surface Groups

Organic functional groups with lower reactivity could be grafted to enhance the hydrophobicity of the surface and protecting the material towards hydrolysis. Further, the pore diameter of mesoporous materials can also be adjusted by varying the alkyl chain length of the silylating agent or by increasing the quantity of the silylating agent.[36] The commonly used surface modifying agents are the trimethyl chlorosilane (Me_3SiCl), trimethyl ethoxysilane ($Me_3Si(OC_2H_5)$) and hexamethyldisilazane [$(Me_3Si)_2NH$].[31,37] Hexamethyldisilazane functionalization was widely used to quantify the number of surface silanols, to passivate the surface silanols and also to depolarize the surface for selective adsorption experiments.[37a,b]

1.3.1.2. Grafting with Reactive Surface Groups

Grafting of the mesoporous silica surfaces with organic units containing reactive functional groups like olefin, cyanide, thiol, amide, halide, *etc* permits further functionalization of the surface as their terminal end contains a reactive functional group. For instance, modification of these reactive materials includes hydroboration[38] and bromination of olefins[39] (vinyl-terminated materials), hydrolysis of cyanide to carboxylic acids,[40] oxidation of thiols to sulphonic acids,[41] nucleophilic substitution of amines and halides.[42] After, modification of these materials with the desired functionalities, catalytically active homogenous transition metal complexes as well as organometallic complexes can be anchored over these organic-inorganic hybrid materials. For instance, the functionalization of Mn (III) schiff base salen complex to surface-modified MCM-41 containing 3-chloro propyl silane (3-CPTS) is feasible by the nucleophilic replacement of the halogen atom.[43]

1.3.1.3. Site-Selective Grafting

The external surface silanols of the mesoporous materials are kinetically more accessible than the internal surface silanols. Hence, in order to minimize the grafting of reactive surface sites on the external surface and thereby to utilize the inner pore channels, it is necessary to passivate the external silanol groups before functionalizing on the internal surfaces.[44] Shepherd *et al.* had passivated the external surface of the MCM-41 surface with dichloro diphenyl silane (Ph_2SiCl_2) first and then 3-aminopropyl triethoxy silane (3-APTS) was grafted over the internal channels for the heterogenization of an active ruthenium cluster. The existence of amine functional groups in the inner pore channels of MCM-41 was confirmed by the high-resolution transmission electron microscopy (HRTEM).[45]

Another approach effectively utilized was the template ion exchange property, for the grafting of Me_3SiCl, without removing the surfactants from the pore channels. The advantage of this method is that this procedure avoids the two-step synthesis procedure and that the grafting exclusively occurs in the external surfaces due to the steric constraint of the surfactants.[46] Following solvent extraction, for the removal of surfactant groups, the internal surface of the materials is free for further modifications while the external surface is passivated.

In another way, Antochshuk and Jaroniec carried out simultaneous grafting and extraction of template molecules by modification of uncalcined MCM-41 with trialkylchlorosilanes. As-synthesized MCM-41 was refluxed in neat trialkylchlorosilane, first by itself, and then with added anhydrous pyridine, followed by multiple washing with different solvents, leading to surfactant-free mesoporous products.[47] The loading of surface organic groups exceeded that on calcined supports that were otherwise treated in a similar way. The advantages of this method include the increased concentration of surface hydroxyl groups and the decreased reduction in pore size of the materials, as this procedure avoids the high temperature calcination process for the removal of surfactant groups.

1.3.2. Co-condensation Reactions

Organic-inorganic hybrid mesoporous materials can be also prepared at room temperature or at higher temperatures by the one-step co-condensation method between tetraalkoxy silanes ($Si(OR')_4$, R' = Et, Me) with one or more organoalkoxy silanes (**R**-$Si(OR')_3$, R' = Et, Me), through the sol-gel process in presence of a structure orientor.[48] Depending on the nature of the **R** groups, a variety of organofunctionalized mesoporous materials attached covalently with the silica surface can be synthesized. The advantages of this method than the grafting procedures include the stability of the inorganic framework even at higher organic loadings, homogenous distribution of the organic groups in the pore channels as well as the single step preparation procedures.[49] Solvent extraction of the as-synthesized materials in an acidic-alcohol mixture helps to remove the occluded surfactants from the pore channels and to obtain the organofunctionalized ordered mesoporous material (Scheme 1.6). Several research groups had employed this co-condensation procedure for the synthesis of organic-inorganic hybrid mesoporous materials under S^+I^-, $S^+X^-I^+$, S^oI^o and N^oI^o pathways.[44,50]

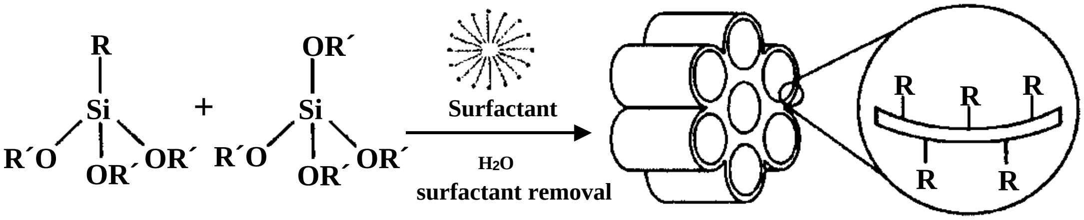

Scheme 1.6. Synthesis of organic-inorganic hybrid mesoporous silicates by co-condensation reactions. [*Source*: Ref. 28d]

1.4. PERIODIC MESOPOROUS ORGANOSILICAS (PMO): ORGANIC-INORGANIC HYBRIDS WITH ORGANIC MOIETY IN THE FRAMEWORK

The diverse applications of periodic mesoporous silica and organic-inorganic hybrid mesoporous materials have stimulated the search for materials with new structures and framework compositions. The combination of organic and inorganic fragments inside the structure of porous materials that are self-assembled into architectures with dimensions spanning multiple length scales can give rise to new materials preserving the unique characteristic of both organic and inorganic materials.[51] Thus an alternative strategy in the synthesis of organic-inorganic hybrid mesoporous materials is to replace one or more of the siloxane links with organic groups (Scheme 1.7).[52] Since the organic groups integrated inside the channel walls is the carrier of the desired property, it finds interesting to tailor the properties of these materials by the replacement of the bridging oxygen group by bridging organic groups in the wall channels. The organic component is capable of modifying the properties of bulk material and using these approach new materials with interesting morphologies can be developed according to the nature of the organic groups in the silicate network.[53]

Inagaki *et al*. have first reported the synthesis of ‘periodic mesoporous organosilica’ (PMO) with organic functional groups uniformly incorporated in the mesoporous walls, using 1,2-bis(triethoxysilyl)ethane as the framework precursor and octadecyl trimethylammonium chloride as the surfactant.[52a] Asefa *et al*. and Melde *et al*. have also described the co-condensation of either 1,2-bis(triethoxysilyl)ethane or 1,2-bis(triethoxysilyl)ethylene with silica precursors to synthesize hexagonal hybrid framework materials, under basic reaction conditions.[52b,c] Melde *et al*. designated their materials as ‘unified organically functionalized mesoporous networks’ (UOFMN), having worm-like channel systems and lacking long-range ordering. Thus the co-condensation of silsesquioxane precursors of the type, $(R'O)_3Si\mathbf{R}Si(OR')_3$, where $\mathbf{R}$ = $-(CH_2)_x-$, $-C_6H_5-$, $-CH{=}CH-$, *etc,* and their self assembly over an organized surfactant species can create organic-inorganic hybrid materials having long-range ordering and organic moiety as component of the solid network.[53] These materials are unique compared to the first generation periodic mesoporous silica materials (PMS), since unlike MCM-41, the bridging organics inside the channel wall of periodic mesoporous organosilicas offer a diversity of function and potential uses. Moreover, organic groups like ethylene, phenyl and biphenyl in the framework exhibits crystalline wall channels and thus the discovery of periodic mesoporous organosilicas is considered as a major breakthrough in the field of materials science.[54] The crystal-like ordering of the wall structures is thought to form through self-organization of the precursor molecules as a result of hydrophobic-hydrophilic interaction of hydrolyzed $(OH)_3Si\text{-}\mathbf{R}\text{-}Si(OH)_3$ species or π-π interactions of aromatic groups. Now, a wide range of synthetic routes to mesoporous organosilicas with different mesophases and morphologies has been reported including the use of cationic, neutral and non-ionic surfactants and surfactant mixtures under basic, acidic and neutral conditions.[55]

Compared to the conventional organic-functionalized heterogeneous mesoporous materials, where the organic groups are '*dangling*' inside the pores of the hybrid mesoporous materials, the periodic mesoporous organosilica materials exhibit quite different pore wall structure and surface properties.[56] Although the conventional grafting of organic functional groups on the inorganic framework offers the advantage of introducing catalysis and adsorption properties, the inactivation of catalytic sites on the inorganic framework through coverage with organic groups as well as the accompanied decrease in porosity of the material highlights the relevance of PMO materials. Other important advantages of the PMO materials than the conventional organic-inorganic hybrid mesoporous materials are due to: (i) organic moieties in PMO are homogeneously dispersed inside the wall channels with a maximum loading of 100%, which are not achievable with the organic pendant groups grafted, (ii) bridging organics inside the channel walls do not block the pores, (iii) the soft organic groups integrated within the channel walls impart interesting physical and mechanical properties of the host and (iv) the organic groups integrated inside the channel walls can be varied to produce a wide range of materials with potentially interesting characteristics.[57]

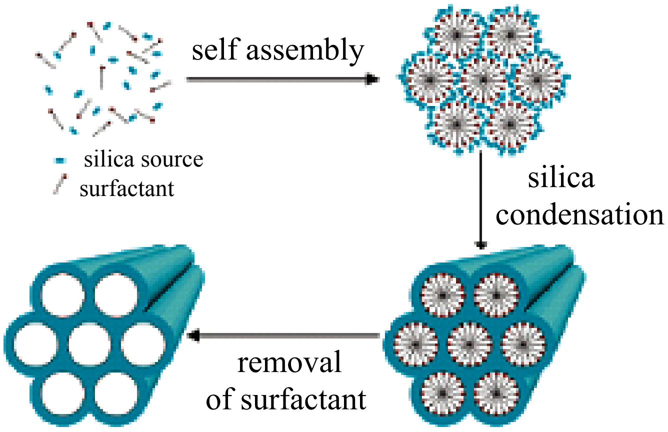

Scheme 1.7. Synthesis of organic-inorganic hybrid mesoporous materials having organic groups in the frame wall positions. Silica source: Bridged Silsesquioxanes, $(R'O)_3Si\mathbf{R}Si(OR')_3$, where **R** = $-(CH_2)_X-$, $-C_6H_5-$, -CH=CH-. [*Source*: Ref. 53a]

The union of the two main branches of chemistry *viz.,* the inorganic chemistry and organic chemistry there by allows the preparation of a myriad of new nanocomposites in which the organic groups can be integrated into an inorganic material. The organosilane compound with two or more alkoxy groups can make stable framework because the alkoxy groups at the both sides of the silsesquioxane precursor will condense to form a three dimensional stable network containing organic groups in the framework with a better periodic arrangement under surfactant templating conditions. These are the first type of mesoporous materials whose framework has a completely uniform distribution of organic groups integrated within the inorganic framework at the molecular level and having a periodic pore arrangement. Further, this is the first type of mesoporous materials having only T type [$Si(OH)R(OSi)_2$] silicons, without any Q type [$Si(OSi)_n(OH)_{4-n}$, n = 2-4] silicon species. However, similar to M41S materials, the hybrid mesoporous materials also posses residual silanol sites, as T^2 type silicon species.[58] The peak intensity ratio of the T^2/T^3 signals of the PMO is almost similar to the Q^3/Q^4 sites, which indicates that the hybrid materials posses similar silanol density as of M41S materials (Scheme 1.8). Further adsorption isotherm of water vapour showed that the hybrid materials has more hydrophobic surface than siliceous MCM-41, which suggests that the organic fragments are exposed on the surface and thereby increase the surface hydrophobicity.[59] Thus it is ideal to mention that this new approach extends the realm of mesoporous materials to *'chemistry of the channel walls'* rather than limiting it to the *'chemistry of the void space'*.[60]

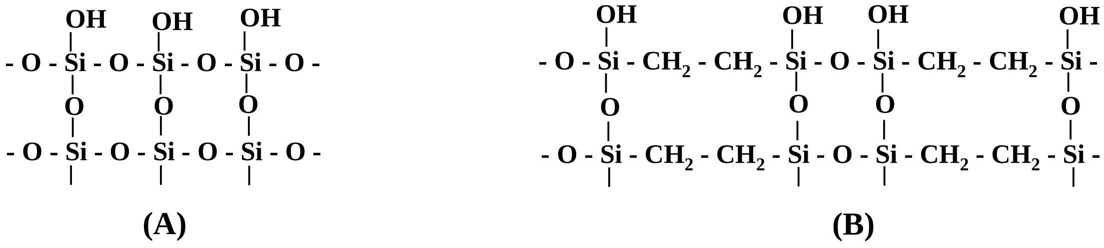

Scheme 1.8. Composition and surface characteristics of: (A) periodic mesoporous silica (PMS) and (B) organosilica (PMO) material having ethane bridges.

1.5. METAL-SUBSTITUTED MESOPOROUS MOLECULAR SIEVES

The advantages of using ordered mesoporous solids in catalysis are due to the relatively large pores, which facilitate mass transfer, and the very high surface area, which allows a high concentration of active sites per mass of material.[3b,11a] Although mesoporous materials posses unique textual as well as morphological features, siliceous M41S materials shows limited catalytic activity in various organic transformations and hence ample modifications are necessary to make them as suitable candidates for various catalytic organic transformations. The incorporation of heteroatoms into the inert framework or walls of pure siliceous mesoporous materials is an important route to modify the nature of the framework. In fact, the first catalytic studies with mesoporous molecular sieves were focused on metal-substituted MCM-41 materials, in which the active species were incorporated into the silicate matrix.[11b] However, since the wall structure of mesoporous silica resembles more to amorphous silica, incorporation of heteroatoms does not lead to the formation of defined sites as in zeolites, but as a rather wide variety of different sites with different local environments. Therefore, the catalytic properties of such materials resemble more to metal-containing amorphous silica rather than the framework-substituted zeolites.[61]

Modification of the framework composition of mesoporous materials is possible by the direct synthesis, *i.e.,* from mixtures containing both silicon and the hetero element to be incorporated or by post synthesis treatment of an initially prepared mesoporous material. The direct method usually results in a homogeneous incorporation of the hetero element while post synthesis methods helps in an increased concentration of heteroatoms on the surface. Various heteroatoms are incorporated into the pore channels of mesoporous supports and it is generally observed that apart from the synthesis conditions, *viz.,* gel pH, temperature and time, the degree of metal incorporation as well as coordination of metal sites in the mesopore structure is dependant on the nature of metal precursor used.[62] Thus, the incorporation of trivalent metal ions such as B, Al, Ga, *etc* in the silica frame walls produces framework negative charges that can be compensated by protons providing acid sites and hence serve as important materials in acid catalysis. The substitution of various transition metals like Ti, V, Cr, Mn, Fe, *etc* helps in the development of mesoporous materials with redox catalytic properties. Although the chemical elaboration of the surfactant templated mesoporous materials has been extensively applied to catalysis, the Si-MCM-41 type mesoporous materials potentially suffers from a plumbing problem. Since the periodic porosity is one-dimensional and nanoscopic in MCM-41, any internal blockage can shutoff the catalyzed walls from reaction.[63] However, the three dimensionally channel oriented mesoporous architectures, like the hexagonal mesoporous silica (HMS) materials, with continuous but aperiodically porous network offer new transport routes and has less diffusion limitations and are reported to be catalytically more active than the M41S materials. For instance, Tanev *et al.* had shown that Ti-HMS catalysts shows improved catalytic activity than Ti-MCM-41 catalysts in the oxidation reaction of 2,6-DTBP, MMA and styrene.[64]

Even though, the catalytic transformations of bulky organic molecules can be carried out in the '*nanoreactors'* of the mesoporous materials, there exist significant differences between metal-substituted zeolites and mesoporous silica materials. A comparison of metal incorporated zeolitic molecular sieves with mesoporous materials shows that the activity and heterogenity of the zeolitic catalysts lie far ahead than the mesoporous molecular sieves.[65] Hence, an important question arise that what causes for the much lower activity observed on the M-MCM-41 samples than the zeolitic metallosilicates, even though they share almost similar metal local environments. Obviously, diffusion limitations and steric constraints due to reactants or transition-state intermediates are not the only factors that govern the activity of metal sites in molecular sieves. The crucial difference in the structure of M41S and zeolite is that the M41S materials have no long-range order and the pore walls are essentially amorphous. Thus, the Si-O-M bonds sitting in the amorphous environment of M41S are supposed to be connected by more comfortable bond angles and are thermodynamically more stable than those of metal incorporated silicates, which had crystalline frameworks. Therefore, the Si-O-M bonds in mesoporous materials should be less reactive and have lower redox potential than those in zeolite samples. Further, since a part of active metal sites can be located inside the walls in mesoporous materials, these sites are not accessible for the reactants and this property was commonly observed when the metal precursor was introduced together with the silica source during the synthesis.[66] Another difference with zeolite concerns the nature of framework itself. In zeolites the number of defect groups like silanols is low, as they are located on the outer surface of the crystals. Hence, zeolites have a relatively high hydrophobic character, well suited for oxidation reactions in aqueous medium.[67] In contrast, mesoporous silica contain large amounts of internal silanol groups, capable of hydrogen bonding with water molecules, which will affect their performance in aqueous catalytic reactions.

The catalytic activity of metal-containing mesoporous materials is strongly influenced by the hydrophobic properties of the support surface, the local environment and the stability of the metal introduced. Hence, bifunctional organic-inorganic hybrid mesoporous materials containing heteroatoms like titanium and organic groups such as methyl silanes were prepared in a one step co-condensation method in order to improve the hydrophobic features of the metal-containing periodic mesoporous silica materials.[68]

The methyl-tethered Ti-MCM-41 showed better epoxidation activity than the non-modified Ti-MCM-41, in the epoxidation reaction of cyclohexene. Bhaumik and Tatsumi synthesized a wide range of organically modified Ti-MCM-41 samples by co-condensation of TEOS, organo- triethoxy silanes like methyl, vinyl, allyl, 3-chloropropyl, pentyl, phenyl and titanium tetrabutoxide.[69] Higher titanium incorporation as well as enhanced epoxide selectivity was observed in presence of organic groups than in their absence and were attributed to the improved hydrophobicity of the organo-modified mesoporous surface.

Akin to periodic mesoporous silicas, periodic mesoporous organosilicas also offer advantages for various surface modifications due to the presence of T^2 type silanol sites. Hence, various transition metals can be incorporated inside the pore channels of these materials by the direct method or by the post synthesis grafting routes. The metal-containing PMO samples are presumed to exhibit high catalytic activity, selectivity and stability due to the presence of organic fragments in the frame wall positions. Various metal ions like Al, Ti, V were incorporated over the PMO materials having ethane fragments in the frame wall positions and they exhibited superior catalytic activity and stability than the conventional M-M41S materials.[70] For instance, titanium-containing PMO materials show exceptional catalytic activity and oxime selectivity in the ammoximation reaction of ketones, whereas the conventional Ti-MCM-41 catalysts are not active for the same reaction.[70a] Among the reasons put forward to explain this dependence was the hydrophobicity of the matrix; as the more hydrophobic the surface, the higher the reaction rate because of the increased concentration of the organic substrate at the active titanium site. One of the major drawbacks of metal-containing M41S materials is their decreased hydrothermal stability. However, because of the presence of organic fragments, especially ethane groups, in the frame wall positions the PMO materials shows better hydrothermal stability than the M41S materials.[71] Thus the presence of hydrophobic organic groups, integrated inside the frame wall positions, improved the catalytic activity and overall structural stability of the mesoporous materials.

1.6. MESOPOROUS SILICA AS SUPPORT OR HOST FOR THE HETEROGENIZATION OF HOMOGENEOUS CATALYSTS

Materials with well-defined pores belong to the most interesting class of compounds, because they can be converted into organic-inorganic hybrid nanocomposites by various surface modifications. The microporous and organized mesoporous materials obtained after the hydrothermal synthesis are in fact a nonporous organic-inorganic hybrid since the organic structure director (template or surfactant) is usually trapped in the cavities of the solid. Hence, to obtain completely porous solid and to introduce reactive organic functional groups inside the channels of ordered materials, it is necessary to remove the entrapped organic species from the as-made samples.

The commonly employed method for the removal of surfactant consist of calcining the materials, in a flow of air, typically >400 ^{o}C. However, the high-cost template reactant is destroyed and such treatments further cause damage to the porous materials, since during calcination high local temperature and water formation may occur, and therefore extra framework sites may be formed.[72] An alternative method involves the removal of the template by mild treatments such as liquid extraction using acidic solutions, alcohols or a mixture of both.[73] This method is especially effective for mesoporous materials where the framework-surfactant interactions are weak (electrostatic, van der Waals or hydrogen bonding interactions) and because of the larger pore sizes. An added advantage of this method is that under acidic extraction conditions, exchange of sodium ions for protons is also achieved simultaneously with the removal of surfactants. Moreover, the mild routes for the removal of templates helps in the reuse of the organic templates for a subsequent synthesis with similar textual properties.[74] The materials obtained after the removal of surfactant groups contains ordered pore channels with abundant silanol sites. These mesoporous hosts can be utilized for the synthesis of organic-inorganic hybrid mesoporous materials having reactive functional groups and have stimulated fundamental research interests in the inclusion of metals and metal complexes inside the mesoporous channels.[75,76]

During the last few years, organic-inorganic hybrid mesoporous materials constitutes an emerging area in the field of materials science and had shown its impact in a wide range of heterogeneous catalysis reactions.[77] However, the main problem encountered in heterogenized catalysts is that the bonds between metal and ligand are often broken and reformed during catalytic reactions, leading to leaching of the metal from the catalyst in the product, thus decreasing the reaction rate and activity.[78] Hence the nature of interaction between the homogenous catalysts and the support surface decides the overall stability and reusability of the heterogenized catalysts and in general, if the anchoring is covalent, it can be robust enough to withstand the harsh conditions of the catalytic reactions. The most common immobilization techniques used for this purpose include grafting or tethering, physical entrapment, ship-in-a-bottle synthesis and supported liquid phase catalysis.[28a,79]

Earlier, the supports used to tether the homogeneous catalyst are the organic polymers, which are soluble in the reaction media. The advantage of this support is that the active sites are distributed through out the reaction solution and hence the catalyst architecture is similar to that of the homogeneous catalyst that it is trying to mimic.[80] Insoluble supports are preferable than the homogeneous supports because of several reasons *i.e.,* they are readily recovered, they have potential applications in flow process and they do not need extra solvents for precipitation. Insoluble organic polymers are effective supports, but the polymer had to be carefully chosen and tuned so as to avoid swelling and to ensure that the homogeneous complex catalyst is tightly bound with the support not merely occluded inside. In contrast to the insoluble organic polymers, inorganic silica materials like amorphous silica gels or mesoporous silicas did not swell or dissolve in organic solvents. However, because of the lack of ordered pore channels, amorphous silica gels are unable to provide the size/shape specificity properties. Hence the immobilization of various homogeneous metal catalysts over solid organic-inorganic hybrid mesoporous supports as a mean of ‘heterogenization’ has particular significance. Heterogenization of useful homogenous catalysts or active centers will improve the overall efficiency of the catalytic process due to: (i) it is easier to separate the catalyst from the liquid by simple filtration, where the homogenous catalysts often leads to complicated and laborious extraction or distillation requirements, (ii) often the catalysts can be regenerated and recycled, (iii) confinement of the catalyst in the mesopores provides a means of introducing the size/shape selectivity and thus a greater specificity to a desired reaction. Moreover, if the functional groups or the catalytic active site was attached firmly to the solid support, the leaching problem, usually encountered in liquid phase reactions, can be greatly reduced.

1.7. PHYSICOCHEMICAL CHARACTERIZATION

Understanding the structural and electronic properties of the catalyst by spectroscopic techniques is one of the major goals in catalysis research because they can provide fundamental information about catalytic structures and surface reaction intermediates under controlled environments and also gives insight into the relation between physical and chemical properties of the catalyst and its activity. In catalytic research, a number of techniques will be used to characterize a sample and a summation of all characterization techniques will reveal the active sites in a catalyst and these in turn will helps in the design of a new catalyst or to improve the catalytic performances. The commonly used characterization techniques, their principles, advantages and limitations are briefly described in this section.

1.7.1. X-Ray Diffraction (XRD)

XRD has been applied as the most important tool to determine the structure of the materials characterized by long-range ordering, to identify bulk phases, to monitor the kinetics of bulk transformations and to estimate particle sizes.[81,82] The XRD method involves the interaction between the incident monochromatized X-rays (like Cu K_α or Mo K_α source) with the atoms of a periodic lattice. X-rays scattered by atoms in an ordered lattice interfere constructively in directions given by Bragg's law: $n\lambda = 2d \sin\theta$, where, λ is the wavelength of the X-rays, d is the distance between two lattice planes, θ is the angle between the incoming X-rays and the normal to the reflecting lattice plane and n is an integer known as the order of reflection.[83]

Bragg peaks are measured by observing the intensity of the scattered radiation as a function of scattering angle 2θ. The angles of maximum intensity enable one to calculate the spacings between the lattice planes and allow phase identifications while the width of diffraction peaks carries information on the dimensions of the reflecting planes. The width of the diffraction lines can be further used to estimate the crystal size by the Debye-Scherrer formula: $D_{hkl} = k\lambda/\beta cos\theta$, where D_{hkl}, λ, β and θ are the volume averaged particle diameter, X-ray wavelength, full width at half maximum (FWHM) and diffraction angle, respectively, and k is a constant, often taken as 1.[83]

Isomorphous substitution of heteroatoms in the framework of molecular sieves can be calculated from the changes in the unit cell parameters and unit cell volume. Unit cell parameter (a_o) of a hexagonal lattice can be calculated from, $a_o= 2d_{100}/\sqrt{3}$ and a cubic lattice can be determined by the following equation: $a_o = d_{211}\sqrt{6}$. The unit cell dimension determined by XRD is also used to calculate the frame wall thickness (FWT) of the channels of the mesoporous materials. A major limitation of XRD is that this technique requires samples, which possess sufficient long-range order. Amorphous phases and small particles give either broad and weak diffraction lines or no diffraction at all, which makes them virtually invisible for XRD.

1.7.2. Porosity Measurements by N_2 Adsorption Method

The most common method of measuring surface area and textural characteristics of catalytic materials is that based on the theory developed by Brunauer, Emmett and Teller (BET), considering the multilayer adsorption. The BET equation can be represented as: $p/V(p_o-p) = 1/cV_m + [(c-1)/cV_m]\ (p/p_o)$, where p is adsorption equilibrium pressure, p_o is saturation vapor pressure of the adsorbate at the experimental temperature, V is volume of N_2 adsorbed at pressure p, V_m is volume of adsorbate required for monolayer coverage and c, a constant that is related to the heat of adsorption and liquefaction.[84] A linear relationship between $p/V(p_o-p)$ and p/p_o is required to obtain the quantity of nitrogen adsorbed. The monolayer volume, V_m is given by $1/(S+I)$, where S is the slope and is equal to $(c-1)/cV_m$ and I is the intercept equal to $1/cV_m$.

The surface area of the catalyst (S_{BET}) is related to V_m, by the equation, $S_{BET} = (V_m/22414)\ N_a\sigma$, where N_a is Avogadro number and σ is mean cross sectional area covered by one adsorbate molecule. The σ value generally accepted for N_2 is 0.162 nm^2.

Several computational procedures are available for the derivation of pore size distribution of mesoporous samples from physisorption isotherms. Most popular among them is the Barrett-Joyner-Halenda (BJH) model, which is based on speculative emptying of the pores by a stepwise reduction of p/p_o, and allowance being made for the contraction of the multilayer in those pores already emptied by the condensate.[85] The mesopore size distribution is usually expressed as a plot of $\Delta V_p/\Delta r_p$ versus r_p, where V_p is the mesopore volume, and r_p is the pore radius.

1.7.3. Scanning Electron Microscopy (SEM)

Scanning electron microscopy is a straightforward technique to probe the morphological features of mesoporous molecular sieve materials. SEM scans over a sample surface with a probe of electrons (5-50 eV) and detects the yield of either secondary or back-scattered electrons as a function of the position of the primary beam. Contrast is generally caused by the orientation that parts of the surface facing the detector appear brighter than parts of the surface with their surface normal pointing away from the detector. The interaction between the electron beam and the sample produces different types of signals providing detailed information about the surface structure and morphology of the sample.[86] When an electron from the beam encounters a nucleus in the sample, the resultant Coulombic attraction leads to a deflection in the electron's path, known as Rutherford elastic scattering. A fraction of these electrons will be completely backscattered, re-emerging from the incident surface of the sample. Since the scattering angle depends on the atomic number of the nucleus, the primary electrons arriving at a given detector position can be used to produce images containing topological and compositional information.[87] A major advantage of SEM is that bulk samples can also be directly studied by this technique.

1.7.4. Transmission Electron Microscopy (TEM)

Transmission electron microscopy is typically used for high resolution imaging of thin films of a solid sample for micro structural and compositional analysis. The technique involves: (i) irradiation of a very thin sample by a high-energy electron beam, which is diffracted by the lattices of a crystalline or semi crystalline material and propagated along different directions, (ii) imaging and angular distribution analysis of the forward scattered electrons (unlike SEM where backscattered electrons are detected) and (iii) energy analysis of the emitted X-rays.[88] In detail, a primary electron beam of high energy and high intensity passes through a condensor to produce parallel rays, which impinge on the sample. As the attenuation of the beam depends on the density and the thickness, the transmitted electrons forms a two-dimensional projection of the sample mass, which is subsequently magnified by the electron optics to produce the so-called bright field image. The dark field image is obtained from the diffracted electron beams, which are slightly off angle from the transmitted beam. Typical operating conditions for TEM instruments are 100-200 keV electrons, 10^{-6} mbar vacuum, 0.5 nm resolution and a magnification of 10^5 to 10^6. The topographic information obtained by TEM in the vicinity of atomic resolution can be utilized for structural characterization and identification of various phases of mesoporous materials, *viz*., hexagonal, cubic or lamellar.[89]

1.7.5. Fourier Transform Infrared Spectroscopy (FT-IR)

Infrared spectroscopy (IR) can be considered as the first and the most important of the modern spectroscopic techniques that has found profound applications in the field of catalysis. This is primarily due to the fact that IR provides actual information on the structure, geometry and orientation of practically all molecules that are present in the reaction mixture, irrespective of the physical state, temperature or pressure. IR is therefore a feasible tool to identify phases that are present in the catalyst or its precursor stages, the adsorbed species, adsorption sites and the way in which the adsorbed species are chemisorbed on the surface of the catalyst.[90]

Infrared spectroscopy is the common form of vibrational spectroscopy and it depends on the excitation of vibrations in molecules or in solid lattices by the absorption of photons. Absorption of an infrared photon occurs only if a dipole moment changes during the vibration. However, it is not necessary that the molecule possess a permanent dipole, it is sufficient if a dipole moment changes during the vibrations. The intensity of the infrared band is proportional to the change in the dipole moment. Although this statement is of little practical value, as the magnitude of dipole moments during the vibrations are not known, it explains why species with polar bonds such as CO, NO and OH exhibit strong IR bands, where as covalent bonds such as C-C absorb infrared light only weakly and molecules such as H_2, N_2 are not infrared active at all.

A variety of IR techniques have been used to attain information on the surface chemistry of different solids. A great advantage of infrared spectroscopy is that the technique can be used to study catalysts *in situ*. In case of porous silicates, the FTIR spectra in the 1300-400 cm^{-1} region provides information about the structural details, whereas the bands in the 4000-3000 cm^{-1} region allows to determine different Brönsted and Lewis acid sites and silanol groups.[91] The band at 980-960 cm^{-1} in the framework region is very important in metal-containing molecular sieves, as this region provides information about the incorporation of metal species in the frame wall positions.[92] Acidic and basic properties as well as their strength can also be estimated using ammonia (NH_3), pyridine (C_5H_5N), carbon dioxide (CO_2), *etc* as probe molecules and their quantitative estimation by FTIR.[93] One drawback of IR is that almost all compounds absorb IR radiation so that the spectra of reaction mixtures can be very complex, hampering straightforward interpretation and assignments. However, data manipulation and processing techniques like deconvolution, spectral subtraction and chemometrics, are helpful in extracting the desired informations.[81]

1.7.6. Fourier Transform Raman Spectroscopy (FT-RS)

Raman spectroscopy (RS) is based on the inelastic scattering of photons, which loose energy by exciting vibrations in the sample. A vibration is Raman active if it changes the polarizability of the molecule. Raman spectroscopy is widely used for the investigation of oxides, supported and bulk metals, supported oxides and has found steadily increasing application for the characterization of supported transition metal oxide catalysts.[94] Similar to infrared spectroscopy, a great advantage of Raman spectroscopy is that the technique can be used to study catalysts *in situ*. All characteristic vibrational features of oxides of the transition metals like V, Cr, Mo and W fall in the frequency range below 1100 cm^{-1} and these oxides have high Raman scattering cross-sections because of their relatively high covalent bond character. Various studies have demonstrated that the simultaneous use of reference compounds and the correlation between Raman frequency and bond length makes RS very well suited to study the molecular structures of supported metal oxides. The usual support materials (particularly, silica and alumina) have very low Raman scattering cross-sections and shows weak absorption bands in the 1100-700 cm^{-1} region. Hence, RS has the advantage that the normal modes of the minority components, namely the transition metal oxides dispersed on the supports, can most frequently be detected with relative ease. A disadvantage of this technique is the small cross sections for Raman scattering, that most of the scattered intensity goes into the Rayleigh band, which is typically about three orders of magnitude greater than the Stokes bands.

1.7.7. Diffuse Reflectance UV-Visible Spectroscopy (DR UV-Vis)

Diffuse reflectance spectroscopy (DRS) is a technique based on the reflection of light in the ultraviolet (UV), visible (VIS) and near-infrared (NIR) region by a powdered sample. In a DRS spectrum, the ratio of the light scattered from an*'infinitely thick'* closely packed catalyst layer and the scattered light from an infinitely thick layer of an ideal non-absorbing (white) reference sample is measured as a function of the wavelength, λ. The scattered radiation, emanating from the sample, is collected in an integration sphere and detected. The most popular continuum theory describing diffuse reflectance effect is the Schuster-Kubelka-Munk (SKM) theory.[95] If the sample is infinitely thick, the diffuse reflection of the sample (R_∞) is related to an apparent absorption (K) and apparent scattering coefficient (S) by the SKM equation: $F(R_\infty) = (1-R_\infty)^2 / 2R_\infty = K/S$. At low concentrations of supported transition metal ions (TMI), this equation is a good representation of the absorption spectrum and allows a quantitative determination of the transition metal ions.

UV-Vis spectroscopy generally deals with the study of electronic transitions between orbital or bands of atoms, ions or molecules. One of the advantages of DRS is that the obtained information is directly chemical in nature since outer shell electrons of the transition metal ions are probed. This further provides information about the oxidation state and coordination environment of transition metal ions in the solid matrices. Thus DRS is a sensitive technique to examine the type of the metal sites, *viz.,* framework or extra-framework, in which that metal ion or cluster exist.[96] For most of the isomorphously substituted metal-containing molecular sieves, transitions in the UV region (200-400 nm) are of prime interest. The disadvantage of DRS is that the signals are usually broad and overlap with each other, leading to a biased spectral analysis. In addition, the origin of the specific electronic transition is sometimes difficult to isolate due to its dependence on the local coordination environment, the polymerization degree and the specific oxidation state.

1.7.8. X-Ray Photoelectron Spectroscopy (XPS)

XPS (also referred by the acronym ESCA, Electron Spectroscopy for Chemical Analysis) is a non-destructive surface analysis technique, based upon one of the fundamental interactions of photons with matter *viz.*, the photoelectric effect.[97] XPS provides information on the elemental composition, the oxidation state of the elements and in favorable cases on the dispersion of one phase over another. In this technique, sample surface is irradiated with X-rays and the emitted photoelectrons are measured. When an atom absorbs a photon of energy hv, a core or valence electron with binding energy E_b is ejected with kinetic energy E_k: $E_k = hv - E_b - \varphi$, where h is Planck's constant, v is the frequency of the exciting radiation, E_b is the binding energy of the photoelectron relative to the Fermi level of the sample and φ is the work function of the spectrometer.

The photoelectrons ejected from an atom in the solid have different kinetic energies, according to the electronic level and the type of atom they come from. As the electronic structure of an atom is a unique fingerprint of this atom, photoelectron spectra allow an excellent elemental analysis of the target sample.

XPS entails emission from both core and valence electrons of the solid, the stimulating X-ray sources being Al K_α (1486.6 eV) or Mg K_α (1253.6 eV). Their photon energy is high enough to reach at least one core level of any element and also their natural line width is small enough to allow the recording of well-resolved photoelectron spectra. XPS spectrum is usually a plot of the intensity of photoelectrons versus binding energy. Since the electrons whose energies are analyzed in XPS arise from a depth of not greater than about 5 nm, this technique is highly surface specific. A set of binding energies is characteristic for an element and hence XPS can be used to analyze the composition of samples, considering the area of the peak and cross section for photoemission.[81]

An experimental problem in XPS is that electrically insulating samples may charge during measurements, as photoelectrons leave the sample. Due to the positive charge on the sample, all XPS peaks in the spectrum shift by the same amount to higher binding energies. Calibration for this effect can be done by using C 1s binding energy of 284.9 eV from carbon contamination, which is present on most of the catalysts. Though XPS provides information about the oxidation state and the chemical environment of a given atom due to shift in the binding energies, the structural information is, however, limited in case of supported vanadium oxides and chromium oxides. For instance, VO_x structures possessing the same oxidation state, *i.e.,* between VO_6, VO_5 and VO_4 and chromium samples containing monochromates, dichromates and polychromates cannot be discriminated by this method. Another disadvantage relates to the use of ultrahigh vacuum conditions, which may result in the reduction of surface metal oxide species in the measurement chamber.[98]

1.7.9. Temperature Programmed Reduction (TPR)

Temperature programmed reaction methods typically involve monitoring surface or (bulk) processes between the solid catalyst and its gaseous environment *via.,* continuous analysis of the gas phase composition as the temperature is raised linearly with time. Instrumentation for temperature-programmed investigations generally consists of a reactor, charged with catalyst, in a furnace that can be temperature programmed and a thermal conductivity detector to measure the concerned active gas of the gas mixture before and after reaction. Temperature programmed reduction (TPR) determines the number of reducible species present in the catalyst and reveals the temperature at which the reduction occurs. An important aspect of TPR analyses is that the sample need not have any special characteristics other than containing reducible metals.[81] In a TPR experiment, the sample is placed in a fixed-bed reactor in a flow of reducing gas mixture and subjected to a linear temperature ramp. The consumption of hydrogen by adsorption/reaction is continuously measured by monitoring the change in composition of the gas mixture after passing through the reactor. The degree of reduction can be calculated from the amount of hydrogen consumed.

1.7.10. Thermal Analyses (TG-DTG and DTA)

Thermo analytical techniques involve the measurements of the response of the solid under study (energy or mass released or consumed) as a function of temperature (or time) dynamically by application of a linear temperature program. Thermogravimetry (TG) is a technique measuring the variation in mass of a sample when it undergoes temperature scanning in a controlled atmosphere. This variation in mass can be either a loss of mass (vapor emission) or a gain of mass (gas fixation). Differential thermal analysis (TGA) is a technique measuring the difference in temperature between a sample and a reference (a thermally inert material) as a function of time or temperature, when they undergo temperature scanning in a controlled atmosphere. The DTA method helps to determine any transformations and provides information on exothermic and endothermic reactions, taking place in the sample, which include phase transitions, dehydration, decomposition, redox or solid-state reactions. Further, for molecular sieves, it provides informations about the desorption of water, oxidative decomposition of occluded organic template species and dehydroxylation of silanol groups in the channel walls.[99]

1.7.11. Solid-State Nuclear Magnetic Resonance Spectroscopy (NMR)

Nuclear magnetic resonance spectroscopy gives information on the interaction of nucleus having a nuclear spin quantum number, *I*, greater than zero with an external magnetic field. The interaction of nuclear spins with the externally applied magnetic field, B_o, and their environment can be described by the spin Hamiltonian H: $H = HZ + HCS + HQ + HD + HJ$, where *HZ* is a Hamiltonian, which describes the interaction of the nuclear spin with the external field B_o (Zeeman Interaction). The chemical shift Hamiltonian *HCS* gives information on the local environment of a nucleus. The chemical shift is measured relative to that of a reference compound (TMS in case of ^{29}Si NMR) and is expressed in Hertz or in ppm with respect to the resonance frequency of the reference compound. *HQ* describes the quadrupolar interaction of the nucleus with the surrounding electric field gradient. *HD* describes the dipolar interaction with other nuclei, while *HJ* describes the interaction with other nuclei through *J*-coupling.

In solid-state NMR, the line shape is determined by dipolar and quadrupolar interactions. The lines are usually broader because the rigid structure of the solid phase prevents the averaging of the dipolar interaction by motions. Since the first order quadrupolar and dipolar interactions are proportional to $(3 \cos^2\theta - 1)$, where θ is the angle between an internuclear vector and the magnetic field, these interactions can be removed, to a first order approximation, by spinning the sample around the so-called magic angle θ with respect to the external magnetic field, for which $3 \cos^2\theta - 1 = 0$, *i.e.,* $\theta = 54.74^o$. This technique is known as Magic Angle Spinning (MAS).[100]

With the advent of sophisticated solid-state NMR techniques, now it is possible to obtain NMR spectra of solids with spectral resolution comparable to that of liquids.[101] Modern high-resolution solid-state NMR spectroscopy allows to elucidate the chemical and structural environment of several atoms in a solid matrix.[102,103] Cross-polarization

(CP) technique does not affect the line width of the spectra, but is applied to improve the sensitivity, *i.e.*, the signal to noise ratio (SNR) of the spectra of nuclei with low natural abundance (*e.g.* ^{13}C, ^{29}Si, ^{31}P, *etc*) and to monitor the spatial proximity of nuclei.[104] CP involves indirect excitation of the less abundant nucleus through magnetization transfer from an abundant spin system (*e.g.* ^{1}H).

1.7.12. Electron Paramagnetic Resonance (EPR)

EPR spectroscopy has been extensively applied in the field of catalysis to investigate the nature of the catalytic site and its environment (symmetry, number and nature of the ligands, *etc*). The high sensitivity of the technique permits the study of low concentrations of active sites and also helps to probe highly reactive paramagnetic intermediates without any spectroscopic interference. The main informations obtained from EPR experiments arises from the g-factor, hyperfine interactions and super hyperfine interactions.[105]

EPR technique is based on the interaction between electron magnetic moment and an external applied magnetic field designated as Zeeman interaction. When a system containing unpaired electrons (spin $\neq 0$) is placed in an external magnetic field H, the energy of the system is given by the equation, $E = \pm (1/2)\, g_e \beta H$. When this system is irradiated by suitable electromagnetic radiation perpendicular to the magnetic field with a frequency ν, the transition between the two Zeeman levels occurs provided the photon energy $h\nu$ is such that the condition, $\Delta E = g_e \beta H = h\nu$ is fulfilled. This is the resonance condition and results in an energy absorption. EPR spectra recording can be performed in a wide range of temperatures, and are generally carried out by placing the powdered samples in silica tubes, typically 5 or 6 mm in outer diameter. The spectrometer usually works with a 9000 MHz klystron (X band). However, for some experiments, other frequencies, such as 23,000 MHz (K band) or 35,000 MHz (Q band) are also used. A major limitation of the technique is that diamagnetic species cannot be observed and hence only a limited type of species can be studied.

1.8. CATALYTIC APPLICATIONS AND PROSPECTS

In recent years, environmental and economic considerations have raised strong interest to redesign commercially important process so that the use of harmful substances and the generation of toxic wastes can be avoided. Zeolite plays a key role in the development of environmentally benign process in the production of fine chemicals. However, zeolites posses severe limitations when large reactant molecules are involved, due to the diffusional restrictions imparted from the small pore channels of microporous solids.[11] Hence, because of the large pore size than the zeolite based porous materials, mesoporous materials stood for the extension of catalytic applications of zeolites for the conversion of bulky molecules.

Through the development of hybrid organic-inorganic mesoporous solids, much progress has been made in the last few years towards the applications of mesoporous solids in various areas of heterogeneous catalysis. The concept of '*heterogenization*' of homogenous catalysts over organic-inorganic hybrid mesoporous materials possessing reactive functional sites provides the prospective for extending the benefits of heterogeneous catalysis to homogeneous systems. These benefits include easier separation of catalyst and reaction products leading to shorter work up times, improved process efficiency and better reuse of the supported catalysts. However, the prime requirement of the heterogenization approach is to maintain the stability of the heterogenized complex, such that it does not decompose or leach out from the solid support to the liquid phase during the course of reaction, and at the same time retains high activity and selectivity. Reactions that have been studied using functionalized mesoporous solids include acid catalysis,[106] base catalysis,[107] oxidations,[108] reductions,[109] enantioselective catalysis[110] and other catalytic reactions that produce fine chemicals.[111]

It has been noted that the confinement of the catalyst or active sites in the mesoporous channels improved the overall activity of the catalysts compared to attachment over amorphous or non-porous silica supports. These improved results apparently stemed out due to the confined environment of the mesopore channels. In some cases, the performance of the mesoporous catalyst was found to be directly depend on the pore size of the mesopore host, since depending on the pore size the accessibility of the active sites in the mesopores gets varied. For instance, in the hydrogenation of olefins (styrene, *trans*- and *cis*- stilbene, α-methyl styrene and limonene), the hydrido chloro carbonyl tris-(triphenylphosphine) ruthenium complex ($RuHCl(CO)(PPh_3)_3$ immobilized over aminopropyl functionalized mesoporous SBA-15 shows superior catalytic activity than the MCM-41 sample, even though both mesoporous supports shows higher conversion and turnover frequency than the unsupported ruthenium complex. The superior catalytic activity of SBA-15 than MCM-41 is attributed to the easier access of substrate molecules to the active sites in SBA-15 due to its larger pore size than the MCM-41 host matrix.[112]

In this section, the catalytic applications and prospects of metal-containing mesoporous materials and organo-modified mesoporous materials for various oxidation, and epoxidation reactions are briefly reviewed.

1.8.1. Oxidation Reactions

The first examples of liquid phase catalytic oxygen transfer dates back to 1936. The so-called Milas reagents were formed by reaction of transition metal oxides with a solution of H_2O_2 in *tert*-butanol resulting in soluble inorganic peracids.[113] These catalysts were used for the vicinal dihydroxylation of olefins but with certain metal oxides like MoO_3 or WO_3, selective epoxidation was observed. From these basics, a great deal of effort has been put into the development of transition metal based catalysts, as homogeneous and heterogeneous, for various selective oxidation reactions.[114]

Based on the key intermediate involved in the oxygen transfer step, the metal catalyzed oxidations can be divided mainly into two categories.[115] The first one involves a peroxometal species, while the second one involves an oxometal pathway. In general, titanium, vanadium and molybdenum catalyzed reactions are believed to occur *via.,* a peroxometal pathway,[116] while chromium[117] and ruthenium[118] catalyzed reactions are supposed to proceed through oxometal species.

Metallosilicate molecular sieves with MFI topologies (*e.g.* TS-1, VS-1) have been extensively investigated as heterogeneous catalysts for various selective oxidation and epoxidation reactions.[119] However, as mentioned earlier, the catalytic properties of these molecular sieves can be utilized only for small molecules, due to the small pore size of these materials. In this regard, the advent of metal-containing mesoporous solids that can accomodate bulky molecules inside the pore channels widened the range of catalysts available for selective oxidation reactions using peroxides and air as oxidants, few of which are summarized in Table 1.3. Further, the advent of various organic-inorganic hybrid mesoporous materials having reactive functional groups helps to immobilize various metal and metal complexes inside the pore channels of the mesoporous materials. Compared to the metal-substituted mesoporous materials, these methods provides better active site isolations and also helps to increase the stability of the metal-containing mesoporous materials, if the bonding between the ligand and metal is robust.

Recently, there is much interest in substituting process that use pollutant oxidants with more environmentally acceptance ones. Besides the prime properties like price and ease of handling, the choice of oxidants depends mainly upon two factors *viz.,* the nature of the corresponding by-product and the active-oxygen content. The former property is important in terms of environmental considerations, while the latter factor influences the overall productivity of the process. In this respect, molecular oxygen is an attractive choice. However, the free radical nature of the reaction restricts its applicability to a rather small number of molecules. Hence, for the catalytic epoxidation and oxidation reactions of a wide variety of organic molecules, organic peroxides as well as hydrogen peroxide was used as single oxygen donors. Even though, organic peroxides are more active oxidants than hydrogen peroxide, they are more expensive and the active oxygen content is rather low. Moreover, usage of organic peroxides generates stoichiometric amount of corresponding alcohols, which in most cases complicates the separation process. Hence the preferred oxidant in most of the oxidation or epoxidation process is hydrogen peroxide, with respect to the active oxygen content (47%) and the nature of by-product formed *viz.,* water.[131]

Table 1.3. Oxidation reactions over surface-modified mesoporous silicas

No.	Catalysts	Reaction	Reference
1	Ti-MCM-41	Epoxidation of styrene, 1-octene, cyclododecene	120
2	Ti-HMS	Epoxidation of cyclooctene, styrene	121
3	V-MCM-41	Oxyfunctionalization of alkanes, hydroxylation of 1-napthol, epoxidation of cyclooctene	122,123
4	V-MCM-48	Selective oxidation of cyclohexane, styrene	124
5	V-HMS	Oxidation of 2,6-DTBP, naphthalene, cyclododecanol	125
6	Cr-MCM-41	Oxidation of 1-napthol, cyclohexane	126
7	Cr-MCM-48	Oxidation of ethyl benzene	127
8	Fe-MCM-41	Epoxidation of styrene	128
9	Co-MCM-41	Oxidation of styrene, benzene, 1-hexene	129
10	Sn-MCM-41	Oxidation of 1-napthol, Bayer-Villiger oxidation reactions	130

Although hydrogen peroxide (H_2O_2) provides distinguishable advantageous feature than the organic peroxides, two main problems are generally encountered when H_2O_2 was used as an oxidant in presence of redox molecular sieves and both these problems are related to the presence of water formed during the reaction. The first and most important problem is related to the irreversible hydrolysis of the siloxy-metal (Si-O-M) units in the active sites. The second problem frequently observed is that, water obstructs the active sites of the catalyst and thereby sterically prevents the alkene, in epoxidation reaction, or hydrocarbons, in oxidation reactions, to react with the active site. This usually results in a decreased activity of the catalyst while the former problem severely limits the reusability of the catalysts.[131,132] Since the commercially available oxidant sources of hydrogen peroxide and organic peroxides, like the *tert*-butyl hydroperoxide, contain water to some extent, use of oxidants like urea-hydrogen peroxide

(UHP) or hydrophobic catalyst surface are better alternatives to overcome such difficulties.[133] However, in heterogeneous systems with clean oxidants like H_2O_2, it is an environmentally friendly alternative to traditional oxidation reactions and hence attention had also been devoted to the synthesis of stable metal-containing mesoporous materials by the judicious decoration of the internal pore size of the mesoporous materials with various organic groups.[68-70] Hence, the development of environmentally friendly, safer and effective heterogeneous redox catalysts seems to be a challenging task to the research community.

1.9. SCOPE AND OBJECTIVES OF THE THESIS

The principal aim of this thesis was to investigate the approach of heterogenization of various transition metals over solid mesoporous supports and organic-inorganic hybrid mesoporous materials for oxidation and epoxidation reactions, under different reaction conditions.

During the last few years, the catalytic transformations of bulky molecules over various metal-containing and organo-modified metal-containing mesoporous materials constitute an interesting research area in the field of fine chemical syntheis.[11a,76a] Hence, the incorporation of various heteroatoms in the framework and pore channels of different mesoporous materials had been systematically studied, characterized and also used as catalysts in various industrially relevant organic transformations. The high surface area, ordered pore channels and high-density silanol sites of the mesoporous molecular sieves were also exploited for the preparation of bifunctional molecular sieves for the heterogenization of catalytically reactive species. Special attention was paid in the synthesis and use of silsesquioxane precursors for the development of periodic mesoporous organosilicas and their metal analogs. Besides, throughout the thesis, much emphasis was placed on catalyst stability evaluations since this step is considered as a prime requirement for the successful development of various metal-containing mesoporous materials. In-depth characterizations of all catalyst systems are highlighted to understand the mode of interaction of the active sites with the mesoporous silicate network and thereby to evaluate the structure-catalytic activity relations and stability of the mesoporous solids.

Vanadium-containing mesoporous materials were active in a number of liquid-phase oxidation reactions using H_2O_2 and TBHP as oxidants.[122,123] However, they show the leaching of active metal sites during oxidation reactions, in presence of aqueous oxidants. Recently, there has been an increasing demand in the synthesis of metal-containing mesoporous materials with better catalytic activity and stability. Hence, it was thought interesting to study in detail the role of commonly used silica sources, *viz.,* fumed silica and tetraethyl orthosilicate in the structural stability and site isolation of vanadium sites in Si(V)-MCM-41 mesoporous materials. Further, the increased demand of organic-inorganic hybrid mesoporous materials and their unique hydrophobic features attracted attention in the development of heterogenized vanadium catalysts over various amino propyl modified mesoporous silica supports and in the development of vanadium-containing periodic mesoporous organosilicas having ethane groups in the frame wall positions.

The design and synthesis of metal-containing mesoporous materials having pore size greater than 25 Å be the main area of research in the last decade, as their high surface area and pore size helps to overcome the limitations of the conventional small pore zeolite catalysts.[134] However, solid materials having pore sizes in between that of zeolites and mesoporous materials (super microporous region) received less attention and hence ordered porous silicas that effectively bridge the existing gap between the typical microporous and mesoporous materials are interesting in the field of heterogeneous catalysis.[135] Hence in search of new metal-containing mesoporous materials having pore size in the super microporous region, bifunctional mesoporous organosilicas having unprecedented organic groups in the pore channels as well as chromium in the frame wall positions were first synthesized. Chromium-containing porous materials having pore size in the super microporous region can be readily obtained by calcination of the chromium-containing organo-functionalized materials and these materials are envisaged to exhibit high catalytic activity and better stability in various liquid phase oxidation reactions, than the conventional metal-containing mesoporous materials. Chromium-containing mesoporous materials reported earlier shows the leaching of active metal sites during liquid-phase reactions.[126,127] Hence, in an attempt to improve the stability of chromium-containing mesoporous materials, ethane-silica hybrid periodic mesoporous organosilicas were synthesized and their catalytic performance was compared with the conventional chromium-containing mesoporous molecular sieves. In-depth characterization of all chromium catalysts are highlighted to understand the nature and location of active chromium sites in the porous network, the role of hydrophobic organic species in dispersing the active chromium sites and also to explore the origin of catalytic activity.

The specific problems chosen are:

(i) Synthesis of periodic mesoporous silica materials like Si-MCM-41, Si-MCM-48, Si-SBA-15 and their surface modification by organic functional groups *via.,* different routes.

(ii) Synthesis of periodic mesoporous organosilicas having organic moieties like ethane ($-CH_2-CH_2-$) in the frame wall positions.

(iii) Synthesis of vanadium-containing mesoporous materials, by various preparation routes, over the periodic mesoporous silica and organosilica materials and application of these materials in the oxidation reaction of naphthalene and cyclohexane and in the epoxidation reaction of cyclooctene and styrene.

(iv) Synthesis of chromium-containing bifunctional mesoporous silicas, chromium-containing ethane-bridged hybrid mesoporous organosilicas and application of these samples in the selective oxidation reaction of cyclohexane using peroxides and air as oxidants.

(v) Detailed characterization of all the new organo-modified, metal-containing mesoporous catalysts.

1.10. OUTLINE OF THE THESIS

The thesis is presented in **SIX** chapters, a brief summary of which is given below.

Chapter 1 presents a general introduction about various physicochemical aspects of periodic mesoporous silica and periodic mesoporous organosilica materials. The different characteristic properties of these materials, their synthesis parameters, formation mechanisms, different approaches for surface-functionalization, characterization techniques and application as supports for different catalytically active transformations are discussed in brief. The scope and objectives of the present work have been outlined at the end of this chapter.

Chapter 2 describes the synthesis of vanadium-containing mesoporous MCM-41 samples by the direct substitution method, grafting method and by the immobilization method. The synthesis procedures of the V-MCM-41 catalysts are probed in detail by using different silica sources in order to account the role of silica sources in the mesoporous structural ordering, stabilization of vanadium sites, catalytic activity and stability. The immobilization of vanadium was carried out over amino propyl modified mesoporous supports like SBA-15 and MCM-41 and an amorphous silica gel, in order to probe the role of surface hydroxyl groups in the anchoring of organic groups as well as to attain information about the nature and coordination of vanadium over different organo-modified supports. All the synthesized catalysts are characterized by XRD, N_2 sorption technique, SEM, TEM, TG-DTG analysis, ICP analysis, solid state ^{13}C CP MAS NMR, ^{29}Si and ^{51}V MAS NMR, FT-IR spectroscopy, FT-Raman spectroscopy, EPR and TPR. The catalytic activity as well as the stability of vanadium catalysts was evaluated in the oxidation reaction of naphthalene and cyclohexane and in the epoxidation reaction of cyclooctene, using *aqueous* hydrogen peroxide (H_2O_2) as well as *tert*-butylhydrogenperoxide (TBHP) as oxidants and are discussed in detail.

Chapter 3 describes the synthesis of vanadium-containing periodic mesoporous organosilica samples, having ethane groups in the frame wall positions, prepared by using cationic surfactants of different chain lengths *viz.,* C18-, C16- and C14-. All the synthesized catalysts are characterized by XRD, N_2 sorption technique, SEM, TEM, TG-DTG analysis, ICP analysis, solid-state ^{13}C CP MAS NMR, ^{29}Si and ^{51}V MAS NMR and FT-Raman spectroscopy. The catalytic activity and stability of hybrid vanadium catalysts was compared with V-MCM-41 catalyst in the epoxidation reaction of styrene, using *aqueous* hydrogen peroxide (H_2O_2) as well as *tert*-butylhydrogenperoxide (TBHP) as oxidants and are discussed in detail.

Chapter 4 deals with the synthesis of bifunctional chromium-containing mesoporous materials, using various organo modifiers like chloro propyl, methyl and vinyl units and their further transformation to chromium-containing small pore silicas. The effect of different chain length organic groups in the percentage of chromium loading, structural shrinkage as well as the dispersion of chromium and the controlled transformation of these bifunctional mesoporous materials to small pore chromium silicas having pore size in the super microporous region are discussed. The catalytic activities of the chromium catalysts were assessed in the oxidation reaction of cyclohexane to cyclohexanol and cyclohexanone using *non-aqueous tert*-butylhydrogenperoxide and air as oxidants under different reaction conditions. The stability as well as reusability of the catalysts were also carried out and are described in detail.

Chapter 5 deals with the synthesis of chromium-containing periodic mesoporous organosilicas having ethane groups in the frame wall positions by two different synthesis routes, using 1,2-bis(triethoxysilyl)ethane as the silica source and 1,2-bis (triethoxysilyl)ethane and tetraethyl orthosilicate as a mixed silica source. The newly developed organo-modified mesoporous chromium samples are characterized by XRD, N_2 sorption technique, TEM, TG-DTA, ICP analysis, solid-state ^{13}C CP MAS NMR and ^{29}Si MAS NMR, FT-IR spectroscopy, FT-Raman spectroscopy, UV-Vis, XPS and TPR.

The catalytic activity of the chromium catalysts were assessed in the oxidation reaction of cyclohexane to cyclohexanol and cyclohexanone using *aqueous* hydrogen peroxide, *non-aqueous tert*-butylhydrogenperoxide and air as oxidants under different reaction conditions and are compared with a conventional Cr-MCM-41 sample. The stability as well as reusability of the catalysts were also carried out and are discussed in detail.

Chapter 6 summarizes the results obtained and the basic findings of the present study.

1.11. REFERENCES

1 D. W. Breck, *Zeolite Molecular Sieves*, Wiley, New York, **1974**.

2 (a) R. Szostak, *Molecular Sieves: Principles of Synthesis and Identification*, Van Nostrand Reinhold, New York, **1989**. (b) R. M. Barrer, *Hydrothermal Chemistry of Zeolites*, Academic Press, New York, **1982**. (c) M. E. Davis, *Acc. Chem. Res*. **1993**, *26*, 111. (d) C. S. Cundy, P. A. Cox, *Chem. Rev*. **2003**, *103*, 663. (e) C. E. A. Krischhock, S. P. B. Kremer, J. Vermant, G. V. Tendeloo, P. A. Jacobs, J. A. Martens, *Chem. Eur. J.* **2005**, *11*, 4306.

3 (a) A. Corma, *Chem. Rev.* **1995**, *95*, 559. (b) A. Corma, *Chem. Rev.* **1997**, *97*, 2373. (c) S. M. Csicsery, *Zeolites* **1984**, *4*, 202. (d) J. H. Clark, D. J. Macquarrie, *Chem. Soc. Rev*. **1996**, *25*, 303.

4 (a) M. E. Davis, C. Saldarroaga, C. Montes, J. Garces, C. Crowder, *Nature* **1998**, *331*, 698. (b) M. E. Davis, C. Montes, P. E. Hathaway, J. P. Arhancet, D. L. Hasha, J. M. Garces, *J. Am. Chem. Soc.* **1989**, *111*, 3919. (c) I. W. C. E. Arends, R. A. Sheldon, M. Wallau, U. Schuchardt, *Angew. Chem. Int. Ed*. **1997**, *36*, 1144. (d) M. E. Davis, *Nature* **2002**, *417*, 813.

5 (a) C. T. Kresge, M. E. Leonowicz, W. J. Roth, J. C. Vartuli, J. S. Beck, *Nature* **1992**, *359*, 710. (b) J. S. Beck, J. C. Vartuli, W. J. Roth, M. E. Leonowicz, C. T. Kresge, K. D. Schmitt, C. T. W. Chu, D. H. Olson, E. W. Sheppard, S. B. McCullen, J. B. Higgins, J. L. Schlenker, *J. Am. Chem. Soc*. **1992**, *114*, 10834. (c) T. Yanagisawa, T. Shimizu, K. Kuroda, *Bull. Chem. Soc. Jpn*. **1990**, *63*, 988. (d) S. Inagaki, Y. Fukushima, K. Kuroda, *J. Chem. Soc., Chem. Commun*. **1993**, 680.

6 (a) Q. Huo, R. Leon, P. M. Petroff, G. D. Stucky, *Science* **1995**, *268*, 1324. (b) D. Zhao, J. Feng, Q. Huo, N. Melosh, G. H. Fredrickson, B. F. Chmelka, G. D. Stucky, *Science* **1995**, *267*, 865. (c) P. T. Tanev, T. J. Pinnavaia, *Science* **1995**, *267*, 865. (d) S. S. Kim, W. Zhang, T. J. Pinnavaia, *Science* **1998**, *282*, 1302. (e) D. M. Antonelli, J. Y. Ying, *Angew. Chem. Int. Ed.* **1996**, *35*, 426. (f) A. Davidson, *Curr. Opinion in Colloid & Inter. Sci*. **2002**, *7*, 92.

7 (a) K. Cassiers, T. Linssen, M. Mathieu, M. Benjelloun, K. Schrijnemakers, P. Van der Voort, P. Cool, E. F. Vansant, *Chem. Mater*. **2002**, *14*, 2317. (b) P. Van der Voort, M. Baltes, E. F. Vansant, *Catal. Today* **2001**, *68*, 121. (c) S. Jun, J. M. Kim, R. Ryoo, Y. S. Ahn, M. K. Han, *Microporous Mesoporous Mater*. **2000**, *41*, 119.

8 T. Linssen, K. Cassiers, P. Cool, E. F. Vansant, *Adv. in Colloid and Inter. Sci.* **2003**, *103*, 121.

9 (a) K. W. Gallis, C. C. Landry, *Chem. Mater*. **1997**, *9*, 2035. (b) K. Cassiers, P. Van Der Voort, B. M. Weckhuysen, R. A. Schoonheydt, E. F. Vansant, *J. Catal*. **2001**, *197*, 160. (c) C. Petitto, A. Galarneau, M-F. Driole, B. Chiche, B. Alonso, F. D. Renzo, F. Fajula, *Chem. Mater*. **2005**, *17*, 2120. (d) A. Sayari, *J. Am. Chem. Soc*. **2000**, *122*, 6504.

10 (a) L. D. Rollmann, *Adv. Chem. Ser*. **1979**, *173*, 389. (b) D. W. Breck, *J. Chem. Edu*. **1964**, *41*, 678.

11 (a) A. Sayari, *Chem. Mater*. **1996**, *8*, 1840. (b) J. Y. Ying, C. P. Mehnert, M. S. Wong, *Angew. Chem. Int. Ed*. **1999**, *38*, 56.

12 F. Schuth, *Angew. Chem. Int. Ed*. **2003**, *42*, 3604.

13 (a) A. E. C. Palmqvist, *Curr. Opinion in Colloid & Inter. Sci*. **2003**, *8*, 145. (b) H-P. Lin, C-Y. Mou, *Acc. Chem. Res*. **2002**, *35*, 927.

14 C. Madsen, C. J. H. Jacobsen, *Chem. Commun*. **1999**, 673.

15 (a) S. Polarz, M. Antonietti, *Chem. Commun*. **2002**, 2593. (b) G. S. Attard, J. C. Glyde, C. G. Goltner, *Nature* **1995**, *378*, 366.

16 (a) R. Ryoo, S. H. Joo, S. Jun, *J. Phys. Chem. B* **1999**, *103*, 7743. (b) J. Lee, S. Yoon, T. Hyeon, S. M. Oh, K. B. Kim, *Chem. Commun*. **1999**, 2177. (c) S. H. Joo, R. Ryoo, M. Kruk, M. Jaroniec, *J. Phys. Chem. B* **2002**, *106*, 4640. (d) S. H. Joo, S. J. Choi, I. Oh, J. Kwak, Z. Liu, O. Terasaki, R. Ryoo, *Nature* **2001**, *412*, 169. (e) A. Lu, W. Schmidt, A. Taguchi, B. Spliethoff, B. Tesche, F. Schuth, *Angew. Chem. Int. Ed*. **2002**, *41*, 3489.

17 J. N. Israelachvili, D. J. Mitchell, B. W. Ninham, *J. Chem. Soc., Faraday Trans*. **1976**, *72*, 1525.

18 J. C. Vartuli, K. D. Schmitt, C. T. Kresge, *Chem. Mater*. **1994**, *6*, 2317.

19 (a) H-P. Lin, C-Y. Mou, *Acc. Chem. Res.* **2002**, *35*, 927. (b) M. Ogura, H. Miyoshi, S. P. Naik, T. Okubo, *J. Am. Chem. Soc*. **2004**, *126*, 10937.

20 J. S. Beck, J. C. Vartuli, G. J. Kennedy, C. T. Kresge, W. J. Roth, S. E. Schramm, *Chem. Mater*. **1994**, *6*, 1816.

21 C. Y. Chen, S. L. Burkett, H. X. Li, M. E. Davis, *Microporous Mater*. **1993**, *2*, 27.

22 (a) A. Monnier, F. Schuth, Q. Huo, D. Kumar, D. I. Margolese, R. S. Maxwell, G. D. Stucky, M. Krishnamurthy, P. Petroff, A. Firouzi, M. Janicke, B. F. Chmelka, *Science* **1993**, *261*, 1299. (b) G. D. Stucky, A. Monnier, F. Schuth, Q. Huo, D. I. Margolese, D. Kumar, M. Krishnamurthy, P. Petroff, A. Firouzi, M. Janicke, B. F. Chmelka, *Mol. Cryst. Liq. Cryst*. **1994**, *240*, 187.

23 (a) A. Firouzi, D. Kumar, L. M. Bull, T. Besier, P. Sieger, Q. Huo, S. A. Walker, J. A. Zasadzinski, C. Glinka, J. Nicol, D. I. Margolese, G. D. Stucky, B. F. Chmelka, *Science* **1995**, *267*, 1138. (b) A. Firouzi, F. Atef, A. G. Oertli, G. D. Stucky, B. F. Chmelka, *J. Am. Chem. Soc*. **1997**, *119*, 3596.

24 (a) Q. Huo, D. I. Margolese, U. Ciesla, P. Feng, P. Sieger, R. Leon, P. Petroff, F. Schuth, G. D. Stucky, *Nature* **1994**, *368*, 317. (b) Q. Huo, D. I. Margolese, U. Ciesla, D. G. Demuth, P. Feng, T. E. Gier, P. Sieger, A. Firouzi, B. F. Chmelka, F. Schuth, G. D. Stucky, *Chem. Mater*. **1994**, *6*, 1176.

25 (a) P. T. Tanev, T. J. Pinnavaia, *Chem. Mater*. **1996**, *8*, 2068. (b) P. T. Tanev, T. J. Pinnavaia, *Science* **1996**, *271*, 1267. (c) S. A. Bagshaw, E. Prouzet, T. J. Pinnavaia, *Science* **1995**, *269*, 1242.

26 A. Sayari, S. Hamoudi, *Chem. Mater*. **2001**, *13*, 3151

27 A. P. Wight, M. E. Davis, *Chem. Rev*. **2002**, *102*, 3589.

28 (a) D. E. De Vos, M. Dams, B. F. Sels, P. A. Jacobs, *Chem. Rev.* **2002**, *102*, 3605. (b) X. Feng, G. E. Fryxell, l. Q. Wang, A. Y. Kim, J. Liu, K. M. Kemner, *Science* **1997**, *276*, 923. (c) D. Brunel, N. Bellocq, P. Sutra, A. Cauvel, M. Lasperas, P.

Moreau, F. D. Renzo, A. Galarneau, F. Fajula, *Coord. Chem. Rev*. **1998**, *178*, 1085. (d) A. Stein, B. J. Melde, R. C. Schroden, *Adv. Mater*. **2000**, *12*, 1403.

29 (a) T. Yokoi, H. Yoshitake, T. Tatsumi, *J. Mater. Chem*. **2004**, *14*, 951. (b) H-P. Lin, L-Y. Yang, C-Y. Mou, S-B. Liu, H-K. Lee, *New J. Chem*. **2000**, *24*, 253. (c) H. Q. Yang, G. Y. Zhang, X. L. Hong, Y. Y. Zhu, *Microporous Mesoporous Mater*. **2004**, *68*, 119.

30 P. M. Price, J. H. Clark, D. J. Macquarrie, *J. Chem. Soc., Dalton Trans*. **2000**, 101.

31 X. S. Zhao, G. Q. Lu, *J. Phys. Chem. B* **1998**, *102*, 1556.

32 J. Liu, X. Feng, G. E. Fryxell, L. Q. Wang, A. Y. Kim, M. Gong, *Adv. Mater*. **1998**, *10*, 161.

33 K. K. Unger, *Porous Silica- Its Properties and Use as Support in Column Liquid Chromatography*, Vol. 16, Elsevier, Amsterdam, **1979**.

34 L. Mercier, T. J. Pinnavaia, *Environ. Sci. Tech*. **1998**, *32*, 2749.

35 J. Liu, G. E. Fryxell, S. Mattigod, T. S. Zemanian, Y. Shin, L. Q. Wang, in Proc. Nanoporous Materials II, Banff, Canada, **2000**.

36 T. Kimura, S. Saeki, Y. Sugahara, K. Kuroda, *Langmuir* **1999**, *15*, 2794.

37 (a) R. Anwander, C. Palm, J. Stelzer, O. Groeger, E. Engelhardt, *Stud. Surf. Sci. Catal*. **1998**, *117*, 135. (b) R. Anwander, I. Nagl, M. Widenmeyer, G. Engelhardt, O. Groeger, C. Palm, T. Roser, *J. Phys. Chem. B* **2000**, *104*, 3532. (c) V. Antochshuk, M. Jaroniec, *J. Phys. Chem. B* **1999**, *103*, 6252. (d) C. P. Jaroniec, M. Kruk, M. Jaroniec, A. Sayari, *J. Phys. Chem. B* **1998**, *102*, 5503.

38 T. Asefa, M. Kruk, M. J. MacLachlan, N. Coombs, H. Grondey, M. Jaroniec, G. A. Ozin, *J. Am. Chem. Soc*. **2001**, *123*, 8520.

39 M. H. Lim, C. F. Blanford, A. Stein, *J. Am. Chem. Soc*. **1997**, *119*, 4090.

40 M. H. Lim, C. F. Blanford, A. Stein, *Chem. Mater*. **1998**, *10*, 467.

41 W. M. Van Rhijn, D. E. De Vos, B. F. Sels, W. D. Bosaert, P. A. Jacobs, *Chem. Commun*. **1998**, 317.

42 (a) J. H. Clark, D. J. Macquarrie, *Chem. Commun*. **1998**, 853. (b) D. Brunel, *Microporous Mesoporous Mater*. **1999**, *27*, 329.

43 P. Sutra, D. Brunel, *Chem. Commun*. **1996**, 2485.

44 M. H. Lim, A. Stein, *Chem. Mater*. **1999**, *11*, 3285.

45 D. S. Shepherd, W. Zhou, T. Maschmeyer, J. M. Malters, C. L. Roper, S. Parsons, B. F. G. Johnson, M. J. Duer, *Angew. Chem. Int. Ed*. **1998**, *37*, 2719.

46 F. De Juan, E. R. Hitzky, *Adv. Mater*. **2000**, *12*, 430.

47 V. Antochshuk, M. Jaroniec, *Chem. Commun*. **1999**, 2373.

48 C. Sanchez, F. Ribot, *New J. Chem*. **1994**, *18*, 1007.

49 (a) S. L. Burkett, S. D. Sims, S. Mann, *Chem. Commun*. **1996**, 1367. (b) D. J. Macquairre, *Chem. Commun*. **1996**, 1961. (c) Q. Huo, D. I. Margolese, G. D. Stucky, *Chem. Mater*. **1996**, *8*, 1147.

50 (a) S. R. Hall, C. E. Fowler, B. Lebeau, S. Mann, *Chem. Commun*. **1999**, 201. (b) F. Babonneau, L. Leite, S. Fontlupt, *J. Mater. Chem*. **1999**, *9*, 175. (c) V. Goletto, V. Dagry, F. Babonneau, *Mater. Res. Soc. Symp. Proc*. **1999**, *576*, 229. (d) L. Mercier, T. J. Pinnavaia, *Chem. Mater*. **2000**, *12*, 188. (e) R. Richer, L. Mercier, *Chem. Commun*. **1998**, 1775. (f) J. Brown, R. Riche, L. Mercier, *Microporous Mesoporous Mater*. **2000**, *37*, 41.

51 (a) D. A. Loy, K. J. Shea, *Chem. Rev*. **1995**, *95*, 1431. (b) K. J. Shea, D. A. Loy, O. Webster, *J. Am. Chem. Soc*. **1992**, *114*, 6700. (c) D. A. Loy, G. M. Jamison, B. M. Baugher, S. A. Myers, R. A. Assink, K. J. Shea, *Chem. Mater*. **1996**, *8*, 656.

52 (a) S. Inagaki, S. Guan, Y. Fukusima, T. Ohsuma, O. Terasaki, *J. Am. Chem. Soc*. **1999**, *121*, 9611. (b) T. Asefa, M. J. MacLachlan, N. Coombs, G. A. Ozin, *Nature* **1999**, *402*, 867. (c) B. J. Melde, B. T. Holland, C. F. Blanford, A. Stein, *Chem. Mater*. **1999**, *11*, 3302.

53 (a) B. Hatton, K. Landskron, W. Whitnall, D. Perovic, G. A. Ozin, *Acc. Chem. Res*. **2005**, *38*, 305. (b) S. Guan, S. Inagaki, T. Ohsuna, O. Terasaki, *J. Am. Chem. Soc*. **2000**, *122*, 5660. (c) M. P. Kapoor, S. Inagaki, *Chem. Mater*. **2002**, *14*, 3509. (d) A. Sayari, S. Hamoudi, Y. Yang, I. L. Moudrakovski, J. R. Ripmeester, *Chem. Mater*. **2000**, *12*, 3857. (e) C. H. Lee, S. S. Park, S. J. Choe, D. H. Park, *Microporous Mesoporous Mater*. **2001**, *46*, 257.

54 (a) S. Hamoudi, S. Kaliaguine, *Chem. Commun*. **2002**, 2118. (b) Y. Lu, H. Fan, N. Doke, D. A. Loy, R. A. Assink, D. A. LaVan, C. J. Brinker, *J. Am. Chem. Soc*. **2000**, *122*, 5258. (c) J. R. Matos, M. Kruk, L. P. Mercuri, M. Jaroneic, T. Asefa, N. Coombs, G. A. Ozin, T. Kamiyama, O. Terasaki, *Chem. Mater*. **2002**, *14*, 1903.

55 S. Inagaki, S. Guan, T. Ohsuna, O. Terasaki, *Nature* **2002**, *416*, 304. (b) M. P. Kapoor, Q. Yang, S. Inagaki, *Chem. Mater.* **2004***, 16,* 1209. (c) W. Wang, S. Xie, W. Zhou, A. Sayari, *Chem. Mater.* **2003**, *15*, 4886. (d) M. P. Kapoor, Q. Yang, S. Inagaki, *J. Am. Chem. Soc*. **2002**, *124*, 15176. (e) K. Okamoto, Y. Goto, S. Inagaki, *J. Mater. Chem*. **2005**, *15*, 4136.

56 C. Y. Ishii, T. Asefa, N. Coombs, M. J. MacLachlan, G. A. Ozin, *Chem. Commun*. **1999**, 2539. (b) K. Nakajima, D. Lu, J. N. Kondo, I. Tomita, S. Inagaki, M. Hara, S. Hayashi, K. Domen, *Chem. Lett*. **2003**, *32*, 950.

57 M. J. MacLachlan, T. Asefa, G. A. Ozin, *Chem. Eur. J.* **2000**, *6*, 2507.

58 S. Inagaki, S. Guan, F. Fukushima, T. Ohsuna, O. Terasaki, *Stud. Surf. Sci. Catal*. **2000**, *129*, 155.

59 (a) M. P. Kapoor, A. K. Sinha, S. Seelan, S. Inagaki, S. Tsubota, H. Yoshida, M. Haruta, *Chem. Commun*. **2002**, 2902. (b) E-B. Cho, K-W. Kwon, K. Char, *Chem. Mater*. **2001**, *13*, 3837.

60 T. Asefa, M. J. MacLachlan, H. Grondey, N. Coombs, G. A. Ozin, *Angew. Chem. Int. Ed*. **2000**, *39*, 1808.

61 R. A. Sheldon, M. Wallau, I. W. C. E. Arends, U. Schuchardt, *Acc. Chem. Res*. **1998**, *31*, 485.

62 (a) M. Janicke, D. Kumar, G. D. Stucky, B. F. Chmelka, *Stud. Surf. Sci. Catal*. **1994**, *84*, 243. (b) M. Hartmann, C. Bischof, *Stud. Surf. Sci. Catal*. **1998**, *117*, 249. (c) Z. Luan, H. He, C. F. Cheng, W. Zhou, J. Klinowski, *J. Phys. Chem. B* **1995**, *99*, 1018.

63 D. R. Rolison, *Science*, **2003**, *299*, 1698.

64 P. T. Tanev, M. Chibwe, T. J. Pinnavaia, *Nature* **1994**, *368*, 321.

65 D. Wei, W. T. Chueh, G. L. Haller, *Catal. Today* **1999**, *51*, 501.

66 (a) R. B. Borade, A. Clearfield, *Catal. Lett*. **1995**, *31*, 267. (b) Q. Kan, V. Fornes, F. Rey, A. Corma, *J. Mater. Chem*. **2000**, *10*, 993.

67 (a) T. Ishikawa, M. Matsuda, A. Yasukawa, *J. Chem. Soc., Faraday Trans*. **1996**, *92*, 1985. (b) A. Jentys, N. H. Pham, H. J. Vinek, *J. Chem. Soc., Faraday Trans*. **1996**, *92*, 3287.

68 (a) A. Corma, J. L. Jorda, M. T. Navarro, F. Rey, *Chem. Commun*. **1998**, 1899. (b) N. Igarashi, S. Kidani, R. Ahemaito, K. Hashimoto, T. Tatsumi, *Microporous Mesoporous Mater*. **2005**, *81*, 97.

69 A. Bhaumik, T. Tatsumi, *J. Catal*. **2000**, *189*, 31.

70 (a) A. Bhaumik, M. P. Kapoor, S. Inagaki, *Chem. Commun*. **2003**, 470. (b) M. P. Kapoor, A. K. Sinha, S. Seelan, S. Inagaki, S. Tsubota, H. Yoshida, M. Haruta, *Chem. Commun*. **2002**, 2902. (c) M. A. Wahab, C-S. Ha, *J. Mater. Chem*. **2005**, *15*, 508. (d) Q. Yang, Y. Li, L. Zhang, J. Yang, J. Liu, C. Li, *J. Phys. Chem. B* **2004**, *108*, 7934. (e) S. Shylesh, A. P. Singh, *Microporous and Mesoporous Mater*. (in press).

71 (a) Q. Yang, Y. Li, L. Zhang, J. Yang, J. Liu, C. Li, *J. Phys. Chem. B* **2004**, *108*, 7934. (b) Y. Xia, W. Wang, R. Mokaya, *J. Am. Chem. Soc*. **2005**, *127*, 790. (c) Q. Yang, J. Yang, Z. Feng, Y. Li, *J. Mater. Chem*. **2005**, *15*, 4268.

72 J. Patarin, *Angew. Chem. Int. Ed.* **2004**, *43*, 1.

73 (a) S. Hitz, R. Prins, *J. Catal*. **1997**, *168*, 194. (b) P. T. Tanev, T. J. Pinnavaia, *Chem. Mater*. **1996**, *8*, 2068.

74 H. Lee, S. I. Zones, M. E. Davis, *Nature* **2003**, *425*, 385.

75 (a) N. Husing, *Angew. Chem. Int. Ed*. **2004**, *43*, 3216. (b) C-H. Lee, T-S. Lin, C-Y. Mou, *J. Phys. Chem. B* **2003**, *107*, 2543. (c) C. D. Nunes, M. Pillinger, A. A. Valente. J. Rocha, A. D. Lopes, I. S. Goncalves, *Eur. J. Inorg. Chem*. **2003**, 3870. (d) L. L. Welbes, A. S. Borovik, *Acc. Chem. Res*. **2005**, *38*, 765.

76 (a) A. Taguchi, F. Schuth, *Microporous Mesoporous Mater*. **2004**, *77*, 1. (b) C. T. Fischel, R. J. Davis, J. M. Garcer, *J. Catal*. **1996**, *163*, 141. (c) R. Ryoo, C. H. Ko, J. M. Kim, R. Howe, *Catal. Lett*. **1996**, *37*, 29.

77 (a) J. Jamis, J. R. Anderson, R. S. Dickson, E. M. Campi, W. R. Jackson, *J. Organomet. Chem*. **2001**, *627*, 37. (b) K. Mukhopadhyay, B. R. Sarkar, R. V. Chaudhari, *J. Am. Chem. Soc*. **2002**, *124*, 9692. (c) C. Baleizao, B. Gigante, M. J. Sabatier, H. Garcia, A. Corma, *Appl. Catal. A. Gen*. **2002**, *288*, 279. (d) S. Xiang, Y. Zhang, Q. Xin, C. Li, *Angew. Chem. Int. Ed*. **2002**, *41*, 821. (e) A. Poppl, P. Baglioni, L. Kevan, *J. Phys. Chem.* **1995**, *99*, 14156. (f) W. Bohlmann, K. Schandert, A. Poppl, H. C. Semmelhack, *Zeolites* **1997**, *19*, 297.

78 D. J. Cole Hamilton, *Science* **2003**, *299*, 1702.

79 (a) W. F. Maier, J. A. Marten, S. Klein, J. Heilmann, R. Parton, K. Vercruysse, P. A. Jacobs, *Angew. Chem. Int. Ed*. **1996**, *35*, 180. (b) N. A. Herron, *Inorg. Chem*. **1986**, *25*, 4714.

80 C. A. McNamara, M. J. Dixon, M. Bradley, *Chem. Rev*. **2002**, *102*, 3275.

81 J. W. Niemantsverdriet, *Spectroscopic Methods in Heterogeneous Catalysis*, VCH, Weinheim, **1993**.

82 (a) S. Biz, M. Occelli, *Catal. Rev-Sci. Eng*. **1998**, *40*, 329. (b) G. Bergeret in: *Handbook of Heterogeneous Catalysis*, Vol. 2, Eds, G. Ertl, H. Knozinger, J. Weitkamp, Wiley-VCH, Weinheim, **1997**, pp. 464-475.

83 W. H. Bragg, W. L. Bragg, *The Crystalline State*, Vol. 1, McMillan, New York, **1949**.

84 S. Brunauer, P. H. Emmett, E. Teller, *J. Am. Chem. Soc*. **1938**, *60*, 309.

85 E. P. Barrett, L. G. Joyner, P. P. Halenda, *J. Am. Chem. Soc*. **1951**, *73*, 373.

86 J. I. Goldstein, H. Yakowitz (Eds.), *Practical Scanning Electron Microscopy*, Plenum Press, New York, **1975**.

87 G. Lawes, *Scanning Electron Microscopy and X-Ray Microanalysis*, John Wiley and Sons Ltd., Chichester, **1987**.

88 J. R. Fryer, *Chemical Applications of Transmission Electron Microscopy*, Academic Press, San Diego, **1979**.

89 J. M. Thomas, O. Terasaki, P. L. Gai, W. Zhou, J. Gonzalez-Calbet, *Acc. Chem. Res*. **2001**, *34*, 583.

90 R. P. Eischens, W. A. Pliskin, *Adv. Catal*. **1958**, *10*, 1.

91 (a) C. C. Freyhardt, M. Tsapatsis, Jr. Balkus, M. E. Balkus, M. E. Davis, *Nature* **1996**, *381*, 295. (b) P. A. Jacobs, W. Y. Martier, *Zeolites* **1982**, *2*, 226.

92 (a) B. Notari, *Stud. Surf. Sci. Catal*. **1987**, *37*, 413. (b) G. N. Vayssilov, *Catal. Rev*. **1997**, 209.

93 J. Ryczkowski, *Catal. Today* **2001**, *68*, 263.

94 P. L. Villa, F. Trifiro, I. Pasquon, *React. Kinet. Catal. Lett*. **1974**, *1*, 341.

95 (a) B. M. Weckhuysen, R. A. Schoonheydt, *Catal. Today* **1999**, *49*, 441. (b) R. A. Schoonheydt, *Diffuse Reflectance Spectroscopy in Characterization of Heterogeneous Catalysts*, F. Delannay (Ed.) Marcel Dekker, New York, **1984**.

96 (a) B. M. Weckhuysen, I. P. Vannijvel, R. A. Schoonheydt, *Zeolites* **1995**, *15*, 482. (b) X. T. Gao, I. E. Wachs, *J. Phys. Chem. B* **2000**, *104*, 1261. (c) X. T. Gao, I. E. Wachs, *J. Catal*. **1999**, *188*, 325.

97 (a) T. A. Carlson, *X-Ray Photoelectron Spectroscopy*, Dowden, Hutchinson & Ross: Stroudsburg, PA, **1978**. (b) D. Briggs, M. P. Seah (Eds.), *Practical Surface Analyses*, Vol. 1: *Auger and X-Ray Photoelectron Spectroscopy* (2nd Ed.), New York, **1990**.

98 (a) B. M. Weckhuysen, D. M. Keller, *Catal. Today* **2003**, *78*, 25. (b) B. M. Weckhuysen, I. E. Wachs, R. A. Schoonheydt, *Chem. Rev*. **1996**, *96*, 3327.

99 C-Y. Chen, H-X. Li, M. E. Davis, *Microporous Mater*. **1993**, *2*, 17.

100 R. A. Wind in A. I. Popov, K. Hallenga (Eds.), *Modern NMR Techniques and Their Applications in Chemistry*, Marcel Dekker Inc., New York, **1991,** pp. 156.

101 M. Mehring, *High Resolution NMR Spectroscopy in Solids*, Springer-Verlag, Berlin, **1976**.

102 (a) G. Engelhardt, D. Michel, *High-Resolution Solid-State NMR of Silicates and Zeolites*, John Wiley and Sons Ltd., Chichester, **1987**. (b) C. A. Fyfe, G. C. Gobbi, J. Klinowski, J. M. Thomas, S. Ramdas, *Nature* **1982**, *296*, 530.

103 G. Engelhardt in: *Handbook of Heterogeneous Catalysis*, Vol. 2, Eds: G. Ertl, H. Knozinger, J. Weitkamp, Wiley-VCH, Weinheim, **1997**, pp. 525-539.

104 (a) A. A. Shubin, O. B. Lapina, D. Courcot, *Catal. Today* **2000**, *56*, 379. (b) H. Eckert, I. E. Wachs, *J. Phys. Chem*. **1989**, *93*, 6796. (c) N. Das, H. Eckert, H. Hu, I. E. Wachs, J. F. Walzer, F. J. Feher, *J. Phys. Chem*. **1993**, *97*, 8240.

105 (a) J. C. Vedrine, *Electron Spin Resonance*, Chapter 5 in: *Characterization of Heterogeneous Catalysts*, F. Delannay (Ed.) Marcel Dekker, New York, **1984**. (b) M. Che, E. Giamello, *Electron Paramagnetic Resonance*, Chapter 5 in: *Spectroscopic Characterization of Heterogeneous Catalysts*, J. L. G. Fierro (Ed.), *Stud. Surf. Sci. Catal*. Vol. 57B, Elsevier, **1990**.

106 (a) W. M. Van Rhijn, D. E. De Vos, W. Bossaert, J. Bullen, B. Wouters, P. Grobet, P. A. Jacobs, *Stud. Surf. Sci. Catal*. **1998**, *117*, 183. (b) W. D. Bossaert, D. E. DeVos, W. M. Van Rhijn, J. Bullen, P. J. Grobet, P. A. Jacobs, *J. Catal*. **1999**, *182*, 156.

107 (a) D. J. Macquarrie, *Green Chem*. **1999**, 195. (b) A. Cauvel, G. Renard, D. Brunel, *J. Org. Chem*. **1997**, *62*, 749. (c) D. J. Macquarrie, D. B. Jackson, *Chem. Commun*. **1997**, 1781. (d) R. A. Sheldon, R. S. Downing, *Appl. Catal. A. Gen*. **1999**, *189*, 163.

108 (a) T. Maschmeyer, R. D. Oldroyd, G. Sankar, J. M. Thomas, I. J. Shannon, J. A. Klepetko, A. F. Masters, J. K. Beattie, C. R. A. Catlow, *Angew. Chem. Int. Ed.* **1997**, *36*, 1639. (b) C. J. Liu, S. G. Li, W. Q. Pang, C. M. Che, *Chem. Commun*. **1997**, 65.

109 (a) R. Anwander, C. P. Gerstberger, O. Groeger, G. Engelhardt, *Chem. Commun*. **1998**, 1811. (b) S-G. Shyu, S-W. Cheng, D-L. Tzou, *Chem. Commun*. **1999**, 2337.

110 (a) N. Bellocq, S. Abramson, M. Laspyras, D. Brunel, P. Moreau, *Tet. Assym*. **1999**, *10*, 3229. (b) S. J. Bae, S-W. Kim, T. Hyeon, B. M. Kim, *Chem. Commun*. **2000**, 31.

111 (a) X. Lin, G. K. Chuah, S. Janicke, *J. Mol. Catal. A. Chem*. **1999**, *150*, 287. (b) G. Gerstberger, C. Palm, R. Anwander, *Chem. Eur. J.* **1999**, *5*, 997.

112 T. Joseph, S. S. Deshpande, S. B. Halligudi, A. Vinu, S. Ernst, M. Hartman, *J. Mol. Catal. A. Chem*. **2003**, *206*, 13.

113 (a) N. A. Milas, S. Sussman, *J. Am. Chem. Soc*. **1936**, *58*, 1302. (b) N. A. Milas, S. Sussman, *J. Am. Chem. Soc*. **1937**, *59*, 2345. (c) N. A. Milas, *J. Am. Chem. Soc.* **1937**, *59*, 2342.

114 K. A. Jorgensen, *Chem. Rev*. **1989**, *89*, 431.

115 (a) R. A. Sheldon, J. Dakka, *Catal. Today* **1994**, *19*, 215. (b) H. E. B. Lempers, R. Garcia, R. A. Sheldon, *J. Org. Chem*. **1998**, *63*, 1408.

116 (a) H. Mimoun, M. Mignard, P. Brechot, L. Saussine, *J. Am. Chem. Soc*. **1986**, *108*, 3711. (b) H. Mimoun, *Catal. Today* **1987**, *1*, 281. (c) E. S. Gould, R. R. Hiatt, K. C. Irwin, *J. Am. Chem. Soc*. **1968**, *90*, 4573. (d) A. Waldemar, A. Corma, I. Reddy, M. Renz, *J. Org. Chem*. **1997**, *62*, 3631.

117 J. Muzart, *Chem. Rev*. **1992**, *92*, 113.

118 C-M. Che, *Pure Appl. Chem*. **1995**, *2*, 225.

119 (a) G. Bellussi, M. S. Rigutto, *Stud. Surf. Sci. Catal*. **1994**, *85*, 177. (b) W. M. Meier, D. H. Olson, Ch. Baerlocher, *Zeolites* **1996**, *17*, 1. (c) P. R. H. Prasad Rao, A. A. Belhekar, S. G. Hegde, A. V. Ramaswamy, P. Ratnasamy, *J. Catal*. **1993**, *141*, 595. (d) T. Selvam, A. P. Singh, *J. Chem. Soc., Chem. Commun*. **1995**, 883.

120 (a) V. Hulea, E. Dumitriu, *Appl. Catal. A. Gen*. **2004**, *277*, 99. (b) A. Corma, P. Esteve, A. Martinez, *J. Catal*. **1996**, *161*, 11. (c) K. A. Koyano, T. Tatsumi, *Microporous Mater*. **1997**, *10*, 259.

121 (a) J. M. R. Gallo, I. S. Paulino, U. Schuchardt, *Appl. Catal. A. Gen*. **2004**, *266*, 223. (b) W. Zhang, M. Froba, J. Wang, P. T. Tanev, J. Wong, T. J. Pinnavaia, *J. Am. Chem. Soc*. **1996**, *118*, 9164.

122 (a) K. M. Reddy, I. Moudrakovski, A. Sayari, *J. Chem. Soc., Chem. Commun*. **1994**, 1059. (b) V. Parvulescu, C. Anastasescu, B. L. Su, *J. Mol. Catal. A. Chem*. **2003**, *3919*, 1.

123 S. Shylesh, A. P. Singh, *J. Catal*. **2005**, *233*, 359.

124 (a) P. Selvam, S. E. Dapurkar, *Appl. Catal. A. Gen*. **2004**, *276*, 257. (b) S. Gomez, L. J. Garces, J. Villegas, R. Ghosh, O. Giraldo, S. L. Suib, *J. Catal*. **2005**, *233*, 60.

125 (a) J. S. Reddy, A. Sayari, *J. Chem. Soc., Chem. Commun*. **1995**, 2231. (b) J. S. Reddy, P. Liu, A. Sayari, *Appl. Catal. A. Gen*. **1996**, *148*, 7.

126 (a) N. Ulagappan, C. N. R. Rao, *Chem. Commun*. **1996**, 1047. (b) A. Sakthivel, P. Selvam, *J. Catal*. **2002**, *211*, 134. (c) A. Sakthivel, S. E. Dapurkar, P. Selvam, *Catal. Lett*. **2001**, *77*, 155.

127 (a) R. J. Mahalaingam, S. K. Badamali, P. Selvam, *Chem. Lett*. **1999**, 1121. (b) S. E. Dapurkar, A. Sakthivel, P. Selvam, *New J. Chem*. **2003**, *27*, 1184.

128 Y. Wang, Q. Zhang, T. Shishido, K. Takehira, *J. Catal*. **2002**, *209*, 186.

129 (a) V. Parvulescu, B. L. Su, *Catal. Today* **2001**, *69*, 315. (b) R. Neumann, A. M. Khenkin, *Chem. Commun*. **1996**, 2643. (c) Q. Tang, Q. Zhang, H. Wu, Y. Wang, *J. Catal.* **2005**, *230*, 393.

130 (a) K. Chaudhari, T. K. Das, P. R. Rajmohanan, L. Lazar, S. Sivasanker, A. J. Chandwadkar, *J. Catal*. **1999**, *183*, 281. (b) A. Corma, M. T. Navarro, L. Nemeth, M. Renz. *Chem. Commun*. **2001**, 2190.

131 M. L. W. Vorstenbosch, Ph.D Thesis, Schuit Institute of Catalysis, Eindhoven University of Technology, The Netherlands, **2002**.

132 S. Shylesh, A. P. Singh, *J. Catal*. **2004**, *228*, 333

133 S. C. Laha, R. Kumar, *J. Catal*. **2001**, *204*, 64.

134 (a) M. Ogawa, N. Yamamoto, *J. Porous Mater*. **1999**, *6*, 19. (b) R. Ryoo, I-S. Park, S. Jun, C. W. Lee, M. Kruk, M. Jaroniec, *J. Am. Chem. Soc*. **2001**, *123*, 1650. (c) M. J. Kim, R. Ryoo, *Chem. Mater*. **1999**, *11*, 487.

135 (a) M. Eswaramoorthy, S. Neeraj, C. N. R. Rao, *Microporous Mesoporous Mater*. **1999**, *28*, 205. (b) J. Aguado, D. P. Serrano, J. M. Escola, *Microporous Mesoporous Mater*. **2000**, *34*, 43.

2.1. INTRODUCTION

Mesoporous silica materials like MCM-41, MCM-48, SBA-15 had received considerable research interests in shape selective heterogeneous catalysis and as host for various kinds of molecules due to their large surface area, uniform pore size and high density internal surface silanols.[1-4] Major advances in understanding and exploiting the synthesis protocols and mechanism of formation of mesoporous materials have allowed designed tailoring of composition, pore size, structure, texture and active site location and density through functionalization. However, a major drawback of mesoporous materials lies in their inherent inert nature towards various organic transformations and hence ample surface modifications are necessary to make them well suitable in the field of catalysis. Among the various surface modifications, the incorporation of transition metals by the direct hydrothermal method as well as by the post synthesis methods are employed as novel techniques to introduce active metal sites in mesoporous materials.[5]

The incorporation of transition metals within the silica framework has been considered as a way of increasing the acidity, ion exchange capacity and catalytic activity of mesoporous silica molecular sieves. However, the methods incorporating metal precursors into the surfactant-silicate gel require specialized synthesis conditions, depending on the respective structures of the materials being synthesized, incorporating metal and the silica sources. In 1994, Reddy *et al.*[6] had first successfully synthesized vanadium-substituted MCM-41 while a detailed characterization of these materials were carried out independently by Tuel *et al.*[7] and Luan *et al.*[8] and they concluded from their studies that: (i) vanadium centers in the as-synthesized and calcined forms of V-MCM-41 had the same coordination state and no direct chemical bonding was formed with the silicate frame work and (ii) vanadium occurs simultaneously in two forms on the support surfaces *viz.,* as framework and extra framework species. However, the framework substituted catalysts suffer three major disadvantages: (i) low metal content, (ii) decaying catalytic activities; where metal is easily leached from the framework during the catalytic reaction and (iii) poor control of the molecular environment of the catalytic site. In this context, considerable efforts have been made to improve the stability of vanadium-containing mesoporous materials under severe reaction reactions. Actually, the solid wall surfaces of MCM-41 type mesoporous materials are too delicate to withstand severe reaction conditions and hence a rapid disorder in mesoporosity is observed after the drastic reaction conditions.[9,10] This usually enhances the leaching of framework substituted metal species to the reaction mixture and thereby limits its further usability. Hence there exists ample opportunity to exploit the surface properties of the mesoporous materials to improve the structural stability and there by the reusability of metal-containing mesoporous materials.

This chapter describes in detail the synthesis, characterization and catalytic applications of vanadium-containing periodic mesoporous silica materials in the oxidation reaction of naphthalene and cyclohexane and in the epoxidation reaction of cyclooctene. The chapter is divided into three sections, the first section describes a comparison in catalytic properties between vanadium -substituted, -grafted and -immobilized mesoporous MCM-41 samples, second section describes the influence of different silica sources in the properties of V-MCM-41 samples and the third section describes the heterogenization of vanadium over aminopropyl modified SBA-15, MCM-41 and an amorphous silica gel sample.

2.2. EXPERIMENTAL

2.2.1. Materials

For the synthesis of Si-SBA-15, Si-MCM-41, organo-modified mesoporous materials and vanadium-containing mesoporous materials, the following reagents were used: tetraethyl orthosilicate (TEOS, 98%, Aldrich), fumed silica (SiO_2, 99.8%, Aldrich), silica gel (S_{BET} = 444 m^2g^{-1}, Loba Chemie), cetyl trimethyl ammonium bromide (C_{16}-TAB, Aldrich), 3-aminopropyltriethoxysilane (3-APTS, Lancanster), vanadyl sulphate ($VOSO_4$. $3H_2O$, Aldrich) and vanadyl acetylacetonate ($VO(acac)_2$, Aldrich). All chemicals were used as received without further purification.

2.2.2. Synthesis of Siliceous Mesoporous MCM-41 and SBA-15 (Si-MCM-41 & Si-SBA-15)

The synthesis of pure siliceous mesoporous MCM-41 and SBA-15 was carried out using an initial molar gel composition of SiO_2-0.39Na_2O-0.48C_{16}-TAB-0.29H_2SO_4-100H_2O and SiO_2-0.023P123-7.8HCl-260$H_2$0, respectively.

In a typical synthesis of MCM-41, 3 g of fumed silica was added to a solution of 1.6 g of NaOH in 40 mL water and stirred for 30 min. To this mixture, a solution of 8.7 g of C_{16}-TAB in 40 mL water was added drop wise. After stirring for another 30 min, 1.4 g of H_2SO_4 was added to the gel mixture so that the pH of the gel mixture is adjusted to approximately 10.5. Finally, 30 mL of water was added to the synthesis gel, stirred for 2 h and autoclaved at 100 ^{o}C for 72 h. The solid product obtained after hydrothermal synthesis was filtered, washed with distilled water, acetone and air-dried. The material was then calcined in air at 540 ^{o}C for 6 h.

In a typical synthesis of SBA-15, 2 g of P123 surfactant was stirred with 20 mL of deionized water at 35 ^{o}C. The mixture was stirred until the surfactant gets dissolved, followed by the addition of 30 g of 2 M HCl solution. The stirring was allowed to run for another 30 min and 4.5 g of TEOS was added drop wise to the stirred solution mixture. The mixture was then stirred for another 24 h and autoclaved at 100 ^{o}C for 48 h. The solid material obtained after hydrothermal synthesis was filtered, washed with distilled water, acetone and air-dried. The material was then calcined in air at 540 ^{o}C for 6 h.

2.2.3. Synthesis of Vanadium-substituted Mesoporous MCM-41 (V-MCM-41)

Vanadium-containing mesoporous MCM-41 materials were synthesized by a one-pot synthesis method using fumed silica and tetra ethyl orthosilicate as silica sources. The gel composition of the mixture is,

$$SiO_2\text{-}xVO_2\text{-}0.17Na_2O\text{-}0.5C_{16}\text{-TAB-}100H_2O$$

where, x varies from 0.025-0.012. In a typical synthesis, 3 g TEOS was added to a solution of 0.2 g of NaOH in 25 mL distilled water and stirred for 1 h. To this mixture, a solution of 2.6 g C_{16}-TAB and 0.04 g vanadyl sulfate was added slowly with vigorous stirring. The mixture was stirred at room temperature for another 5 h and then autoclaved at 100 °C for 4 days. For comparison purposes, respective silica polymorphs are also prepared by the same method but with out the addition of vanadyl sulfate. The solid material obtained after the hydrothermal treatment was then filtered, washed well with distilled water and acetone and then dried at 80 °C for 3 h. The surfactant occluded inside the pores of the mesoporous material was removed by calcination at 540 °C for 6 h.

The vanadium-containing solid samples obtained from fumed silica sources are denoted as VMS while the samples obtained from TEOS silica source are denoted as VMT and the input Si/V gel ratios were denoted in parenthesis. The MCM-41 silica polymorph obtained from fumed silica and tetraethyl orthosilicate silica sources were named as SMS and SMT, respectively.

2.2.4. Synthesis of Vanadium-grafted Mesoporous MCM-41 (V/MCM-41)

The grafting of vanadyl acetylacetonate on MCM-41 support was carried out by adding 1 g of the calcined MCM-41 sample to a solution of 0.15 g of $VO(acac)_2$ salt in 50 mL ethanol, so as to obtain a vanadium loading of ~1 wt%. After addition, the solution was stirred at room temperature for 2 h and at 70 °C for 5 h, and finally the mixture was dried by removing the solvent using a rotary evaporator. The as-synthesized material was calcined in air at 540 °C for 6 h.

2.2.5. Functionalization of 3-APTS over SBA-15, MCM-41 and Silica gel by Post Synthesis Grafting (NH_2-SBA-15/NH_2-MCM-41/ NH_2-SG)

Prior to functionalization, the support silica materials were dehydrated at 150 °C for 3 h to remove the physisorbed water molecules. Post synthesis modification was done by refluxing 1 g of the silica sample with 2.2 mmol of 3-APTS in 50 mL of toluene, under nitrogen atmosphere. The mixture was then allowed to run for 6 h at 100 °C. Finally, the material was filtered, washed with toluene, and then soxhlet extracted using a mixture of diethyl ether (100 mL) and dichloromethane (100 mL) for 24 h and vacuum dried.

In order to probe the role of solvents during grafting, the grafting procedures were also repeated with other solvents such as dichloromethane, acetone and chloroform.

2.2.6. Immobilization of $(VO)^{2+}$ cations over amino propyl-terminated Mesoporous Silica and Silica gel (VO-NH_2-SBA-15/ VO-NH_2-MCM-41/ VO-NH_2-SG)

Vanadyl cations were immobilized over aminopropyl modified silica materials by treating NH_2-SBA-15/NH_2-MCM-41/NH_2-SG samples with an alcoholic solution of vanadyl sulphate. Typically, 1 g of organo amine functionalized silica was stirred with a 0.01 M ethanolic solution of vanadyl sulfate for 6 h at 60 ^oC, under nitrogen atmospheres. The process was repeated twice for a maximum coordination of vanadyl groups on the amine functionalized silica samples. Finally, the pale green colored mixture was filtered, washed with ethanol and acetone and vacuum dried. The material was then soxhlet extracted with ethanol (100 mL) for 12 h to remove the unanchored vanadium species.

For comparison, the same procedure was repeated on non-modified (without amino propyl groups) SBA-15, MCM-41 and Silica gel samples, to evaluate the role of amino groups in the anchoring of vanadium species.

2.2.7. Instruments for Characterization

Powder X-ray diffraction (XRD) patterns of MCM-41 samples were recorded on a Rigaku D MAX III VC Ni-filtered Cu K_α radiation, λ=1.5404 Å, between 1.5 to 10° (2θ) with a scanning rate of 1^o/min and a step size of 0.02^o. X-ray diffraction patterns of SBA-15 samples were collected on a Siemens D5005 diffractometer using Cu K_α (λ = 1.5404 Å) radiation. The diffractograms were recorded in the 2θ range of 0.5 to 5^o with a step size of 0.01^o and a step time of 10 s.

The specific surface area, total pore volume and average pore diameter were measured by N_2 adsorption-desorption method using NOVA 1200 (Quanta chrome) instrument. The samples were activated at 200 ^oC for 6 h under vacuum and then the adsorption-desorption was conducted by passing nitrogen over the sample, which was kept under liquid nitrogen. Pore size distribution (PSD) was obtained by applying the Barrett-Joyner-Halenda (BJH) pore analysis applied to the desorption branch of nitrogen adsorption-desorption isotherms.

Transmission electron micrographs (TEM) were obtained on a JEOL JEM 1200 EX instrument at an acceleration voltage of 120 kV. Samples for TEM analysis were prepared by sonicating the powdered samples for 30 min in isopropanol, followed by depositing two drops on a holey carbon film supported by a copper grid.

Fourier transform infra red (FT-IR) spectra of the solid samples were taken in the range of 4000 to 400 cm^{-1} on a Shimadzu FTIR 8201 instrument. Prior to analysis, the samples were flushed in nitrogen atmosphere at 100 ^{o}C for 3 h and the spectra were accquired at 4 cm^{-1} resolution and averaged over 48 scans. Raman measurements were done on a Jobin Yron TRIAX 550 triple grating spectrometer equipped with cryogenic charge-coupled device camera and diode pumped frequency-doubled solid state Nd:YAG laser of 532 nm (Model DPSS 532-400, Coherent Inc., USA).

Diffuse reflectance UV-Vis spectra (DR UV-Vis) of the solid samples were recorded in the range 200-800 nm in a Shimadzu UV-2101 PC spectrometer equipped with a diffuse reflectance attachment, using $BaSO_4$ as the reference. Specifically for the hydrated samples, the catalysts were kept under ambient conditions for 2 h while for the dehydrated samples, the catalysts were treated in dry air atmosphere at 550 ^{o}C for 5 h and flushed with an inert atmosphere, repeatedly, before taking the spectra. The absorption edge energy values were determined from the energy intercept of a linear fit passing through the near-edge region in a plot of $[F(R\alpha)hv]^{1/2}$ versus hv, where the first parameter refers to the Kubelka–Munk (KM) function and hv is the energy of incident photon. Electron paramagnetic resonance (EPR) spectra of the solid samples were recorded at room temperature conditions operating at X-band frequency on a Bruker EMX spectrometer.

Thermal analysis (TG-DTA) of the mesoporous samples was performed using a Pyris Diamond TGA analyzer under air atmosphere (80 mL/min) from ambient to 1000 °C at a heating rate of 10 °C/min. Temperature programmed reduction (TPR) was carried out on a Micromeritics Autochem 2910 catalyst characterization system, equipped with a TCD detector. Fresh, dried samples were pretreated by passing high purity (99.9%) argon (20 mL/min) at 500 ^{o}C for 3 h. After cooling to ambient temperature, the argon atmosphere is replaced by 5% H_2/Ar mixture. The samples were heated in this atmosphere to 800 ^{o}C at a heating rate of 10 ^{o}C/min and ~ 100 mg of calcined sample was used for all the experiments. The water produced during the reduction was condensed in a cold trap immersed in a slurry of isopropanol and liquid nitrogen.

Solid-state ^{13}C CP MAS NMR and ^{29}Si MAS NMR spectra were recorded on a Bruker MSL 300 NMR spectrometer with a resonance frequency of 75.5 MHz and 59.6 MHz for ^{13}C and ^{29}Si using 4 mm zirconia rotors and a sample spinning frequency of 3 kHz. ^{13}C spectra were collected with 70^{o} rf pulses and 5 s delay while ^{29}Si spectra were collected with 70^{o} rf pulses and 30 s delay, with ~6000 scans. The chemical shifts were referenced to glycine and TMS, respectively, for ^{13}C and ^{29}Si. ^{51}V MAS NMR was recorded under a magnetic field of 7.05 T, on a DSX 300 spectrometer. The samples were spun using 4 mm diameter zirconia rotors at 7 kHz and the spectra were obtained with a pulse length of 3 μs and recycle delay of 500 ms. Chemical shifts were referenced against liquid $VOCl_3$ by using ammonium metavanadate as a secondary reference.

2.3. COMPARISON IN CATALYTIC PROPERTIES BETWEEN VANADIUM -SUBSTITUTED (V-MCM-41), -GRAFTED (V/MCM-41) AND -IMMOBILIZED (VO-NH_2-MCM-41) CATALYSTS

Vanadium-containing mesoporous materials prepared by the direct hydrothermal methods (V-MCM-41, V-MCM-48, V-HMS, *etc*) and by the post synthesis grafting methods over different mesoporous supports were active catalysts in a number of liquid phase oxidation reactions using H_2O_2 as an oxidant.[5-9] However, drawbacks of these framework substituted materials lies in their low metal content, lower activity- as a great part of the active sites are well buried inside the pore channels, and the gradual decrease in catalytic activity after each cycle. On the contrary, grafting of vanadium precursors over solid mesoporous supports help to achieve a high percentage of metal loading and also help to disperse the active metal sites by suitably tuning the preparation procedures. However, it is difficult to control the dispersity of the grafted metal species, so tiny metal oxide species can form preferentially even at relatively low metal loading and the inherent leaching problem always confuses on the heterogeneity of the grafted catalysts. Hence, several attempts have been made to heterogenize transition metal catalyst over organic-inorganic hybrid mesoporous materials having reactive functional sites to extend the benefits of the homogeneous catalyst to heterogeneous systems *viz*., easier separation of catalyst and reusability of the supported catalysts.[11,12] Thus, the heterogenization of vanadium catalysts over organic-inorganic hybrid mesoporous solids, is anticipated to show better activity and better stability due to the improved hydrophobicity imparted to the support surface because of the presence of organic groups.

This section describes the surface properties and catalytic activity differences of vanadium-containing mesoporous samples prepared by the direct hydrothermal method, post synthesis grafting method and immobilization method over an amino propyl modified mesoporous MCM-41 sample, in the oxidation reaction of naphthalene.

2.3.1. CHARACTERIZATION

2.3.1.1. Powder X-Ray Diffraction

The uniqueness of mesoporous structure, phase purity, degree of orderedness and unit cell parameters of MCM-41 and vanadium-modified MCM-41 samples were determined from powder X-ray diffraction. Figure 2.1 shows the XRD patterns of V-MCM-41, V/MCM-41 and VO-NH_2-MCM-41 samples, which shows important differences in the long-range ordering and characteristic diffraction patterns of mesoporous materials prepared by the different methods. The well-defined XRD patterns of Si-MCM-41 and V-MCM-41 can be indexed to the (100), (110), (200) and (210) Bragg reflections, characteristic of materials with hexagonal (*p6mm*) mesophases with long range ordering. Further, a slight shift of the characteristic (100) peak to lower angle with a corresponding linear increase in the *d* spacing and unit cell values is noted for V-MCM-41 sample than the corresponding silica polymorph (Table 2.1). The increase in the hexagonal unit cell parameter compared with its silica polymorph is taken as an indication for the incorporation of vanadium, as the V-O bond distance (1.8 Å) is longer than the Si-O bond distance (1.6 Å). [6]

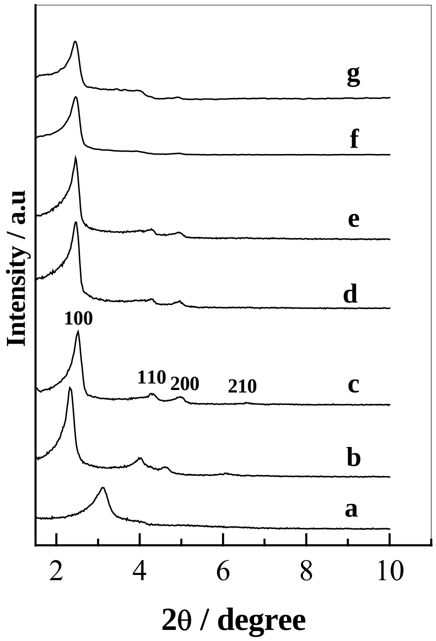

Figure 2.1. X-ray diffraction patterns of vanadium-containing mesoporous materials: (a) MCM-41 silica polymorph, (b) V-MCM-41 (55), (c) Si-MCM-41, (d) V/MCM-41 (*as syn.*), (e) V/MCM-41 (*cal.*), (f) NH_2-MCM-41 and (g) VO-NH_2-MCM-41.

Compared to Si-MCM-41 and V-MCM-41, the V/MCM-41 and VO-NH_2-MCM-41 samples show an intensity decrease for the characteristic (100) peak with a loss in long range ordered peaks. These results relates to a partial structural collapse of the mesoporous material, after post synthesis modifications, and such change are more pronounced for the vanadium-immobilized samples than the V/MCM-41 samples. These structural changes arise from the inherent poor hydrothermal stability of M41S materials and thus the high-temperature reflux treatments may dissociate some of the pore walls and thereby decrease the long-range structural ordering.[13] The well-ordered mesoporous structure obtained for the vanadium-incorporated V-MCM-41 sample may be due to the simultaneous condensation between metal and silicon species in presence of the organic micelles, thereby influencing the unit cell parameters, wall thickness and the long-range ordering. However, for the post synthesis modified catalyst systems, since the metal species are mainly on the surface the aforementioned interactions are limited and hence leads to peak broadening with the loss of long-range ordered peaks.[14] These results are better explained from Fig. 2.1 a&b, where the V-MCM-41 material shows an intense XRD reflection with more ordered hexagonal structures than the parent silica polymorph prepared under the same conditions, but without vanadium. Hence, the better structural ordering of the V-MCM-41 sample explains the increased surfactant-silicate interaction in the presence of metal salts as they compete to enter the silica framework and thus may act like a promoter for the condensation of the silicate species and thereby for its reorganization.[15]

2.3.1.2. Transmission Electron Microscopy

Transmission electron microscopy (TEM) is generally used as an indispensable tool for the characterization of mesoporous supports. Figure 2.2 shows the TEM images of V-MCM-41, V/MCM-41 and VO-NH_2-MCM-41 samples. TEM of V-MCM-41 sample shows hexagonally arranged pore channels, when viewed along the pore direction, and the presence of parallel lattice fringes, on a side view analysis. The presence of equidistant parallel fringes shows the nature of separation between the layers and the well-packed unique arrangement further points to the addition of such monolayers. These kinds of results are valuable as they support the assumption that the deposition of 2-3 monolayers of silicate precursor on the isolated surfactant micellar rod and their subsequent further condensation results in the formation of long range ordered mesoporous materials.[1] A comparison of the TEM images between vanadium incorporated and post synthesis modified MCM-41 samples shows that the latter methods had damaged the regular structural ordering of the mesoporous materials (Fig. 2.2 c&d).

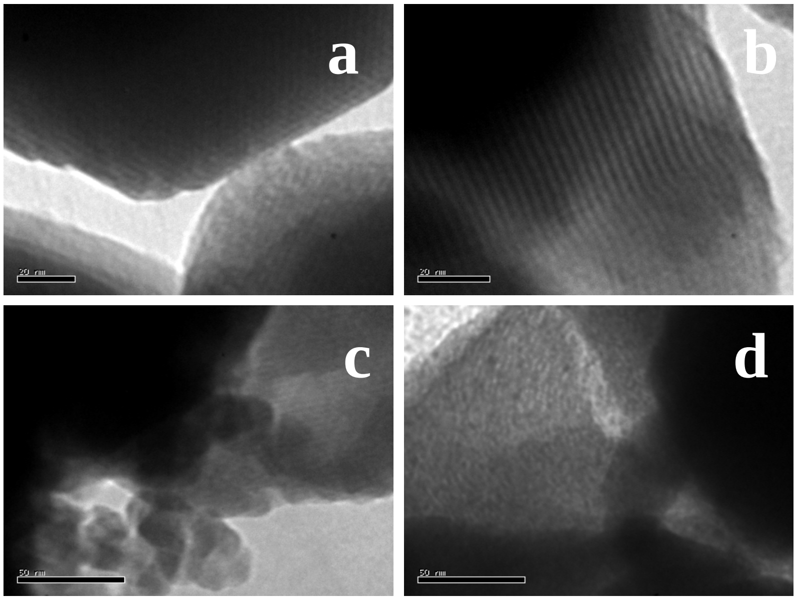

Figure 2.2. TEM images of: (a) V-MCM-41 (*viewed along the pore direction*), (b) V-MCM-41 (*parallel fringes, side on view*), (c) VO-NH$_2$-MCM-41 and (d) V/MCM-41.

2.3.1.3. N$_2$ Adsorption and Desorption

The textual properties of vanadium-containing mesoporous materials were determined from N$_2$ adsorption-desorption isotherms. The surface area of the samples determined by the BET method shows that, compared to the silica polymorph, the surface area is higher for the V-MCM-41 sample while for V/MCM-41 and VO–NH$_2$-MCM-41 catalysts the surface area is decreased. The MCM-41 silica polymorph shows a surface area of 711 m^{2}g^{-1} and an increase of 198 m^{2}g^{-1} is observed for the V-MCM-41 catalyst. However, the V/MCM-41 and the vanadium immobilized VO–NH$_2$-MCM-41 material shows ~28% and ~59% surface area decrease compared to Si-MCM-41. The decrease in surface area for the post synthesis modified catalysts is due to the presence of the bulkier organic moieties inside the pore channels. After calcination, the surface area of the post synthesis modified materials had shown an increase from their as-synthesized counterparts and restored to almost 90% of the original value and may be due to the removal of the bulky acetyl acetonate and organic amino propyl groups and the BET results are summarized in Table 2.1.

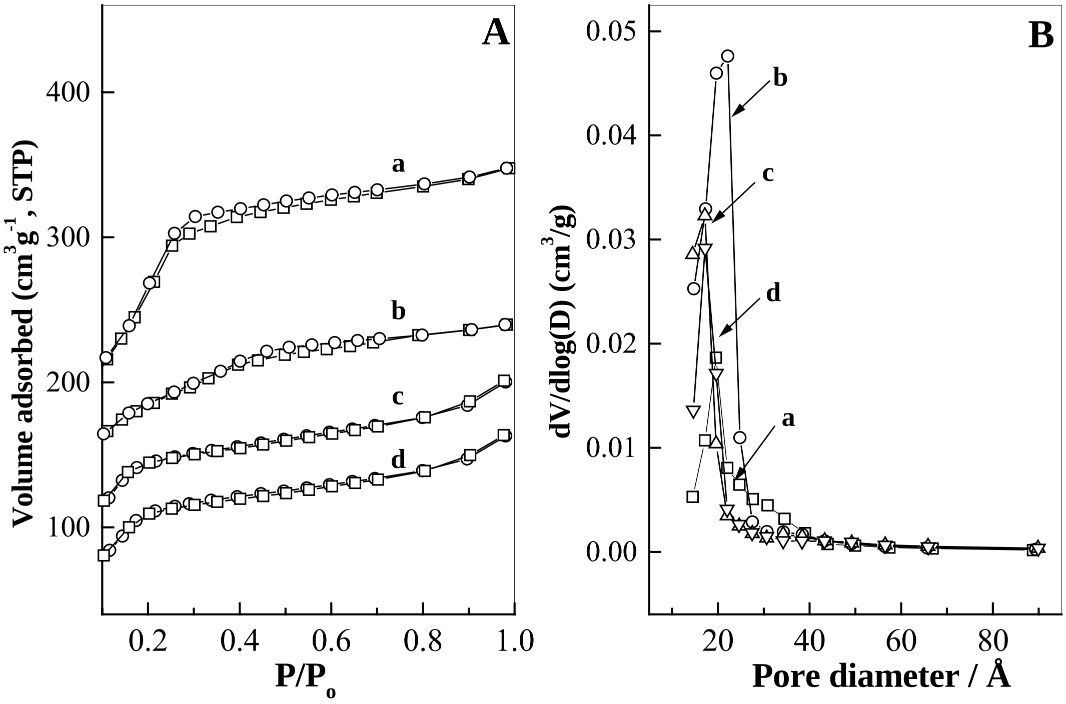

Figure 2.3. (A) Nitrogen adsorption-desorption and (B) Pore size distribution curves of: (a) V/MCM-41, (b) V-MCM-41 (55), (c) NH_2-MCM-41 and (d) VO-NH_2-MCM-41.

N_2 physisorption analysis of the vanadium-containing samples were carried out to probe the structural ordering, since if the material had a regular pore structure it will show a steep increase in adsorption isotherms due to the capillary condensation at specific N_2 partial pressures.[16] N_2 adsorption-desorption isotherms of all samples show a sharp capillary condensation step at P/P_o = 0.2-0.3, with completely reversible isotherms characteristic for ordered mesoporous materials of Type IV, according to the IUPAC classification (Fig. 2.3A). The pore size distributions (PSD) of the mesoporous samples were determined from the BJH method. It was observed that the pore size distribution of the V-MCM-41 sample is quite narrow than the V/MCM-41 and VO-NH_2-MCM-41 samples, indicating uniformity in the pore structures for the V-MCM-41 sample (Fig. 2.3B) and are in accordance with the XRD and TEM results.

Table 2.1. Properties of Vanadium-containing MCM-41 catalysts

Catalyst	V (%) [a]	a_o (Å) [b]	Surface Area (m^2g^{-1})	Pore Volume (ccg^{-1})	TPR [c]	
					$T_{max.}$ (°C)	AOS
Si-MCM-41	-	40.4	845	0.68	-	-
V/MCM-41 (*cal.*)	0.196	41.4	797	0.64	504	3.3
VO-NH_2-MCM-41 (*as syn*)	0.281	41.1	342	0.58	-	-
VO-NH_2-MCM-41 (*cal.*)	0.262	40.6	782	Nd	501	3.4
V-MCM-41 (55)	0.192	39.3	909	0.53	412	4.5
MCM-41 Silica polymorph [d]	-	36.5	711	0.37	-	-

[a] Determined by ICP-OES analysis.

[b] Unit cell parameter calculated using, $a_o = 2d_{100}/\sqrt{3}$.

[c] Temperature of maximum hydrogen consumption (T_{max}) and the average oxidation state (AOS) after reduction.

[d] Mesoporous support synthesized hydrothermally without the addition of vanadyl sulfate.

2.3.1.4. Thermal Analyses

In order to evaluate the thermal stability of V-MCM-41, V/MCM-41 and VO-NH_2-MCM-41 samples, TG-DTG/DTA analysis of as-synthesized samples was conducted in air from room temperature to 1000 °C (Fig. 2.4).

The TGA curves of as-synthesized V-MCM-41 and its corresponding silica polymorph shows three steps of weight loss. The weight loss below 100 °C is due to the loss of physisorbed water molecules (first step), the weight loss in the range 200-280 °C is attributed for the combustion of the hexagonally packed surfactants (second step) and the weight loss in the range 530-570 °C arises due to the water loss formed by the condensation of the silanol groups (third step).[17] The decomposition of surfactants is supported by the sharp exothermic peak at 300 °C from the DTA plots. However, the percentage weight loss of the surfactants is larger for V-MCM-41 catalyst (>43%) than the corresponding MCM-41 silica polymorph (>35%). This result suggest that the interaction between the surfactant and silicate species is more in presence of metal salts, in the present hydrothermal synthesis, and hence induces a better arrangement of the hexagonal structure. The TGA plot of V/MCM-41 catalyst also shows a weight loss at 100 °C, due to the loss of physisorbed water molecules. This step was followed by two sharp weight losses at 240 °C and 310 °C, attributed to the decomposition of the acetyl acetonate groups of the anchored vanadyl acetylacetonate complexes (Fig. 2.4c). This result shows that the decomposition of acetyl acetonate groups occurs in a stepwise manner rather than as a concerted reaction.

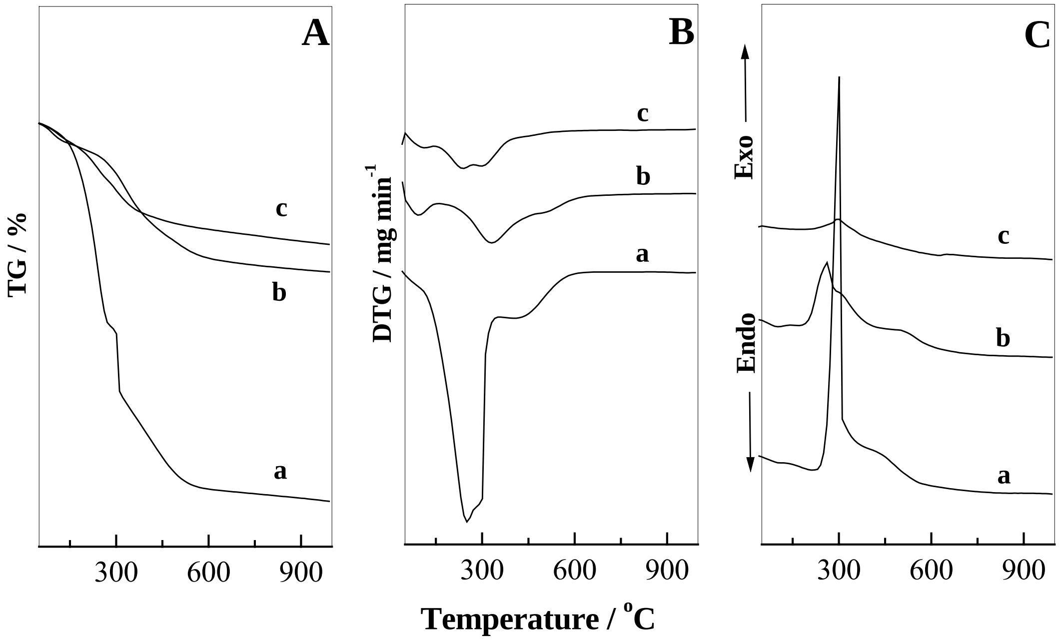

Figure. 2.4. (A) TG, (B) DTG and (C) DTA plots of: (a) V-MCM-41 (55), (b) VO-NH$_2$-MCM-41 and (c) V/MCM-41.

On the contrary, the TGA curves of VO-NH_2-MCM-41 catalyst show a weight loss below 100 °C, a sharp, distinct weight loss at 300-340 °C and after 500 °C (Fig. 2.4b). As mentioned, the first weight loss arises from the desorption of physisorbed water while the second peak develops from the burning of the amino propyl groups from the pores of the support and the third peak is mainly due to water loss formed by the condensation of silanol groups.[18,19] The DTA patterns further supports the above results as it shows a strong exothermic peak around 310 °C, and thus attributed these loss to the decomposition of the 3-APTS groups.

2.3.1.5. FT-IR Spectra

Presence of isolated surface silanols, hydrogen bonded hydroxyl groups and amorphous structure of the wall is evidenced from the IR spectrum of the calcined Si-MCM-41 sample (Table 2.2).

Table 2.2. IR band assignments and corresponding wave numbers obtained for Si-MCM-41 and Vanadium-containing MCM-41 catalysts

Catalyst	ν_{OH} (Si-OH)	ν_{as} (Si-O-Si)	ν (Si-OH) / ν_{as} (Si-O-V)	ν_s (Si-O-Si)
Si-MCM-41	3749	1080, 1230	972	801
V-MCM-41	3653	1078, 1224	976	805
V/MCM-41	3657	1078, 1228	974	804
VO-NH_2-MCM-41	3710	1091, 1235	965	807

Figure 2.5 shows the FT-IR spectra of V-MCM-41 and post synthesis modified vanadium samples. FT-IR spectra of V-MCM-41 and its corresponding silica polymorph is shown in Figure 2.5A. The band observed at 800 cm^{-1} is due to the symmetric stretching vibrations of the Si-O groups, and the sharp band observed at 1080 cm^{-1} is assigned to the asymmetric stretching of the Si-O vibrations, and its increased intensity correlates to a higher concentration of the siloxane groups. Furthermore, a strong band is observed in the mid-infrared region at 960 cm^{-1}, and are attributed to the incorporation of

various heteroatoms at the framework positions of porous metallo-silicates.[20] Since MCM-41 has properties between those of amorphous materials and zeolites, literature reveals with unambigituy for its assignment and are generally attributed for the presence of Si-O-V bands and/or to the perturbations in the rocking-mode vibrations of Si-OH moieties due to adjacent metal ions. Moreover, the shifting of 960 and 1080 cm^{-1} peaks to lower and higher frequencies, respectively, after metal substitution is an indication for the presence of metal in the framework of the mesoporous materials.[17,20]

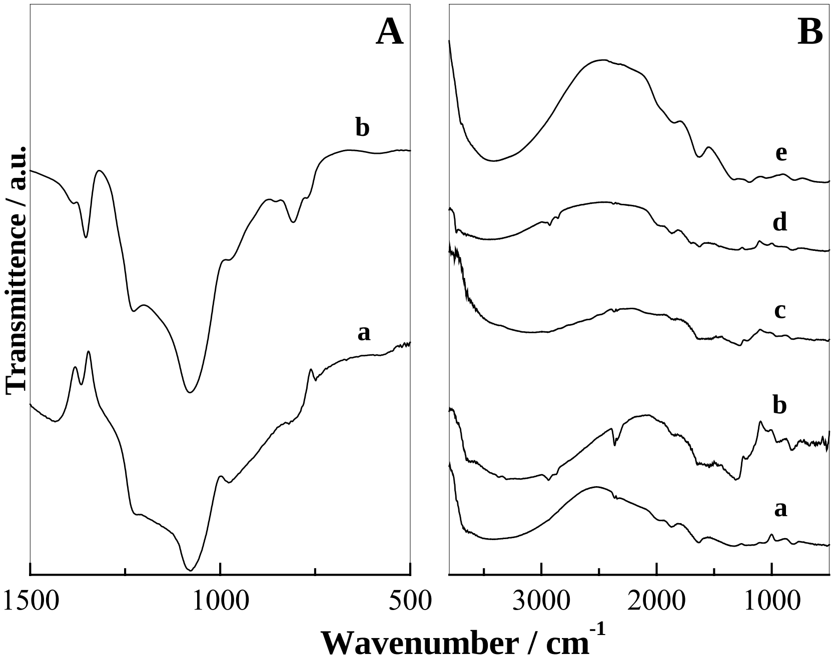

Figure 2.5. Infra red spectra of: (A) (a) MCM-41 silica polymorph, (b) V-MCM-41 (55) and (B) (a) Si-MCM-41, (b) NH_2-MCM-41, (c) VO-NH_2-MCM-41, (d) V/MCM-41 (*as syn.*) and (e) V/MCM-41 (*cal.*).

In the hydroxyl region (3600-3200 cm^{-1}) the broad band observed is assigned to the silanol groups inside the channels of Si-MCM-41 and the decreased intensity of the silanol groups after post synthesis modifications shows the active participation of these surface silanols (Fig. 2.5B). The grafting of VO(acac)$_2$ groups is confirmed by the presence of bands in the region of 1600-1200 cm^{-1} and at 2950-2850 cm^{-1}, as these vibrations are attributed to the presence of acetylacetonate ligands of the adsorbed complex.[21] For the NH_2-MCM-41 material, weak bands at 2960 cm^{-1} and 2850 cm^{-1} are observed for the C-H stretching vibrations while the N-H vibrations are observed at 3360, 3290 and 1520 cm^{-1}, respectively.[11] A closer examination of the amine peaks after vanadium immobilization shows that the peaks get shifted to lower wave numbers and the decrease in wave number indicates the possible anchoring of the vanadium species on the active sites. These results prove that the organo siloxane groups of 3-APTS had linked to the silica surfaces by the condensation reaction, for the formation of Si-O-Si bonds, and not through electrostatic interactions or by hydrogen bonding interactions between the amine groups and the Si-OH groups. After calcination, all bands belongs to the organic groups disappeared which proves the removal of organic groups from the pore channels of the mesoporous support.

2.3.1.6. UV-Vis Experiments

UV-Vis spectroscopy is a useful and reliable technique to obtain information about the coordination of vanadium in various molecular sieves and in particular to detect the presence of framework and extra framework metal species.[7] The UV-Vis spectra of the vanadium-containing mesoporous samples are shown in Figure 2.6. The band observed at 220 nm is typical for siliceous materials but new bands are appeared in the 250-500 nm range after vanadium introduction and their peak positions varied with respect to the method of synthesis of mesoporous vanadium samples.

Direct information about the oxidation state and coordination of vanadium species can be interpreted from the color of the materials prepared. The color of the dehydrated calcined vanadium catalysts is white and on hydration (contact with atmosphere) the color abruptly changes to yellowish. The change in color is due to the modification in the coordination environment of the vanadium species (V^{5+}) from the isolated tetrahedral coordination (T_d, 260 nm) to its distorted octahedral coordination ($O_{h,}$, 340-400 nm) by contacting with two water molecules in the atmosphere, due to the hydrophilic nature of the MCM-41 samples.[22] Compared to V-MCM-41 sample, the abrupt color transition of post synthesis modified vanadium samples indicates that a greater percentage of vanadium atoms are on the wall channels, hence the water molecules can easily access the site for higher coordination.

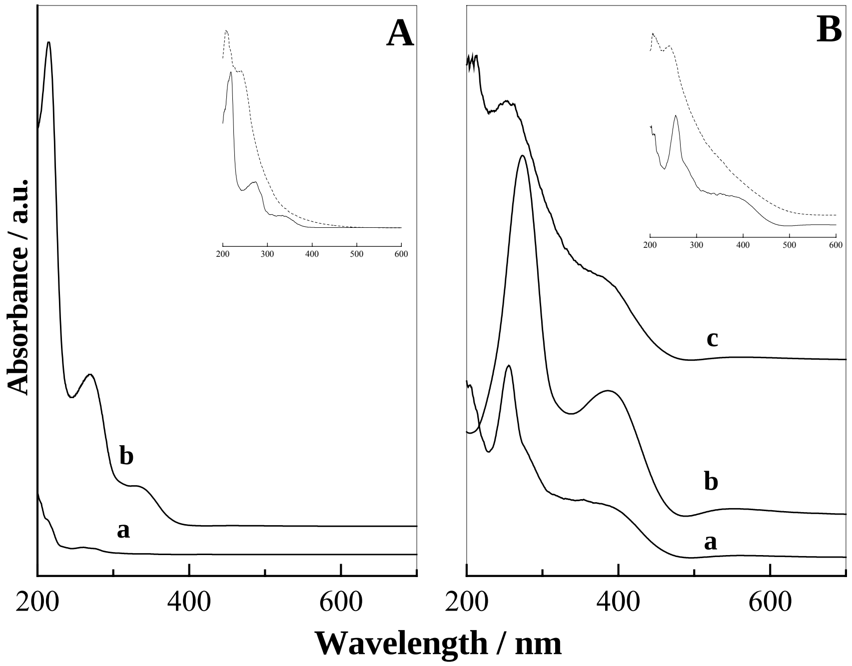

Figure 2.6. Diffuse reflectance UV-Vis spectra of: (A) (a) Silica polymorph, (b) V-MCM-41 (55) and (B) (a) V/MCM-41 (*as syn.*), (b) V/MCM-41 (*cal.*) and (c) VO-NH_2-MCM-41. Inset in (A) & (B) shows the hydrated (*solid lines*) and dehydrated (*dotted lines*) spectra of V-MCM-41 (55) and V/MCM-41 samples, respectively.

The UV-Vis spectra of all vanadium samples show three intense absorption bands in the UV region, at 220 nm, 280 nm and at 340 nm. The band observed at 220 nm is typical of siliceous materials but bands in the 250-350 nm range shows the presence of anchored vanadium. The absorption bands at 280 nm and 340 nm are assigned to the low energy charge transfer bands between V=O electron transfer from $(\pi)t_2$ to (d)e and $(\pi)t_1$ to (d)e of tetrahedrally coordinated V^{5+} ions. However, the VO-NH_2-MCM-41 sample lacks the characteristic d-d transition of $(VO)^{2+}$ ions usually observed in the visible region (600- 800 nm). Hence, it is possible that the V^{4+} species may change its oxidation state from $^{+}4$ to $^{+}5$ during the drying process and thus the concentration of V^{4+} groups on the support surfaces may be low. Moreover, since the d-d transitions are ~10-30 times lower than the high intense charge transfer (CT) transitions in the 250-400 nm range, a decreased intensity in the low frequency region is also expected.

The UV-Vis spectra of calcined, dehydrated V-MCM-41 and V/MCM-41 catalysts show a greater percentage of tetrahedral vanadium species in the peak fitting curves and are almost devoid from the band above 330 nm (Fig. 2.6, inset). In detail, the dehydrated V-MCM-41 catalyst shows ~90% of tetrahedral species, in the 240-280 nm region and the dehydrated V/MCM-41 catalyst shows an almost disappearance of the 360 nm peak. This result shows the high affinity of atmospheric water molecules to form coordination with the surface tetrahedral vanadium species to penta- or hexacoordinated vanadium sites.

2.3.1.7. UV-Vis Absorption Edge Energy Measurements

The UV spectrum of vanadium consists of the lower energy charge-transfer (LCT) band associated with an O to V electron transfer, while the optical band gap energy is represented by the energy edge. The optical absorption edge energy is defined as the minimum photon energy required to excite an electron from the highest occupied molecular orbital (HOMO, at the top of the valence band in semiconductor domains) to the lowest unoccupied molecular orbital (LUMO, at the bottom of the conduction band). There are two basic types of electronic transitions, direct and indirect.[23] In direct transitions, only photons excite electrons, while indirect transitions require concerted vibrations and energy from the crystal lattice (phonons). The energy dependence of the absorption coefficient (α) for semiconductors in the region near the absorption edge is given by $\alpha \infty (h\nu - E_o)^{\eta} / h\nu$, where $h\nu$ is the energy of the incident photon and E_o is the optical absorption edge energy and the exponent η depends on the type of optical transition caused by photon absorption.

In crystalline semiconductors, where crystal momentum is conserved and electron transitions obey well-defined selection rules, η is 1/2, 3/2, 2 and 3 when the transitions are direct allowed, direct forbidden, indirect-allowed and indirect-forbidden, respectively.[24] In amorphous, homogeneous semiconductors, the value of η is 2 irrespective of the type of transition found in crystalline materials of the same composition. With an appropriate choice of η, a plot of $(\alpha h\nu)^{1/\eta}$ vs $h\nu$ is linear near the edge and the intercept of the line on the abscissa at $(\alpha h\ \nu)^{1/\eta} = 0$ gives the optical absorption edge energy E_o.

In the diffuse reflectance experiments, UV-Vis reflectance data cannot be used directly to measure absorption coefficients (α) because of scattering contributions to the reflectance spectra. Scattering coefficients, however, depend weakly on energy and $F(R_\infty)$, where $F(R_\infty)$ is the Kubelka-Munk (KM) function for an infinitely thick sample, and can be assumed to be proportional to the absorption coefficient within the narrow range of energy containing the absorption edge features. Then, a plot of $(F(R_\infty)\ h\nu)^{1/\eta}$ vs $h\nu$ can be used to determine the absorption edge energy. Thus, as in the case of a particle in a box, where the separation between energy levels decreases with increasing box size, the band gap energy of a real system decreases as the domain size increases. Wei *et al.* studied a series of vanadium model compounds with different, but well-defined, local symmetry of vanadium, using the classical way of opting $\eta = 1/2$.[25] The symmetry and domain size of vanadium model compounds and values of edge energies summarized in Table 2.3 shows that the edge energy decreases monotonically with an increasing domain size. The domain size, the so-called molecular cage size, could be defined by the nearest neighbour ligands (oxygen in the present case) coordinating the vanadium centre. This is quite useful in determining the local structure of vanadium, since domain size sensitively varied with the symmetry.

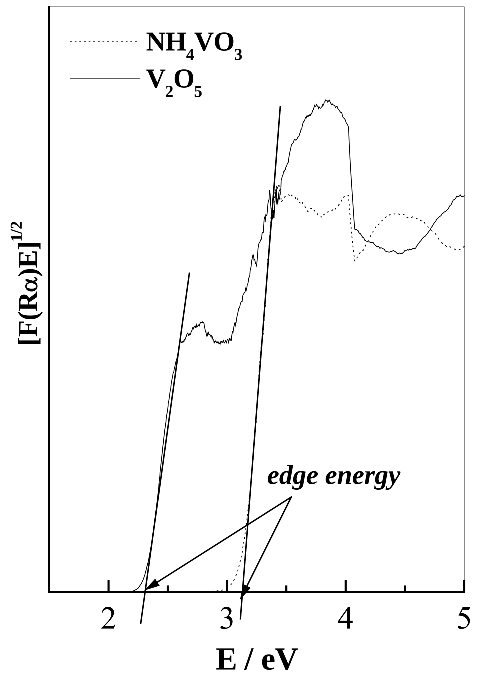

Figure 2.7. Determination of absorption edge energy of vanadium model compounds, with reference to UV-Vis spectral data.

The edge energies, determined from the intercept of a straight line fitted through the rise of the function $[F(R_\infty)\ h\nu]^{1/2}$ plotted versus hν, for V_2O_5 and NH_4VO_3 is shown in Figure 2.7.[26] The edge energy is 2.3 eV for V_2O_5 and 3.2 eV for NH_4VO_3. The decrease in edge energy for V_2O_5 implies an increased polymerization of vanadium (V) species, with increasing surface density of vanadia. In the present vanadium-containing mesoporous samples, the edge energy values are in the range 3-4 eV and a comparison with vanadium model compounds shows that the formation of tetrahedral vanadium species is more for V-MCM-41 sample, while the post synthesis modified catalysts are more vulnerable towards the higher coordinated vanadium species.[27] Thus vanadium in V-MCM-41 sample can be tentatively attributed to be tetrahedrally coordinated, supporting the framework incorporation. The fact that the edge energy of calcined V/MCM-41 sample is lower than V-MCM-41 sample relates to the presence of tetrahedral vanadium species, co-existing with octahedral polymeric species (Table 2.3).

Further, compared to the hydrated samples, the dehydrated samples show an increase in the edge energy values showing the possible transformation of the square pyramidal/octahedral coordination to its tetrahedral coordination upon expulsion of the coordinated water molecules. Thus the increase in edge energy values upon dehydration shows a decreased electron density on the vanadium atom, which may arise from the loss of electron donating H_2O species.

Table 2.3. Absorption edge energy values of calcined Vanadium-containing MCM-41 samples and Vanadium model compounds

Sample	Absorption edge energy / eV	Domain Size	Local symmetry
V-MCM-41 (H)	3.67	-	-
V-MCM-41 (D)	4.11	-	-
V/MCM-41	3.31	-	-
VO-NH_2-MCM-41	3.60	-	-
Na_3VO_4	3.21	1.729	Tetrahedral
NH_4VO_3	3.23	1.735	Distorted tetrahedral
V_2O_5	2.30	1.978	Square pyramidal
PbV_2O_6	2.05	2.075	Distorted octahedral

H = Hydrated sample, D = Dehydrated sample

2.3.1.8. Temperature Programmed Reduction

H_2-TPR profiles of the calcined V-MCM-41, V/MCM-41 and VO-NH_2-MCM-41 samples taken in the 100-800 ^{o}C temperature range show that the reduction temperature maxima (T_{max}), which qualitatively reflects the reducibility of the supported vanadia, and the average oxidation state (AOS) values varies over the direct synthesized and post synthesis modified mesoporous vanadium catalysts (Table 2.1). For comparison purpose, the reduction profile of pure V_2O_5 is also included in Figure 2.8. It was found that pure V_2O_5 exhibits multiple (three) reduction peaks and the three peaks obtained are due to the reduction sequence: $V_2O_5 \rightarrow V_6O_{13} \rightarrow V_2O_4 \rightarrow V_2O_3$. The reduction profiles for bulk vanadia reported in literature vary widely, probably because of the differences in factors such as method of preparation, level of impurities, partial pressure of H_2 used, rate of heating, reduction conditions, *etc.*[28]

Various detailed studies performed over V/SiO_2 catalysts confirm that the reduction peak observed at 430 ^oC is due to surface dispersed tetrahedral vanadium phases and the peak observed after 550 ^oC for bulk-vanadium phases.[29,30] Usually, as the particle size of vanadium species increase, the species are more difficult to reduce due to bulk diffusion limitations, resulting a shift in the reduction peaks to higher temperatures. In the present case, the V-MCM-41 sample exhibits sharp reduction peak at 430 ^oC, which may results from the reduction of monomeric or low oligomeric surface dispersed tetrahedral vanadium species. In contrast, the calcined V/MCM-41 and VO-NH_2-MCM-41 catalysts show a higher shift in the main reduction peak and are at ~510 ^oC (Fig. 2.8). The single T_{max} obtained for all samples represents a single stage reduction of the surface V^{5+} to surface V^{3+} while the higher T_{max} for crystalline V_2O_5 arises from the more difficult reduction of the internal V^{5+} sites in the V_2O_5 crystalline lattice during H_2-TPR.[31] Moreover, a careful analysis between the reduction profiles of calcined V/MCM-41 and VO-NH_2-MCM-41 samples shows that the V/MCM-41 sample exhibit a distinct tailing of the 510 ^oC band, indicating the formation of less reducible polymeric '*bulk-like*' vanadia species, which may exist in a highly dispersed state on the support surface.[32,33] However, such shoulder like peaks (at ~570 ^oC), are devoid over the immobilized vanadium sample. Thus it can be pointed that immobilization provides a probable $(-(CH_2)_3\text{-}NH_2)_3VO^{2+}$ anchoring and hence during calcination these organic spacers inhibit the agglomerization of the vanadium species and thus the formation of bulk-like vanadia species is not prominent over the calcined VO-NH_2-MCM-41 sample.

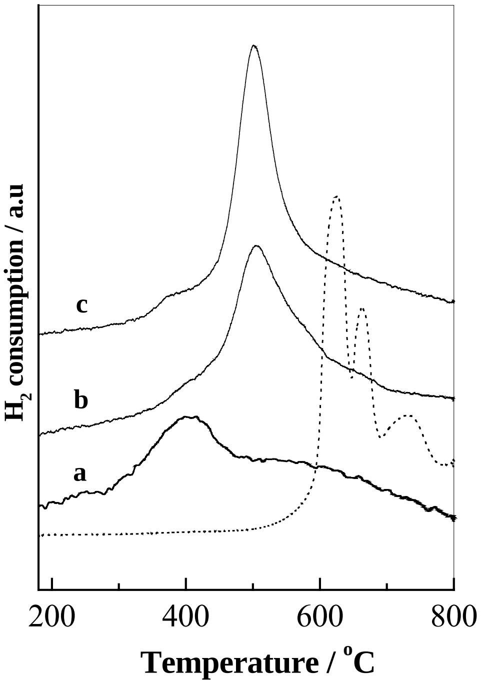

Figure 2.8. H_2-TPR reduction profiles of: (a) V-MCM-41 (55), (b) V/MCM-41 and (c) VO-NH_2-MCM-41. The dotted line shows the reduction profile of pure V_2O_5.

2.3.2. CATALYTIC OXIDATION OF NAPHTHALENE

2.3.2.1. Reaction Procedure

Naphthalene oxidation reactions were performed in a 25 mL round bottom flask using 30 wt.% *aqueous* H_2O_2 and 70 wt.% *aqueous* TBHP as oxidants. The reactant mixtures of naphthalene (1 g, 7.8 mmol), H_2O_2 (30 wt.%, 2.67 g, 23.56 mmol) and acetonitrile (10 mL) solvent were added to catalyst (10% of naphthalene) and heated at a constant temperature of 80 °C under magnetic stirring (*ca.* 800 rpm). After reactions, the reaction mixture was cooled to room conditions and the oxidized products were analyzed on a gas chromatograph (HP 6890) equipped with a flame ionization detector (FID) and a capillary column (5 μm cross linked methyl silicone gum, 0.2 mm × 50 m) and were further confirmed by GC-MS (Shimadzu 2000 A).

2.3.2.2. Catalytic Results

The conversion obtained for V-MCM-41, V/MCM-41 and VO-NH_2-MCM-41 catalysts in the oxidation reaction of naphthalene is visualized in Figure 2.9A. For the V-MCM-41 and VO-NH_2-MCM-41 catalysts, the conversion increases gradually with time and reaches a maximum of 13.5 % and 16.0 %**,** respectively, after 24 h run. No hydroxylated products (napthols) were detected for the calcined samples and after 24 h the selectivity to 1,4 napthoquinone (1,4 NQ) and pthallic anhydride (PTA) is 58 % and 42 % for the V-MCM-41 catalyst and 54 % and 46 % for the VO-NH_2-MCM-41 catalyst. However, for the V/MCM-41 catalyst the conversions are abrupt even in the early stages of the reaction and are almost steady through the run and show 16.4 % naphthalene conversion after 24 h with a 1,4 NQ and PTA selectivity of 40 % and 60 %, respectively. The higher catalytic activity of the V/MCM-41 and VO-NH_2-MCM-41 catalyst shows that the post synthesis modifications have made the active metal sites well exposed and accessible for the reactant molecules but for the V-MCM-41 catalyst since a part of the active sites are buried inside the pore channels, the vanadium sites are not completely accessible for the diffused reactant molecules and hence the difference.[34]

In the oxidation reaction of naphthalene as shown in Scheme 2.1, the polarity of the reactant (naphthalene) and the primary products formed (napthols) are different that the reactant is non-polar while the primary products are polar. Hence hydrophobic catalysts can enhance the conversion rates as it can suitably adsorb the reactant molecules while hydrophilic catalysts can adsorb the formed napthols preferentially and thereby to convert them to its further oxidized products. Accordingly, an interesting observation is the difference in the selectivity behaviour of the V/MCM-41 catalyst before and after calcinations, as the as-synthesized V/MCM-41 catalyst shows the formation of hydroxylated products (napthols) during the initial stages of the reaction (>15 %/6 h) while its calcined counterpart shows only the presence of more oxidized products without any hydroxylated primary products. Since the presence of bulkier organic groups on the as-synthesized V/MCM-41 catalyst makes the catalyst surface hydrophobic, the oxidation of naphthalene will be more than that of napthols, as these compounds are desorbed rapidly from the hydrophobic surface of the as-synthesized V/MCM-41 material. However, for the calcined V/MCM-41 catalyst, since calcination decomposes all the organic moieties, the surface becomes hydrophilic and thus the oxidation of napthols is more pronounced. So it is apparent that hydrophilic-hydrophobic interactions also plays a key role in the selectivity of hydroxylated products during the hydroxylation reactions.[35]

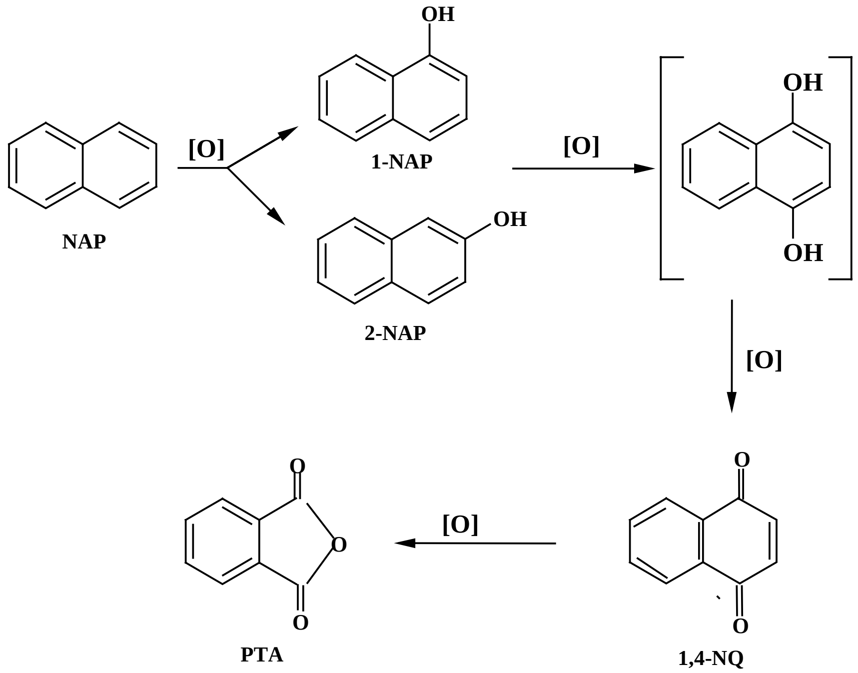

Scheme 2.1. Possible reaction scheme for the oxidation of naphthalene

2.3.2.3. Recycle Studies

Since small amounts of leached metal species can have a significant effect on the entire catalytic activity, heterogenity of the present vanadium catalysts was investigated in detail using a series of leaching studies, giving much attention towards the V-MCM-41 catalyst.

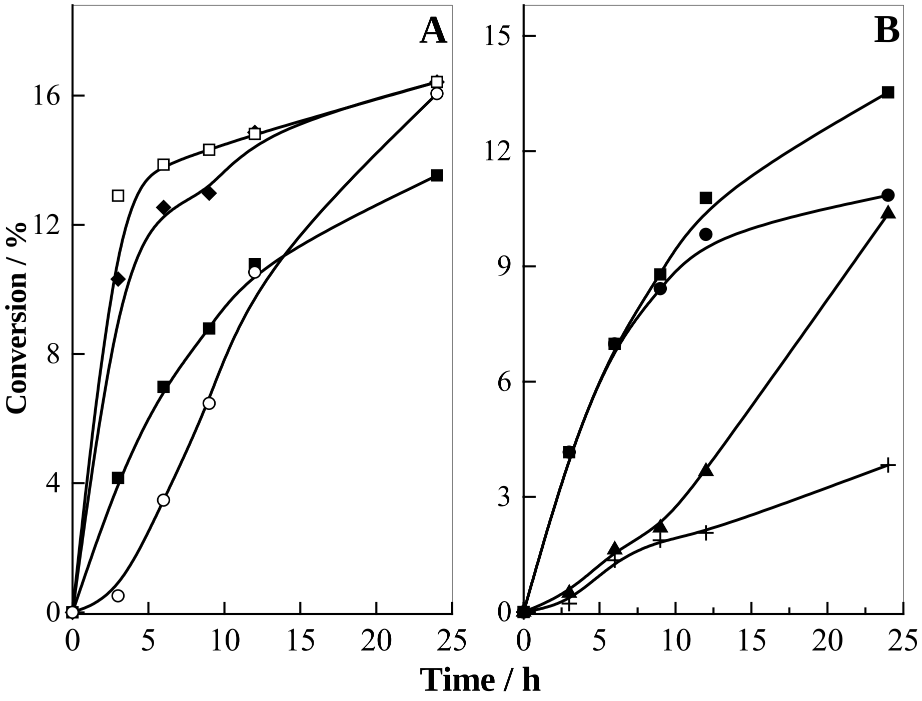

Figure. 2.9. (A) Influence of reaction time in the conversion of naphthalene over: (■) V-MCM-41 (55), (◆) V/MCM-41 (*as syn.*), (□) V/MCM-41 (*cal.*), (O) VO-NH_2-MCM-41 and (B) Various leaching studies performed on V-MCM-41 (55) catalyst: (■) fresh cycle, (●) resubmission of the catalyst removed hot filtrate after 6 h of run, (▲) activity of the '*filtrate*' after stirring the catalyst in solvent-oxidant mixture and (+) activity of the '*catalyst*' after stirring in an ~1M H_2O_2 solution.

Catalytic activity of the used catalysts by simple washing with $CHCl_3$ and washing followed by calcination show a decrease in activity of the V-MCM-41 and V/MCM-41 catalyst systems (< 10 % after 24 h). However, in both cases, no pthallic anhydride (PTA) was detected and hence infer to the loss of weakly bonded extra framework vanadium species and thereby decreasing the further oxidation of quinone products.

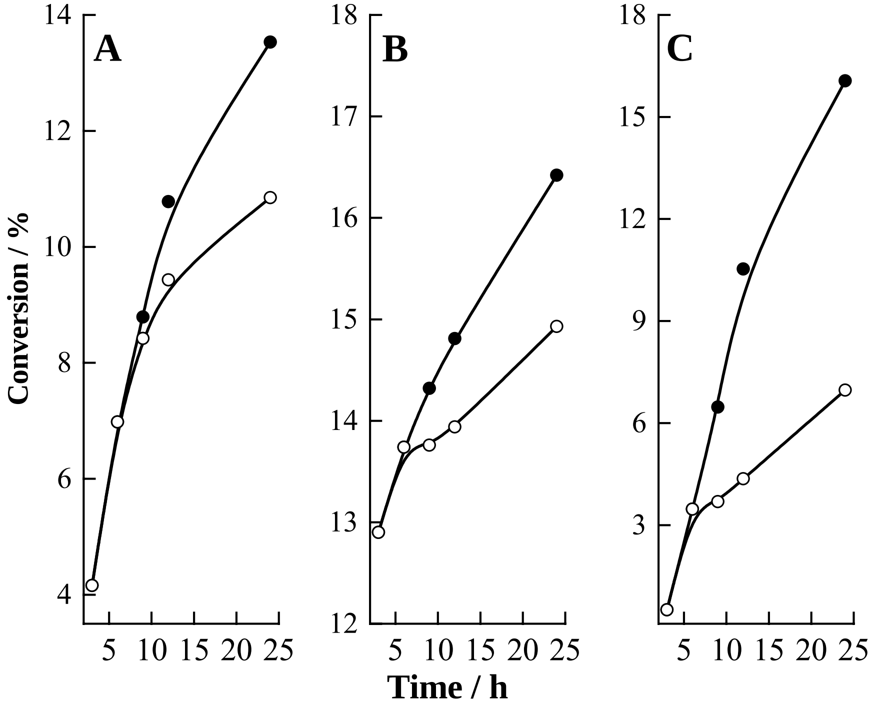

Figure 2.10. Hot filtration experiments of vanadium-containing MCM-41 samples: (A) V-MCM-41 (55), (B) V/MCM-41 and (C) VO-NH_2-MCM-41, (●) fresh cycle and (○) filtration after 6 h run.

From hot filtration experiments, it was observed that the V-MCM-41 and V/MCM-41 catalyst shows the leaching of active vanadium species from the frame wall positions, even after the removal of catalyst (Fig. 2.10A&B).[36] Hence, in order to attain more evidence for what causes the exact leaching phenomenon in this reaction, two separate leaching studies are also performed with the V-MCM-41 catalyst. The catalyst was first stirred in an acetonitrile-H_2O_2 mixture for 2 h at 80 ^{o}C and the catalyst removed filtrate was applied under the reaction conditions with substrate. The second experiment was performed by treating the catalyst in H_2O_2 (~1M) for 2 h and then the catalyst was applied under identical reaction conditions with the substrate and oxidant (Fig. 2.9B). Interestingly, for the reaction**,** where the 'catalyst' stirred in H_2O_2 solution and applied to the reaction condition shows a decreased conversion while the 'filtrate' obtained from the solvent-oxidant mixture shows an increased conversion rate, showing the major role of *aqueous* oxidants in the leaching of active metal sites. On the contrary, the vanadium-immobilized VO-NH_2-MCM-41 catalyst shows limited leaching of active vanadium sites. This interesting result suggests that the high-density amino propyl groups on the mesoporous support improves the hydrophobicity of the catalyst and binds the VO^{2+} ions effectively and thus exhibits improved heterogenity than the V-MCM-41 and V/MCM-41 catalyst systems (Fig. 2.10C). Thus the stability of vanadium-containing mesoporous catalysts prepared by different methods, under the present reaction condition, can be rationalized in the following order, VO-NH_2-MCM-41>>V-MCM-41>V/MCM-41.

The decreased stability of the V-MCM-41 catalyst is mainly due to the interaction of *aqueous* H_2O_2 (30 wt%) on the defect sites of the mesoporous material, which may detach some of the vanadium species residing on extra framework positions, (species observed in the UV-Vis spectra, >300 nm). Furthermore, the decreased heterogenity of the V-MCM-41 catalysts may arise from: (i) calcination treatments itself, as during calcination the water formed due to the decomposition of the template molecules can break some of the Si-O-V bonds and these species get leached out and dispersed on the support surface, similar to impregnated metal complexes, (ii) under drastic oxidation reaction conditions even the mesopore wall structure itself gets collapsed, since the frame wall thickness (FWT) of the M41S materials is lower and this may also contributes to the leaching of the vanadia species in a definite environment.[34] These leached out vanadium species can interact with the water molecules present in the oxidant and can form well-homogenized different vanadium peroxo species, thus enhances the oxidation of the organic substrates faster as reaction progresses.[37] Accordingly, the XRD patterns of the spent V-MCM-41 catalyst shows a decrease in the peak intensities with a corresponding decrease in the unit cell values, pointing the loss of heteroatoms from the framework positions.

Thus the present study point out two important conclusions: (i) the stability of the V-MCM-41 sample was less under polar solvents and hence improvements in frame wall structure can lead to structurally stable, catalytic active V-MCM-41 catalysts, (ii) even though the hexagonal structural features of Si-MCM-41 get disordered after the two step post synthesis modifications, amino propyl immobilized mesoporous vanadium samples are more active and stable than the V-MCM-41 catalysts, which suggest that the presence of organic groups helps to improve the hydrophobicity and thereby the catalytic activity and stability of the metal-containing mesoporous samples. These points are further verified and described in the next sections for the development of an active, stable and recyclable vanadium-containing mesoporous catalyst.

2.4. PROPERTIES OF V-MCM-41 CATALYSTS PREPARED WITH FUMED SILICA AND TETRAETHYL ORTHOSILICATE SILICA SOURCES

Mesoporous molecular sieves with transition metals incorporated into the framework had attracted great interest in catalytic oxidation process, especially for the production of fine chemicals. Among them, one of the well-studied metal-containing mesoporous material is the V-MCM-41, because of its catalytic potential for selective oxidation reactions using peroxides as oxidants. However, the rapid structural disordering and the leaching of extra framework vanadium species always confuses on the heterogenity of these mesoporous silicates. This limitation is generally attributed to the presence of thin pore walls of MCM-41 samples, which may gets seriously damaged under strong oxidizing reaction conditions, thus losses its long range mesoscopic order and thereby limits its further applicability. Even though, the wall thickness of the M41S materials can be improved by various post-synthesis modifications on the silica surfaces it seems to be a better alternative to take care on the synthesis step itself, since it is known that the hydrolysis and condensation of various silica sources are altering and shows interesting properties with the gel pH and other pre-treatment conditions.[38] Hence, it is of importance to probe systematically the role of commonly used silica sources in the synthesis of metal-containing mesoporous materials at a particular pH and under a particular gel ratio, as it provides a qualitative idea about the active metal site isolations in various reported literature procedures and thus provide more insights in to the nature of interaction of the silica species with the structure directors, metal ions, *etc*.[39,40]

This section describes the influence of the two commonly used silica sources *viz.,* fumed silica and tetraethyl orthosilicate in the structural stability, nature of vanadium sites and the catalytic activity of Si(V)-MCM-41 materials.

2.4.1. CHARACTERIZATION

2.4.1.1. Powder X-Ray Diffraction

Figure 2.11 shows the XRD patterns of as-synthesized Si-MCM-41 and V-MCM-41 samples synthesized from fumed silica and tetra ethyl orthosilicate silica sources. Even though higher hydrothermal synthesis temperature can incorporate a greater percentage of metal into the silica framework, the sequential problem of the dissolution of the micelles at higher temperatures, which may affect the long-range structural ordering, limits the present hydrothermal treatments at 100 ◦C, but with more cooking time. A comparison of the XRD patterns between the vanadium-containing mesoporous materials and the respective siliceous counterparts shows a better structural ordering for the vanadium-containing MCM-41 samples than the Si-MCM-41 samples. These discrepancies shows the effect of vanadium in the synthesis gel as its salt like influence may helps to orient the surfactant-silicate assembly in a more ordered way than under metal free systems. Thus, even though the same surfactant was used for the synthesis of vanadium-containing mesoporous materials and their corresponding silica counterparts, the discrepancies in the XRD patterns arise due to the following reasons: (i) due to the large V-O bond distance than the Si-O bond distance and (ii) the thickening of pore wall due to the transition metal promoted cross linking of the amorphous silica walls. The well-defined XRD patterns of the as-synthesized V-MCM-41 samples prepared using both silica sources can be indexed to the Bragg reflections, (100), (110), (200) and (210), characteristic of materials with hexagonal structure. Thus, irrespective of the silica source, the as-synthesized V-MCM-41 materials had shown an almost similar XRD reflection pattern, with the presence of all long range ordered peaks.

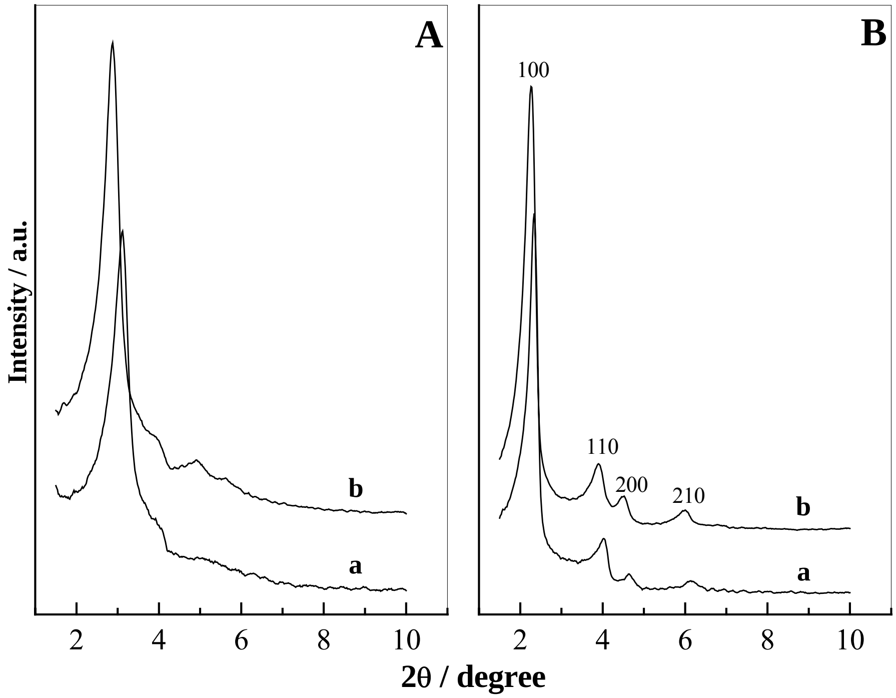

Figure 2.11. XRD patterns of as-synthesized samples: (A) Si-MCM-41 and (B) V-MCM-41, (a) from fumed silica source and (b) from TEOS silica source

Figure 2.12 represents the XRD patterns of VMS and VMT samples synthesized with different Si/V gel ratios. Attempts to synthesize V-MCM-41 samples with an Si/V ratio of 30, resulted in broad XRD peaks with an absence of long range ordered peaks, when the H_2O/Si gel ratio is 60. However, by changing the H_2O/Si ratio to 100, high-quality XRD patterns are observed for V-MCM-41 materials with a Si/V ratio of even 25. These results suggest the importance of homogeneous gel mixtures in the synthesis of Si-MCM-41 and M-MCM-41 materials, where the presence of excess water make it easier to orient the surfactant-silicate assembly than it would be under thick gel conditions. In addition, it is also reasonable that the addition of more water may increase the effective head group area of the surfactants, which in turn may reduce the packing parameter value ($g = V/a_o l$), resulting in materials of good quality. Further, the increase in the unit cell values (a_o) compared with pure MCM-41 shows the incorporation of vanadium in the molecular sieve framework, since the V-O bond distance (1.8 Å) is longer than the Si-O bond distance (1.6 Å) and are given in Table 2.4.[6]

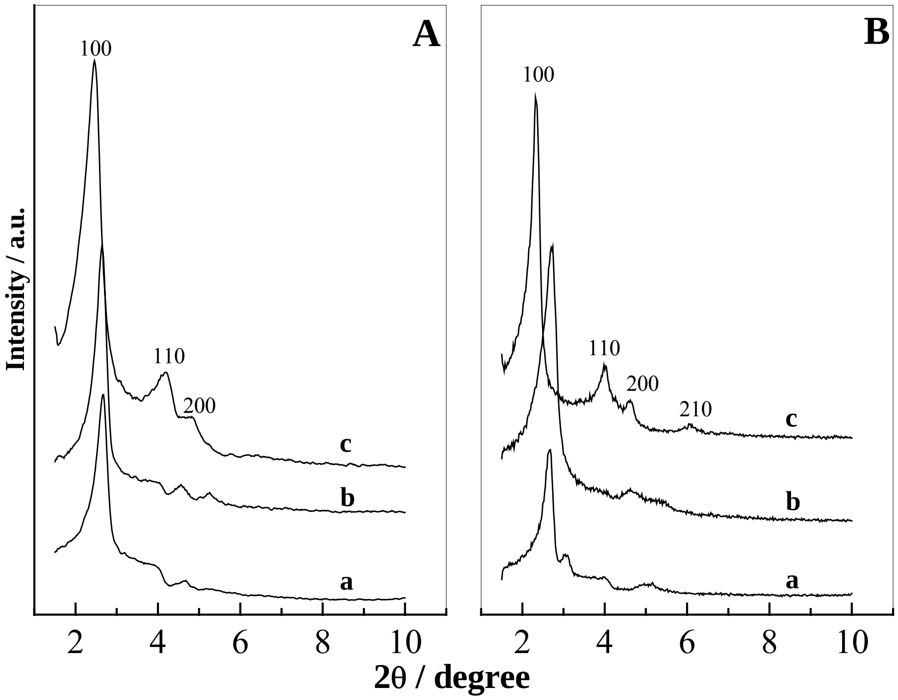

Figure 2.12. XRD patterns of: (A) VMT samples and (B) VMS samples, (a) Si/V = 80, Si/V=55 and (c) Si/V= 25.

To evaluate whether the increased structural ordering of V-MCM-41 samples results from more condensed silica species or to the increased interaction between the silica species and surfactants, two common processes are opted for the removal of the surfactants, *viz.,* solvent extraction and calcination (Fig. 2.13). Interestingly, the samples obtained after extraction show an almost similar peak intensity and ordering, like the as-synthesized samples, while after calcination the material obtained from the fumed silica source shows XRD patterns with an approximately twofold lower intensity, than the TEOS synthesized sample, with a loss in their long range ordered peaks. This result relates to the difference in the nature of silanol condensation and thus indicates that the silica source had a role in the quality of MCM-41 materials. Thus, the decreased intensity of the VMS catalyst after calcination, may arise due to the increased surface hydroxyl condensation which in turn may increase the wall thickness of the material and thereby its stability.

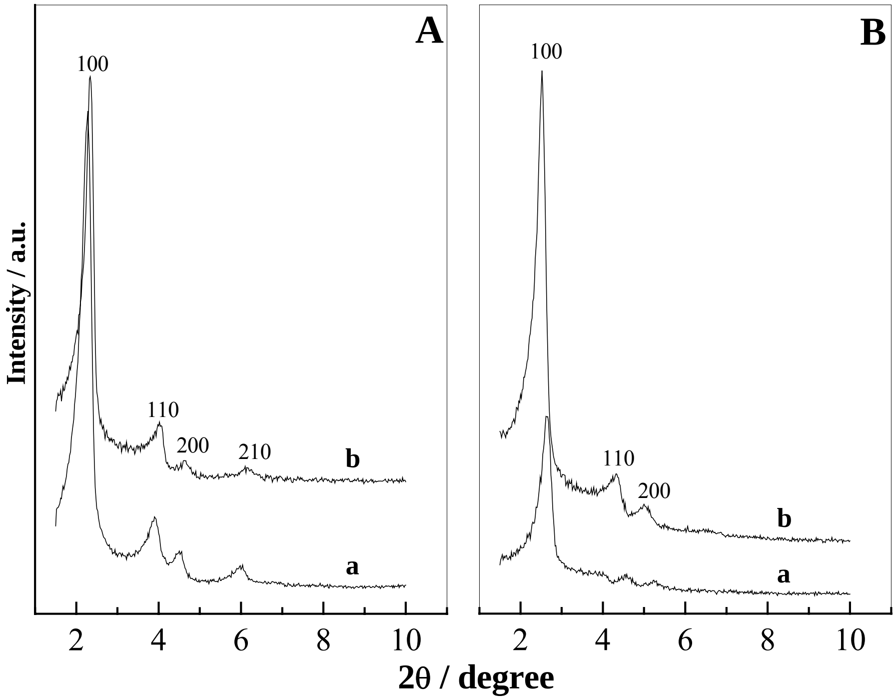

Figure 2.13. XRD patterns of: (A) surfactant-extracted and (B) calcined V-MCM-41 samples, (a) VMS (55) and (b) VMT (55).

In order to further ascertain the above discrepancies, one has to probe in detail the chemistry behind the nature of hydrolysis and its further condensation procedures when using silica sources of a different nature. Tetra ethyl orthosilicate, a quarternary alkoxide having monomeric structure, produce silicate species of smaller chains during its hydrolysis and subsequent condensation steps. Contrary the fumed silica source, itself polymeric in nature, produce oligomeric silicates of larger sizes and hence the condensation of such silica species around the micelles is faster producing materials of good quality.[38] However, during calcinations, the remaining silanol groups may get condensed faster thereby increasing the wall thickness of the material at the expense of (100) face intensity. But the increased intensity of the TEOS prepared samples still after calcination may be due to the following reasons: (i) during hydrolysis, the precursor TEOS used produce ethanol as by product and the formed alcohol may have a significant role in the formation of well ordered, more intense XRD patterns by increasing the curvature between the surfactant and silicate species. Since the formed ethanol can accumulate near the hydrophilic surfactant head group, the effective area of the surfactant gets increased and these in turn may reduce the packing parameter values, resulting in hexagonal mesoporous materials of high quality and (ii) due to the decreased silicate condensation.[39]

The above results are supported from the increased lattice contraction exhibited by the VMS materials than the VMT materials and are usually related to the extent of cross linking of the non-condensed residual silanol groups upon calcination (Table 2.4). Thus the significant lattice contraction observed for the VMS catalyst obviously show the increased cross-linked inorganic framework, when using silica source of polymeric nature as the inorganic backbone. These results had significance, especially in the liquid-phase oxidation reaction of M-MCM-41 materials with *aqueou*s H_2O_2 as oxidant, as the water present in the oxidant can deteriorate the thin frame walls of mesoporous silicates and enhances the leaching of the isomorphously substituted metal sites. Thus the nature of silica precursor used in the synthesis of Si(V)-MCM-41 materials plays a key role in affecting the overall structural stability of MCM-41 materials which in turn may arise from the difference in the rate of hydrolysis and subsequent condensation procedures. Besides, the absence of peaks corresponding to crystalline V_2O_5 in both the preparation methods shows that the metal ions were either atomically dispersed or may exist in an amorphous dispersed state on the surface of mesoporous supports.

Table 2.4. Properties of Vanadium-containing mesoporous VMS and VMT samples

Catalyst	V (%) [a]	Unit cell shrinkage (%)	Surface Area (m^2g^{-1})	Pore Diameter (D_p, Å)	Wall Thickness (ω_t, Å) [b]	$Q^4/(Q^3+Q^2)$ [c]
VMS (25) [d]	0.98	4.0	852	25.1	16.3	-
VMS (55)	0.67	10.0	909	23.8	15.7	2.04
VMS (83)	0.36	12.4	828	22.9	15.6	-
SMS	0.0	14.8	711	21.9	14.5	1.63
VMT (25)	0.76	0.8	1103	25.2	18.3	-
VMT (55)	0.50	9.5	1060	21.6	17.1	1.15
VMT (83)	0.21	10.1	1036	20.9	16.5	-
SMT	0.0	10.3	905	19.3	16.0	0.84

[a] Vanadium content determined by ICP-OES analysis.

[b] Wall thickness = a_o-D_p, where $a_o = 2d_{100}/\sqrt{3}$, [c] Relative peak area from ^{29}Si MAS NMR.

[d] Numerals in parentheses stands for the input Si/V gel ratios.

2.4.1.2. N_2 Adsorption and Desorption

N_2 adsorption-desorption isotherms of all samples show type IV isotherms with an inflection in the P/P_o range of 0.2-0.4, with completely reversible isotherms, but without any hysterisis loops, characteristic of ordered mesoporous materials. Figure 2.14 show the sorption isotherms and pore size distribution (PSD) curve obtained for the VMS (25) and VMT (25) sample.

The specific surface area, pore volume and pore diameter of both V-MCM-41 materials and their silica analogous are listed in Table 2.4. From table, it is interesting to note that the surface area, pore diameter and the wall thickness of the V-MCM-41 materials are higher than their corresponding silica polymorphs. Since the same chain length surfactant (C16-) was used for the synthesis of Si-MCM-41 materials and vanadium-containing mesoporous materials, an almost similar pore size is expected in all cases. However, the observed increase in pore size after vanadium substitution shows the effect of metal salts in the synthesis procedures and in the subsequent hydrothermal treatments.

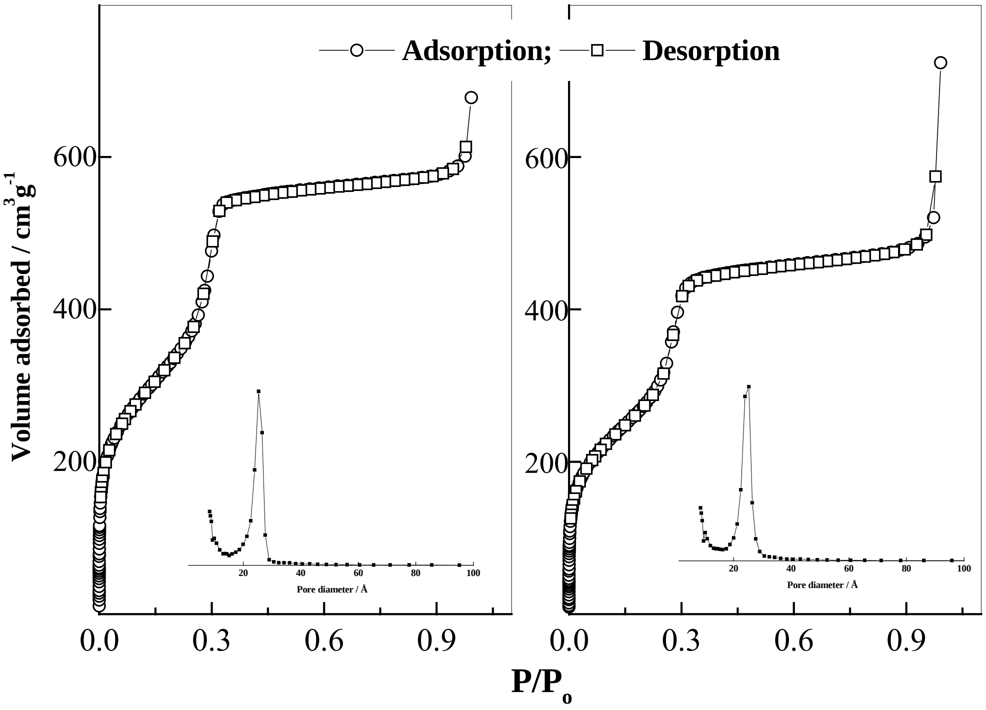

Figure 2.14. Nitrogen adsorption-desorption isotherms and pore size distribution plots (*insert*) of: (A) VMT (25) and (B) VMS (25) samples.

Usually metal (here, vanadium) gets incorporated into the silica framework of mesoporous materials in two ways: (i) a part of vanadium may be distributed along the pore walls and may combine with the hydroxyl groups to form a tetrahedral environment while the next part may be well exposed on the pore wall surfaces as external surface species causing a possible decrease in the pore size and pore volume, (ii) vanadium gets incorporated deep into the silica framework with tetrahedral coordination causing a possible increase in the pore size.[22] For zeolites, metal incorporation usually increases their pore size due to the crystalline framework and due to the longer bond length of M-O groups than Si-O groups. However, such a classification is not possible in MCM type materials due to its amorphous structure where an increase or a decrease in pore size is observed with the experimental protocols. Thus, the former way of metal incorporation does not cause any significant change in the pore size values while the latter way of metal incorporation may increase the channel width and hence exhibits larger pore sizes than the corresponding silica support surface. Hence the increase in pore size of vanadium-containing materials compared with the respective silica polymorphs shows that vanadium gets incorporated inside the silica framework due to the increased cationic size of V^{5+} ions (0.49 Å) than the Si^{4+} ions (0.26 Å).

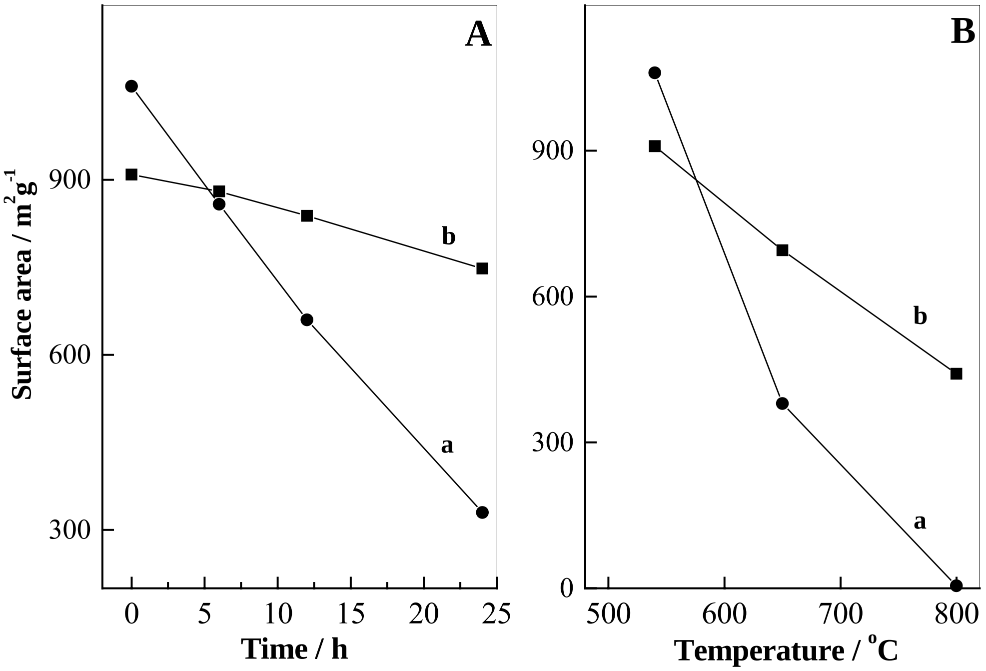

Figure 2.15. Surface area differences as a function of: (A) water vapour exposure rate and (B) calcination temperature, (a) VMT (55) sample and (b) VMS (55) sample.

The thermal and hydrothermal stability of the VMS and VMT samples were analyzed by increasing the calcination temperature up to a high value of 800 °C and by refluxing in water for 24 h and the changes observed in the surface area are depicted in

Figure 2.15. It is interesting that the VMT catalyst shows a complete loss of surface area after 800 °C calcination and a surface area decrease of ~70 % is observed after 24 h water treatments while the VMS catalyst shows only a moderate decrease of ~50 % and ~17 %, respectively, after the drastic thermal and hydrothermal treatments. These results further support the findings from the XRD measurements and show the increased thermal and hydrothermal stability of the V-MCM-41 catalyst prepared from the fumed silica source. Thus the increased thermal resistance and hydrothermal stability of the VMS catalyst arise reasonably from the increased silica condensation and thus confirms that the silica source had a significant role in the physical properties of the V-MCM-41 catalysts.

2.4.1.3. ^{29}Si MAS NMR Spectra

Figure 2.16 shows the ^{29}Si MAS NMR spectra of calcined Si-MCM-41 and V-MCM-41 materials and their relative peak proportion values were given in Table 2.5. Because of the amorphous nature of silica walls and the presence of wide range of T-O-T bond angles, usually M41S related materials show broad peaks in the –90 to -110 region and the bands are centered at -92 ppm, -100 ppm and -110 ppm assigned to the $Si(OSi)_x(OH)_{4-x}$ framework units, where x can have values of 2 (Q^2 site), 3 (Q^3 site) and 4 (Q^4 site).[41]

Presence of Q^2 sites is noted for the Si-MCM-41 sample prepared from tetraethyl orthosilicate silica source while similar sites are not observed in the spectra of Si-MCM-41 synthesized from fumed silica source. Thus the decreased intensity (from PXRD) of the fumed silica samples after calcination procedure relates to more silanol condensation and thereby increases the wall thickness of the material at the expense of mesopore ordering. In addition, a significant decrease in the Q^3/Q^4 ratio with a peak broadening of the Q^4 site is observed for the V-MCM-41 samples than the corresponding silica counterparts. The decrease in intensity of the Q^2 and Q^3 sites and the corresponding increase in Q^4 site of V-MCM-41 materials show that vanadium substituted in the silica framework and promotes the condensation of silanol groups.[41]

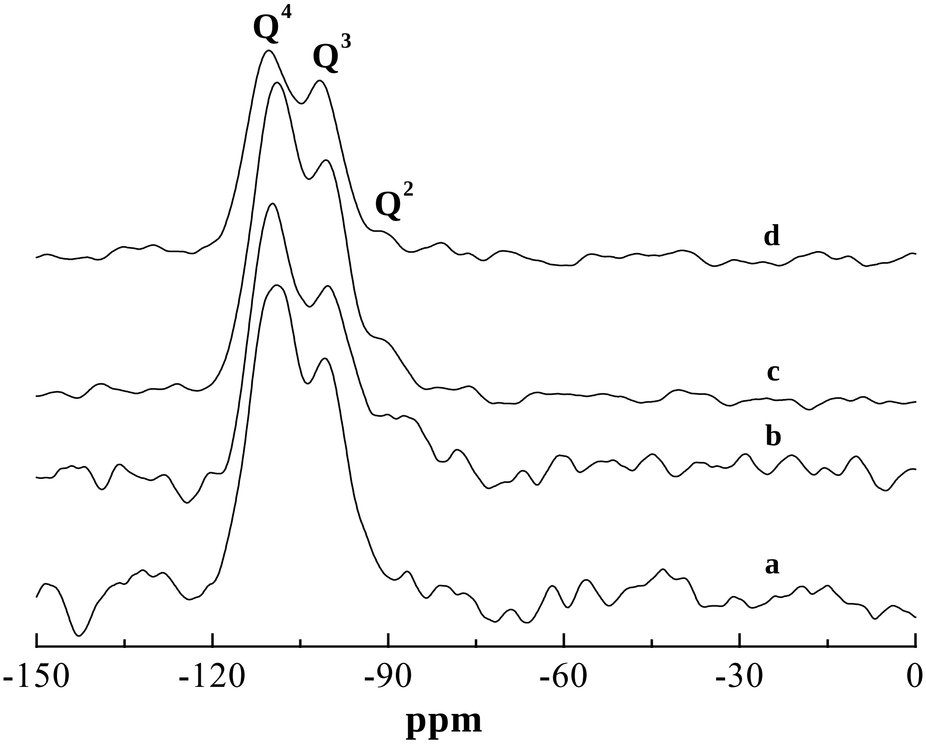

Figure 2.16. ^{29}Si MAS NMR results of calcined Si-MCM-41 and V-MCM-41 samples: (a) SMS, (b) SMT, (c) VMS and (d) VMT.

2.4.1.4. UV-Vis Experiments

Figure 2.17 shows the diffuse reflectance UV-Vis spectra of VMS and VMT samples. The UV-Vis spectra of both samples shows the presence of sharp bands at ~260 nm and ~340 nm for the tetrahedral V^{5+} ions inside the silica walls and the tetrahedral V^{5+} ions on the wall surfaces (extra framework species). The color of all V-MCM-41 catalysts is white after calcination (dehydrated), which turns yellowish (hydrated) during atmospheric exposure; the changes are more prominent for VMS samples, indicating a greater percentage of vanadium species on the wall surfaces. The color transformation of the materials shows a possible modification in the oxidation state of the vanadium species from its original tetrahedral coordination to the square pyramidal/octahedral coordination by the coordination of two water molecules from the atmosphere and the red shift increases with the percentage of vanadium loading.

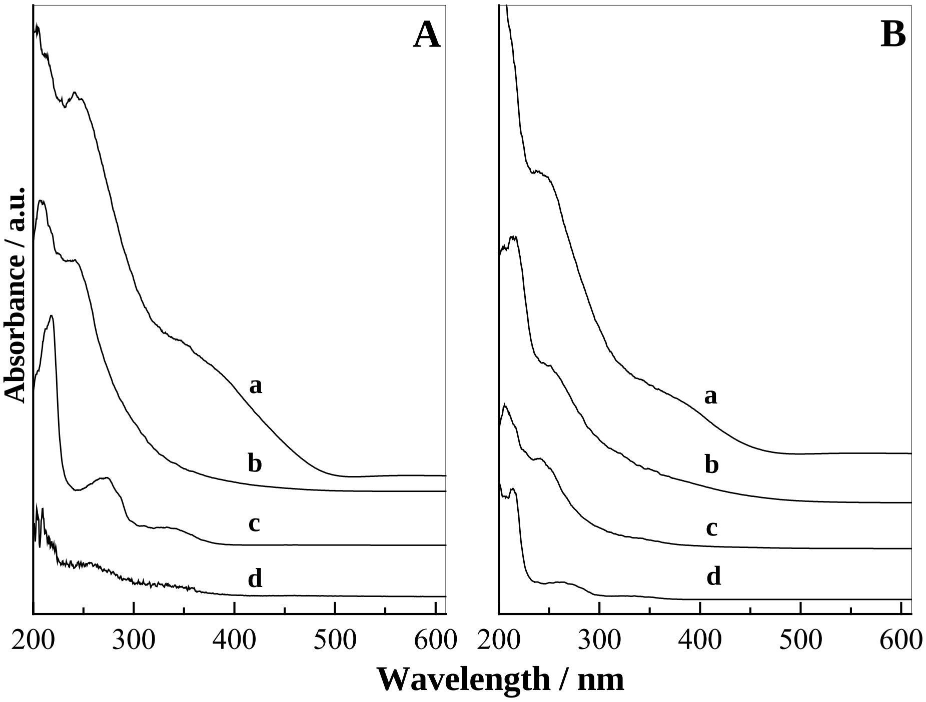

Figure 2.17. UV-Vis spectra of calcined V-MCM-41 samples: (A) VMT samples and (B) VMS samples, a = Si/V (25), b = Si/V (55) (*dehydrated*), c = Si/V (55) and d = Si/V (80).

As noted by Luan *et al.* it is observed that the absorption in the 260 nm region does not gets influenced by moisture treatments while the bands above 300 nm gets modified under various treatments (Fig. 2.17).[7] This behaviour confirms the presence of two different kinds of vanadium species on the mesoporous samples, one well buried inside the pore channels which are thermally and chemically stable, while the other species lies on the hexagonal wall surfaces which can easily undergo modifications. However, for the vanadium samples with a Si/V ratio greater than 55, the band after 300 nm is not prominent, even in the hydrated state, and this suggests that at lower vanadium contents nonaccessible tetrahedral vanadium sites are present and hence the water molecules cannot access the vanadium sites to increase the coordination. Further, the absence of bands in the visible region (>400 nm) proves the absence of aggregated V_2O_5 species over both VMS and VMT samples.

Table 2.5. Relative proportion of UV-Vis spectra and the corresponding absorption edge energy values of VMS and VMT samples

Sample	Percentage of 260 nm site	Absorption edge energy (eV)
VMS- 55 (H)	78	3.6
VMS- 55 (D)	>95	4.1
VMT- 55 (H)	71	3.3
VMT- 55 (D)	91	3.6

H = Hydrated sample, D = Dehydrated sample

2.4.1.5. EPR and ^{51}V MAS NMR Spectra

The EPR spectra of as-synthesized vanadium-containing mesoporous materials, recorded at room temperature, are given in Figure 2.18A. Since the vanadium source used for the synthesis of vanadium-containing mesoporous materials is vanadyl sulphate (V^{4+}, d^1) in as-synthesized state the material usually exhibits the characteristic eight-line hyperfine splitting (hfs) patterns due to the interaction of the unpaired electron with the nuclear spin of the ^{51}V nuclei (I = 7/2, natural abundance = 99.8%).[42] However, the V-MCM-41 sample prepared from fumed silica source (VMS) only shows the typical hyperfine splitting pattern, while the material prepared from TEOS silica source shows the absence of hyperfine splitting patterns. The well-resolved hyperfine splitting patterns obtained for the VMS sample indicates that the $(VO)^{2+}$ ions are dispersed inside the pore channels of the MCM materials and the observed g values ($g_{\parallel}$ = 1.945, $g_{\perp}$ = 1.997) and the hyperfine coupling constants ($A_{\parallel}$ = 185 G and $A_{\perp}$ = 68 G) are in well agreement with the values for $(VO)^{2+}$ ions with a distorted pesudo octahedral coordination.[43] Sayari *et al*. attributed the absence of EPR signals in vanadium-containing mesoporous materials for the presence of V^{4+} ions in highly symmetrical lattice positions and to the electronic degeneracy and associated very short relaxation times.[5] Selvam *et al*. also noted such kinds of results for V-MCM-41 materials and had assigned this behaviour for the aerial oxidation of V^{4+} to V^{5+} due to the high pH and hydrothermal synthesis conditions used in the synthesis of V-MCM-41 materials.[44] Since the VMS and VMT samples differ only with respective to the silica source, the former assignment is more possible and thus the present study shows that such anomalous results may also arise from the nature of silica sources which may have a role in the transformation of V^{4+} to V^{5+} or in the stabilization of V^{4+} species.

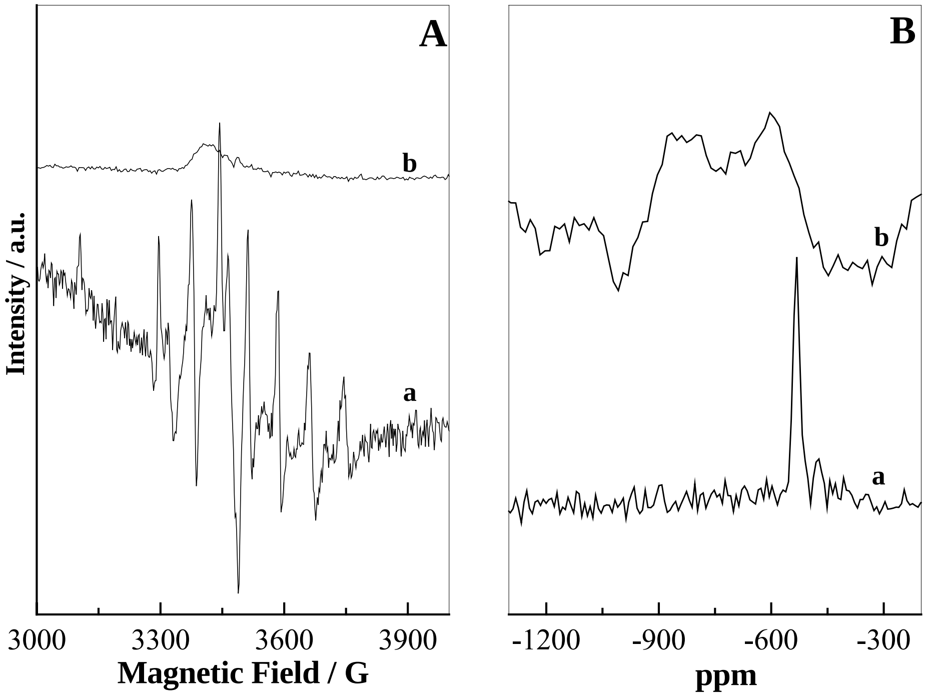

Figure 2.18. (A) EPR and (B) ^{51}V MAS NMR spectra of V-MCM-41 samples: (a) VMS (55) and (b) VMT (55).

In order to ascertain whether the absence of hfs patterns for VMT catalyst arise from any agglomerated V_2O_5 species, ^{51}V MAS NMR experiments were carried out and the results are depicted in Figure 2.18B. Since vanadium is 99.8% abundant and has a large magnetic moment and short spin relaxation times, judicial experimental procedures can provide information on the local coordination of vanadium atoms in the silica framework. Eckert and Wachs described how the mass spectra vary over different magnetic field strengths and showed in detail the peak assignment values of supported vanadium catalysts and vanadium model compounds.[45] In general, tetrahedrally coordinated vanadium sites shows signals at -500 to -540 ppm, while octahedrally coordinated V_2O_5 species shows signals at -300 ppm. Since no signals are observed in the -300 ppm region for the VMS and VMT samples, the formation of octahedrally coordinated V_2O_5 can be neglected and thus suggests that most of the added vanadium is incorporated into the silica framework as tetrahedral coordination with the oxygen ligands. However, similar to EPR results, a sharp difference in spectra between the V-MCM-41 catalysts is noticed, that the VMS catalyst shows a sharp peak at -530 ppm while the vanadium sample prepared using TEOS silica source shows a less intense and broad peak with two maxima after -500 ppm. The presence of disordered peaks suggest that vanadium exists not in a perfect tetrahedral position in VMT catalyst but as disordered tetrahedral sites or the presence of different tetrahedral vanadium species on the VMT sample may be responsible for the multiple peak positions after -500 ppm, consistent with the earlier results.[25]

2.4.1.6. Raman Spectra

Figure 2.19 depicts the Raman spectra of VMT and VMS samples, and for comparison, with the spectrum of pure V_2O_5. The Raman bands observed at 480 and 620 cm^{-1} arise from the three fold and four fold siloxane rings while the bands at 810 and 970 cm^{-1} is assigned to the siloxane bridges and the silanol groups, which may arise from the inorganic backbone of the amorphous MCM-41 silica surface.[43,46] The VMS sample shows a strong band at 1030 cm^{-1}, which is characteristic of isolated terminal $(SiO)_3V{=}O$ groups being tetrahedrally coordinated while this band is not so prominent for the VMT sample. However, both the samples produce bands at 1070 and 920 cm^{-1} and are attributed to the perturbed silica surfaces, which may arise due to the interference of neighboring vanadium atoms or due to Si-O-V moieties.[47] According to Can Li, high frequency bands corresponds to shorter V-O bonds and hence the bands greater than 1000 cm^{-1} in the present case may corresponds to the V=O species, which may arise from the isolated terminal metal sites.[48] Further, in agreement with the UV-Vis and ^{51}V MAS

NMR results, the Raman spectra did not show any band characteristic of crystalline V_2O_5, which are usually observed around 995, 703 and 530 cm^{-1}.

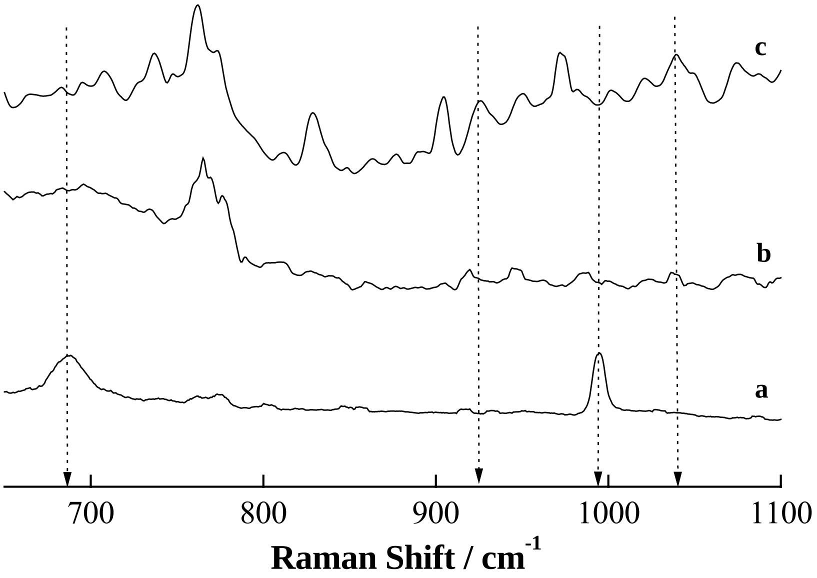

Figure 2.19. Raman spectra of vanadium-containing samples: (a) V_2O_5, (b) VMT (55) and (c) VMS (55).

Thus structural characterization results show that the material prepared from fumed silica source displays better thermal and hydrothermal stability than the TEOS synthesized vanadium samples while spectroscopic studies shows that vanadium exists in different tetrahedral environment over the different silica source synthesized vanadium samples. From UV-Vis and absorption edge energy analysis it is noted that the TEOS synthesized mesoporous vanadium catalyst shows a greater percentage of framework incorporated tetrahedral sites than the fumed silica catalyst, but the peak broadening of the ^{51}V NMR spectra of VMT sample reveals that the symmetry of vanadium species is not perfectly tetrahedral but as more distorted states and the water of coordination is less pronounced. Contrary, the sharp and distinct ^{51}V NMR peak and the greater percentage of extra framework vanadium species in the VMS catalyst (supported by the rapid colour change during hydration process) shows that the material consists of well exposed $(SiO)_3V{=}O$ species located probably near the pore mouth, which allows an easy change in the coordination state of vanadium species upon hydration and rehydration process. Hence, considering the above spectral results and the suggestions put forward by Wei *et al.* a possible representation of the vanadium sites on the two silica samples is shown in Scheme 2.2.[25]

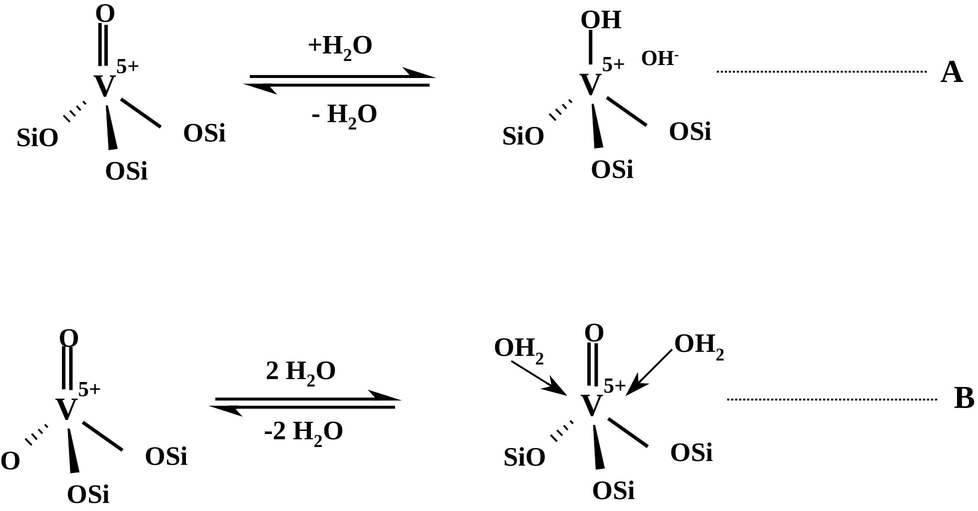

Scheme 2.2. Possible representation of vanadium sites in: (A) VMT samples and (B) VMS samples.

2.4.2. CATALYTIC EPOXIDATION OF CYCLOOCTENE

2.4.2.1. Reaction Procedure

Epoxidation reactions were performed in a 10 mL round bottom glass batch reactor fitted with a water-cooled condenser using *aqueous* H_2O_2 (30%) and TBHP (70%) as oxidants. The reactant mixtures of cyclooctene (0.92 g, 8.3 mmol), H_2O_2 (0.26 g, 2.2 mmol) and acetonitrile solvent (5 mL, dried over 4 Å molecular sieves) were added to catalysts (10% of cyclooctene) and heated by an oil bath at a temperature of 70 ^{o}C under magnetic stirring (*ca.* 800 rpm). The oxidized products were analyzed on a gas chromatograph (HP 6890) equipped with a flame ionization detector (FID) and a capillary column (5 μm cross linked methyl silicone gum, 0.2 mm × 50 m) and were further verified by GC-MS (Shimadzu 2000 A). The presence of unreacted oxidant at the end of each reaction was checked by means of standard iodometric titration (for H_2O_2 oxidant) and GC analysis (for TBHP oxidant).

2.4.2.2. Catalytic Results

Table 2.6 lists the conversion datas of VMS and VMT catalyst of different vanadium loadings under *aqueous* H_2O_2 and TBHP oxidants. In accordance with the characterization results, the fumed silica synthesized vanadium catalysts (VMS) showed a better catalytic activity than the VMT catalysts. Since catalysis is a surface phenomenon, the improved catalytic results of the VMS catalysts may relate to the greater percentage of extra framework metal species than the TEOS synthesized VMT catalysts.

An interesting result observed from the experimental part relies in the increased catalytic activity of the VMS (55) catalyst than the higher vanadium-containing VMS (25) catalyst. Earlier literature reports assigned such behaviour for the formation of M-O-M bonds and/or to the loss of structural integrity of the mesoporous material at higher metal loadings.[49] However, in the present case, the VMS (25) sample had shown well-ordered XRD patterns (Fig. 2.12B) and hence the decreased conversion obtained may accounts for the slight oligomerisation of vanadium species at higher metal loadings. Generally, octahedrally coordinated metal species are less active in epoxidation reactions due to the lack of free coordination sites. Thus the low cyclooctene conversion obtained for the VMS (25) catalyst proves that the material may contain dimeric/oligomeric vanadia species, and are supported by its higher H_2O_2 decomposition rates (Table 2.6). However, for the TEOS synthesized V-MCM-41 catalysts the conversion increases monotonically with the vanadium content.

Table 2.6. Epoxidation of cyclooctene over Vanadium-containing catalysts synthesized using different silica sources[*]

Catalyst	Cyclooctene conversion [a] mol.%	H_2O_2 conversion %	TOF [b] h^{-1} ($x10^2$)	Epoxide selectivity mol.%
VMS (25)	28 (20)	78 (56)	10.4	97
VMS (55)	50 (34)	53 (47)	39.0	>99
VMS (80)	34	n.e	06.7	100
VMT (25)	33 (11)	53 (39)	17.0	>99
VMT (55)	23 (14)	46 (31)	15.7	100
VMT (80)	11	n.e	13.5	100

<u>Reaction Conditions</u>: T (^oC) = 70, cyclooctene: H_2O_2 (mol/mol) = 4.0; cyclooctene: TBHP (mol/mol) = 1.0; catalyst weight = 10% of cyclooctene, solvent, CH_3CN (mL) = 5, reaction time (h) = 12.

[a] (Cyclooctene conversion/theoretically possible conversion) x100.

[b] Turnover frequency (TOF) = moles of substrate converted/mole of vanadium/h.

[*] Values in parentheses show the results over TBHP oxidant. n.e. = not evaluated.

It is known that solvents had a profound influence in the catalytic activity and stability of various metal-containing mesoporous silicates and the properties are attributed to the difference in the chelating abilities of the polar group of the solvent molecule with the metal sites. Apart from this, the role of solvents in oxidation reactions are too complicated to diagnose, since it vary with various factors such as polarity, solubility of the reactants and formed products, diffusion limitations, *etc*.[50] Hence in the present reaction, the activity of the catalysts was verified with a series of solvents of different polarity. Even though a solvent free atmosphere is appreciated under the present environmental regulations, negligible activity of the catalysts (< 2 %), under solvent free conditions, urged the use of diluents for enhanced conversion rates. Among the solvents used, acetonitrile shows enhanced conversion rates and the catalytic activity follows the order CH_3CN > $(CH_3)_2CO$ > CH_3OH, irrespective of the catalyst sample. The enhanced activity of the polar aprotic solvent may arise from a decreased phase separation between the aromatic alkene portion and the aqueous oxidant part, which in turn may allows an easy transport of the active oxygen species for the epoxidation process.[34] Usually, usage of more protic solvents increases the acidity of the catalyst surface and thereby increases the cleavage of the formed epoxide to their corresponding diol moieties.[50] However, in the present epoxidation reaction of cyclooctene the large stability of the formed epoxide (epoxy cyclooctene) may be the reason for the increased selectivities (> 98%) even after longer time durations (24 h) and in presence of catalyst with higher vanadium contents.

2.4.2.3. Recycle Studies

In order to monitor whether the activity of the V-MCM-41 materials arise from stable mesoporous materials, two leaching studies were carried out: (i) the catalyst applied under the reaction condition was removed after a definite time interval and the filtrate was monitored for further reaction rates, (ii) the catalyst was stirred at the reaction condition (2 h) in presence of solvent and to the catalyst removed 'hot filtrate', substrate and oxidant was added to probe the conversion rates. Indeed the former way of analysis is more crucial and hence the first-step leaching study was also carried out under hot and cold conditions.

Sheldon *et al.* showed for chromium-containing porous silicates, that cold filtration steps show less conversion rates than hot filtration steps due to the re-adsorption of dissolved metal ions from solution to catalyst surface on cooling.[51] However, the present studies on V-MCM-41 materials indicate that the leaching of vanadium species from MCM-41 matrix occurred under both hot and cold conditions, over both the catalyst systems (Fig. 2.20). Further a combination of the above two stability tests explicitly shows that *aqueous* H_2O_2 is actually promoting the leaching of active metal sites in case of V-MCM-41 catalyst systems. Hence, the leaching of vanadium in VMS catalysts is attributed to the loss of extra framework metal sites while for the VMT catalyst, the mesopore structure degradation may be the reason for leaching, on consideration of the large attenuation in the XRD patterns for H_2O_2 treated VMT catalysts.

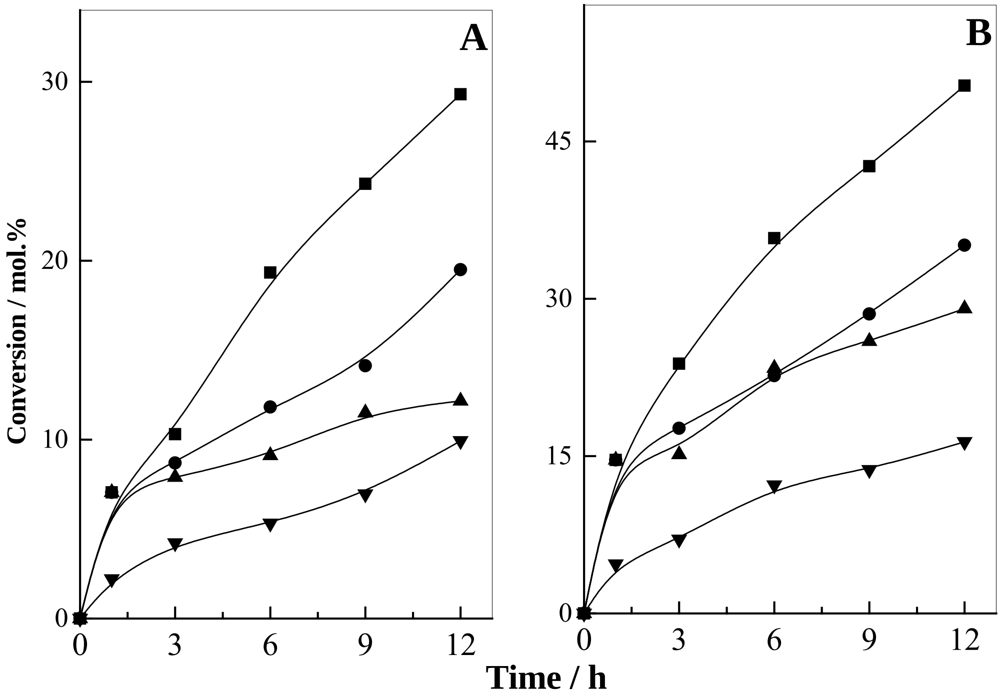

Figure 2.20. Various leaching studies performed over (A) VMS and (B) VMT catalysts: (■) fresh cycle, (●) hot filtration experiments after 1 h run, (○) cold filtration experiments after 1 h run, (▲) application of catalyst-acetonitrile stirred '*filtrate*' to the reaction condition with substrate and oxidant.

Interestingly, though the conversion rates are lower with the TBHP oxidant, the crucial point relies that the spent VMT catalyst retains ~70% of the structural ordering (from XRD patterns) in place of completely amorphous material obtained after H_2O_2 treatments. Thus usage of TBHP as an oxidant implies a possible reusability of the mesoporous catalyst materials, since regular structural patterns of mesoporous materials may always tend the metal sites more accessible for the diffused reactant species.[15] Hence the comparatively improved structural stability observed for VMS catalysts, after H_2O_2/TBHP treatments, show that the inorganic backbone arising from the fumed silica source is better than the TEOS synthesized mesoporous catalysts. Further since the vanadium species in V-MCM-41 materials are never bound to four silicate species after calcinations, for a profound applicability and re-usability of V-MCM-41 catalysts, usage of oxidants with lower water content, catalysts with lower vanadium contents and a judicious choice of the silica source (fumed silica instead of TEOS) be the crucial steps.

2.5. IMMOBILIZATION OF VANADYL CATIONS $[(VO)^{2+}]$ OVER AMINOPROPYL MODIFIED MESOPOROUS Si-SBA-15, Si-MCM-41 AND SILICA GEL

The heterogenization of homogeneous catalysts on mesoporous solids represent an interesting research area and had expanded with considerable refinements in the synthesis procedures as it provides potential advantages over the homogeneous counterparts like easy separation of the catalyst, with enhanced activities.[52] Earlier, various metal complexes are occluded inside the pores of the mesoporous support (like *'ship in a bottle'* technique) or grafted to the internal silanol sites and as a result the activity of the catalysts are questionable due to the leaching of the confined metal complexes under drastic liquid-phase reaction conditions.[53] However, the immobilization of homogeneous metal catalysts by strong chemical bonding to organo modified mesoporous materials enhances their potential in a dual manner- by making them truly heterogeneous and with increased activity. Because of this reason, literature displays a wide spectrum of organo tethered mesoporous materials with active functionalities, and among them, thiol (-SH) and amine ($-NH_2$) terminated mesoporous materials receive more attention than the other active pendant groups (-Cl, -OH, $(-PPh_3)_3$) for the immobilization of various traditionally used active homogeneous catalysts.

Since the V-MCM-41 catalysts prepared with fumed silica and tetraethyl orthosilicate silica source, described in Section 2.4, still posses serious drawbacks due to their low metal content, lower activity- as a great part of the active sites are buried inside the pore channels and the gradual decrease in catalytic activity after each cycle, the heterogenization of vanadyl cations were attempted over organic-inorganic hybrid mesoporous materials having reactive amino propyl functional groups. Even though literature shows several reports over amine-functionalized mesoporous materials, a proper comparison or a comprehensive understanding about the structural changes as well as the binding of aminopropyl groups over SBA-15, MCM-41 and silica gel surfaces during post synthesis modifications is highly limited. This section describes in detail the influence of solvents used for the grafting of the aminopropyl groups, the effect of amino groups anchored towards the structural stability of the mesoporous silicas and the nature of vanadium species formed over aminopropyl modified SBA-15, MCM-41 and Silica gel surfaces.

2.5.1. CHARACTERIZATION

Post synthesis grafting methods are employed, for the functionalization of aminopropyl groups over mesoporous silica samples, since it was known that the co-condensation of TEOS and 3-APTS groups can cause severe damage to the mesopore structural ordering in an acidic route (SBA-15 synthesis), compared to the basic synthesis as performed over MCM-41.[54] The aminopropyl groups introduced in an acidic media can get easily protonated and disturb the surfactant-silicate assembly, leading to disordered mesophases in the direct synthesis of NH_2-SBA-15 materials. In addition, the disordering also arise due to the following reasons: (i) formation of zwitterions, due to the interaction of the amine and silanol groups, prevents the interaction of the oligomerized silicates with the surfactants, (ii) interaction of the amine with the hydrophilic ethylene oxide (EO) groups of the surfactant chain and the repulsion between the hydrophilic tail of the amino propyl groups with the hydrophobic propylene oxide (PO) groups of the block copolymer, (iii) cross linking of the ammonium groups with the silanols and the variation in the pH of the gel mixture.[55] Because of these factors and for a better comparison of the structural changes happening during the anchoring of the 3-APTS groups, post synthesis modifications are more suitable as it provides more insights about the properties of the support surfaces than the ‘one-pot’ co-condensation method.

2.5.1.1. Elemental Analyses

For the functionalization of 3-APTS over mesoporous as well as silica gel supports, toluene was used as the dispersing medium. Nitrogen elemental analysis showed that the percentage of amine loading varies in the order MCM-41>Silica gel> SBA-15, which corresponds to ~76%, ~70% and ~66%, respectively, used for the functionalization. Since the amount of 3-APTS added was same over the three support materials, the observed discrepancies in the percentage of amine loading may arise from the difference in the number and nature of silanol/siloxane bonds on the support surface.

In order to probe whether the solvents used had any effect in the percentage of 3-APTS functionalization, instead of toluene, the grafting procedures are extended using solvents like dichloromethane, acetone and chloroform over MCM-41. It was found that, after 6 h, the percentage of amine loading varies in the order, toluene (~76%), chloroform (~70%), acetone (~63%) and dichloromethane (~59%). Thus, among the solvents tried, toluene shows the best level of amine functionalization with a percentage loading greater than 70%. In addition, from XRD patterns, it is also observed that the structural ordering of the resultant functionalized mesoporous materials (NH_2-MCM-41) also differs according to the nature of the solvent used. Thus, dichloromethane refluxed mesoporous MCM-41 sample retains the structural ordering intact while the sample refluxed in toluene shows the lowest structural ordering. A comparison of this result with the elemental analysis data suggests that the improved mesopore structure obtained in low boiling solvents relates to the decrease in the percentage of aminopropyl loadings. These results emphasize the importance of solvents used for organo functionalization studies. Hence, if the goal is to increase the percentage of aminopropyl groups, toluene as solvent gives the best results, while mesopore structural ordering is retained over low boiling solvents, having lesser amount of functionalized amine groups.

The percentage of vanadium-immobilized over the 3-APTS functionalized samples, estimated by ICP analysis, shows an almost similar level of vanadium over NH_2-MCM-41, NH_2-SBA-15 and NH_2-silica gel samples (Table 2.9). Meanwhile, the samples prepared without using 3-APTS spacer shows the absence of vanadium, which highlights the role of amino groups in stabilizing the vanadium complexes.

2.5.1.2. Powder X-Ray Diffraction

The small angle X-ray diffraction (XRD) patterns of SBA-15, NH_2-SBA-15 and $(VO)^{2+}$ cations immobilized aminopropyl modified SBA-15 samples are given in Figure 2.21A, while the corresponding MCM-41 samples are given in Figure 2.21B.

The XRD pattern of pristine SBA-15 shows three (hkl) reflections of (100), (110) and (200) in the 2θ range of 0.8-2^{o} indexed to two-dimensional (2D) hexagonal *p6mm* symmetry, indicating a highly ordered hexagonal structure.[2] In the same way, the pristine MCM-41 solid sample shows four Bragg reflexes with (hkl) reflections of (100), (110), (200) and (210) for a highly ordered hexagonal symmetry. After 3-APTS grafting, the width of the (100) peak of both mesoporous materials gets narrowed which may relate to the homogenous distribution of the pore structure brought about by the attachment of aminopropyl groups inside the mesopore channels. However, the decrease in intensity of the (100) peak, after post synthesis modifications, shows the partial structural collapse of the mesoporous materials or to the flexibility induced in the silica framework due to the strain generated from the functionalized organic groups.[11] A comparison in the XRD pattern between the two mesoporous materials, after modifications, shows that the long range ordered (110), (200) and (210) peaks gets disappeared in MCM-41 while SBA-15 preserves its structural features intact even after vanadyl cation immobilization. These results show that the mesoporous structural disordering is pronounced over MCM-41 than the SBA-15 solids during surface modifications.

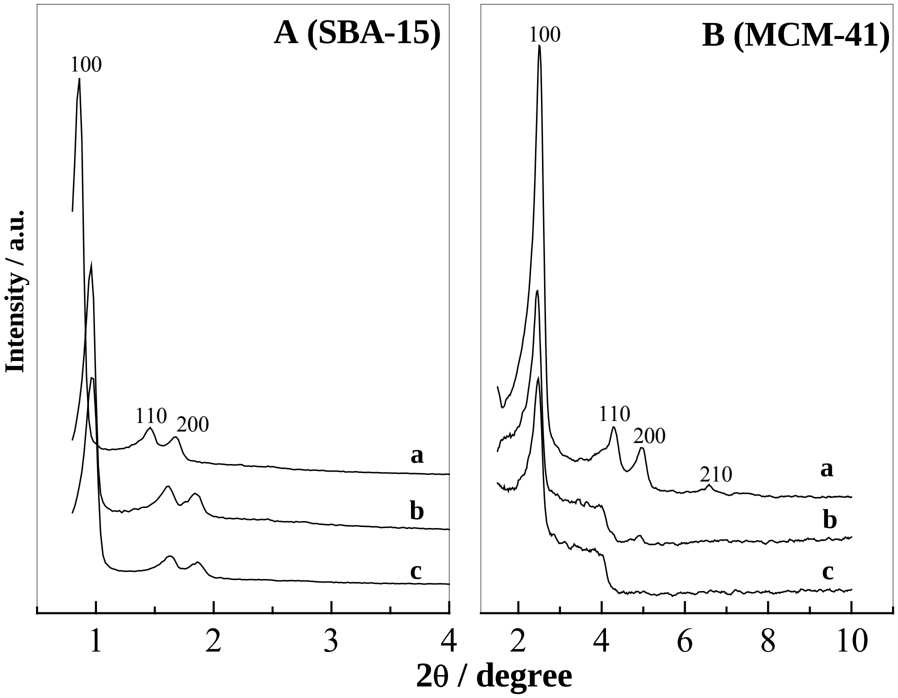

Figure 2.21. XRD patterns of (A) SBA-15 and (B) MCM-41 samples: (a) calcined support sample, (b) aminopropyl modified sample and (c) vanadium-immobilized aminopropyl sample.

2.5.1.3. Transmission Electron Microscopy

Evidence that the ordered structural features are preserved over SBA-15 samples than MCM-41 samples, after silylation reactions and subsequent metal immobilization, is directly provided from the transmission electron microscopy (TEM) images (Fig. 2.22). TEM of pristine mesoporous SBA-15 and MCM-41 samples show the images of channels and framework when the electron beam is passed perpendicular to the pore, demonstrating a highly ordered pore structure. After silylation, the hexagonal arrangement of SBA-15 preserves and after $(VO)^{2+}$ cation immobilization distinct spots of nano-sized metal sites in the ordered mesopore channels are clearly observed. However, for MCM-41, a significant decrease in the channel ordering is observed after silylation and after vanadium immobilization the structural degradation becomes more pronounced, that the MCM-41 structure undergoes a morphological change by agglomeration to large debris.

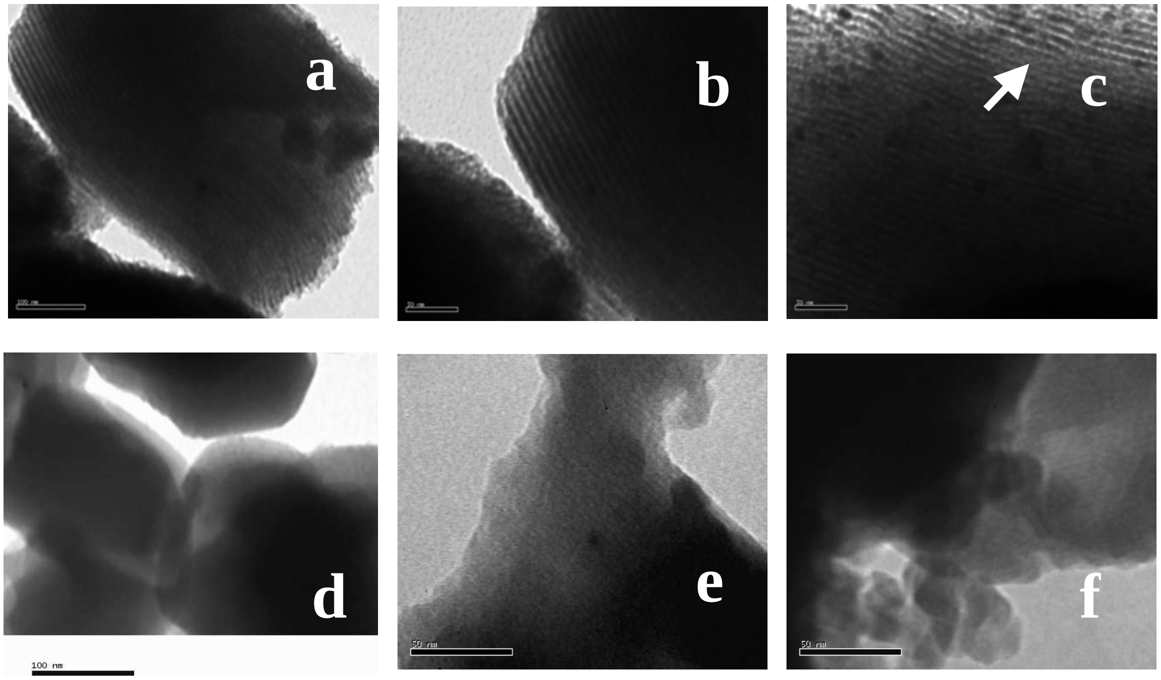

Figure 2.22. Transmission electron micrographs of: (a) Si-SBA-15, (b) NH_2-SBA-15, (c) VO-NH_2-SBA-15, (d) Si-MCM-41, (e) NH_2-MCM-41 and (f) VO-NH_2-MCM-41.

2.5.1.4. N_2 Adsorption and Desorption

Nitrogen adsorption-desorption isotherms of calcined, aminopropyl modified and vanadyl cations immobilized SBA-15 and MCM-41 samples are shown in Figure 2.23. Both the pristine mesoporous solids show Type IV isotherms, according to the IUPAC classification. SBA-15 samples show a sharp increase in the N_2 adsorption step at a higher P/P_o value (~0.7) and a distinct hysterisis loop with an almost parallel adsorption and desorption step (Type H1). The increased sharpness in the N_2 condensation step points to the uniformity of the mesopore structure.[2] Moreover, the width of the hysterisis loop did not change significantly after vanadyl cation immobilization showing the preservation of pore arrangement after the modifications.

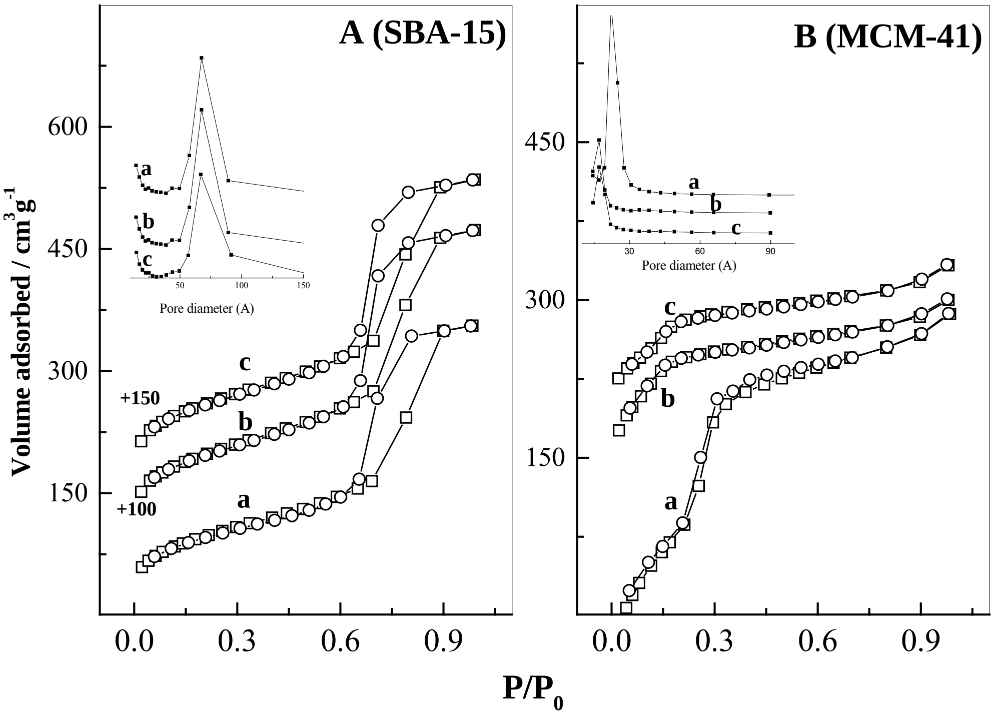

Figure 2.23. Nitrogen adsorption-desorption isotherms and pore size distribution curves (*insert*) of (A) SBA-15 and (B) MCM-41: (a) calcined sample, (b) aminopropyl modified sample and (c) vanadium-immobilized aminopropyl sample.

N_2 isotherm of Si-MCM-41 displays no hysterisis suggesting that the pore size is uniform and also the framework of the silica is composed of cylindrical channels without any intersecting disordered channels. However, compared to the pristine MCM-41 silica, the modified samples lack the sharpness in the N_2 condensation step relating a possible structural disordering. In addition, the pore size distribution (PSD) curves, obtained from the adsorption plot of the isotherm, show a sharp unimodal peak after modifications in SBA-15 samples while for MCM-41 samples the PSD curves get slightly broadened showing materials with less ordered pore structures (Fig. 2.23, insert). Thus, the physisorption results indicate that the textural properties of SBA-15 is almost preserved while MCM-41 samples show significant differences after 3-APTS grafting and are in accordance with the XRD and TEM results.

The specific surface area of SBA-15, MCM-41 and silica gel are 810, 849 and 444 m^2g^{-1}, respectively. The reduction in surface area after amino propyl modification is ~31% for SBA-15, ~40% for MCM-41 and ~37% for silica gel and the textural properties of all samples are summarized in Table 2.7. The significant decrease in surface area for the modified mesoporous materials shows that the anchoring of 3-APTS had occurred inside the mesopore channels and thereby reduces a large extent of their textural qualities. However, the reduction in surface area is rather less pronounced after the immobilization of the vanadyl cations.

Table 2.7. Characteristics of Vanadium-immobilized mesoporous samples and silica gel

Sample	Unit cell parameter (Å) [a]	Surface Area (m^2g^{-1})	Pore Volume (ccg^{-1})	Pore Diameter (Å)	Wall Thickness (Å) [b]
SBA-15	114	810	0.93	72	42
NH_2-SBA-15	107	559	0.82	67	40
VO-NH_2-SBA-15	104	532	0.78	67	37
MCM-41	40	849	0.68	32	8
NH_2-MCM-41	42	505	0.61	24	18
VO-NH_2-MCM-41	41	320	0.58	28	13
SG	-	444	n.d	n.d	-
NH_2-SG	-	279	n.d	n.d	-
VO-NH_2-SG	-	240	n.d	nd	-

[a] Unit cell parameter = $2d_{100}/\sqrt{3}$,

[b] Wall thickness = unit cell parameter – pore diameter, n.d = not determined.

The difference in structural ordering between SBA-15 and MCM-41 samples during modifications relates to the inherent property difference between the two mesoporous materials, for example, the difference in hydrothermal stability. In the present case, the wall thickness of pristine MCM-41 material is observed at 8 Å, which corresponds to only 3$[SiO_4]^{4-}$ layers where as SBA-15 posses an approximately five-fold increased wall thickness of 45 Å, which corresponds to around 10$[SiO_4]^{4-}$ layers. Hence, it is reasonable that the high temperature organo functionalization and subsequent synthesis procedures may cause some dissociation in the silica framework of MCM-41 and thus accounts for the partial structural collapse of the material after modifications. Thus the increased pore wall thickness and thereby the increased structural stability of the silica framework in SBA-15, prepared under acidic conditions, than the MCM-41 framework, prepared under basic conditions, explains the better stability of the SBA-15 solids than MCM-41 during surface modifications.[38]

Besides, the explanations after post synthesis modifications needs more attention because SBA-15 is not an extended form of MCM-41, having better stability and wall thickness. Generally, the calcined SBA-15, prepared below 100 °C synthesis temperature, possesses large amounts of micropores, where as MCM-41 is devoid from such pore size discrepancies. The formation of micropores is related to the penetration of hydrophilic EO chains (of P123 surfactant) into the silica framework, which upon calcination provides heterogenity in pore structure.[56] However, in high temperature SBA-15 synthesis, the degree of hydration around the EO blocks decreases, which in turn results in the redistribution of the EO blocks to the core region of the micelles leading to materials devoid of micropores. From *t*-plot analysis, it was observed that the present SBA-15 samples are free from micropores and the micropore volume amounts to only ~15% of the total pore volume of the sample. Kruk *et al.* suggested that the triblock copolymers, used as the structure orientor in SBA-15 synthesis, are polydisperse mixtures having a range of molecular weights, *i.e.,* they contains appreciable amounts of diblock EO-PO units as well as free PO units. These units which are not participating in the cooperative assembly process between surfactant and oligomerized silicate are believed to be involved in the creation of domains, which constitute to the complementary porosity of the SBA-15 samples.[57] Moreover, Galarneau *et al*. observed that a microporous corona surrounds the mesopores of the SBA-15 samples prepared at temperatures of 100-120 °C.[58] Thus even though SBA-15 samples show the absence of micropores from *t*-plot analysis, in reality, the materials prepared at 100 ^{o}C possesses micropores and these discrepancies arise due to the sensitive assumptions adopted in the BET equation and also due to the lack of an appropriate reference isotherm.[59] Hence, for a better comparison of SBA-15 and MCM-41 mesoporous materials, SBA-15 samples prepared at least at 100 ^{o}C (as in the present synthesis procedure) or greater are the optional candidates as these synthesis procedures remove the micropores in the samples, to a greater extent, otherwise the material may exhibit different adsorption properties due to the presence of micropores and mesopores.

2.5.1.5. FT-IR Spectra

FT-IR spectroscopy has been extensively used to study the surface properties of silica samples and, in particular, the stretching vibrations of surface silanols (v_{OH}) are very informative. The v_{OH} stretching vibrations observed in the 3600-3200 cm^{-1} region are attributed to the hydrogen bonded silanol groups and the sharp bands at ~3740 cm^{-1} for the isolated surface silanol groups. Stretching vibrations of geminal silanols are also observed in the same region of isolated silanols and hence it is very difficult to get distinguished them in the IR spectral patterns. However, Takei *et al*. suggested that the shoulder band observed around 3600 cm^{-1} relates to the presence of hydrogen bonded and isolated geminal silanols.[60]

In the present study, after 3-APTS functionalization, a complete disappearance of the isolated peak at 3740 cm^{-1} or a sharp decrease in its intensity with a peak shift to lower value was observed showing the role of surface silanols during modifications (Fig. 2.24). Moreover, it is also observed that the intensity of the hydrogen bonded silanol groups in the 3600-3200 cm^{-1} get decreased after 3-APTS functionalization. Generally, the free and the geminal silanol sites are the active silanol sites participating in the condensation reactions with the silylating agents while the hydrogen bonded silanol groups will not participate due to the efficient hydrophilic networks formed among themselves.[61] However, the present results imply that the hydrogen bonded silanol groups are also vulnerable in the reaction with aminopropyl groups.

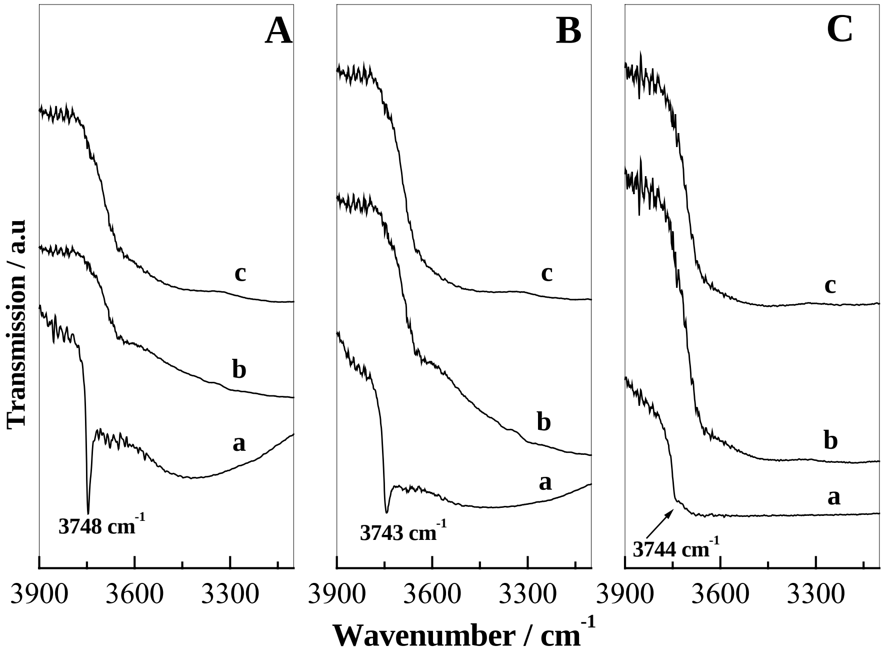

Figure 2.24. OH vibrations in the IR spectra of (A) SBA-15, (B) MCM-41 and (C) Silica gel: (a) calcined sample, (b) aminopropyl modified sample and (c) vanadium-immobilized aminopropyl sample.

Removal of surfactants from the pore channels of mesoporous materials and the attachment of aminopropyl groups over the silica surfaces was also examined by IR spectroscopy (Fig. 2.25). For surfactant removal from Si-SBA-15 and Si-MCM-41 materials, calcination procedures are employed on consideration that a complete removal of the surfactant groups can favour a uniform distribution of 3-APTS groups over the support surface and also to avoid the clogging of the aminopropyl moieties in the pore openings. The absence of strong absorptions in the range 3000-2700 cm^{-1} for the calcined SBA-15 and MCM-41 sample indicates the removal of surfactants, while the insertion of amino propyl groups were confirmed from the presence of N-H bending mode vibrations at 1520 cm^{-1} and at 3360, 3290 cm^{-1} corresponding to that of primary amines and the C-H stretching vibration of methylene groups at 2960, 2850 and 1660 cm^{-1}.[19,62,63] These results corroborate the attachment of aminopropyl groups on the solid supports. However, these bands appeared with less intense over the mesoporous supports while for the NH_2-

SG sample the bands are clearly observed with high intense patterns. Further a shift of the Si-OH band toward lower wave number (from 965 to 955 cm^{-1}) is noted after 3-APTS grafting and is probably due to the interaction between the $-NH_2$ groups and the silanol groups through hydrogen bonding, as illustrated in Scheme 2.3.[62b] After vanadium immobilization a shift in the amine peak to lower wave number is observed. These results explicitly indicate the anchoring of the vanadyl cations on the tethered $–NH_2$ groups and also prove that the organo siloxane groups had linked to the silica surfaces by the formation of Si-O-Si bonds and not through any electrostatic interactions or by hydrogen bonding interactions between the amine groups and the Si-OH groups.[34]

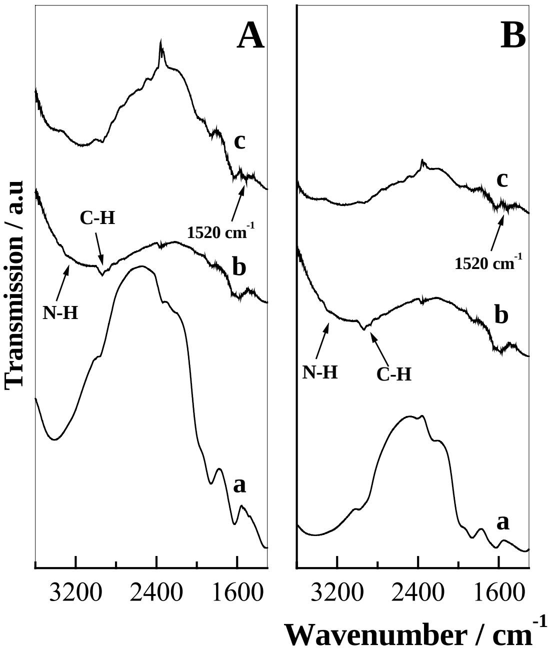

Figure 2.25. FT-IR spectra of (A) SBA-15, (B) MCM-41 and (C) Silica gel: (a) calcined sample, (b) aminopropyl modified sample and (c) vanadium-immobilized aminopropyl sample.

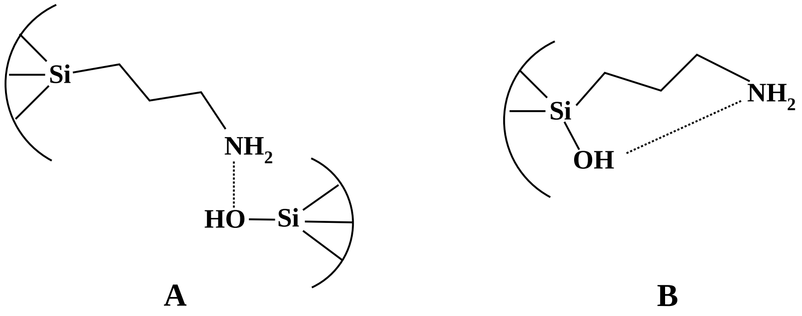

Scheme 2.3. Possible hydrogen bonding interactions: (A) intermolecular and (B) intramolecular Si-OH····NH_2 bridges.

2.5.1.6. ^{29}Si MAS NMR Spectra

NMR experiments were used to prove the anchoring of the silylating agents and to understand how these silylation procedures affect the structural properties of the support materials.

^{29}Si MAS NMR of propylamine functionalized silica materials exhibit peaks at –110, -101, -92 (sh), -65 and –57 ppm which are usually assigned to the Q^4 ($Si(OSi)_4$), Q^3 ($Si(OH)(OSi)_3$), Q^2 ($Si(OH)_2(OSi)_2$), T^3 ($SiR(OSi)_3$) and T^2 ($Si(OH)R(OSi)_2$) sites, respectively (Fig. 2.26). For comparison, the spectra of calcined parent support samples are also given in Figure 2.27. The broad resonance peaks from -90 to -110 ppm, of calcined samples, are indicative for a range of Si-O-Si bond angles and the formation of more tetrahedral silicon environments. Compared to parent silica samples, amine-functionalized silica samples shows a decrease in the Q^3 and Q^2 values with a corresponding increase in the percentage of Q^4 sites showing that the silylating agents effectively consumes the geminal as well as the free silanol sites.

In general, the Q^3 sites are considered to be rich with isolated Si-OH groups, which may be free or hydrogen bonded, while the Q^2 sites posses the geminal silanol sites (Scheme 2.4).[61] A decrease in the Q^3 and Q^2 values after silylation, over all the support materials, shows that these silanol groups are highly accessible to the silylating agents. Q^3+Q^2/Q^4 ratio indicates the presence of silanol groups residing on the support surface and a lower Q^3+Q^2/Q^4 value for propylamine functionalized samples suggest that the material posses few residual silanols, resulting in pore wall structure with higher degree of silica condensation.[64]

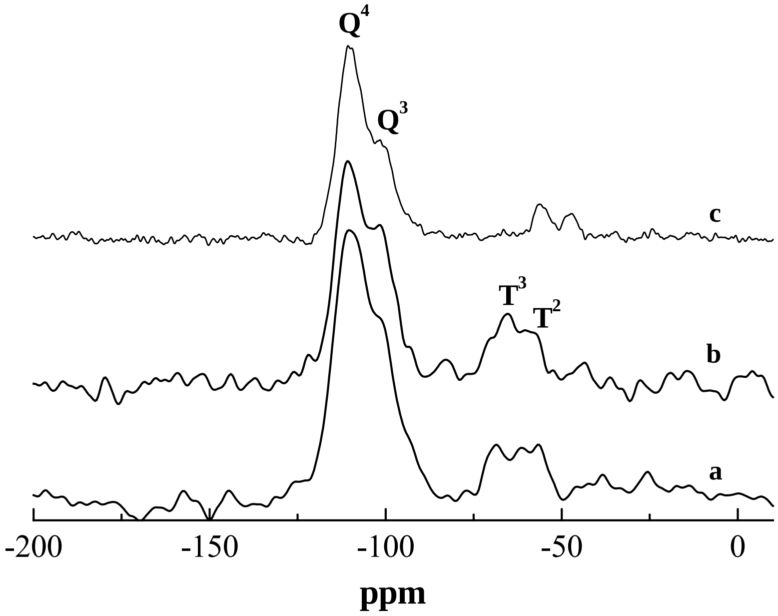

Figure 2.26. ^{29}Si MAS NMR results of aminopropyl modified silica samples: (a) NH_2-SBA-15, (b) NH_2-MCM-41 and (c) NH_2-SG.

Among the support samples, the higher Q^3+ Q^2/Q^4 ratio in MCM-41 indicates that MCM-41 possesses abundant silanol groups than SBA-15 and silica gel and these results explain the higher amine loading over MCM-41 sample than the other two samples (from elemental analysis). In addition, after 3-APTS functionalization, it was observed that the population of T^3 sites is more over MCM-41 than SBA-15 and silica gel. Thus the differences in the T^2/T^3 results, summarized in Table 2.8, shows that the population of silanol produced on the attached 3-APTS groups is more on silica gel, followed by SBA-15 and MCM-41, and suggests that the 3-APTS groups are randomly distributed over the silica gel sample than the mesoporous materials.[63] Usually, the 3-APTS groups interacts with one or two silanol groups of the support surface and get attached to the support as $SiC(SiO)(OH)_2$ or as $SiC(SiO)_2(OH)$, due to hydrolysis of the alkoxy groups. As mentioned, the isolated and the geminal silanol sites are the active silanols participating in the condensation reactions with the silylating agents, while the hydrogen bonded silanol groups will not actively participate due to the efficient hydrophilic networks formed among themselves. In the present synthesis, prior to post synthesis modification, water treatments or any out gassing temperature treatments was not carried out to enhance the number of silanol groups and thereby to increase the percentage of silylation. Thus the decreased T^2/T^3 ratio in NH_2-MCM-41 shows that more silanes are linked to each other than in the pore channels of NH_2-SBA-15 and NH_2-silica gel surface. Further, the ratio of silicon from the organic groups to the total silicon present, $\{\Sigma T^n/\Sigma(T^n+Q^n)\}$, shows an increased value in case of MCM-41 (13.7) than SBA-15 (13.0) and silica gel (11.8).

Table 2.8. ^{29}Si MAS NMR datas of pristine silica supports and amine-functionalized silica supports

Sample	Q^3+Q^2/Q^4	T^2/T^3	T^2+T^3/Q^2+Q^3	$\Sigma T^n/\Sigma\ (T^n+Q^n)$
SBA-15	0.47	-	-	-
NH_2-SBA-15	0.24	1.28	0.75	13.0
MCM-41	0.59	-	-	-
NH_2-MCM-41	0.31	0.62	0.65	13.7
SG	0.33	-	-	-
NH_2-SG	0.18	2.51	0.85	11.8

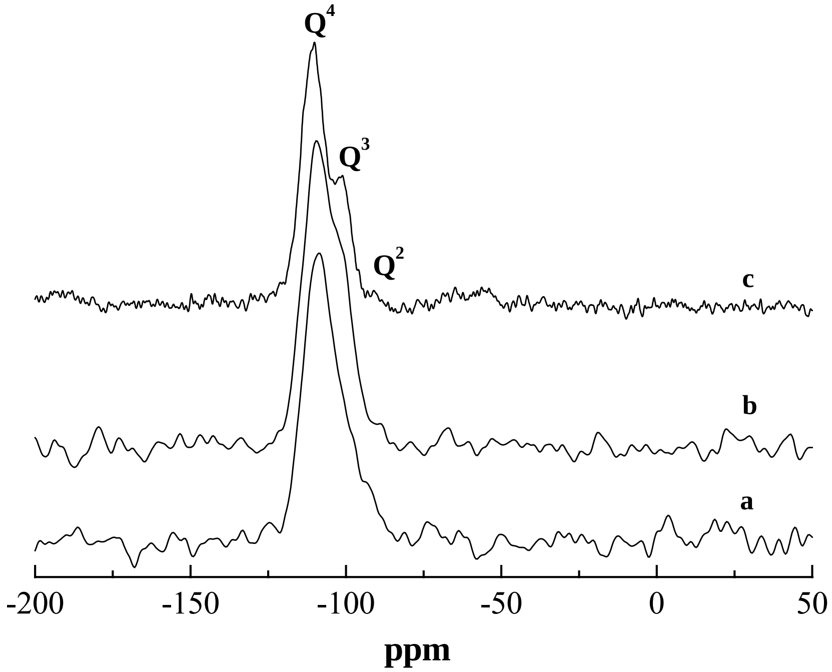

Figure 2.27. ^{29}Si MAS NMR results of calcined samples: (a) SBA-15, (b) MCM-41 and (c) Silica gel.

Hence, from the NMR interpretations, it can be concluded that more silanes are grafted on MCM-41 than the large pore SBA-15 and amorphous silica gel sample. Since steric factors do not affect the grafting of silanes on the support surface, as the pore diameter of the two mesoporous supports is sufficiently higher than the molecular size of silane, the decreased surface coverage over SBA-15 surface may be due to the blockage of some organic groups near the pore mouth because of the complementary textual characteristics of SBA-15. Since the silylation steps were performed under higher temperatures, it is also possible that the flexible wall structure of the MCM-41 sample gets deteriote to produce more silanol groups. These *in situ* formed silanol groups may also participate in the reaction with the organo silanols to enhance the percentage of 3-APTS groups than the hydrothermally stable SBA-15 sample. Proof for the formation of such silanols is not explored, but the increased structural collapse as well as the increased 3-APTS loading of the NH_2-MCM-41 sample than the NH_2-SBA-15 sample accounts for this suggestion. Thus, the more disordered structural features of the NH_2-MCM-41 material (from XRD/TEM/N_2 sorption measurements) after organic modification rely on a greater fixation of the trialkoxy organosilanes with the surface silanols and the increased consumption of the silanol groups may trigger the structural disordering.

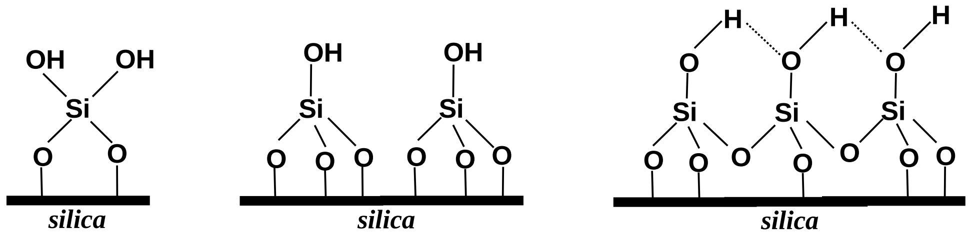

geminal silanols	isolated silanols	vicinal (hydrogen bonded) silanols
IR: 3600 cm^{-1}	**IR: 3745 cm^{-1}**	**IR: 3600-3200 cm^{-1}**
^{29}Si NMR: -92 ppm	**^{29}Si NMR: -102 ppm**	**^{29}Si NMR: -102 ppm**

Scheme 2.4. Schematic representation of the silanol groups in silica surfaces and their respective IR and NMR values.

2.5.1.7. UV-Vis Experiments

The UV-Vis spectra of vanadium-immobilized aminopropyl samples are given in Figure 2.28A. Even though, the vanadium species anchored on the amino groups are $(VO)^{2+}$, after all manipulations, the silica gel supported vanadium complexes are yellowish in color while the mesoporous supported vanadium catalysts are pale green colored. From the color of the complexes prepared, it is probable that the oxidation state of vanadium residing over mesoporous NH_2-SBA-15, NH_2-MCM-41 and NH_2-silica gel samples are different.

UV-Vis spectra of all as-synthesized materials show three intense absorption bands in the UV region, at 220, 280 and 340 nm. The band observed at 220 nm is typical of siliceous materials but bands in the 250-350 nm range show the presence of anchored vanadium. The absorption bands at 280 nm and 340 nm are assigned to the low energy charge transfer bands between V=O electron transfer from $(\pi)t_2$ to (d)e and $(\pi)t_1$ to (d)e of tetrahedrally coordinated V^{5+} ions.[65] However, all samples lack the characteristic d-d transition of $(VO)^{2+}$ ions usually observed in the visible region (600-800 nm). Hence, it is possible that some of the V^{4+} species may change its oxidation state from $^{+}4$ to $^{+}5$ during the drying process and thus the concentration of V^{4+} species on the support surfaces is low. Moreover, since the d-d transitions are ~10-30 times lower than the high intense charge transfer (CT) transitions in the 250-400 nm range a decreased intensity in the low frequency region is also expected.[11]

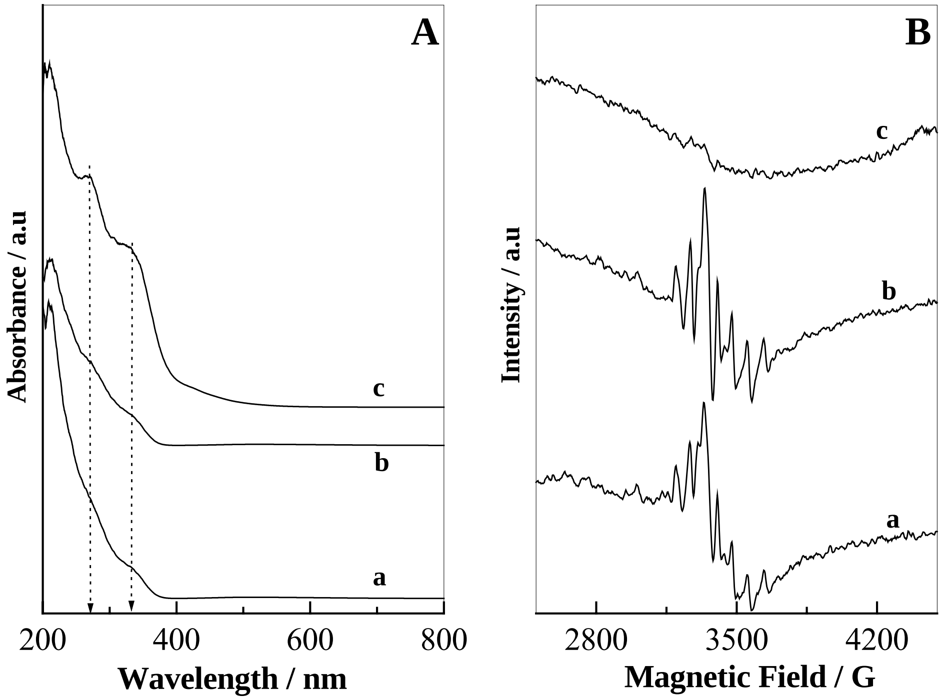

Figure 2.28. (A) UV-Vis and (B) EPR spectra of vanadium-immobilized silica samples: (a) VO-NH_2-SBA-15, (b) VO-NH_2-MCM-41 and (c) VO-NH_2-SG.

Among the three vanadium-immobilized samples, NH_2-silica gel supported vanadium catalyst shows high intense UV patterns. These results support the yellowish color of the VO-NH_2-silica gel sample and for an increased amount of V^{5+} species. Since the surface coverage of aminopropyl groups was least over the silica gel sample, it is also reasonable that the amino groups are not able to stabilize vanadium in the tetravalent state. However, the increased percentage of amino groups as well as the pore confinement in mesoporous materials may help to stabilize a part of the vanadyl cations in the tetravalent state than over the silica gel surfaces and these results are confirmed from the epr spectral patterns.

2.5.1.8. EPR Spectra

The EPR spectra of vanadium-immobilized NH_2-SBA-15, NH_2-MCM-41 and NH_2-SG samples, recorded at room temperature, are given in Figure 2.28B. All the as-synthesized mesoporous samples, exhibit the anisotropic eight-line hyperfine splitting patterns due to the interaction of the unpaired electron (V^{4+}, $3d^1$) with the nuclear spin of vanadium nuclei (I = 7/2). The well-resolved hyperfine splitting patterns obtained for the vanadium-containing mesoporous catalysts indicates that the $(VO)^{2+}$ ions are dispersed inside the pore channels of the mesoporous materials and the observed g values and the hyperfine coupling constants are typical of $(VO)^{2+}$ ions with distorted pseudo octahedral coordinations.[43]

In accordance with UV-Vis analysis, the silica gel immobilized vanadium sample lacks the hyperfine splitting patterns, which confirms that the entire vanadium anchored over NH_2-SG, is in $^+5$ oxidation state. This interesting result suggest that the structural and textural features of mesoporous materials are more suitable for the entrapment of metal complexes in specific oxidation states than over the conventional silica gel samples. However, a combination of the UV-Vis and epr analysis shows that, all the vanadium immobilized samples depicts sharp ligand to metal UV-Vis charge transfer (LMCT) transitions in the 200-400 nm, typical of V^{5+} species, while the epr patterns shows the presence of V^{4+} in case of mesoporous samples. Since epr is a sensitive characterization technique, where even ppm level of vanadium can get detected, it is speculated that the concentration of V^{4+} over the mesoporous materials is very less. Hence, the spectral characterization results show that the V^{4+} species over NH_2-silica gel sample is more vulnerable to change its oxidation state to the EPR silent V^{5+}, while the mesopore structural characteristics of SBA-15/MCM-41 help to retain a part of vanadium in its tetravalent state.

2.5.2. CATALYTIC OXIDATION OF CYCLOHEXANE

2.5.2.1. Reaction Procedure

Cyclohexane oxidation reactions were performed in a 10 mL round bottom flask fitted with a water-cooled condenser, using 30 wt.% *aqueous* H_2O_2 as an oxidant. The reactant mixtures of cyclohexane (0.8 g, 10 mmol), oxidant (1.12 g, 10 mmol) and acetonitrile solvent (5 mL) were added to 0.1 g of catalyst and heated at a constant temperature of 80 ^{o}C under magnetic stirring (*ca.* 800 rpm). After reactions, the reaction mixture was cooled to room conditions and the catalyst was separated from the reaction mixture by centrifugation. The oxidized products were analyzed on a gas chromatograph (HP 6890) equipped with a flame ionization detector (FID) and a capillary column (5 μm cross linked methyl silicone gum, 0.2 mm × 50 m).

2.5.2.2. Catalytic Results

The catalytic activity of the heterogenized vanadyl complexes in the oxidation reaction of cyclohexane with *aqueous* hydrogen peroxide (30 % H_2O_2) is given in Table 2.9. For comparison purpose, the activity over an isomorphously substituted vanadium-containing MCM-41 catalyst (V-MCM-41) is also included in Table 2.9. From table it is apparent that the vanadium-immobilized mesoporous catalysts show more activity and turn over frequency (TOF) than the framework substituted V-MCM-41 catalyst. The increased catalytic activity of the immobilized vanadium catalysts than the V-MCM-41 catalyst may arise from active metal site isolations, *i.e.,* attachment of catalyst to a support, in such a way that the catalytic sites no longer interact with each other. Thus effective site isolation, better coordination of the metal with the ligands and the tight attachment of ligands to the support, all may favour the high catalytic activity of the immobilized vanadium catalysts than the V-MCM-41 catalyst.[34,66] Further, it is worth meaning to mention that all the vanadium-immobilized aminopropyl catalysts had shown an almost similar conversion and TOF values. This result suggests the presence of similar vanadium structures over all the immobilized catalysts, and hence the coordination of vanadium is presumed to be similar over all the support systems.

Table 2.9. Oxidation of cyclohexane over Vanadium-immobilized catalysts using H_2O_2 as an oxidant

Catalyst	V (%) [a]	Conv. (mol.%)	Selectivity (%) [b]		TOF ($h^{-1}, 10^{-2}$) [c]	Vanadium Leaching (%) [a]
			Cy-ol	Cy-one		
VO-NH_2-SBA-15	0.92	21	58	42	9	11
VO-NH_2-MCM-41	0.95	19	62	38	8	13
VO-NH_2-SG	0.93	18	54	46	8	31
V-MCM-41	0.98	15	52	48	6	22

Reaction Conditions: T (°C) = 80; cyclohexane: oxidant (mol/mol) = 1; catalyst weight = ~10% of cyclohexane; solvent, CH_3CN (mL) = 5; time (h) = 12.

[a] Vanadium content determined by ICP-OES analysis.

[b] Cy-ol = cyclohexanol; Cy-one = cyclohexanone.

[c] Turnover frequency (TOF) = moles of cyclohexane converted/mole of vanadium/h.

The slightly improved catalytic performance of the vanadium-immobilized mesoporous catalysts than the VO-NH_2-SG catalyst can be explained from pore confinement effect, in which the substrate favorable interaction with both the pore walls as well as the catalyst molecule, enhance the conversion rate than the silica gel surfaces. Further, from the present results a reasonable question arise that, whether V^{4+}-O-$O^{\cdot}$ species or V^{5+}-O-$O^{\cdot}$ species is the active vanadium site for the present reaction. Since vanadium-immobilized NH_2-SBA-15 sample shows higher cyclohexane conversion, the epr spectrum of this sample is taken after its treatment with *aqueous* H_2O_2. The addition of H_2O_2 immediately changed the color of the catalyst from pale green to yellowish and the epr analysis shows the absence of eight-line hyperfine splitting patterns. Thus H_2O_2 treatment changed the oxidation state of heterogenized vanadium from its $^{+}4$ state to the epr silent $^+5$ state and hence it is possible that the active vanadium peroxo complex species be the V^{5+}-O-O$^{\cdot}$ species.[11,37]

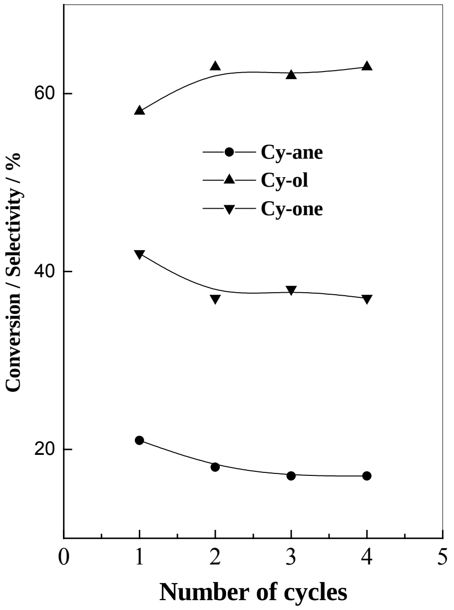

Figure 2.29. Recycling studies carried out over VO-NH_2-SBA-15 catalyst.

2.5.2.3. Recycle Studies

In order to assess whether the activity of the heterogenized vanadium catalysts arise from stable mesoporous materials, metal leaching studies are carried out. ICP-OES analysis was used to determine the percentage of vanadium leached out into the liquid mixture during reactions. It was found that among the mesoporous vanadium catalysts, the extent of leaching gets decreased in the order VO-NH_2-SG>V-MCM-41>VO-NH_2-MCM-41>VO-NH_2-SBA-15 (Table 2.9). Thus, the percentage of vanadium leaching in V-MCM-41 and VO-NH_2-silica gel samples is ~2-3 times higher than vanadium-immobilized NH_2-SBA-15 and NH_2-MCM-41 catalysts. The increased leaching of vanadium from the VO-NH_2-SG sample is related to the weak anchoring of the 3-APTS groups over the silica gel surface (increased T^2 sites from NMR results) and the further breakage of -Si-O-Si*- (Si* related to the silicon of organosilane) bonds in presence of *aqueous* oxidant. However, the decreased heterogenity of V-MCM-41 catalyst is related to the high temperature calcination used for the template removal and also due to the structural collapse of the mesoporous material in presence of *aqueous* oxidants

In addition, several recycling runs were carried out over the VO-NH_2-SBA-15 catalyst (Fig. 2.29). Results showed that during the first recycle (second run) the conversion get slightly decreased, whereafter the conversion and product selectivity remained more or less the same. Thus, the leveling off conversion and selectivity during subsequent cycles (up to fourth run) shows the existence of tightly held, isolated vanadium sites since if the metal is leached out, during subsequent recycling tests, the conversion as well as selectivity should varied. All these results point to the novelty of heterogenizing metal complexes in mesoporous materials through organo-tethered groups and the enhanced catalytic activity as well as the better stability of the organic-inorganic hybrid mesoporous hosts is attributed to the active metal site isolations, more hydrophobic environments as well as the spatial restrictions imparted from the concave silica surface in SBA-15 and MCM-41 than the convex silica surface of the silica gel sample.[67]

2.6. REFERENCES

1 J. S. Beck, J. C. Vartuli, W. T. Roth, M. E. Leonowicz, C. T. Kresge, K. D. Schmitt, C. T. W. Chu, D. H. Olson, E. W. Sheppard, S. B. McCullen, J. B. Higgins, J. L. Schlenker, *J. Am. Chem. Soc*. **1992**, *114*, 10834.

2 D. Zhao, Q. Huo, J. Feng, B.F. Chmelka, G.D. Stucky, *J. Am. Chem. Soc*. **1998**, *120*, 6024.

3 J. Y. Ying, C. P. Mehnert, M. S. Wong, *Angew. Chem. Int. Ed*. **1999**, *38*, 56.

4 A. Stein, B. J. Melde, R. C. Schroden, *Adv. Mater*. **2000**, *12*, 1403.

5 (a) A. Sayari, *Chem. Mater*. **1996**, *8*, 1840. (b) A. Corma, *Chem. Rev*. **1997**, *97*, 2373.

6 (a) K. M. Reddy, I. Moudrakovski, A. Sayari, *JCS., Chem. Commun.* **1994**, 1059. (b) P. Selvam, S. E. Dapurkar, *J. Catal*. **2005**, *229*, 64.

7 Z. Luan, J. Xu, H. He, J. Klinowski, L. Kevan, *J. Phys. Chem*. **1996**, **100**, 19595.

8 S. Gontier, A. Tuel, *Microporous Mater*. **1995**, *5*, 161.

9 J. S. Reddy, P. Liu, A. Sayari, *Appl. Catal. A Gen*. **1996**, *148*, 721.

10 Y. Deng, C. Lettmann, W. F. Maier, *Appl. Catal. A Gen*. **2001**, *214*, 31.

11 C-H. Lee, T-S. Lin, C-Y. Mou, *J. Phys. Chem. B* **2003**, *107*, 2543.

12 J. Evans, A. B. Zaki, M. Y. El-Sheikh, S. A. El-Safty, *J. Phys. Chem. B* **2000**, *104*, 10271.

13 L. Chen, T. Horiuchi, T. Mori, K. Maeda, *J. Phys. Chem. B* **1999**, *103*, 1216.

14 N. Lang, P. Delichere, A. Tuel, *Microporous Mesoporous Mater*. **2002**, *56*, 203.

15 V. Parvulescu, C. Anastasescu, B. L. Su, *J. Mol. Catal. A. Chem*. **2003**, *3919*, 1.

16 M. Kruk, M. Jaroniec, *Chem. Mater*. **2001**, *13*, 3169

17 S. C. Laha, P. Mukherjee, S. R. Sainkar, R. Kumar, *J. Catal*. **2002**, *207*, 1.

18 S. Shylesh, S. Sharma, S. P. Mirajkar, A. P. Singh, *J. Mol. Catal. A. Chem*. **2004**, *212*, 219.

19 W. Wang, Y-H. Tseng, J. C. C. Chan, S. Cheng, *J. Catal*. **2005**, *233*, 266.

20 G. N. Vayssilov, *Catal. Rev*. **1997**, 209.

21 J. R. Sohn, *Zeolites*, **1986**, *6*, 225.

22 S. Lim, G. L. Haller, *J. Phys. Chem. B* **2002**, *106*, 8437. (b) K. J. Chao, C. N. Wu, H. Chang, L. J. Lee, S-F. Hu, *J. Phys. Chem. B* **1997**, *101*, 6341.

23 K. A. Smith, *Semiconductors*, Cambridge University Press, Cambridge, **1978**.

24 J. Tauc, *Amorphous and Liquid Semiconductors*, J. Tauc (Ed.) Plenum, London, **1974**.

25 D. Wei, H. Wang, X. Feng, W. T. Chueh, P. Ravikovitch, M. Lyubovsky, C. Li, T. Takeguchi, G. L. Haller, *J. Phys. Chem. B* **1999**, *103*, 2113.

26 R. S. Weber, *J. Catal*. **1995**, *151*, 470.

27 D. G. Barton, M. Shtein, R. D. Wilson, S. L. Soled, E. Iglesia, *J. Phys. Chem. B* **2000**, *104*, 1516.

28 M. M. Koranne, G. G. Goodwin jr., G. Marcelin, *J. Catal*. **1994**, *148*, 369.

29 C-B. Wang, G. Deo, I. E. Wachs, *J. Catal*. **1998**, *178*, 640.

30 X. Gao, S. R. Bare, B. M. Weckhuysen, I. E. Wachs, *J. Phys. Chem. B* **1998**, *102*, 10842.

31 H. Brendt, A. Martin, A. Bruckner, E. Schreier, D. Muller, H. Kosslick, G. U. Wolf, B. Lucke, *J. Catal*. **2000**, *191*, 384.

32 B. Solsona, T. Blasco, J. M. Lopez Nieto, M. L. Pena, F. Rey, A. Vidyal Moya, *J. Catal*. **2001**, *203*, 443.

33 E. V. Kondratenko, M. Cherian, M. Baerns, D. Su, R. Schlogl, X. Wang, I. E. Wachs, *J. Catal*. **2005**, *234*, 136.

34 S. Shylesh, A. P. Singh, *J. Catal*. **2004**, *228*, 333.

35 H. Jing, Z. Guo, D. G. Evans, X. Duan, *J. Catal*. **2002**, *212*, 22.

36 R. A. Sheldon, M. Wallau, I. W. C. E. Arends, U. Schudhardt, *Acc. Chem. Res.* **1998**, *31*, 485.

37 H. Mimoun, L. Saussine, E. Daire, M. Postel, J. Fischer, R. Weiss, *J. Am. Chem. Soc.* **1983**, *105*, 3101.

38 (a) K. Cassiers, T. Linssen, M. Mathieu, M. Benjelloun, K. Schrijnemakers, P. Vander Voort, P. Cool, E. F. Vansant, *Chem. Mater*. **2002**, *14*, 2317. (b) R. Mokaya, *J. Phys. Chem. B* **1999**, *103*, 10204.

39 S. Shylesh, A. P. Singh, *J. Catal*. **2005**, *233*, 359.

40 A. E. C. Palmqvist, *Curr. Opinion in Colloid and Inter. Sci*. **2003**, *8*, 145.

41 W. Zhang, M. Froba, J. Wang, P. T. Tanev, J. Wong, T. J. Pinnavaia, *J. Am. Chem. Soc*. **1996**, *118*, 9164.

42 S. K. Mohapatra, P. Selvam, *Catal. Lett*. **2004**, *93*, 47.

43 M. Mathieu, P. Vander Voort, B. M. Weckhuysen, R. R. Rao, G. Catana, R. A. Schoonheydt, E. F. Vansant, *J. Phys. Chem. B* **2001**, *105*, 3393.

44 P. Selvam, S. E. Dapurkar, *Appl. Catal. A. Gen*. **2004**, *276*, 257.

45 H. Eckert, I. E. Wachs, *J. Phys. Chem*. **1989**, *93*, 6796.

46 K. J. Chao, C. N. Wu, H. Chang, I. J. Lee, S. Hu, *J. Phys. Chem. B* **1997**, *101*, 6341.

47 X. Gao, S. R. Bare, B. M. Weckhuysen, I. E. Wachs, *J. Phys. Chem. B* **1998**, *102*, 10842.

48 G. Xiong, C. Li, H. Li, Q. Xin, Z. Feng, *Chem. Commun*. **2000**, 677.

49 (a) N. N. Trukhan, V. N. Romannikov, E. A. Paukshtis, A. N. Shmakov, O. A. Kholdeeva, *J. Catal*. **2001**, *202*, 110. (b) O. A. Kholdeeva, A. Derevyankin, A. N. Shmakov, N. N. Trukhan, E. A. Paukshitis, A. Tuel, V. N. Romannikov, *J. Mol. Catal. A. Chem*. **2000**, *158*, 417.

50 A. Corma, P. Esteve, A. Martinez, *J. Catal*. **1996**, *161*, 11.

51 H. E. B. Lempers, R. A. Sheldon, *J. Catal*. **1998**, *175*, 62.

52 (a) B. Marler, U. Oberhagemann, S. Vortmann, H. Gies, *Microporous Mater*. **1996**, *6*, 375. (b) D. E. De Vos, B. F. Sels, P. A. Jacobs, *Adv. Catal*. **2001**, *46*, 1.

53 D. Brunel, *Microporous Mesoporous Mater*. **1999**, *27*, 329.

54 A. S. M. Chong, X. S. Zhao, *J. Phys. Chem. B* **2003**, *107*, 12650.

55 (a) D. Zhao, J. Feng, Q. Huo, N. Melosh, G. H. Fredrickson, B. F. Chmelka, G. D. Stucky, *Science* **1998**, *279*, 548. (b) J. A. Melero, G. D. Stucky, R. Grieken, G. Morales, *J. Mater. Chem*. **2002**, *12*, 1664.

56 M. S. Morey, S. O'Brien, S. Schwarz, G. D. Stucky, *Chem. Mater*. **2000**, *12*, 898.

57 M. Kruk, M. Jaroniec, C. H. Ko, R. Ryoo, *Chem. Mater*. **2000**, *12*, 1961.

58 A. Galarneau, H. Cambon, T. Martin, L-C. de Menorval, D. Brunel, F. D. Renzo, F. Fajula, *Stud. Surf. Sci. Catal*. **2002**, *141*, 395.

59 A. Galarneau, H. Cambon, F. D. Renzo, F. Fajula, *Langmuir* **2001**, *17*, 8328.

60 T. Takei, K. Kato, A. Meguro, M. Chikazawa, *Colloids Surf. A*. **1999**, *150*, 77.

61 X. S. Zhao, G. Q. Lu, *J. Phys. Chem. B* **1998**, *102*, 1556.

62 (a) A. B. Bourlinos, Th. Karakoatas, D. Petridis, *J. Phys. Chem. B* **2003**, *107*, 920. (b) G. Sartori, F. Bigi, R. Maggi, R. Sartorio, D. J. Macquarrie, M. Lenarda, L. Storaro, S. Coluccia, G. Martra, *J. Catal*. **2004**, *222*, 410.

63 H. Yoshitake, T. Yokoi, T. Tatsumi, *Chem. Mater*. **2002**, *14*, 4603.

64 W. H. Zhang, X-B. Lu, J-H. Xiu, Z-L. Hua, L-X. Zhang, M. Robertson, J-L. Shi, D-S. Yan, J. D. Holmes, *Adv. Funct. Mater*. **2004**, *14*, 516.

65 M. Chatterjee, T. Iwasawa, H. Hayashi, Y. Onodera, T. Ebina, T. Nagase, *Chem. Mater*. **1999**, *11*, 1368.

66 J. M. Thomas, T. Maschmayer, B. F. G. Johnson, D. S. Shephard, *J. Mol. Catal. A. Chem*. **1999**, *141*, 139.

67 J. M. Thomas, R. Raja, *Stud. Surf. Sci. Catal*. **2004**, *148*, 163.

3.1. INTRODUCTION

The catalytic activity as well as the stability of the mesoporous vanadium silica catalysts, described in Chapter 2, suggest that mesoporous organic-inorganic hybrid vanadium catalyst shows better heterogenity than the conventional V-MCM-41 catalysts. Although, the organic-inorganic hybrid aminopropyl immobilized vanadium catalyst shows better catalytic performance, the drawbacks of this class of materials relates to: (i) the lack of structural ordering of the materials at high organic loadings, (ii) the uneven distribution of the organo-functionalized groups on the support and (iii) the blocking of the pore channels of the mesoporous materials by the organic groups grafted inside, which will make the active sites inaccessible for larger molecules. In this context, it was worthy to synthesize organic-inorganic hybrid vanadium-containing mesoporous materials having organic groups in the frame wall positions.

The increasing demand of advanced materials for nanotechnology has stimulated research towards the specific design of nanostructured materials with tailored chemical and physical characteristics. Bridged silsesquioxanes, which were introduced by means of sol-gel synthesis more than a decade ago, represent the initial point to synthesize attractive hybrid materials with a wide variety of tunable properties.[1,2] The use of these organic linkers helps to prepare new nanocomposites with structuration at different scales. In this sense, much progress has been made in the last years for the preparation of new class of organic-inorganic hybrid materials, named as periodic mesoporous organosilicas (PMO), utilizing surfactant templated condensation of organosilanes with two or three trialkoxysilyl groups bridged by an organic linker group.[3-5] From a catalytic point of view, these materials can provide improved hydrophobicity which is increased by a suitable choice of the organo siloxane precursor, $(R'O)_3Si\mathbf{R}Si(OR')_3$, where $\mathbf{R}$ = $-(CH_2)_x-$, $-C_6H_5-$, $-CH{=}CH-$. Until now, a variety of organo-bridged hybrid mesoporous materials have been prepared and among them, because of the exceptionally high stability, ethane-bridged organic groups attracted considerable attention.[6-8]

This chapter describes the synthesis, characterization and catalytic properties of periodic mesoporous organosilicas and vanadium-containing mesoporous organosilicas, having ethane groups (-CH_2-CH_2-) in the frame wall positions, synthesized using cationic surfactants of various chain lengths *viz.*, C_{18}-, C_{16}- and C_{14}.

3.2. EXPERIMENTAL

3.2.1. Materials

For the synthesis of periodic mesoporous organosilica samples and their vanadium analogs, the following reagents were used: 1,2-bis(triethoxysilyl)ethane (BTEE, Aldrich), octadecyl trimethyl ammonium bromide (C_{18}-TAB, Aldrich), cetyl trimethyl ammonium bromide (C_{16}-TAB, Aldrich), tetradecyl trimethyl ammonium bromide (C_{14}-TAB, Aldrich), and vanadyl sulphate ($VOSO_4$. $3H_2O$, Aldrich). All chemicals were used as received without further purification.

3.2.2. Synthesis of Vanadium-containing Periodic Mesoporous Organosilicas having Ethane groups in the Frame wall Positions (V-PMO)

The synthesis of dimethylene silica hybrid periodic mesoporous organosilicas (PMO) and vanadium-containing hybrid mesoporous organosilicas (V-PMO) were carried out using an initial molar gel composition of 1BTEE-0.67C_n-TAB-3.20NaOH-420H_2O and 1BTEE-0.67C_n-TMABr-0.036VO_2-3.20NaOH-420H_2O, respectively, using alkyl trimethyl ammonium surfactants of various chain lengths (C_n-TAB, n = 18, 16, 14).

In a typical synthesis of V-PMO, an aqueous solution of 4.5 g C_{18}-TAB surfactant in 2.0 g sodium hydroxide was added slowly with vigorous stirring to a previously stirred solution of vanadyl sulphate in 6 g BTEE for homogenization. The final gel, having a molar composition of 1BTEE-0.67C_{18}-TAB-0.036VO_2-3.20NaOH-420 H_2O, was stirred for another 20 h at ambient temperature and then allowed to reflux for an additional 40 h at 95 °C. The white precipitate obtained was then collected by vacuum filtration, washed well with deionized water and finally dried at 80 °C for 2 h.

The surfactant inside the pores of the hybrid materials was removed by two methods: (a) by stirring 1 g of as-synthesized material with an HCl-EtOH (0.5 g - 100 mL) mixture at 70 ^{o}C for 6 h (V-PMO-E) and (b) by calcining the material in air at 540 ^{o}C for 6 h (V-PMO-C).

3.2.3. Instruments for Characterization

Powder X-ray diffraction patterns of the hybrid samples were recorded on a Rigaku D MAX III VC Ni-filtered Cu K_{α} radiation, λ=1.5404 Å, between 1.5 to 10° (2θ) with a scanning rate of 1^{o}/min and a step size of 0.02^{o}.

The specific surface area, total pore volume and average pore diameter were measured by N_2 adsorption-desorption method using NOVA 1200 (Quanta chrome) instrument. The samples were activated at 200 ^{o}C for 6 h under vacuum and then the adsorption-desorption was conducted by passing nitrogen over the sample, which was kept under liquid nitrogen. Pore size distribution (PSD) was obtained by applying the Barrer-Joyner-Halenda (BJH) pore analysis applied to the desorption branch of nitrogen adsorption-desorption isotherms.

Diffuse reflectance UV-Vis spectra of the samples were recorded in the range 200-800 nm in a Shimadzu UV-2101 PC spectrometer equipped with a diffuse reflectance attachment, using $BaSO_4$ as the reference. Specifically for the hydrated samples, the catalysts were kept under ambient conditions for 2 h while for the dehydrated samples, the catalysts were treated in dry air atmosphere at 550 ^{o}C for 5 h and flushed with an inert atmosphere, repeatedly, before taking the spectra.

Solid-state ^{13}C CP MAS NMR and ^{29}Si MAS NMR spectra were recorded on a Bruker MSL 300 NMR spectrometer with a resonance frequency of 75.5 MHz and 59.6 MHz for ^{13}C and ^{29}Si using 4 mm zirconia rotors and a sample spinning frequency of 3 kHz. ^{13}C spectra were collected with 70^{o} rf pulses, 5 s delay while ^{29}Si spectra were collected with 70^{o} rf pulses, 30 s delay and in both cases with ~6000 scans. The chemical shifts were referenced to glycine and TMS, respectively, for ^{13}C and ^{29}Si. ^{51}V MAS NMR was recorded under a magnetic field of 7.05 T, spinning at 7 kHz, on a DSX 300 spectrometer. Chemical shifts were referenced against liquid $VOCl_3$ by using ammonium metavanadate as a secondary reference. Raman measurements were done on a Jobin Yron TRIAX 550 triple grating spectrometer equipped with cryogenic charge-coupled device camera and diode pumped frequency-doubled solid state Nd:YAG laser of 532 nm (Model DPSS 532-400, Coherent Inc., USA).

3.3. CHARACTERIZATION

3.3.1. Powder X-Ray Diffraction

The powder X-ray diffraction patterns of as-synthesized and surfactant-extracted hybrid mesoporous organosilicas (PMO) synthesized using different chain length surfactants are shown in Figure 3.1. The C_{18}- surfactant shows better-resolved, distinct XRD patterns than the C_{16}- and C_{14}- chain length surfactants. These results suggest that longer alkyl chain surfactant yield more ordered and more stable mesoporous materials because longer alkyl chains being more hydrophobic, produce better defined cylindrical micelles. Interestingly, addition of the C_{18}- surfactant to the gel mixture resulted in an easy precipitation of the organosilicates, showing a strong interaction of the surfactant with the anionic oligomerized organosilicate species.[9,10] However, for the C_{16}- chain surfactant, precipitation was initiated only after prolonged stirring and for the short chain C_{14}- surfactant, the material precipitated out only after 5-10 h refluxing. These results indicate that an increase in the chain length of the surfactant (C_{18}-) helps to rearrange the organo silane to the hexagonal structure with high ordering. For the other surfactants (C_{16}-, C_{14}-), the decreased surfactant-organosilicate interactions and the less hydrophobic features may be the reason for the absence of long range ordered XRD peaks.

The XRD patterns of as-synthesized, surfactant-extracted and calcined V-PMO materials, synthesized with different chain length structure directors, are depicted in Figure 3.2 (A-C). The material obtained from the long chain C_{18}- surfactant showed the characteristic peaks in the low angle ($2\theta < 5^{o}$) indexed to the (100), (110) and (200) Bragg reflections.[2a] The surfactant-extracted materials displayed larger peak intensities than the as-synthesized samples. This may arise from the enhancement of contrast density between frameworks and pore channels. However, the V-C_{16}- and V-C_{14}- PMO samples showed only one broad peak without any higher-ordered Bragg reflections. From a comparison of the (100) peak intensity and peak width it is obvious that the scattering domain size becomes smaller, when smaller chain length surfactants were used for the synthesis of nanoporous hybrid materials. Furthermore, contrary to the results obtained with vanadium-containing M41S materials, a slight decrease in *d* spacing is noted for the V-PMO materials, as compared with the corresponding hybrid mesoporous materials (Table 3.1).[11] Though the V-O bond length (1.8 Å) is larger than the Si-O bond length (1.6 Å), it seems that the changes in the local bond angles due to the incorporation of the vanadium ions may compensate for the increase in the bond length. After calcination, a decrease in (100) peak intensity, long-range ordering and lattice contraction is observed, showing the further cross-linking of the framework silanols and/or the lack of ordering between adjacent pores.

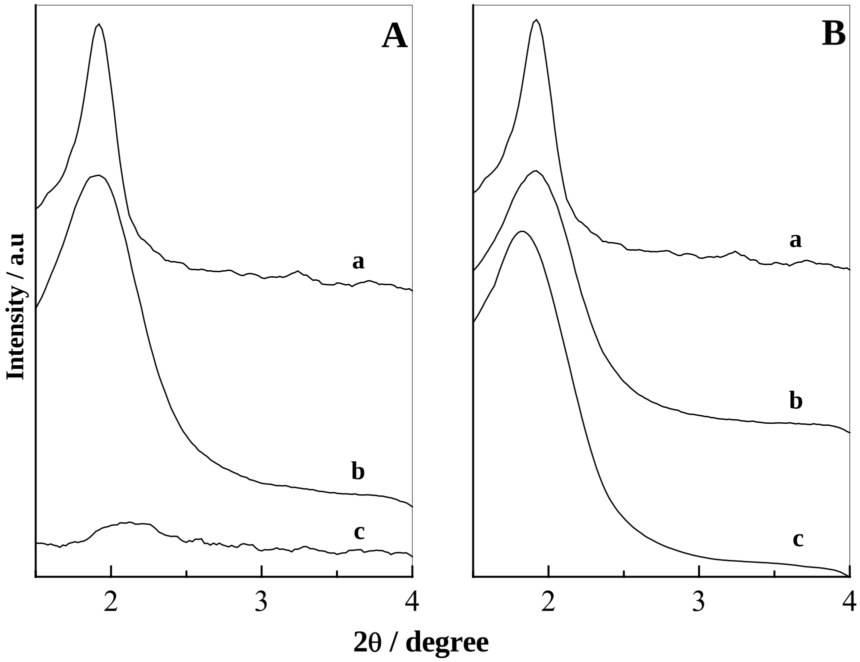

Figure 3.1. XRD patterns of organosilica samples: (A) as-synthesized and (B) surfactant-extracted samples, (a) C_{18}-PMO, (b) C_{16}-PMO and (c) C_{14}-PMO.

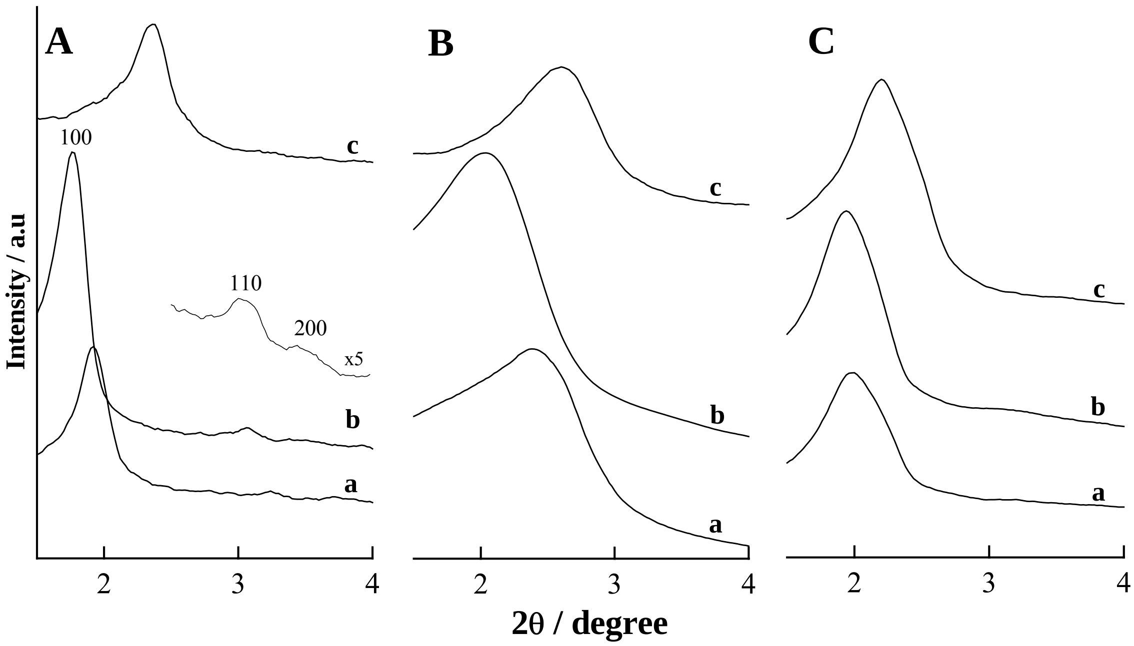

Figure 3.2. XRD patterns of (A) V-C_{18}-, (B) V-C_{16}-, and (C) V-C_{14}- PMO samples: (a) as-synthesized, (b) surfactant-extracted and (c) calcined samples.

In addition to the structural ordering, ICP-OES analysis showed that the hydrophobic nature and chain length of surfactant also plays a vital role in the percentage of vanadium incorporation (Table 3.1). Even though there is no stoichiometric incorporation of vanadium under the present synthesis conditions, it is likely that a large part of the metal remains in the gel solution when C_{16}- and C_{14}- surfactants were used. Thus, when the amount of vanadium incorporation was measured as a function of surfactant chain length, the percentage of vanadium was found high over the more hydrophobic chain length templated mesoporous solids. This result is related to the nature of bonding angle of vanadium and silicon, which means that if the surfactant chain length is long enough and more hydrophobic, it can form a large pore channel and the incorporated vanadium can be arranged along the pore channel more easily than in the small pore channel produced by the short chain length surfactants. Thus, longer alkyl chains being more hydrophobic produce well-defined cylindrical micelles and large pore channel, which in turn helps in a better incorporation of vanadium in the framework of the hybrid mesoporous materials. Hence, the present results show that vanadium can be incorporated more easily in the order of surfactant chain length, C_{18}-> C_{16}- > C_{14}-, showing that metal incorporation in the mesoporous solids also depend on the hydrophobicity of the surfactants.[12-16]

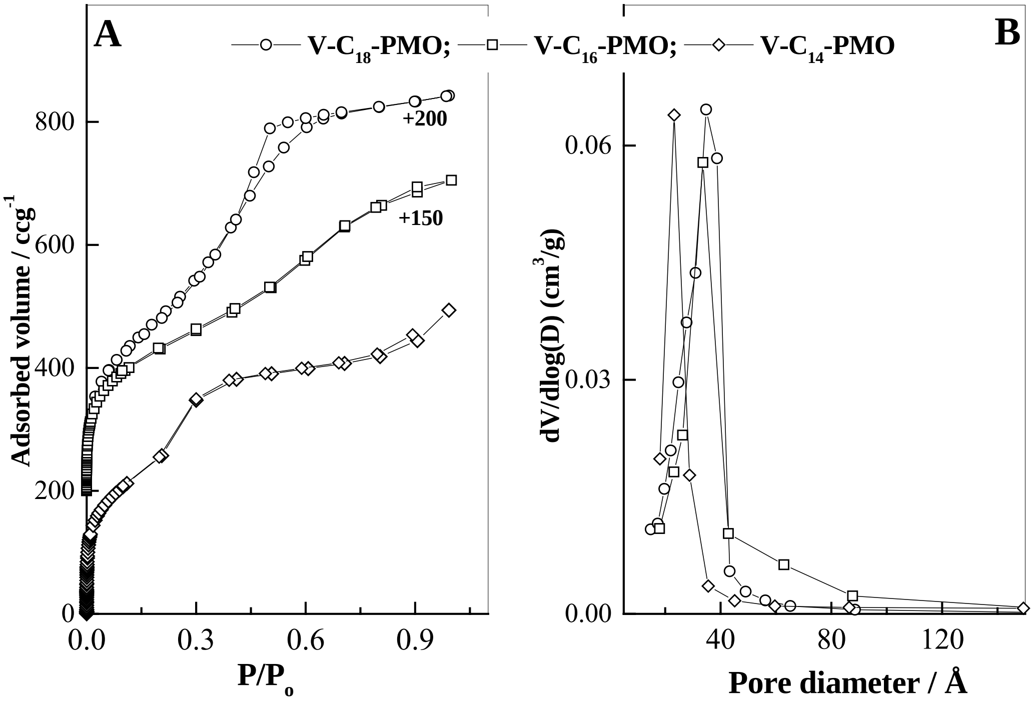

Figure 3.3. (A) Nitrogen adsorption-desorption isotherms and (B) pore size distribution plots of surfactant-extracted V-PMO samples. The isotherms are shifted along the *y* axis as indicated.

3.3.2. N_2 Adsorption and Desorption

N_2 adsorption-desorption analysis of the surfactant-extracted V-PMO samples showed Type IV isotherms, with a sharp increase in adsorption at P/P_o = 0.2-0.4, characteristic of materials with uniform mesopore structure (Fig. 3.3). It is known that the inflection position in N_2 isotherms depends on the diameter of the mesopores and the sharpness usually indicates the uniformity of the mesopores, due to capillary condensation of N_2.[17] Accordingly, the relative pressure for the vanadium-containing samples increased as the alkyl chain length gets increased, with narrow pore size distributions. Furthermore, the isotherms of the V-C_{14}- and V-C_{16}- samples show completely reversible isotherms, while the V-C_{18}- sample shows hysterisis. This hysterisis loop observed at high-pressure region for the long chain templated material indicates that the larger pores were filled at higher relative pressures. However, the calcined samples lost the sharpness in the capillary condensation step, suggesting a partial collapse of the mesostructure, as observed from the XRD measurements.

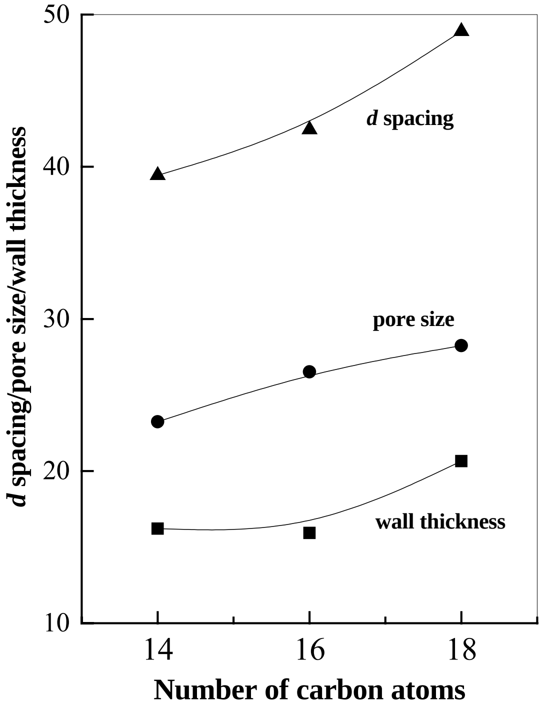

Figure 3.4. Plot of *d* spacing, pore size and wall thickness of calcined V-PMO materials *vs* number of carbon atoms in the surfactant chain.

The BET surface area, pore volume and pore diameter of the ethane-bridged hybrid materials calculated from the adsorption isotherms increase monotonically with the surfactant chain length and are tabulated in Table 3.1. A correlation of the textural properties and interplanar spacing of the calcined V-PMO materials with the surfactant chain length is further shown in Figure 3.4. The specific surface area of the surfactant-extracted V-PMO materials are in the range 702-877 m^2g^{-1}, while the calcined materials show a decrease of ~10-20% in surface area from the extracted materials. In addition, a decrease in pore size and an increase in wall thickness are noted for the V-PMO samples relative to the PMO samples. Even though, the same surfactant was used in the synthesis of organosilicas and corresponding vanadium-containing organosilicas, the decrease in pore size of the V-PMO materials shows the effect of vanadium and its interaction with the BTEE silica source in the synthesis gel. Usually, vanadium is incorporated in the mesoporous framework in two ways. First, it may be distributed along the pore walls and combine with two hydroxyl groups to form a tetrahedral coordination. This generally decreases the pore size of the material. Second vanadium may be incorporated deep inside the silica framework and the pore size may increase. Thus contrary to the observations with the V-MCM-41 samples, where a regular increase in pore size is observed with the vanadium loading (Section 2.4), the decrease in pore size of V-PMO than the pristine PMO samples shows that vanadium exist on the wall surface rather than incorporated deep in the frame wall positions.[11,13]

Table 3.1. Properties of V-PMO samples prepared from different chain length surfactants

Sample	V/Si (mol.%) [a]	Unit cell parameter (Å) [b]	Surface Area (m^2g^{-1})	Pore Volume (cm^3g^{-1})	Pore Diameter (Å)
V-C_{18}-PMO	0.39	54	877 (753)	0.83	34
C_{18}-PMO	-	55	912	0.85	36
V-C_{16}-PMO	0.16	49	734 (646)	0.78	34
C_{16}-PMO	-	49	720	0.81	34
V-C_{14}-PMO	0.13	48	702 (631)	0.76	32
C_{14}-PMO	-	47	711	0.78	32

[a] Determined by ICP-OES analysis. [b] Unit cell parameter = $2d_{100}/\sqrt{3}$.

3.3.3. Electron Microscopy

Figure 3.5 shows the TEM image of C_{18}-PMO and vanadium-containing C_{18}-PMO sample. Unlike the literature reports over ethane-bridged hybrid mesoporous materials, the present samples show a wormlike pore arrangement, with disordered channel structures.[18]

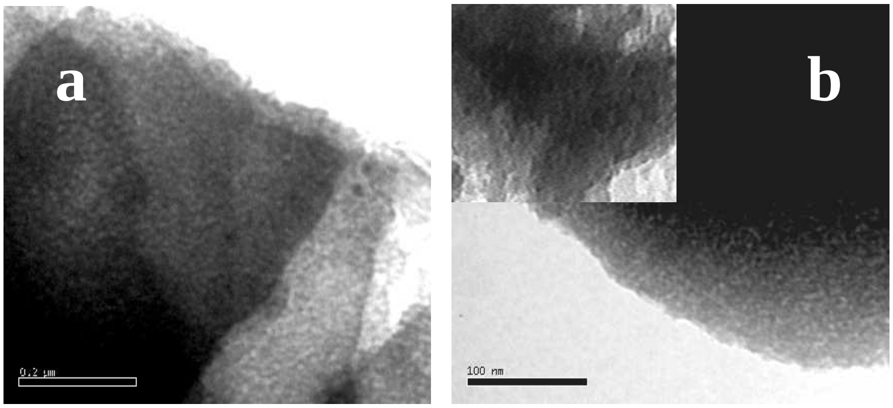

Figure 3.5. TEM images of: (a) C_{18}-PMO and (b) V- C_{18}-PMO, insert in (b) shows the zoom over the TEM image.

Usually, periodic mesoporous organosilicas (PMO) show new symmetries and rich morphologies than the periodic mesoporous silica (PMS) materials under various structure directors/treatment conditions due to the presence of integrated organic groups. The formation of unusual, 2D cubic and 3D hexagonal mesophases in presence of cationic surfactants is a good and rare example for such behaviour, while M41S silicates hardly show such a nature due to the higher anionic charge density.[19] Moreover, SEM images shows a systematic difference in the morphology of the hybrid samples when surfactants of different alkyl chain lengths were used (Fig. 3.6). The organovanadium silica hybrid material prepared using C_{18}- surfactant showed distinct hexagonal facetted tubes of *ca.* ~8-10-μm in diameter. In contrast, the C_{16}- templated material showed flake-like structures of different sizes and shapes of *ca.* ~5-7-μm in the entire region scanned. However, the material synthesized with the C_{14}- surfactant showed disordered hexagonal-like faces of *ca.* ~3-4-μm diameter, with the presence of spherical structures (Fig. 3.6

c&d). The systematic morphological differences suggest that slight changes in the gel conditions of PMO can lead to materials with unexpected morphologies, which in turn is attributed to the organic species integrated in the wall positions.

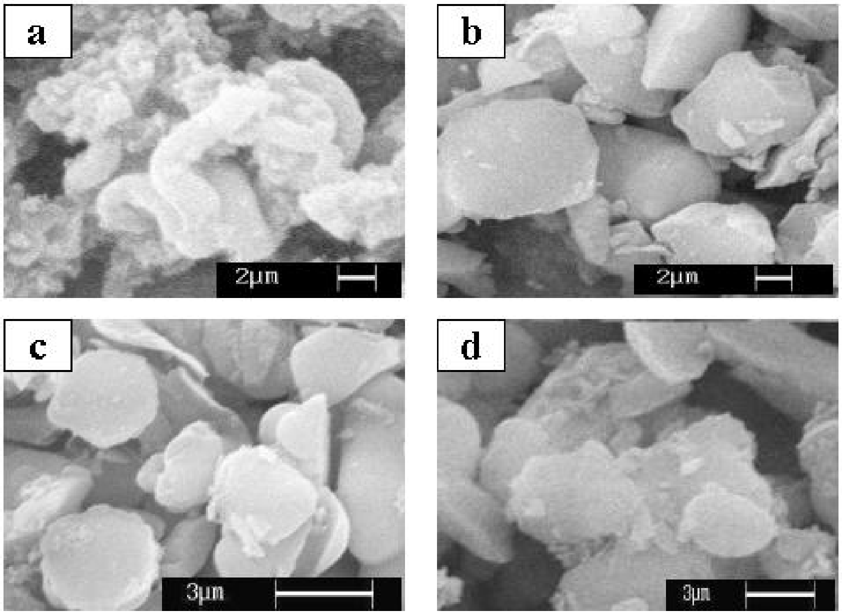

Figure 3.6. SEM images of V-PMO samples: (a) V-C_{18}-, (b) V-C_{16}-, (c) and (d) V-C_{14}-.

3.3.4. ^{29}Si MAS NMR Spectra

^{29}Si MAS NMR spectra of surfactant-extracted V-PMO samples showed the presence of two peaks, one at –57 ppm for the T^2 sites, (C(OH)**Si**-$(OSi)_2$) and other at –68 ppm for the T^3 sites, (C**Si**-$(OSi)_3$). The spectra are devoid of Q^n silicons (Q^n = **Si**$(OSi)_n(OH)_{4-n}$, n = 2-4), showing a complete retention of the bridging organic groups (Fig. 3.7).[3] Thus, during the synthesis of hybrid materials and vanadium-containing hybrid materials no silicon-carbon bond cleavage of the BTEE precursor had occurred. Figure 3.6B further shows the silicon NMR results of surfactant-extracted C_{18}-PMO, V-C_{18}-PMO and calcined V-C_{18}-PMO sample. From figure it is apparent that after calcination, the V-C_{18}-PMO sample devoids T^n sites and shows the presence of Q^n sites, which indicates that the calcination treatments had removed the organic groups from the wall positions and thereby enhance structural disordering and lattice contraction.

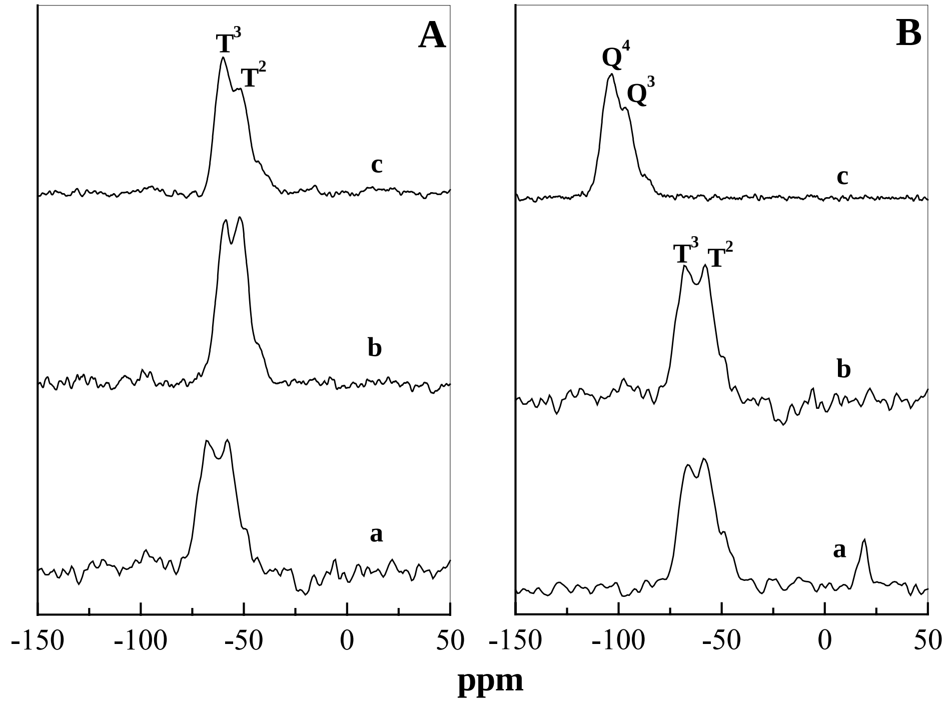

Figure 3.7. ^{29}Si MAS NMR plots of: (A) surfactant-extracted V-PMO samples, (a) V-C_{18}-PMO, (b) V-C_{16}-PMO, (c) V-C_{14}-PMO and (B) hybrid samples prepared using C_{18}-surfactant, (a) C_{18}-PMO, (b) V-C_{18}-PMO and (c) calcined V-C_{18}-PMO.

3.3.5. ^{13}C CP MAS NMR Spectra

^{13}C CP MAS NMR of all vanadium-containing hybrid samples showed a single sharp signal at 5.6 ppm, corresponding to the Si-CH_2-CH_2-Si fragment, proves the intactness of the bridge after the extraction process (Fig. 3.8).[3] The absence of peaks in the 10-30 ppm region indicates the complete removal of the occluded surfactant species, and the absence of peaks at 15 and 58 ppm, assigned to SiO-CH_2-CH_3 species, confirms that the hydrolysis of the organo silane monomers is complete. Thus, NMR results confirm that the porous network of surfactant-extracted hybrid samples is comprised of $_{1.5}$OSi-$(CH_2)_2$-$SiO_{1.5}$ units.[3-5]

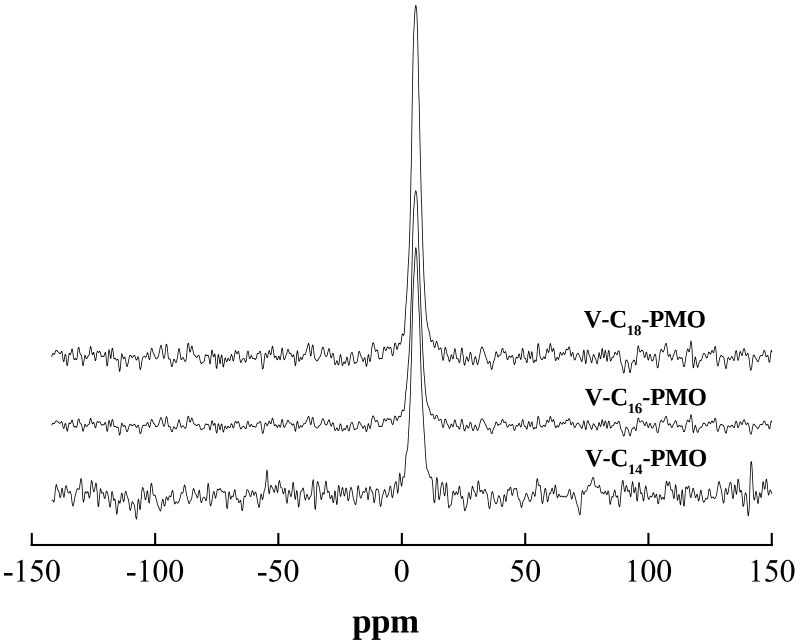

Figure 3.8. ^{13}C CP MAS NMR spectra of surfactant-extracted vanadium-containing PMO samples.

3.3.6. UV-Vis Experiments

Figure 3.9 depicts the UV-Vis spectra of V-PMO samples obtained using different chain length surfactants and, for comparison, with the spectrum of crystalline V_2O_5 and V-MCM-41. The as-synthesized V-PMO materials were white in color, while after calcination and exposure to ambient conditions the material became pale yellowish (V-C_{18}-) and the process is reversible during hydration and dehydration. The absorption bands observed at 260 nm and 340 nm are usually assigned to the low energy charge transfer bands between V=O electron transfer from $(\pi)t_2$ to (d)e and $(\pi)t_1$ to (d)e of tetrahedrally coordinated V^{5+} ions. In detail, for V-C_{18}-PMO, the 260 nm band (~83%) is assigned to the low energy charge transfer transition between the tetrahedral oxygen atoms and the central V^{5+} ions inside the wall surface while the presence of bands above 300 nm (~17%) indicates higher coordinated vanadium atoms in extra-framework positions, due to the possible hydration effects after calcination.[11] Thus, the higher ratio of 260 nm band is a good indication for the presence of tetrahedral vanadium in frame wall positions. However, for the V-C_{16}- and V-C_{14}-PMO samples the 260 nm band is broadened without any red shift and the absence of peak above 300 nm shows that tetrahedral symmetry may be the local structure for the comparatively short chain surfactants. These results indicates that vanadium resides in distorted tetrahedral environment in V-PMO samples, due to the amorphous pore wall nature of the mesoporous materials.[20] In addition, the absence of peaks in the visible region confirms that the materials essentially contain tetrahedrally coordinated V^{5+} species having terminal V=O bands and that the vanadium species are isolated and highly dispersed on the support surface (Fig. 3.9).

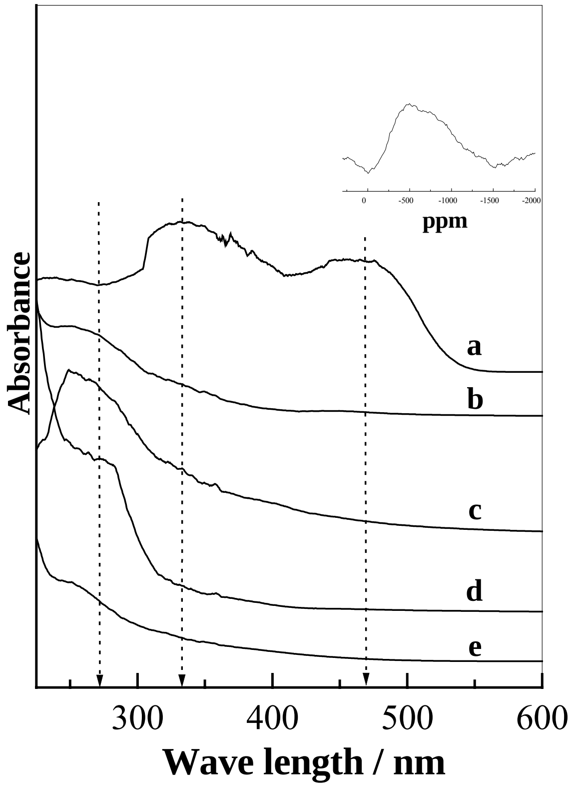

Figure 3.9. Diffuse reflectance UV-Vis spectra of V-PMO samples, V-MCM-41 and V_2O_5: (a) V_2O_5, (b) V-C_{18}-, (c) V-C_{16}- (d) V-C_{14}- and (e) V-MCM-41. Inset shows the ^{51}V MAS NMR spectrum of calcined V-C_{18}-PMO sample.

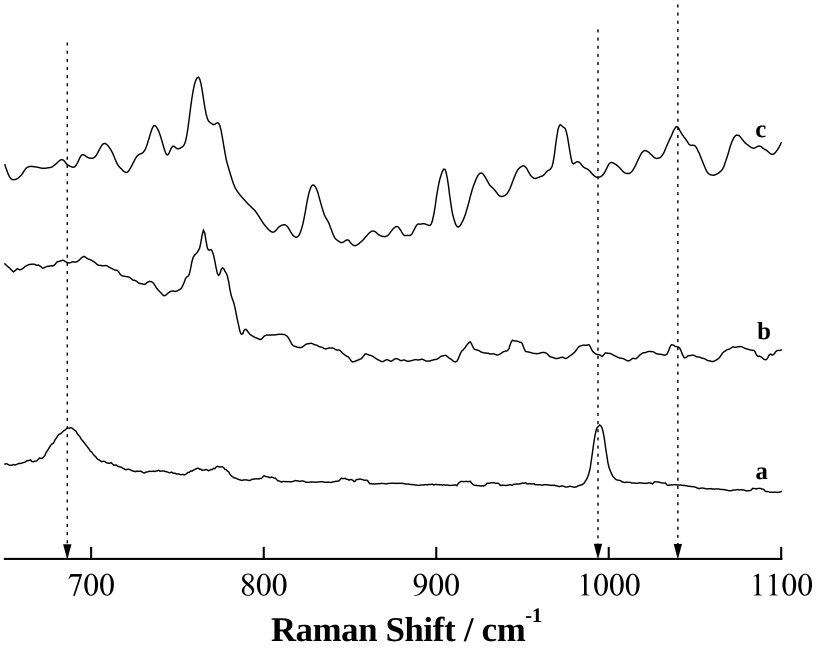

Figure 3.10. Raman spectra of: (a) V_2O_5, (b) V-C_{18}-PMO and (c) V-MCM-41.

3.3.7. ^{51}V MAS NMR and FT-Raman Spectra

The ^{51}V MAS NMR spectrum of the calcined V-C_{18}-PMO material was given in Figure 3.9 (inset). Since no signals were observed in the –300 ppm region, the formation of crystalline V_2O_5 can be avoided. Therefore, it is assigned that most of the vanadium is incorporated in the hybrid silica framework as tetrahedral sites with oxygen ligands. However, unlike the sharp signals observed for V-MCM-41 materials, the V-PMO sample produces a less intense, broad signal after -500 ppm, showing that vanadium exists in disordered tetrahedral environment on the support surfaces.[13,21] Hence, to gain a better understanding about the nature of vanadium residing over the hybrid samples, Raman analysis was carried out and was compared with a V-MCM-41 material and pure V_2O_5 (Fig. 3.10). Interestingly, the V-PMO and V-MCM-41 sample showed an intense band at 1039 cm^{-1} attributed to the stretching vibrations of short V=O bonds of isolated vanadium tetrahedra.[22]. Furthermore, as noted from UV-Vis and ^{51}V NMR, the Raman analysis also confirms that the V-PMO material devoid crystalline V_2O_5 peaks, which are usually observed at 995 and 695 cm^{-1}.[22,23] Thus, the information collected from all spectroscopic techniques confirms that the vanadium species in the hybrid materials are isolated and dispersed on the support surface.

3.3.8. Hydrothermal Studies

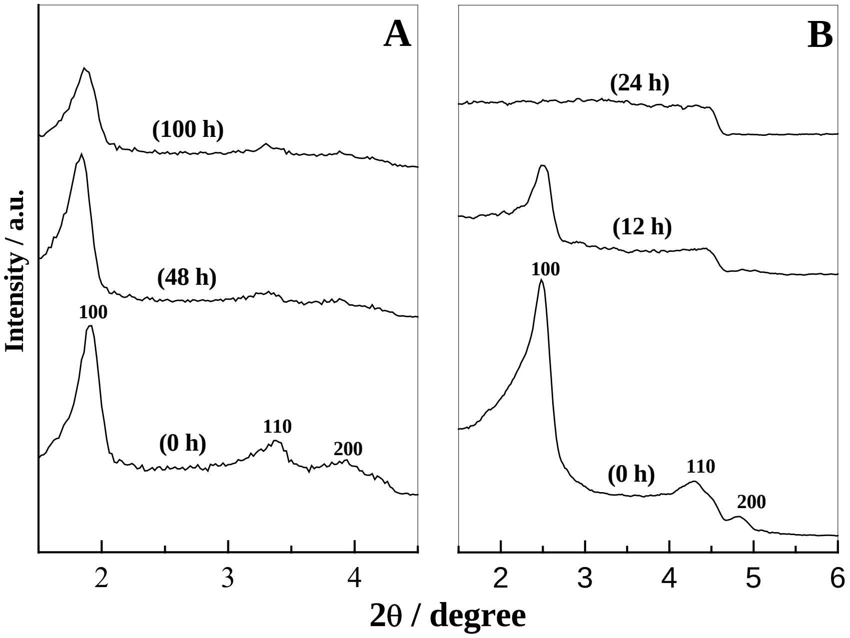

Figure 3.11. XRD patterns of: (A) C_{18}-PMO and (B) Si-MCM-41 samples before and after reflux in boiling water. Numbers in parenthesis represents the reflux time in water.

For potential application of the developed hybrid materials in heterogeneous catalysis and separation science, it is desirable that the material posses high hydrothermal stability. Hence, the hydrothermal stability of the ethane-bridged hybrid material was evaluated by refluxing the materials in water (1 g/100 mL) for various time periods and the changes are compared with a Si-MCM-41 material. XRD patterns shows that the organosilicas having ethane groups in the frame wall positions retains its structural ordering even after 100 h reflux in boiling water and exhibits the characteristic (100) and (110) diffraction peaks (Fig. 3.11A). Meanwhile, the Si-MCM-41 sample shows large attenuation in the XRD pattern, after a 12 h reflux time, and the structure gets completely destroyed after 24 h reflux time (Fig. 3.11B).

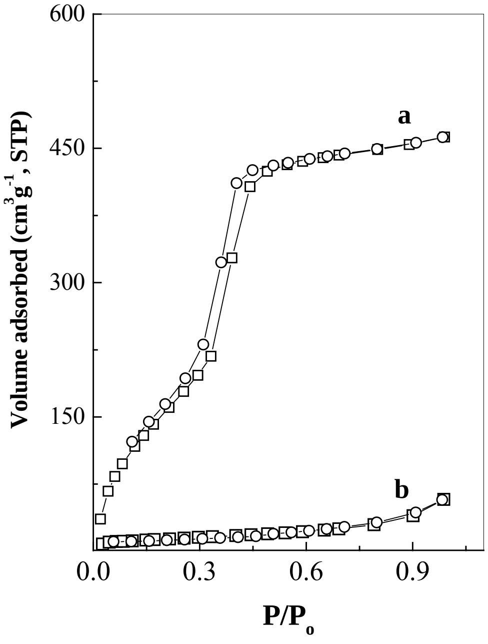

Figure 3.12. N_2 adsorption-desorption isotherms of: (a) C_{18}-PMO and (b) Si-MCM-41 after reflux in boiling water for 100 h and 24 h, respectively.

N_2 adsorption-desorption isotherm of the samples are also measured after reflux in boiling water, *i.e.,* after 100 h for the hybrid organosilica sample and after 24 h for the Si-MCM-41 sample. In accordance with the XRD measurements, the hybrid sample retains the type IV isotherm, with a slight shift in the P/P$_o$ to lower values, while the Si-MCM-41 sample shows a completely destroyed structure after 24 h reflux (Fig. 3.12). Moreover, it was also observed that the surface area and pore volume of the hybrid sample gets reduced to only ~30% and ~35% after 168 h reflux time (1 week) while for Si-MCM-41 the surface area and pore volume reduced to >70% and >90% of the original value, after 24 h reflux time. Since Q^3/Q^4 ratio of Si-MCM-41 material parallels the T^2/T^3 sites of PMO sample, the higher hydrothermal stability of the hybrid organosilica sample explicitly arise from the presence of the homogenously dispersed ethane groups in the frame wall positions, which may enhance the hydrophobicity of the material than the conventional Si-MCM-41.[24] These results had significance in heterogeneous catalysis as a more ordered mesoporous channel can expose the active sites better for the diffused reactant species and hence the PMO materials can be reused for several catalytic runs.[25]

3.4. CATALYTIC EPOXIDATION OF STYRENE

3.4.1. Reaction Procedure

Epoxidation reactions were carried out in a round bottom glass batch reactor fitted with a water-cooled condenser, using *aqueous* H_2O_2 (30%) and TBHP (70%) as oxidants. The reactant mixtures of substrate (8 mmol), oxidant (2 mmol), and acetonitrile solvent (5 mL, dried over 4 Å molecular sieves) were added to the catalyst (10% of styrene) and heated in an oil bath at 70 ^oC, under magnetic stirring (*ca.* 800 rpm). After reaction, the reaction mixture was cooled to room conditions and the catalyst was separated from the reaction mixture by centrifugation. The oxidized products were analyzed on a gas chromatograph (HP 6890) equipped with a flame ionization detector (FID) and a capillary column (5 μm cross-linked methyl silicone gum, 0.2 mm × 50 m) and were further verified by GC-MS (Shimadzu 2000 A). The presence of residual oxidant at the end of reaction was checked by means of standard iodometric titration.

3.4.2. Catalytic Results

In order to understand, how the pore size, morphology and hydrophobicity influence the catalytic properties, the surfactant-extracted and calcined V-PMO catalysts were applied in the liquid phase epoxidation reaction of styrene (Table 3.2). Figure 3.13 shows the kinetic results of styrene epoxidation over V-C_{18}-PMO catalyst in presence of *aqueous* H_2O_2 and *tert*-butylhydroperoxide (TBHP) oxidants. The low styrene conversion obtained with TBHP than H_2O_2 oxidant is related to the low percentage of active oxygen content in TBHP (7.5%) than the H_2O_2 oxidant (47%).

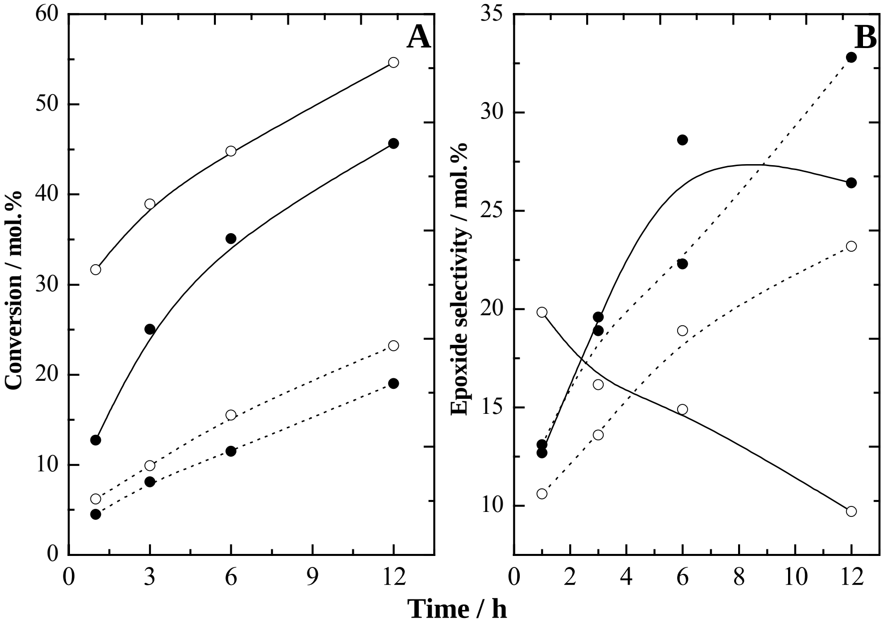

Figure 3.13. (A) Styrene conversion and (B) styrene oxide selectivity observed over V-C_{18}-PMO catalyst: (o) calcined catalyst and (●) surfactant-extracted catalyst, where solid lines represent the catalytic activity using H_2O_2 oxidant and dotted lines represent the activity using TBHP oxidant.

In the absence of catalyst or vanadium-free hybrid materials, a very low styrene conversion was noted and the product obtained was mainly benzaldehyde. Addition of V-PMO catalyst increased the styrene conversion, showing a good utilization of H_2O_2 by the tetrahedral vanadium sites prevailing inside the hybrid organosilica matrix. The V-PMO catalyst prepared from the C_{18}- surfactant showed better conversion than the samples prepared from the relatively short-chain templated V-C_{16} and V-C_{14}-PMO. This may be due to lower vanadium concentrations in the short chain templated samples or to the decreased mesostructural ordering of the hybrid materials, when using surfactants having carbon numbers of 16 and 14. In fact, Parvulescu *et al*. showed for V-MCM-41 samples that the structural ordering can also influence the catalytic properties of the mesoporous materials, since for a structurally ordered material all the active sites are readily available for the diffused reactant species.[25] Hence, any of the above factors or a combination of both, may result in the higher conversion rates of the C_{18}- templated vanadium catalyst.

Styrene oxide and benzaldehyde are the main products observed in the epoxidation reaction of styrene with H_2O_2 over surfactant-extracted ethane-bridge containing V-PMO catalysts. However, an equal percentage of phenyl acetaldehyde as that of styrene oxide is also noted over the calcined V-PMO catalysts and V-MCM-41 (Table 3.2). This result shows that, because of the hydrophobic $-CH_2-CH_2-$ groups in surfactant-extracted V-PMO catalyst, the formed epoxide, which is polar in nature desorbs quickly and thereby limits its further transformations. Earlier literature reports over TS-1 catalyst show that, the formation of phenyl acetaldehyde occurred through isomerization or rearrangement of the formed styrene epoxide product.[26] However, recent *in situ* NMR and EPR studies revealed that styrene oxide and phenyl acetaldehyde are formed by two competing processes and that phenyl acetaldehyde is not formed from further reaction of styrene oxide.[27]

In the present kinetic studies with V-C_{18}-PMO-C catalyst, it was observed that the percentage of benzaldehyde and styrene oxide decreased at longer reaction time. The decrease in the percentage of benzaldehyde is due to its over oxidation to benzoic acid (Scheme 3.1, route (iv)). However, a corresponding increase in the percentage of phenyl acetaldehyde with styrene oxide was not observed and hence it is reasonable that the formation of aldehyde is not at the expense of the epoxide product. Therefore, it is expected that styrene oxide and phenyl acetaldehyde may form by two competing processes or mechanisms over the organovanadium hybrid catalysts. In addition, blank experiment shows benzaldehyde as the major product, with selectivity >99 % (Table 3.2). However, the presence of vanadium catalysts helps to decrease the benzaldehyde selectivity, as observed over many titanium-containing catalysts, with an increase in the formation of the styrene oxide and/or phenyl acetaldehyde.[28] Hence, the presence of catalyst helps to shift the formation of products in favour of route (ii) or (iii) (Scheme 3.1). Thus, the formation of all three main products, *viz.*, benzaldehyde, styrene oxide and phenyl acetaldehyde, is anticipated to proceed in three parallel routes or that the active oxygen species for each formation is different.

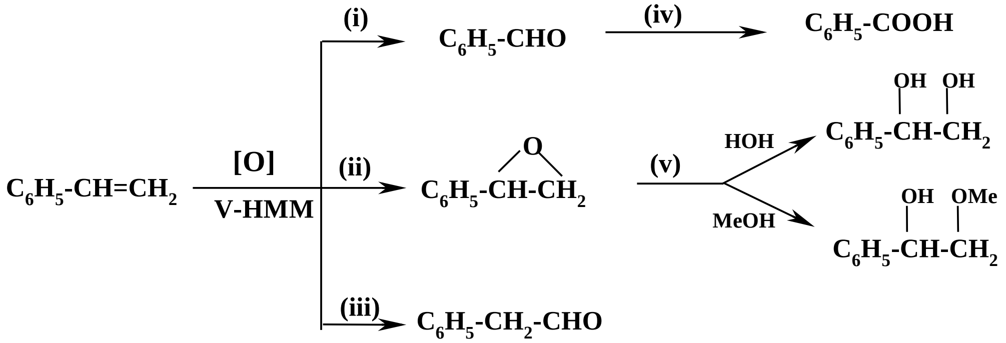

Scheme 3.1. Reaction scheme for the epoxidation of styrene

Table 3.2 further shows the styrene conversions and epoxide selectivities obtained over organovanadium silicates and a V-MCM-41 catalyst. The calcined V-PMO samples showed a higher styrene conversion and epoxide selectivity than the conventional V-MCM-41 catalyst. Since octahedrally coordinated metal species are less active in epoxidation reactions, due to the lack of free coordination sites, the increased catalytic activity of the V-PMO catalyst suggests the presence of well-isolated vanadium sites of tetrahedral nature, in agreement with the characterization results. Furthermore, a comparison in the decomposition rate of H_2O_2 over V-PMO-E and V-PMO-C / V-MCM-41 catalyst shows that the rate of oxidant decomposition is much faster inside the pore channels of silicas than in the pores of organosilicas (Table 3.2). Thus, the retrieval of silanol groups after decomposition of the organic groups in V-PMO catalysts and the inherent hydrophilic nature of the MCM-41 surfaces are responsible for the higher peroxide decomposition. More interestingly, even though the organic fragments in the V-PMO catalyst gets decomposed at higher calcination temperatures, the improved catalytic activity and epoxide selectivity show that the hydrophobic features still remained in the material, akin to earlier observations.[29]

Table 3.2. Epoxidation of styrene with *aqueous* H_2O_2 over V-PMO catalysts

Catalyst [a]	Styrene conversion (mol.%) [b]	H_2O_2 conversion (%)	Product distribution / %		
			Epoxide	Benzaldehyde	Others [c]
No catalyst	8	n.e	-	100	-
C_{18}-PMO	12	n.e	1	99	-
V-C_{18}-PMO-E	35	48	29	62	9
V-C_{18}-PMO-C	45	61	15	58	27
V-C_{18}-PMO-C [d]	32	55	12	54	34
V-C_{18}-PMO-C [e]	33	n.e	10	28	62 [f]
V-C_{16}-PMO-E	24	47	14	71	15
V-C_{16}-PMO-C	39	56	10	76	14
V-C_{14}-PMO-E	31	n.e	22	67	11
V-C_{14}-PMO-C	38	54	15	69	16
V-MCM-41-C	37	73	9	62	29
V-MCM-41-E	18	n.e	10	70	20

Reaction Conditions: catalyst (g), 0.1; T (°C), 70; substrate:oxidant (mol/mol), 4; solvent (5 mL), CH_3CN; time (h), 6.

[a] E stands for surfactant-extracted sample and C stands for calcined sample.

[b] (Styrene conversion/theoretically possible styrene conversion) x 100.

[c] Phenyl acetaldehyde, diols and acids. [d] using acetone as solvent. [e] methanol as solvent.

[f] mainly 1-methoxy-1-phenyl-etan-2-ol. n.e. = not evaluated.

It is generally considered that solvents have a remarkable influence in the catalytic activity and stability of metal-containing mesoporous materials. Hence, the influence of solvents in the epoxidation reaction of styrene was probed using aprotic and protic solvents such as acetonitrile, acetone and methanol. For V-C_{18}-PMO catalyst, the conversion of styrene and the selectivity to styrene epoxide follows the order CH_3CN >

CH_3OH > $(CH_3)_2CO$ and CH_3CN > $(CH_3)_2CO$ > CH_3OH, respectively (Table 3.2). Previously, the increased activity of titanium-containing catalysts in presence of acetonitrile was explained in terms of: (i) electrophilicity of the titanium sites, so that the CH_3CN molecules do not form stable complexes with the titanium atoms and (ii) selective poisoning of the active sites by the basic solvent molecule.[28] In addition to the above points, the enhanced catalytic activity in presence of polar aprotic solvents may also relates to the decreased phase separation between the aromatic alkene portion and the aqueous oxidant part, which in turn may allow an easy transport of the active oxygen species for the epoxidation process.[11a] Usually, the usage of more protic solvents increases the acidity of the catalyst surface and thereby increases the cleavage of the formed epoxide to their corresponding diol moieties. With methanol as a solvent, because of the alcoholysis reactions, an increased formation of 1-methoxy-1-phenyl-etan-2-ol is noted at the expense of benzaldehyde, styrene oxide and phenyl acetaldehyde (Table 3.2, Entry No. 6). Thus, protic solvents lead to an easy cleavage of the epoxide ring with the subsequent formation of diols in presence of water, or ether-like products in presence of alcoholic solvents (Scheme 3.1, route (v)).[28] These results show the relevance of solvents in epoxidation reactions and thus imply that a judicious choice of solvent can enhance the selectivity of speculated products, like styrene oxide, as in the present case.

3.4.3. Recycle Studies

In order to evaluate whether the catalytic activity of V-PMO materials arise from stable mesoporous materials, heterogenity studies were also conducted. Hence, as a first experiment, several recycling runs were performed over the newly developed vanadium-containing catalyst, V-C_{18}-PMO-C. Figure 3.14A shows that during the first recycle (second run), styrene conversion slightly decreased, whereafter the conversion as well as the product selectivity remained more or less the same. The slight decrease in conversion during the second run is due to the removal of trace amounts of extra-framework metal species.[11b] However, the leveling off the conversion and selectivity during subsequent cycles shows the existence of tightly held, isolated vanadium sites. Hence the constant yield of epoxide, even under three runs, shows that the vanadium atoms are tetrahedrally coordinated inside the framework of the PMO materials and are not prone to leaching, due to the hydrophobic environment of the pore channels.

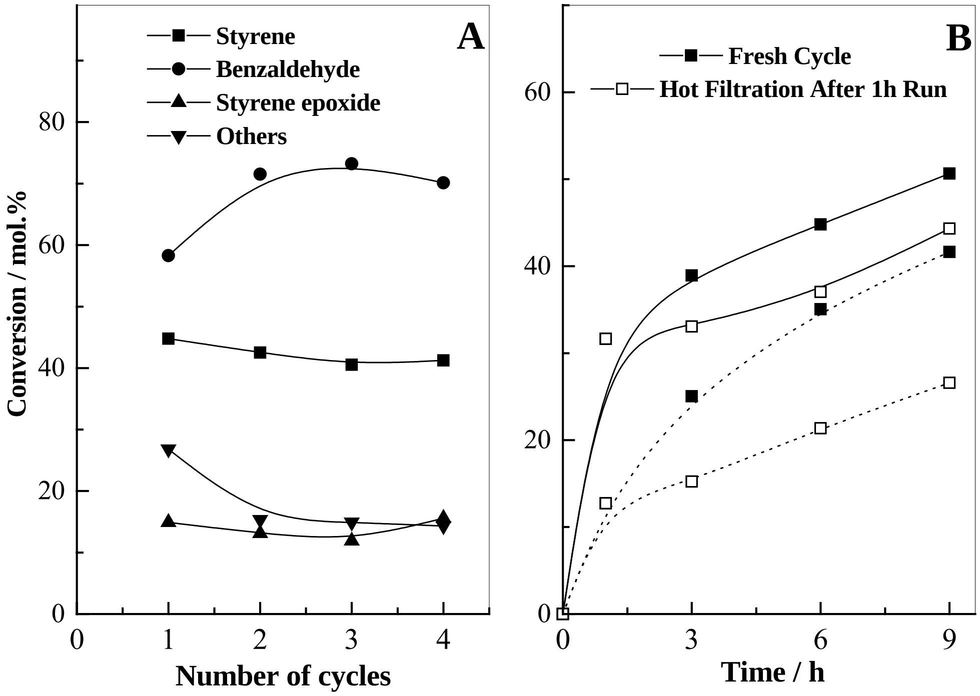

Figure 3.14. Recycling/leaching studies performed over vanadium-containing PMO catalysts: (A) shows the reusability of the V-C_{18}-PMO catalyst and (B) shows the hot filtration tests, solid lines represents the result of calcined V-C_{18}-PMO catalyst while the dotted lines represents the result of surfactant-extracted V-C_{18}-PMO catalyst.

Further, in order to know how the bridged organic fragments stabilize the vanadium species, hot filtration experiments were performed over the calcined and surfactant-extracted V-C_{18}-PMO catalyst. Figure 3.14B shows that compared to the calcined catalyst, the surfactant-extracted V-PMO catalyst showed better stability and resist the leaching of vanadium species. Hence, the present V-PMO materials have better stability and well-isolated active sites with more hydrophobic environments and are promising heterogeneous catalysts for various (ep)oxidation reactions.

3.5. REFERENCES

1 K. J. Shea, D. A. Loy, *Chem. Mater*. **1989**, *1*, 572.

2 D. A. Loy, K. J. Shea, *Chem. Rev*. **1995**, *95*, 1431

3 S. Inagaki, S. Guan, Y. Fukushima, T. Ohsuna, O. Terasaki, *J. Am. Chem. Soc*. **1999**, *121*, 9611.

4 T. Asefa, M. J. MacLachlan, N. Coombs, G. A. Ozin, *Nature* **1999**, *402*, 867.

5 B. J. Melde, B. T. Holland, C. F. Blanford, A. Stein, *Chem. Mater*. **1999**, *11*, 3302.

6 T. Asefa, M. J. MacLachlan, H. Grondey, N. Coombs, G. A. Ozin, *Angew. Chem. Int. Ed*. **2000**, *39*, 1808.

7 C-Y. Ishii, T. Asefa, N. Coombs, M. J. MacLachlan, G. A. Ozin, *Chem. Commun*. **1999**, 2539.

8 S. Inagaki, S. Guan, T. Ohsuna, T. Terasaki, *Nature* **2002**, *416*, 304.

9 S. Hamoudi, Y. Yang, I. L. Moudrakovski, S. Lang, A. Sayari, *J. Phys. Chem. B* **2001**, *105*, 9118.

10 M. Kruk, M. Jaroniec, A. Sayari, *J. Phys. Chem. B* **1997**, *101*, 583.

11 (a) S. Shylesh, A. P. Singh, *J. Catal*. **2004**, *228*, 333. (b) P. Selvam, S. E. Dapurkar, *J. Catal*. **2005**, *229*, 64.

12 S. Hamoudi, Y. Yang, I. L. Moudrakovski, S. Lang, A. Sayari, *J. Phys. Chem. B* **2001**, *105*, 9118.

13 C. Lim, G. L. Haller, *J. Phys. Chem. B* **2002**, *106*, 8437.

14 Q. Huo, D.I. Margolese, G.D. Stucky, *Chem. Mater*. **1996**, *8*, 1147.

15 D. Khushalani, A. Kuperman, G.A. Ozin, K. Tanaka, J. Garcer, M.M. Olken, N. Coombs, *Adv. Mater*. **1995**, *7*, 842.

16 M. Kruk, M. Jaroniec, Y. Sakamoto, O. Terasaki, R. Ryoo, C.H. Ko, *J. Phys. Chem. B* **2000**, *104*, 292.

17 Z. Luan, H. He, W. Zhou, C. F. Cheng, J. Klinowski, *JCS., Faraday Trans*. **1995**, *91*, 2955

18 W. Guo, X. S. Zhao, *Microporous Mesoporous Mater*. **2005**, *85*, 32.

19 (a) M. P. Kapoor, S. Inagaki, *Chem. Mater*. **2002**, *14***,** 3509. (b) A. Sayari, S. Hamoudi, Y. Yang, I. L. Moudrakovski, J. R. Ripmeester, *Chem. Mater*. **2000**, *12*, 3857.

20 W. Zhang, M. Froba, J. Wang, P. T. Tanev, J. Wong, T. J. Pinnavaia, *J. Am. Chem. Soc*. **1996**, *118*, 9164.

21 D. Wei, H. Wang, X. Feng, W. T. Chueh, P. Ravikovitch, M. Lyubovsky, C. Li, T. Takeguchi, G. L. Haller, *J. Phys. Chem. B* **1999**, *103*, 2113.

22 M. Mathieu, P. Vander Voort, B. M. Weckhuysen, R. R. Rao, G. Catana, R. A. Schoonheydt, E. F. Vansant, *J. Phys. Chem. B* **2001**, *105*, 3393.

23 L-X. Dai, K. Tabata, E. Suzuki, T. Tatsumi, *Chem. Mater*. **2001**, *13*, 208.

24 S. Inagaki, S. Guan, F. Fukushima, T. Ohsuna, O. Terasaki, *Stud. Surf. Sci. Catal*. **2000**, *129*, 155.

25 V. Parvulescu, C. Anastasescu, B. L. Su, *J. Mol. Catal. A: Chem*. **2003**, *3919*, 1

26 M. A. Uguina, D. P. Serrano, R. Sanz, J. L. G. Fierro, M-L. Granados, R. Mariscal, *Catal. Today* **2000**, *61*, 263.

27 J. Zhuang, G. Yang, D. Ma, X. Lan, X. Liu, X. Han, X. Bao, U. Mueller, *Angew. Chem. Int. Ed*. **2004**, *43*, 6377

28 V. Hulea, E. Dumitriu, *Appl. Catal. A: Gen*. **2004**, *277*, 99.

29 A. Bhaumik, M. P. Kapoor, S. Inagaki, *Chem. Commun*. **2003**, 470.

30 M. P. Kapoor, A. Bhaumik, S. Inagaki, K. Kuraoka, T. Yazawa, *J. Mater. Chem*. **2002**, *12*, 3078.

4.1. INTRODUCTION

Soon after the discovery of mesoporous materials of the M41S family by Mobil researchers, ordered mesoporous materials possessing high content of organic groups constitute an active research area.[1-6] These organic-inorganic hybrid mesoporous materials with reactive groups are unique as they offer potential advantages than the pristine silica for various surface modifications, and are widely explored in the field of catalysis, separation science, adsorption, sensing and so forth.[7-12] In general, there are two methods by which organic groups of desired functionality can be functionalized over mesoporous materials, *viz.*, direct co-condensation method and post synthesis grafting method.[7-9] Post synthesis method is the commonly and routinely used procedure for the synthesis of organic-inorganic hybrid mesoporous materials, as this procedure can lead to a higher concentration of surface organic groups. In this method, a surface reaction of the silanol groups of mesoporous materials (surfactant-free) with the desired organic coupling groups is effectively utilized. However, the time-consuming two-step synthesis procedure, instability of the inorganic framework at higher loadings and the inhomogeneous distribution of organic groups make the process less demanding.[8,13] On the other hand, the direct co-condensation method helps to modify the surface of mesoporous materials in a single step with controllable as well as homogenous distribution of organic species. Moreover, following this method, organic-rich mesoporous materials can be prepared and on an average 40-50 % silicon atoms carrying organic groups can be synthesized.[14-16] However, many of the synthesis methods reported in literature shows that at higher loadings, materials with very low channel ordering as well as inhomogenity in the functionalized organic groups are obtained. Hence, careful and judicious synthesis procedures are needed in the synthesis of organic-inorganic hybrid mesoporous materials, unless results in the disordering of the mesoporous material with concomitant phase separations, *viz.*, organosilica rich and silica rich phases.

One of the well-studied and widely used mesoporous catalyst support is the one-dimensional channel oriented, MCM-41 due to their unique high surface area, hexagonal channel arrays as well as simple synthesis protocols.[1,17] Although numerous synthesis procedures are available in literature for the single site functionalization on MCM related materials, very few reports and limited success are obtained over bifunctional groups.[15,16,18-20] Bifunctional mesoporous materials containing organic groups and transition metals are versatile that their applications can be tuned in diverse areas, where the organic groups play the role of providing improved hydrophobicity and the presence of metals provide the desired catalytic property.[21,22] Thus the current state-of-art method has to be improved so that one can design a periodic mesoporous silica material having bifunctional sites of tunable pore sizes. For the past decade, the design and synthesis of porous materials having pore size >30 Å be the main area of research, utilizing the chain length of the surfactant groups, micelle expanders and using various polymeric surfactants.[23,24] However, solid materials having pore sizes in between that of zeolites and mesoporous materials (super microporous region, 16-22 Å) received less attention and hence ordered silicas that effectively bridge the existing gap between the conventional microporous zeolites and the mesoporous materials is of particular interest.[25-28]

Earlier such materials are synthesized using surfactants of short alkyl chain length like the hexyl trimethyl ammonium surfactant or octyl trimethyl ammonium surfactants or short chain neutral templates. Unfortunately, these materials show poorly ordered structure, reveal the tendency to collapse the pore structures upon storage and the reproducibility of synthesis procedures are not promising.[29-33] Therefore, one of the major goals in the synthesis of porous materials was the development of materials having pores in the borderline between microporous and mesoporous materials with catalytic properties. Such a material further allows shape selective catalytic transformations, which are not possible with the zeolite catalysts. Very recently, Bagshaw *et al.* showed the synthesis of microporous materials using ω-hydroxy-bolaform surfactants while Sun *et al.* had shown that using adamantamine as surfactant one can prepare porous materials in the super-microporous region.[26,30] In an another way, small pore silicas with lower unit cell dimensions can be prepared from alkyl trimethyl ammonium surfactants, due to the exceptionally large degree of shrinkage upon surfactant removal by calcination process.[25,34-36] Thus, by increasing the calcination temperature one can tailor the *d* spacing and pore size of mesoporous materials, but highly disordered materials are obtained. Hence, new synthesis methods for ordered porous silicas having pore sizes in the super microporous region is alluring, as their unique structural and textual features can be utilized in the field of heterogeneous catalysis.

This chapter describes a new route towards the synthesis of materials having tailorable pore sizes, typically in the supermicroporous region, and more importantly with a catalytic functionality. The objective of this method is three fold: (i) to synthesize metal containing organic-inorganic hybrid mesoporous materials, (ii) to bridge the gap between the mesoporous and microporous materials from the mesopore region and (iii) to observe the effect of organosilanes in the dispersion of the catalytic active sites as well as its catalytic performance than the conventional metal-containing mesoporous materials. A hallmark of the present synthesis procedures is that the preparation of bifunctional mesoporous materials that have functional groups inside the mesoporous matrix can be designed according to the requirement and hence a variety of materials can be prepared using the synthesis procedure reported herewith.

4.2. EXPERIMENTAL

4.2.1. Materials

Tetraethyl orthosilicate (TEOS, Aldrich), cetyl trimethyl ammonium bromide (C_{16}-TAB, Aldrich), 3-chloropropyl triethoxy silane (Cl-ES, Lancanster), triethoxy vinyl silane (Vi-ES, Lancanster), trimethoxy methyl silane (Me-MS, Lancanster), sodium hydroxide (NaOH, Loba Chemie) and chromium nitrate ($Cr(NO_3)_3.6H_2O$, Loba Chemie). All chemicals were used as received without further purifications.

4.2.2. Synthesis of Organofunctionalized Silicas

Organic functionalized mesoporous silica samples were synthesized using the following gel composition: (1-*x*)TEOS-*x*X-ES-0.25C_{16}-TAB-0.25Na_2O-60H_2O. The amount of organosilane was varied from x = 15-60 in case of all organosilanes. The synthesis procedure for chloro propyl functionalized mesoporous silica was typically followed as follows. In a 250 ml plastic bottle, a solution of C_{16}-TAB (2.6 g, 7.1 mmol), NaOH (0.57 g, 14.2 mmol) in water (30 g) was prepared under room conditions and was stirred for 15 minutes. To this mixture, a solution of TEOS silica source (5 g, 24 mmol) as well as Cl-ES (0.90 g, 4.5 mmol, x = 15%) was added slowly with vigorous stirring for approximately 30 min. The mixture was stirred for 6 h under room conditions and then aged at a temperature of 100 ^{o}C for 48 h. The product obtained was then filtered, washed with copious amounts of water and dried under ambient conditions for 5 h to obtain a white fine powder. A similar procedure was carried out for the other organosilanes, that instead of Cl-ES, Vi-ES and Me-MS was added with the TEOS silica source. The Me-MS sample prepared with 40% and above loadings as well as Cl-ES and Vi-ES samples prepared with 50% and 60% loadings remain as a thick gel after aging. For these samples the solvent was removed by simple evaporation and the thick, jelly, solid material was crushed with a mortar to obtain a pale yellowish powder sample. The surfactant occluded inside the pores of the hybrid samples was removed by stirring the as-synthesized sample with an HCl-EtOH mixture (0.5 g/100 mL) at 60 ^{o}C for 6 h. The product was then filtered, washed well with ethanol and dried in vacuum. The surfactant-extracted samples obtained from chloro propyl sample is denoted as Cl-E_x, vinyl silane is denoted as Vi-E_x, methyl silane is denoted as Me-E_x, where x stands for the amount of organosilane added. Porous silica samples were also prepared from the as-synthesized samples by calcination at 540 ^{o}C for 12 h, under air atmospheres, at a heating ramp of 1^{o}/min. The calcined samples obtained from chloro propyl sample was denoted as Cl-C_x, vinyl silane is denoted as Vi-C_x, methyl silane is denoted as, Me-C_x where x stands for the amount of organosilane added.

4.2.3. Synthesis of Chromium-containing Organosilicas

Organic functionalized chromium-containing mesoporous silica samples were synthesized using the following gel composition: (1-*x*)TEOS-*x*X-ES-0.25C_{16}-TAB-0.25Na_2O-*y*Cr_2O_3-60H_2O. The amount of organosilane was varied from *x* = 15-60 in case of all organosilanes and *y* varies from 0.018-0.005, Si/Cr = 27-100. A typical synthesis procedure for chromium-containing chloro propyl functionalized mesoporous silica was as follows. In a 250 ml plastic bottle, a solution of C_{16}-TAB (2.6 g, 7.1 mmol), NaOH (0.57 g, 14.2 mmol) in water (30 g) was prepared under room conditions and was stirred for 15 minutes. To this mixture, a solution of silica source (TEOS, 5 g, 24 mmol) as well as Cl-ES (0.90 g, 4.5 mmol, *x* = 15%) was added slowly with vigorous stirring for approximately 30 min. An aqueous solution of chromium nitrate (0.34 g, 0.8 mmol, *y* = 0.018) was then added to the above mixture with vigorous stirring. The mixture was stirred for 6 h under room conditions and then aged at a temperature of 100 ^{o}C for 48 h. The product obtained was then filtered, washed with copious amounts of water and dried under ambient conditions for 5 h to obtain a green fine powder. A similar procedure was carried out for the other organosilanes that instead of Cl-ES, Vi-ES and Me-MS was added with the TEOS silica source. Chromium-containing Me-MS and Vi-ES samples prepared with 30% and above organic loadings as well as Cl-ES sample prepared with 40% and above loadings remain as a thick gel after aging. For these samples the solvent was removed by simple evaporation and the thick, jelly, solid material was crushed with a mortar to obtain a green powder sample. For comparison, a chromium-containing MCM-41 sample was also prepared under the present synthesis conditions, but without the addition of any organosilane source. The surfactant occluded inside the pores of the hybrid samples was removed by stirring the as-synthesized sample with an HCl-EtOH mixture (0.5 g/100 mL) at 60 ^{o}C for 6 h. The product was then filtered, washed well with ethanol and dried in vacuum. The surfactant-extracted, chromium-containing chloro propyl sample is denoted as C_yClE$_x$, vinyl silane is denoted as C_yViE$_x$, methyl silane is denoted as C_yMeE$_x$, where *x* stands for the amount of organosilane added and *y* stands for Si/Cr ratio. Chromium-containing small pore silica samples were also prepared from the as-synthesized samples by calcination at 540 ^{o}C for 12 h, under air atmospheres, at a heating ramp of 1 ^{o}/min. The calcined samples obtained from chloro propyl sample was denoted as C_yClC_x, vinyl silane is denoted as C_yViC_x and methyl silane is denoted as C_yMeC_x. The surfactant-extracted Cr-MCM-41 sample, prepared without any organosilanes, is denoted as CRE while the calcined sample is denoted as CRC.

4.2.4. Instruments for Characterization

PXRD patterns of the samples were recorded on a Rigaku D MAX III VC instrument using Ni-filtered Cu K_α radiation (λ=1.5404 Å), with a scan rate of 1 ^{o}/min and a step size of 0.02^{o}.

N_2 adsorption-desorption isotherms, pore size distributions as well as the textural properties of the materials were determined at -196 ^{o}C by a NOVA 1200 (Quanta chrome) instrument. Before analysis, the samples were activated at 200 ^{o}C for 6 h under vacuum and then the adsorption-desorption was conducted by passing nitrogen into the sample, which was kept under liquid nitrogen. Pore size distribution and average pore size of the surfactant-extracted hybrid samples were obtained from the adsorption branch of the isotherms using the Barrer-Joyner-Halenda (BJH) method. The pore diameter of the calcined ordered porous silicas was estimated using a geometrical equation derived under the assumption of a 2-D hexagonal honeycomb porous structure.

$$w_d = cd_{100}\,(\rho V_p/1 + \rho V_p)^{0.5} \qquad \text{equ. 4.1}$$

where c is a constant equal to 1.213 for cylindrical pore geometry, ρ is the pore wall density equal to 2.2 gcm^{-3} for silicas, V_p is the primary pore volume and d_{100} is the (100) XRD interplanar spacing.

TEM images were obtained on a JEOL JEM-1200 EX instrument at an acceleration voltage of 120 kV. Samples were prepared by sonicating the powdered samples for 30 min in isopropanol, followed by depositing two drops on a holey carbon film supported by a copper grid.

Thermal analysis (TG-DTG/DTA) of the hybrid samples was carried out in a Pyris Diamond TGA analyzer with a heating rate of 10 ^{o}C/min, under air atmospheres.

Solid-state ^{13}C CP MAS NMR and ^{29}Si MAS NMR spectra were recorded on a Bruker MSL 300 NMR spectrometer with a resonance frequency of 75.5 MHz and 59.6 MHz for ^{13}C and ^{29}Si using 4 mm zirconia rotors and a sample spinning frequency of 3 kHz. ^{13}C NMR spectra were collected with 70^o rf pulses and 5 s delay while ^{29}Si NMR spectra were collected with 70^o rf pulses and 30 s delay, with ~6000 scans. The chemical shifts were referenced to glycine and TMS, respectively, for ^{13}C and ^{29}Si.

Raman spectra were measured using a Bruker RFS 100/S spectrometer equipped with a Nd:YAG laser (1064 nm) and an InGaAs detector. Powdered samples were pressed into a stainless steel sample holder and run in the open atmosphere. A laser power of 75 mW was used. Spectra were acquired from 4000 to 25 cm^{-1} at a resolution of 4 cm^{-1}. In order to increase the signal-to-noise ratio 2000 scans were coadded. Temperature studies were performed by placing the powdered sample into a Specac Environmental Chamber™ DRIFTS cell modified with a near-infrared transparent quartz window. In order to enable quantitative measurement of intensity changes boron nitride powder was physically mixed (1 wt %) with the powdered sample. Boron nitride is stable to high temperatures and its Raman spectrum contains a single, intense band at 1365 cm^{-1} (no band overlap with the samples measured here). After measuring the Raman spectrum at room temperature the sample was heated *in situ* in flowing artificial air (20 mL/min) to 100 °C, held for 60 minutes, and then cooled to room temperature where the Raman spectrum was remeasured. This process was then repeated at 200 °C, 300 °C and 400 °C for each sample.

Diffuse reflectance UV-Vis spectra were recorded in the 200-600 nm range with a Shimadzu UV-2101 PC spectrometer equipped with a diffuse reflectance attachment, using $BaSO_4$ as the reference. The as-synthesized samples were kept at 100 ^oC for 5 h while the calcined samples were treated in dry air atmosphere at 550 ^oC for 5 h and flushed with an inert atmosphere, repeatedly, before the spectra was taken.

Temperature programmed reduction (TPR) was carried out on a Micromeritics Autochem 2910 catalyst characterization system, equipped with a TCD detector. Fresh, dried samples were pretreated by passing high purity (99.9%) argon (20 mL/min) at 500

°C for 3 h. After cooling to ambient temperature, the argon atmosphere is replaced by 5% H_2/Ar mixture. The samples were heated in this atmosphere to 800 °C at a heating rate of 10 °C/min and approximately 100 mg of calcined sample was used for all the experiments. The water produced during the reduction was condensed in a cold trap immersed in a slurry of isopropanol and liquid nitrogen.

XPS measurements were performed on a VG Microtech ESCA 3000 instrument, using non-monochromatized Mg K_α radiation at pass energy of 50 eV and an electron takeoff angle of 60°. Base pressure in the analysis chamber was 4×10^{-10} Torr. The overall energy resolution of the instrument is better than 0.7 eV, determined from the full width at half maximum (FWHM) of the $4f_{7/2}$ core level of the gold surface. The error in all the binding energy (B.E) values was within ±0.1 eV. Binding energy was corrected by using the C 1s peak of carbon at 284.9 eV as reference.

4.3. CHARACTERIZATION

4.3.1. Powder X-Ray Diffraction

XRD patterns of surfactant-extracted organic-functionalized mesoporous silica samples with different percentage of organic groups are shown in Figure 4.1. The surfactant-extracted samples shows larger peak intensities than the as-made samples and these differences arise due to the enhanced contrast in electron density after the removal of the surfactant from the pore channels than the surfactant-silicate samples.[37] Regardless of organosilane, the intensity of the (100) peak as well as higher ordered reflections decreased with an increase in the percentage of organosilica loading up to 50%, where after no reflections are observed. With methylsilanes no XRD peaks are observed at a high loading of 50%, while the chloro propyl and vinyl- pendant silica samples retain one small peak in the low angles. Notably, a decrease in (100) spacing or an increase in 2θ value is observed with the organosilane loading. The reduction in unit cell size with the percentage of organic pendant groups indicate that the organic groups gets loaded in the frame wall positions and it is interesting that with respect to the nature of organosilane, the unit cell shrinkage varies (Fig. 4.3A).

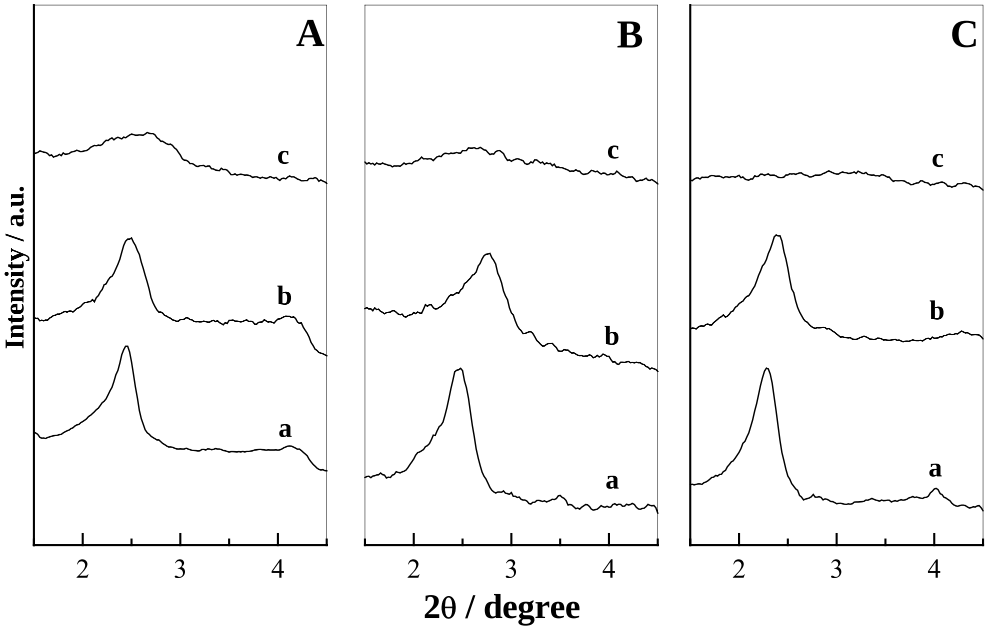

Figure 4.1. XRD patterns of organosilica samples: (A) Cl-E$_x$, (B) Vi-E$_x$ and (C) Me-E$_x$; (a) 15% loading, (b) 30% loading and (c) 50% loading.

Observing the effect of reduction in (100) values with the percentage of organo functionalization, the unit cell shrinkage in presence of an inorganic cation was further probed. Since chromium is presumed to anchor on the defect sites of porous materials and thereby reduce the pore size of the material, chromium nitrate is considered as an ideal precursor, so that mesoporous material with tailorable pore sizes and with a catalytic functionality can be prepared.[38] The XRD patterns of chromium-containing organosilica materials, prepared using organosilanes and chromium are shown in Figure 4.2. All samples show the characteristic reflections of mesoporous materials having 2D hexagonal arrangement of pore channels. This result shows that in presence of organo modifiers (15%) and chromium (~2%), no phase separation had occurred. However, XRD patterns are featureless for structural interpretation for chromium-containing mesoporous samples synthesized with greater than 15% organic groups, except the chloro propyl terminated chromium sample. Thus a high concentration of vinyl or methyl silanes (>15%) and chromium in the synthesis gel may restrict the condensation of the silicate species to form stable inorganic framework while the chloro propyl pendant mesoporous sample retains one reflection up to a loading of 50%.

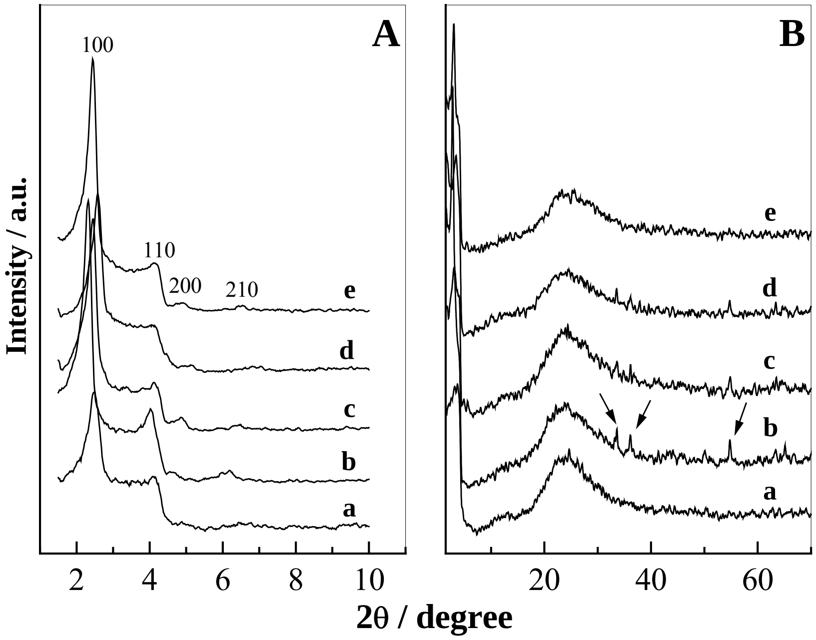

Figure 4.2. XRD patterns of: (A) surfactant-extracted hybrid chromium-containing samples and (B) calcined samples; (a) Si-MCM-41, (b) Cr-MCM-41, (c) methyl chromium silica, (d) vinyl chromium silica and (e) chloro propyl chromium silica.

Compared to surfactant-extracted samples, chromium-containing organosilicas shows a pronounced contraction after calcination (Table 4.2, Fig. 4.2B). The enhanced pore size shrinkages may arise due to the low degree of silica condensation or due to the strong interactions between the surfactants and the inorganic salts. So after calcination, chromium-containing porous materials with *d* spacing as low as 26 Å can be adequately prepared. Notably, it was also observed that compared to the non-modified chromium sample, the organo-modified chromium samples shows the absence of Cr_2O_3 in the wide-angle XRD patterns. Thus the presence of larger organo spacers introduced into the synthesis gel, like the chloro propyl, reduces the formation of Cr_2O_3 (denoted by arrows in Fig. 4.2B) and its formation decreased with the chain length of the organosilanes. These results demonstrate that by a judicious choice of the Si-R groups, chromium-containing porous materials without any crystalline Cr_2O_3 species can be synthesized with a Si/Cr ratio as low as 27.

4.3.2. Elemental Analyses

Elemental analyses of the hybrid samples were carried out for a better understanding about the percentage of organic group functionalization. The mole percentage of organosilanes loaded versus the input concentration of organosilanes is shown in Figure 4.3B. Despite the high amounts in the synthesis gel, the final products contain fewer organosilanes and at higher loadings the percentage of incorporation is very less. In addition, the percentage of organic functionalization varied with respect to the nature of the organosilane and it was found that the methyl- groups show less functionalization while the vinyl- and chloro propyl- terminated samples show an almost similar loading.

In the present synthesis, hydrophobic organosilanes are taken due to the consideration that organoalkoxy silanes having hydrophobic ends can orient more effectively around the water-micelle interface and can intercalate in to the hydrophobic regions of the surfactant micelles, during co-condensation reactions. Thus the primary reason for the differences in the percentage of organic group functionalization may arise from the different hydrolysis and condensation of the TEOS and organosilanes and with respect to the size, hydrophilic-hydrophobic property as well as inductive effects, the percentage incorporation of organosilanes varied (Fig. 4.3B).[39] Besides, because of the inductive effects of the methyl groups in the methyl alkoxy silanes, its hydrolysis/condensation with TEOS will be less, leading to low methyl loadings. Hence, at a higher percentage of methyl loading (typically > 30%), the gel mixture becomes viscous and lead to distinct phase separations. Moreover, the homocoupling of the hydrolyzed organosilanes rather than the co-condensation between TEOS and organosilanes may also enhance phase separation and the formation of more viscous solids at higher organosilane loadings. Thus if the organic groups are not condensed with the inorganic chain of TEOS it will disturb the surfactant-silicate assembly, leading to materials having poor channel structures.[41] Because of this reason, even though the input amount of organosilanes is high, after reflux and washing steps it gets easily removed and thereby reduces the percentage of organic loading. Thus it is likely that the methyl alkoxy silanes are not sufficiently hydrophobic to get entrapped with the micelle groups to produce a rigid framework. The systematic differences observed with different organosilanes suggest that, if the chain length is long, it can be intercalated with the surfactant groups in the condensation process while if the chain length is small it may disturb the surfactant-silicate assembly leading to organic-inorganic hybrid materials having poorly ordered mesoporous structures, with low organic loadings. Hence, the increased unit cell shrinkage observed with the percentage of vinyl- and chloro propyl organic groups may arise due to the increased condensation reactions between the silicate and organosilicate species and the high temperature employed in the synthesis provides a better hydrolysis of the alkoxy silanes, which may enhance the condensation rate between the silicates and the organosilicates.

In an attempt to understand the effect of temperature in the hydrolysis and condensation of organosilanes, the syntheses of organo-modified mesoporous materials are also carried out under room temperatures. However, after surfactant removal by solvent extraction or calcination, the XRD patterns are featureless, even for the ClE_{15} sample, which shows that the stability of the materials was less for the samples synthesized under room temperatures. Elemental analysis results show that only ~6% of chloro propyl groups loaded over the mesoporous support, when the input amount was 15%. The decreased stability as well as the lower loading of organic groups, under room temperature synthesis, may arise due to the difference in the hydrolysis/condensation rates of both silica species. The hydrolysis rate of trialkoxy organo silanes are generally slower than the rate of TEOS due to the electron donating ability of the alkyl groups bonded to the silicon of the Si-R species.[14-16] For instance, the hydrolysis rate of Si-CH_3 proceeds much slower than the other Si-R species used and are supported by the lower loading of methyl groups, from the elemental analysis. Thus the differences in the percentage of functional groups incorporated depend on the intrinsic properties of the organosilanes itself. Hence, in order to increase the surface coverage of organic groups and to enhance the condensation rate between the organosilanes and TEOS, the synthesis was carried out at a higher temperature *viz.*, 100 °C.

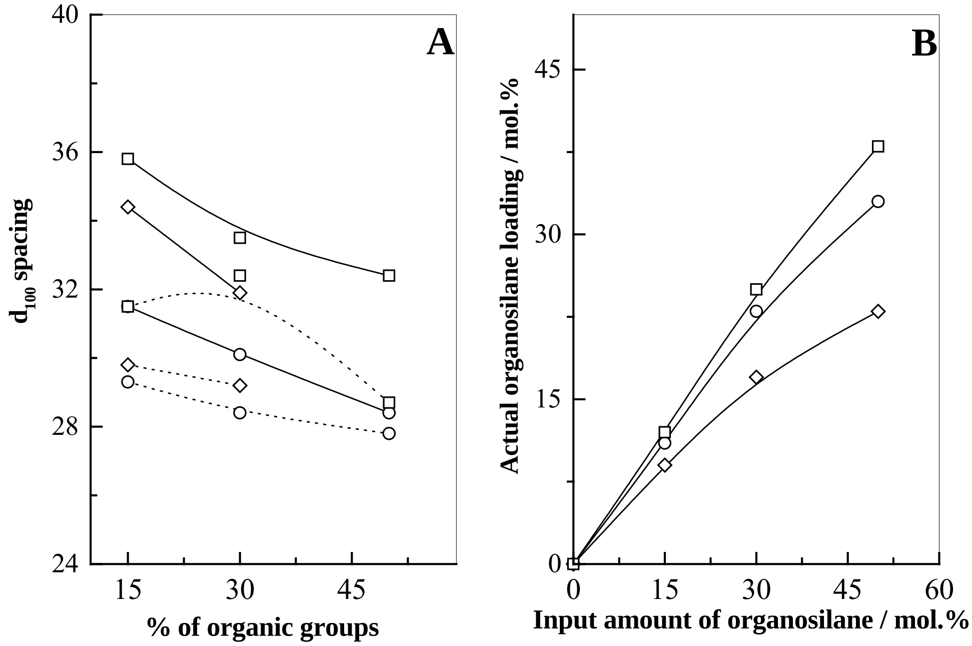

Figure 4.3. (A) d_{100} spacing as a function of percentage of organic group loading over MCM-41: (□) Cl-E_x, (○) Vi-E_x, (◇) Me-E_x, solid lines for surfactant-extracted samples and dotted lines for calcined samples and (B) Input and output elemental analysis results of: (□) Cl-E_x, (○) Vi-E_x and (◇) Me-E_x.

4.3.3. N_2 Adsorption and Desorption

N_2 adsorption-desorption analysis of surfactant-extracted chromium-containing samples having 15% chloro propyl groups show type IV isotherms with a capillary condensation step in the low-pressure region ($P/P_o \sim 0.2$) and an almost constant adsorption in the high-pressure region (Fig. 4.4). Increasing the content of chloro propyl groups in the pore channels resulted in a shift in the type of isotherm and at >15% chloro propyl loading the isotherm changed from type IV to type I. According to IUPAC classification, type IV isotherms relates to capillary condensation steps, characteristics of the mesoporous materials (20-500 Å), while type I isotherms are characteristic of microporous or super microporous materials (<20 Å).[32] The vinyl and methyl pendant sample also shows type I isotherms even with 15% organic loading. The change in type of isotherm with the percentage of organic group loading is accompanied by a concomitant decrease in the textural qualities of the samples.

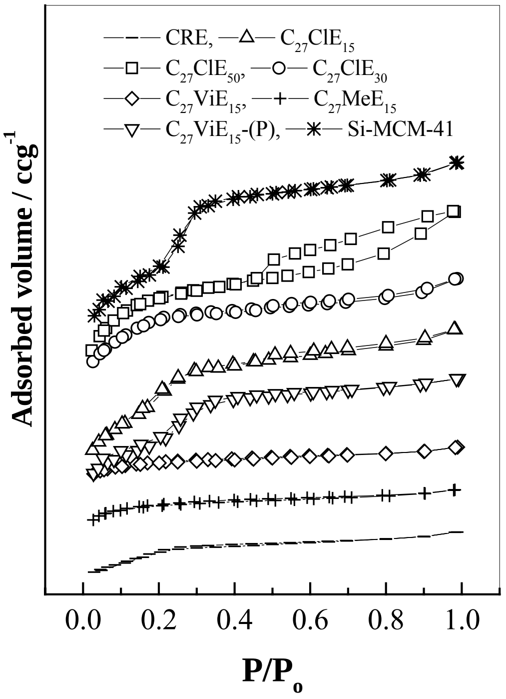

Figure 4.4. Nitrogen adsorption-desorption isotherms of surfactant-extracted chromium-containing mesoporous organosilicas.

Table 4.1. Structural properties of organo-functionalized chromium samples [a]

Sample	d_{100} (Å)	S_{BET} (m^2g^{-1})	S_{EX} (m^2g^{-1})	V_t (cm^3g^{-1})	V_p (cm^3g^{-1})	D_p (Å)
$C_{27}ClE_{15}$	35.8	581	41	0.29	0.47	28
$C_{27}ClE_{30}$	34.6	583	119	0.28	0.44	26
$C_{27}ClE_{50}$	32.9	441	204	0.22	0.37	25
$C_{27}ViE_{15}$	31.5	320	33	0.28	0.34	26
$C_{27}ViE_{15}$-(P)	36.7	535	38	0.27	0.41	30
$C_{27}MeE_{15}$	34.4	412	58	0.16	0.31	27
CRE	38	455	63	0.11	0.39	30

[a] d_{100}, XRD (100) interplanar spacing; S_{BET}, specific surface area; S_{EX}, external surface area; V_t, total pore volume; V_p, primary pore volume; D_p, pore diameter by BJH method.

The BET surface area, pore volume and the pore size observed for all the surfactant-extracted samples are given in Table 4.1. In particular, the external surface area as well as the difference between the total pore volume and primary pore volume increases after 15% loading of organic groups in case of chloro propyl pendant samples. Such changes may possibly relate to the development of secondary porosity. Since secondary porosity was not observed for materials prepared with 15% organosilanes, the additional porosity of the materials observed at higher organosilane loadings may probably results from the phase separations, *viz.*, silica rich and organosilica rich phases. These results are supported by the distinct hysterisis loop observed in the high-pressure regions of $C_{27}ClE_{50}$ sample (Fig. 4.4).[14] A detailed picture of the property of the materials was further obtained from the pore size distribution (PSD) curves. As suggested for the phase separation behaviour for higher organosilane loaded samples (>15%), it is noteworthy that the $C_{27}ClE_{30}$ and $C_{27}ClE_{50}$ sample shows secondary porosity at >35 Å (Fig. 4.5A). Thus, the lack of structural ordering or featureless XRD patterns observed with higher organic loadings might relate to the phase separations.

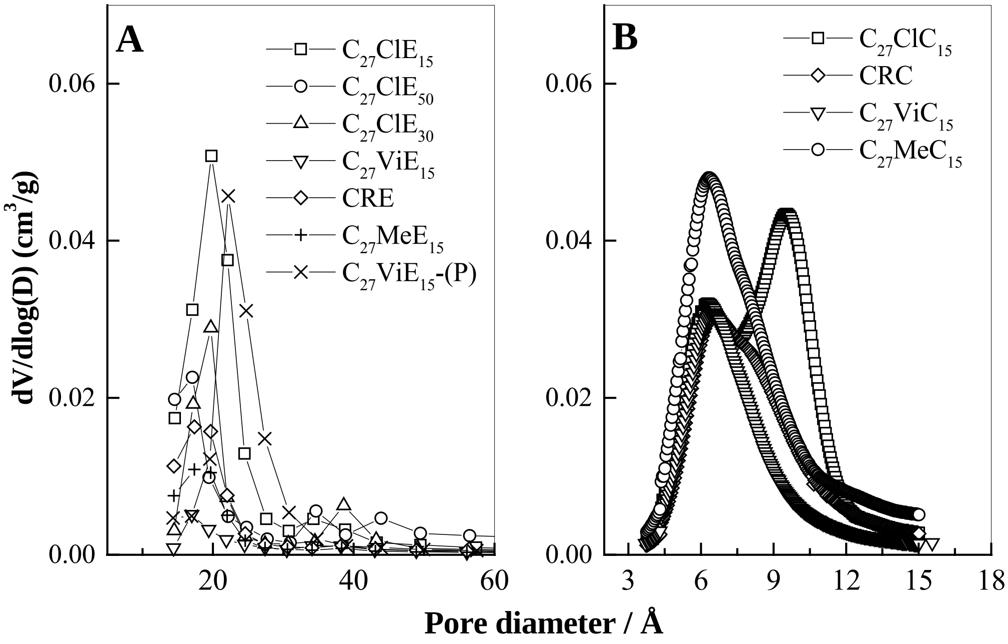

Figure 4.5. (A) Barrett-Joyner-Halenda (BJH) pore size distribution plots of surfactant-extracted chromium-containing organosilica samples and (B) Horvath-Kawazoe (HK) pore size distribution plots of calcined chromium samples.

Among the chromium-containing hybrid samples, the $C_{27}ViE_{15}$ sample shows an unusual sharp decrease in the textural qualities. This result is attributed to the uncontrolled polymerization of the vinyl groups in presence of chromium in the synthesis gel. In order to confirm this pore blockening, an additional experiment was carried out that to an alcoholic solution of Si-MCM-41, vinyl silane and chromium was added at different time intervals. The N_2 adsorption-desorption of this sample [$C_{27}ViE_{15}$- (P)] is shown in Figure 4.4. Contrary to the direct synthesized $C_{27}ViE_{15}$ sample, this sample retains the capillary condensation step with improved textural qualities showing that the vinyl groups had undergone polymerization but in a controlled manner (Table 4.1). Since the vinyl silane is added 1 h before the addition of chromium salts in $C_{27}ViE_{15}$- (P), it is anticipated that the vinyl silane get fixed over the support sample and in presence of chromium salts they undergo controlled polymerization and effectively cover the inner walls of the mesoporous material, with better wall thickness.

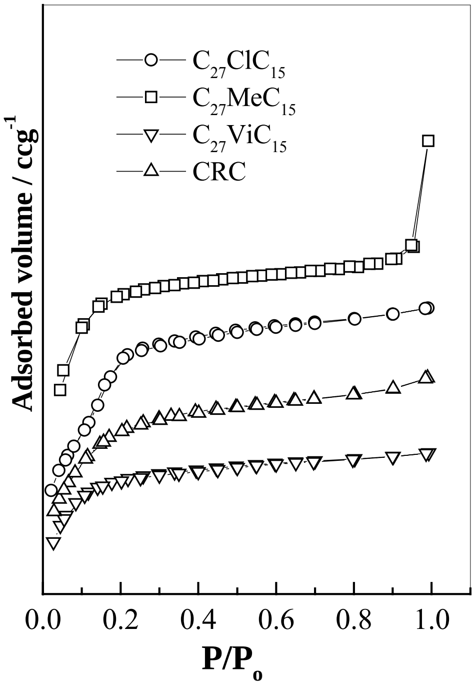

Figure 4.6. Nitrogen adsorption-desorption isotherms of calcined chromium samples.

The formation of ordered super micropores in the samples, after calcination, was further deduced from the N_2 sorption isotherms. Nitrogen adsorption-desorption isotherms of calcined chromium-containing materials having 15% organosilanes are shown in Figure 4.6. The adsorption isotherms are of type I and are similar to the isotherms observed with the short chain templated materials.[26-29] The isotherms shows a condensation in the low-pressure region, somewhere around P/P_o = 0.15-0.2, indicating the formation of pores less than 20 Å diameter, typically in the super microporous region. Since the position of capillary condensation step correlates to the pore diameter of the material, the observed differences before and after calcination shows that the pore size of the material can be tailored by the judicious choice of organic species in the synthesis gel. However, it is difficult to compare the present samples with the pore diameters reported in literatures for small pore materials. Since the pore sizes are mainly examined by gas adsorption studies, where the calculation methods are highly inefficient, differences up to 10 Å can be obtained and thus, in certain cases, produces material with larger unit cell size but with low pore sizes.[14,40] Among the calcined samples, the $C_{27}ClC_{15}$ sample retains a condensation step, in the low-pressure region, relating a better structural ordering. Further, the textural properties of all calcined porous chromium-silica samples are given in Table 4.2. Thus, a combination of the XRD results and adsorption studies suggest that small pore chromium silicas having smaller *d* spacing, higher surface areas and pore sizes in the border line between mesoporous and microporous materials, around 20 Å (equ 1) and below 8 Å (HK) (Fig. 4.5B), can be prepared by a judicious choice of organosilanes. The synthesis routes explained suggest that if surfactants of shorter alkyl chain length are used for the assembly process, chromium-silica samples having still lower pore sizes can be adequately prepared.

Table 4.2. Structural properties of small-pore chromium silicas [a]

Sample	d_{100} (Å)	S_{BET} (m^2g^{-1})	S_{ex} (m^2g^{-1})	V_t (cm^3g^{-1})	V_p (cm^3g^{-1})	D_p		
						w_d	DFT	HK
$C_{27}ClC_{15}$	28.5	719	50	0.31	0.42	23	25	9
$C_{27}ViC_{15}$	26.3	672	70	0.26	0.30	20	20	6
$C_{27}MeC_{15}$	28.4	808	72	0.29	0.38	22	20	7
CRC	30.2	711	83	0.27	0.35	25	23	7

[a] w_d, pore diameter determined using equation 4.1; DFT, pore diameter determined using density functional theory method; HK, pore diameter determined using Horvath-Kawazoe method. Other notations are similar as in Table 4.1.

4.3.4. Transmission Electron Microscopy

The structural ordering and pore array of the chromium samples was further evaluated by TEM analysis. TEM images of the small pore chromium-silica samples show poorly ordered structures akin to the worm-like channel morphologies observed with the amine templated HMS samples.[15,16] In detail, the $C_{27}ClC_{15}$ sample show worm-like structures, $C_{27}ViC_{15}$ sample shows spongy like images, $C_{27}MeC_{15}$ sample show several small particles, each of disordered channels, can be observed from the TEM images (Fig. 4.7). The disordered or spongy like structures appeared for the chromium-containing samples is related to the distortion in the pore channels brought about by the high temperature calcinations. These results indicates that the incorporation of organic groups as well as the nature of organosilanes has an important influence in the morphology and long range ordering of the final materials.

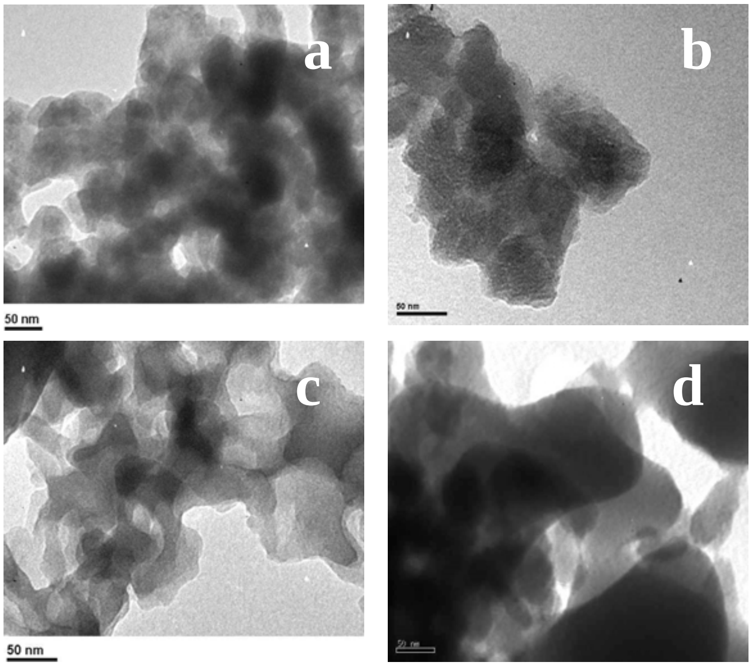

Figure 4.7. TEM images of: (a) $C_{27}ClC_{15}$ (b) $C_{27}ViC_{15}$ (c) $C_{27}MeC_{15}$ and (d) CRC.

4.3.5. Thermal Analyses

Thermal analyses of as-synthesized and surfactant-extracted hybrid samples were carried out to investigate the structural stability of the organic-inorganic hybrid nanocomposites (Fig. 4.8).

The as-synthesized 15% chloro propyl functionalized mesoporous sample ($C_{27}ClA_{15}$) showed a weight loss below 100 ^{o}C (< 3%) attributed to the loss of adsorbed water molecules. This loss was followed by a distinct, sharp weight loss starting from 150-500 ^{o}C, attributed to the combined decomposition of the surfactant groups and the organosilanes (~40%). DTA plot of this sample show that the decomposition process occurs in steps (240-350 °C and 350-500 °C) rather than a concerted reaction. This loss between 240-350 °C can be ascribed to the surfactant decomposition, while the loss between 350-500 °C is due to the decomposition of the functionalized organic groups.

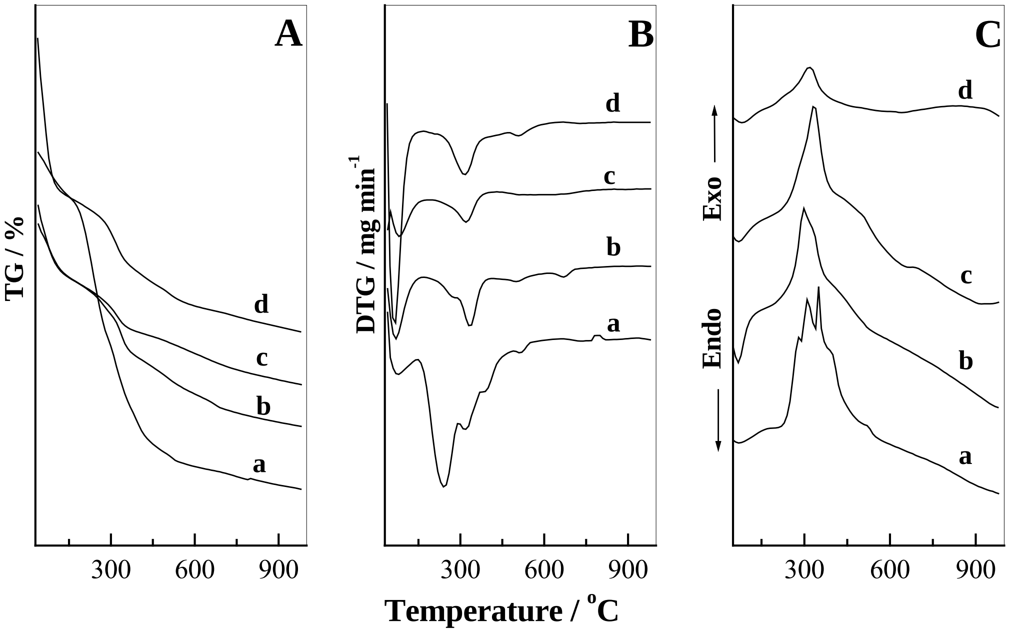

Figure 4.8. (A) TG, (B) DTG and (C) DTA plots of: (a) $C_{27}ClA_{15}$, (b) $C_{27}ClE_{15}$, (c) $C_{27}ViE_{15}$ and (d) $C_{27}MeE_{15}$.

For surfactant-extracted samples, however, no weight loss was observed in the range 240-350 °C implying that the extraction process had removed all surfactant groups. It is noteworthy that the chloro propyl pendant sample shows the maximum weight loss (T >300 °C) followed by vinyl and methyl groups and the decomposition peak maxima varied with respect to the nature of the organic groups introduced. This result correlates the findings from elemental analysis that chloro propyl silanes show maximum functionalization than the vinyl and methyl silanes. Another observation noted from the derivative plots of surfactant-removed samples is the difference in weight loss at temperatures less than 100 °C, for the removal of physisorbed water groups (Fig. 4.8B).

Since the surfactant extraction treatment conditions are similar for all the samples, the significant weight loss observed below 100 °C for MeE_{15} sample, than the chloro propyl and vinyl- pendant samples may relate to the surface hydrophobic-hydrophilic properties of the developed samples. Thus, the presence of higher chain length organic pendant groups (increased carbon number in ClE_{15} and ViE_{15}) makes the mesoporous surface more hydrophobic while the smaller methyl groups in the pores retains the sample hydrophilic similar to the pristine MCM-41 surface. The decreased concentration of methyl groups in the MeE_{15} sample may also explain the above result.

4.3.6. ^{29}Si MAS NMR Spectra

^{29}Si MAS NMR of surfactant-extracted, chromium-containing mesoporous organosilicas exhibit peaks at -110, -100, -91 (sh), -65 and -57 ppm which are usually assigned to Q^4 [$Si(OSi)_4$, siloxane], Q^3 [$Si(OH)(OSi)_3$, single silanol], Q^2 [$Si(OH)(OSi)_3$, geminal silanol], T^3 [$SiR(OSi)_3$] and T^2 [$Si(OH)R(OSi)_2$] sites, respectively (Fig. 4.9).[14-16] The unmodified sample (Si-MCM-41) shows the presence of broad resonance peaks from -90 to -110 ppm, indicative for a range of Si-O-Si bond angles, and it is noteworthy that the sample contains large amounts of Q^3 sites showing a reduced framework cross linking. Compared to Si-MCM-41, chromium and organic pendant group containing samples show a decrease in the Q^3+Q^2 sites showing that the material posses few residual silanols, resulting in siliceous pore wall structure with higher degree of silica condensation (Table 4.3). The decrease in the Q^3 and Q^2 signals after organo functionalization suggests that the functionalization proceeds by the simultaneous cooperative assembly or co-condensation of the TEOS and the organosilanes at the structure-orienting micelle interface. Presence of Q^3 sites, even after organic group loading, suggest that the decreased structural regularity observed for vinyl and methyl silanes (>15%) does not arise from the lack of charge balancing silanols and hence it is apparent that further modifications in the current synthesis can incorporate more organosilanes.[42] However, such a possibility can be utilized for the synthesis of multi-functional organic-inorganic hybrid mesoporous materials, by various post synthesis modifications. In particular, it can be noted that the Q^3+ Q^2/Q^4 ratio is lower for the chloro propyl containing samples. This observation support the results observed from the elemental analysis that an increase in the chain length of the organic pendant groups, helps to intercalate with the surfactant groups in the self assembly process, leading to a better incorporation with better framework cross linking. In addition, the chloro propyl pendant mesoporous organosilica sample shows an increased surface coverage of organic groups than the vinyl and methyl pendant organosilica samples. All these results suggest that more hydrophobic organosilanes can better orient themselves around the water-micelle interface and can intercalate into the hydrophobic region of the surfactant species in the co-condensation reaction process.

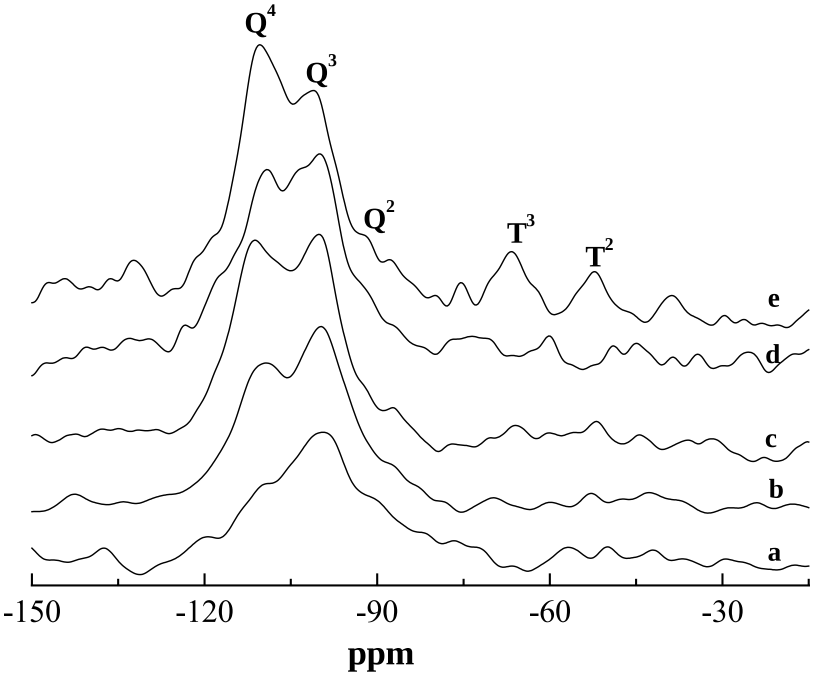

Figure 4.9. Solid-state ^{29}Si MAS NMR plots of surfactant-extracted chromium-containing mesoporous organosilica samples: (a) Si-MCM-41, (b) CRE, (c) $C_{27}MeE_{15}$, (d) $C_{27}ViE_{15}$ and (e) $C_{27}ClE_{15}$.

Table 4.3. ^{29}Si MAS NMR data of organo-functionalized chromium samples

Sample	Q^3+Q^2/Q^4	T^2/T^3	$\Sigma T^n/\Sigma(T^n+Q^n)$	T^2+T^3/Q^2+Q^3	SC [a]
$C_{27}ClE_{15}$	0.88	1.00	0.11	0.13	22
$C_{27}ViE_{15}$	0.96	1.18	0.04	0.05	12
$C_{27}MeE_{15}$	1.21	1.32	0.05	0.06	9
CRE	1.77	-	-	-	
Si-MCM-41	2.08	-	-	-	

[a] SC = Surface Coverage = $(T^2+T^3)/(Q^2+Q^3+T^2+T^3)$

4.3.7. ^{13}C CP MAS NMR Spectra

^{13}C CP MAS NMR shows the presence of functionalized organic groups inside the MCM-41 pore channels and the absence of surfactant species, after the solvent extraction process. Absence of signals at 15 and 58 ppm, assigned to the SiO-CH_2-CH_3 species, and in the range 50-70 ppm, for surfactant groups, indicates that the hydrolysis of the organo silane monomers is complete and the surfactant had removed from the pore channels of the MCM-41 framework. These results are supported by the negligibly low amounts of nitrogen (from surfactant) from the CHN elemental analysis. The ^{13}C CP MAS NMR spectra of chloro propyl pendant mesoporous sample shows three peaks at 9, 26 and 45 ppm corresponding to the carbon atoms of the propyl chain while the methyl pendant organosilica sample shows the presence of a sharp peak at -7 ppm, for the methyl carbon atoms.[43] These results confirm that the chloro propyl and methyl groups are functionalized in the developed samples and the organic groups are not decomposed during the synthesis conditions (Fig. 4.10 a&d).

In synthesis of organic-inorganic hybrid mesoporous materials, a particularly interesting organic pendant group is the vinyl silane, since the double bond is stable under the synthesis conditions and is sufficiently reactive to follow further post synthesis modifications. Generally, in carbon NMR, the vinyl carbon atoms show peaks at 129 and at 138 ppm.[3] However, the vinyl terminated mesoporous chromium sample shows an ill-defined NMR spectrum. Such a result suggests that the vinyl groups had undergone some kind of coupling or oligomerisation reaction and the presence of chromium salts may promotes such reactions (Fig. 4.10b). For comparison, the ^{13}C CP MAS NMR of the $C_{27}ViE_{15}$- (P) is also shown in Figure 4.10c. The post synthesis modified sample also shows ill-defined peaks, but small peaks are observed at 129 ppm and at 138 ppm. These results support the findings from nitrogen adsorption studies that the polymerization of vinyl silanes is different in the two synthesis methods *viz.*, direct co-condensation method and post synthesis grafting method.

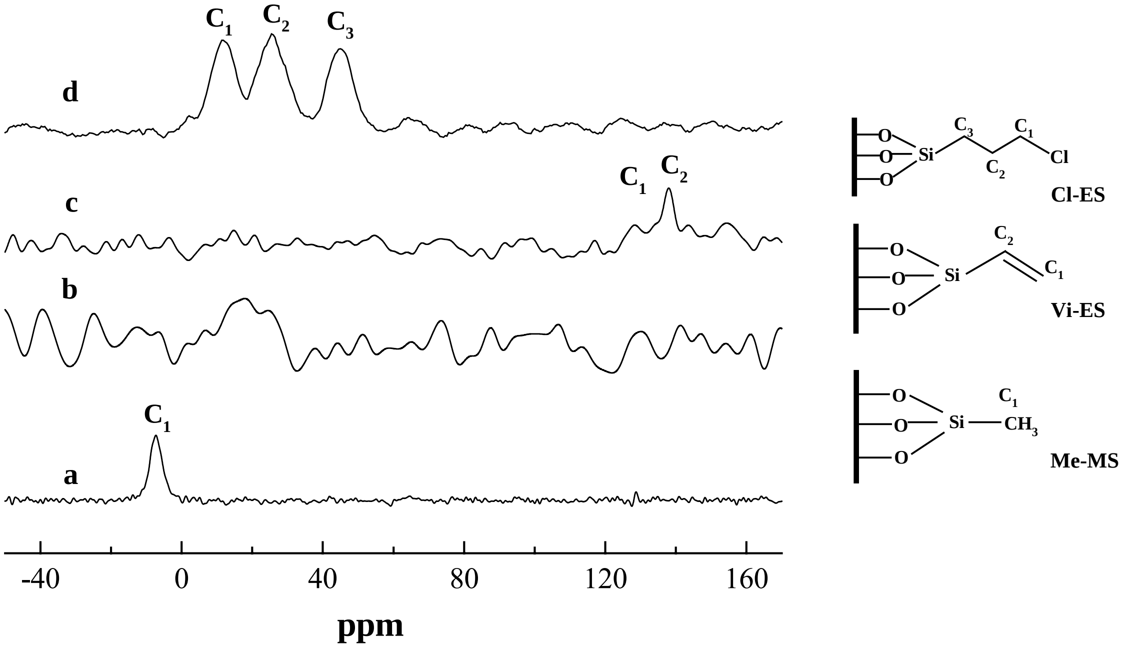

Figure 4.10. Solid-state ^{13}C CP MAS NMR plots of surfactant-extracted chromium-containing mesoporous organosilica samples: (a) $C_{27}MeE_{15}$, (b) $C_{27}ViE_{15}$, (c) $C_{27}ViE_{15}$-(P) and (d) $C_{27}ClE_{15}$.

4.3.8. FT-Raman Spectra

Raman spectra were recorded for all mesoporous materials with and without chromium loading. The peaks assignments are listed in Table 4.4. The bands at 1000 and 795 cm^{-1} are similar in position to those previously reported in these mesoporous siliceous materials and are assigned to the stretching modes of surface silanols (ν O_3Si-OH) and siloxane bridges (Si-O-Si).[44,47] The band at 1600 cm^{-1} has also been observed and assigned to the deformation mode of water (δ H_2O). The vinyl pendant samples (ViE_{15} and $C_{27}ViE_{15}$) showed a peak at 2984 cm^{-1}, which is assigned to the symmetric stretching mode of CH_2. This band was previously observed by Li *et al.* at 2988 cm^{-1} in sol-gels containing vinyl triethoxysilane.[49] The weak asymmetrical stretching mode seen by these authors at 3072 cm^{-1} was not observable in the present spectra. Similarly, the C=C stretching mode observed at 1608 cm^{-1} was not resolved; it was overlapped by the water deformation mode. Samples containing chloro propyl pendants (ClE_{15}, $C_{27}ClE_{15}$, $C_{27}ClE_{30}$, $C_{27}ClE_{50}$) contained a weak band at 1275 cm^{-1}, which is assigned to the CH_2-Cl stretching mode. This mode was observed at 1280 cm^{-1} using infrared spectroscopy by Kun'ko *et al.*[50] Measurements made after calcinations at temperatures up to and including 400 °C showed no significant decrease in the intensity of these bands (except δ H_2O, which decreased). For samples containing methyl pendant groups (MeE_{15}, $C_{27}MeE_{15}$) unique bands due to ν_s and ν_{as} (CH_3) (2923 and 2970 cm^{-1}, respectively) were observed only following calcination, once all traces of surfactant were removed.

Raman spectra of chromium-containing samples did not show any distinct peaks due to chromium oxide species indicating that the transition metal is very well dispersed. Close inspection often showed a shoulder at 980 cm^{-1} when chromium was in the sample. This could be due to the asymmetric stretching mode of dehydrated monochromate (CrO_4^{2-}) however spectra were not conclusive. For comparison, a sample of the siliceous mesoporous material was impregnated with the same amount of chromium (2%) and calcined at 500 °C. A weak but discernible peak at *circa.*, 870 cm^{-1} appeared (assigned to either hydrated monochromate or hydrated polychromate species).[38,45,48] Thus it is apparent that the chromium added during synthesis was clearly stabilized in a manner absent in post-synthesis impregnation.

Table 4.4. Assignment of peaks for Raman spectra of hybrid chromium samples

Assignment	Literature (cm^{-1})	This study (cm^{-1})
v_a $(CH_3\text{-}N)^+$ (surfactant)	3038 [44]	3032
v_s $(CH_3\text{-}N)^+$ (surfactant)	2971 [44]	2964 (w)
v_s $(CH_3\text{-}R)$ (surfactant)	2893 (sh) [44]	2922 (sh)
v_a (CH_2) (surfactant)	2899 [44]	2890
v_s (CH_3)	-	2890
v_s (CH_2) (surfactant)	2853 [44]	2854
δ (H_2O)	1620 [44]	1600
δ_a (CH_3) (surfactant)	1446 [44]	1450
δ_a (CH_3)	1410 [46]	1410
δ_s (CH_3) (surfactant)	1306 [44]	1300
δ_s (CH_3)	-	1270
v $(O_3Si\text{-}OH)$	971 [45], 978 [47]	1000
v (dehydr. CrO_4^{2-})	980 [45, 48, 38]	980 (sh)
v (Si-O-Si)	812 [45], 791 [47]	795
v $(C\text{-}N)^+$ surfactant	761	759
v (Si-C)	530 [46]	522
v (4-fold siloxane rings)	484 [45]	-
δ_s (O-Si-O)	450 [45]	-

4.3.9. UV-Vis Experiments

Diffuse reflectance UV-Vis analysis of the as-synthesized and calcined chromium samples is shown in Figure 4.11 A&B. All the as-synthesized chromium samples were pale green in color and following calcination changed to an intense yellow color. The green color of the material implies the presence of trivalent chromium ions in octahedral geometry while the yellow color would imply the presence of high-valent chromium ions in tetrahedral coordination. UV-Vis spectra of as-synthesized samples show two sharp absorption bands at 440 nm and 610 nm typical of d-d transitions corresponding to the $^4A_{2g}(F)$ to $^4T_{1g}(P)$ and $^4A_{2g}(F)$ to $^4T_{2g}(F)$ transitions, for the trivalent chromium ions (Cr^{3+}) in octahedral coordination (Fig. 4.11A).

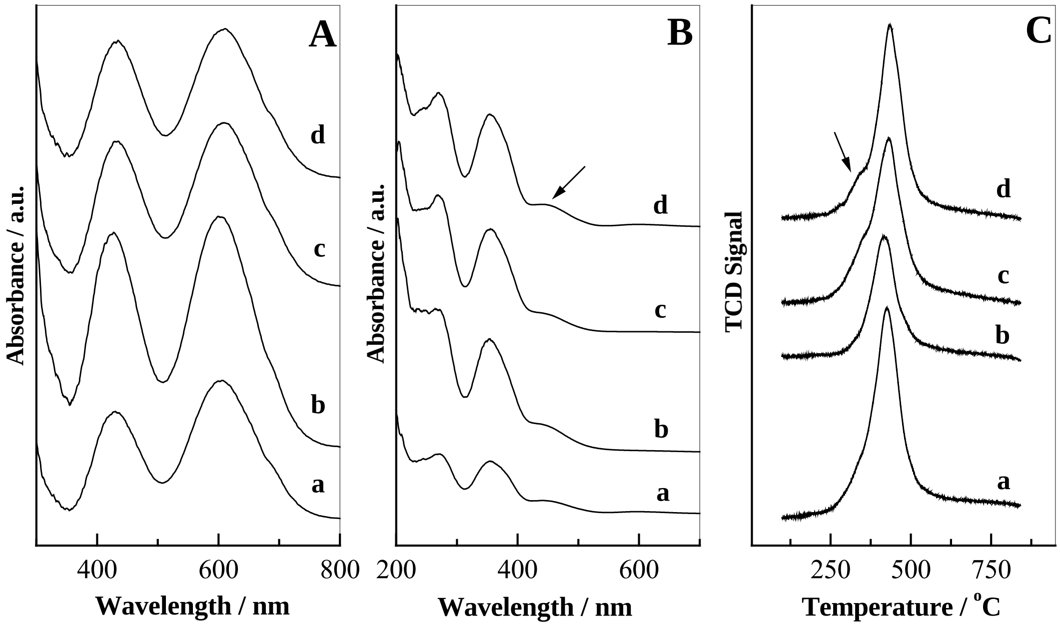

Figure 4.11. UV-Vis spectra of: (A) as-synthesized chromium-containing mesoporous samples, (B) calcined chromium samples and (C) H_2-TPR results of calcined chromium samples: (a) chloro propyl chromium silica, (b) vinyl chromium silica, (c) methyl chromium silica and (d) Cr-MCM-41.

The spectra of calcined chromium samples show bands at 270, 340 and 450 nm. The sharp bands observed at 270 nm and 340 nm are assigned to the O to Cr (VI) charge transfer transitions of chromate species while the weak band centered at 450 nm is assigned to the charge transfer bands associated with dichromate- or polychromate- type species (Fig. 4.11B). These results indicate that the major species formed over the calcined chromium samples be the monochromate species [38]. However, closer analysis of the peaks shows that, except $C_{27}ClC_{15}$, all other chromium samples show a distinct tailing of the band to higher wavelengths. This may possibly arise due to the presence of Cr_2O_3 species, as observed from the XRD analysis.

4.3.10. Temperature Programmed Reduction

Temperature programmed reduction measurements (H_2-TPR) were generally used to investigate the different oxidation states of the transition metal-containing mesoporous materials. Kevan *et al*. pointed out that, the reduction temperature values is dependant on the reduction conditions like H_2 partial pressure, heating rate and final reduction temperature and hence comparison of the reduction values with various literature reports is inappropriate, as they show variations with the experimental set up procedures.[51] H_2-TPR profiles of the calcined chromium-catalysts in the 100-800 ^oC temperature range is shown in Figure 4.11C. The reduction temperature maxima (T_{max}) (425-438 ^oC) as well as the hydrogen consumption of the small pore chromium-silica catalysts vary with the nature of organosilanes added and are given in Table 4.5. The peak observed at this region is attributed to the reduction of Cr^{6+} to Cr^{3+}.[52] This result supports the observations about the presence of Cr (VI) species in the calcined small pore chromium-silica materials. However, the peak maximum gets shifted to lower temperatures for the smaller organosilane prepared chromium catalysts ($C_{27}ViC_{15}$, $C_{27}MeC_{15}$) and the CRC sample showed an additional, distinct peak maxima at ~413 ^oC. Lowering of the reduction peak for the chromium sample prepared with smaller organosilanes and without any organosilane may results from the formation of agglomerated chromium species, as noted with the XRD and UV-Vis analysis.

Table 4.5. XPS Binding energy values, Surface atomic concentration and H_2-TPR datas of small-pore chromium samples

Samples	Si 2p	O 1s	Cr/Si (ICP)	Surface Cr/Si ratio	Cr $2p_{3/2}$ B.E. (eV)	TPR	
						T_{max} (^oC)	H_2 Consum. (µmol/g)
$C_{27}ClC_{15}$	103.4	532.7	0.023	0.010	578.2	438	766
$C_{27}ViC_{15}$	103.3	532.7	0.024	0.019	578.3	434	760
$C_{27}MeC_{15}$	103.3	532.8	0.023	0.019	577.8	430	834
CRC	103.2	532.8	0.025	0.018	577.6	425	428
Si-MCM-41	103.4	532.8	-	-	-	-	-

4.3.11. X-Ray Photoelectron Spectroscopy

High-resolution XP spectra of the Cr 2p core level of the samples were also recorded, as XPS measurements provide valuable information about the oxidation state and chemical environment of chromium due to the shift in binding energies (B.E), *i.e.,* Cr $2p_{3/2}$ and Cr $2p_{1/2}$. In general, Cr (VI) compounds exhibit sharp peaks at higher binding energies, ~579.5 eV, while Cr (III) species show peaks at ~576.6 eV.[53] The Cr $2p_{3/2}$ binding energy of chromium in all the as-synthesized mesoporous materials shows a B.E at ~577.6 eV. However, for the calcined porous chromium silica samples the value shifted to a higher energy, characteristic of Cr (IV) species and hence concludes that the calcination treatments had changed the Cr (III) ions to Cr (VI) (Table 4.5).[54] For the CRC and $C_{27}MeC_{15}$ sample, an intensity decrease as well as a broadening of the Cr $2p_{3/2}$ peak to lower value was noted. This may arise due to the existence of Cr_2O_3 species in the samples, as determined by the UV-Vis studies. However, since the Cr (VI) can be easily reduced to Cr (III) under the high vacuum in the ESCA chamber or under the influence of X-ray beams used during XPS measurements, an accurate estimation of different oxidation states is not explored by this method.[38] The relative dispersion of chromium ions on the catalyst surface estimated from the XPS techniques are also tabulated in Table 4.5. Generally, the metal-to-silicon atomic ratio can be considered as the relative dispersion of transition metal ions on the framework of porous supports and hence the bulk Cr/Si ratio was compared with the Cr/Si ratio determined from the XPS analysis. In accordance with the ICP metal analysis, it was observed that the surface Cr/Si molar ratio increases with an increase in the percentage of chromium in the small pore chromium-silica samples. This indicates that the chromium atoms are not truly incorporated inside the framework since a large part of chromium species are detected in the surface.

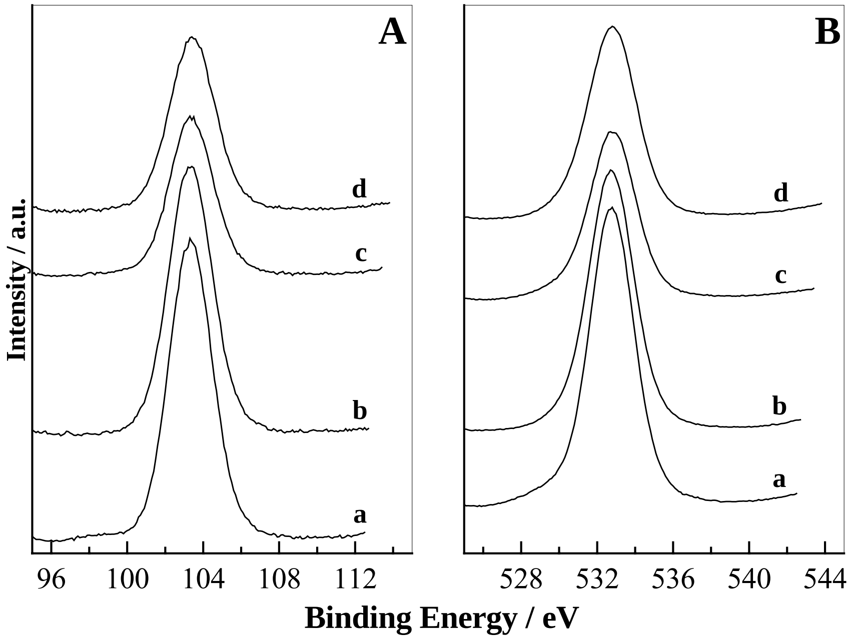

Figure 4.12. XPS plots of (A) Si 2p and (B) O 1s: (a) $C_{27}ClC_{15}$, (b) $C_{27}ViC_{15}$, (c) $C_{27}MeC_{15}$ and (d) CRC.

The Si 2p and O 1s core level XP spectra of the calcined porous chromium silica catalysts were shown in Figure 4.12. The Si 2p core level shows a peak around 103.2 eV characteristic of silicon and among the calcined samples the $C_{27}ClC_{15}$ shows sharp Si 2p peaks. The O 1s XP spectra of the MO/SiO_2 samples usually arise from the contribution of oxygen from the support and the oxygen from the introduced metal oxide systems.

Hence in the present case, the contributions may arise from the oxygen of the support silica (O 1s from SiO_2) and from the oxygen of chromia species (O 1s from Cr_2O_3). The XP spectra of calcined chromium samples show a main peak at ~532.8 eV characteristic for the O 1s, arising entirely from the framework species. However, in addition to the peak at 532.8 eV, the calcined Cr-MCM-41 (CRC) and $C_{27}MeC_{15}$ sample shows a relatively broad band and a tailing of this band to lower energy value (Fig. 4.12B). Deconvolution of the O 1s XP spectra of these samples show a second peak with a maximum at ~530 eV. This peak may possibly arise from the oxygen of the chromia species, as noted from the XRD and UV-Vis analysis.

4.4. OXIDATION OF CYCLOHEXANE USING *non-aqueous* TBHP AND AIR AS OXIDANTS

4.4.1. Reaction Procedure

Cyclohexane oxidation reactions were carried out in a 10 mL round bottom flask fitted with a water-cooled condenser using *non-aqueous tert*-butylhydroperoxide (TBHP) as an oxidant. For that, a stock solution of *tert*-butylhydroperoxide in cyclohexane was prepared by extraction of TBHP (70%) in cyclohexane. Phase separation was promoted by the addition of NaCl in the aqueous layer and finally the organic layer was dried over $MgSO_4$.[55] The reactant mixtures of cyclohexane (10 mmol, E-Merck, 99%, dried over 4 Å molecular sieves), oxidant (10 mmol, E-Merck) and acetone solvent (5 mL, E-Merck, 99%, dried over 4 Å molecular sieves) was added to 0.1 g of catalyst and was heated at a constant temperature of 70 ^{o}C under magnetic stirring (*ca*. 800 rpm).

The aerial oxidation of cyclohexane was carried out in a high-pressure autoclave (Parr 4843) using 20 mL (185 mmol) of cyclohexane in presence of 0.2 g of catalyst, under solvent free condition at different temperature (100-160 ^{o}C) and air pressures (1.3-5.5 MPa).

After reactions, the reaction mixture was cooled to room conditions and the catalyst was separated from the reaction mixture by centrifugation. The oxidized products were analyzed on a gas chromatograph (HP 6890) equipped with a flame ionization detector (FID) and a capillary column (5 μm cross linked methyl silicone gum, 0.2 mm × 50 m). The formation of carboxylic acid side products was determined by GC analysis after conversion to the respective methyl esters.[55,56]

4.4.2. Catalytic Results in Presence of *non-aqueous* TBHP as an Oxidant

Selective oxidation reaction of cyclohexane to a mixture of cyclohexanone and cyclohexanol (so-called K-A oil), under mild conditions, is of considerable relevance in the production of Nylon 6 and Nylon 66.[57] Hence, the present small pore chromium samples are applied as catalysts in the oxidative transformation of cyclohexane and the catalytic activity was compared with a Cr-MCM-41 catalyst synthesized without any organic spacers (Table 4.6). The main products obtained are cyclohexanol (A) and cyclohexanone (K) with trace amounts of cyclohexylhydroperoxide (CHHP) as well as cyclohexyl-*tert*-butylperether (CHTB). The samples prepared using organic spacers showed higher conversion than the conventional Cr-MCM-41 catalyst and among them, the $C_{27}ClC_{15}$ catalyst shows maximum conversion followed by $C_{27}ViC_{15}$, $C_{27}MeC_{15}$ and Cr-MCM-41, after 5 h run. The decreased catalytic activity of CRC and $C_{27}MeC_{15}$ catalysts might be due to the aggregation of chromium species, as noted from UV-Vis and XPS, and the agglomeration of such species may reduces the accessibility of the individual chromium atoms and therefore the number of active sites. Hence the enhanced activity of the $C_{27}ClC_{15}$ catalyst can be assigned to: (i) the wormhole-like channel morphology obtained, which may facilitate a better access for the cyclohexane molecules to the active chromium sites (from TEM images), (ii) the improved hydrophobicity relations between the oxidant and catalyst and (iii) the absence of Cr_2O_3 clusters, which create all the active chromium sites available for the substrate molecules. Thus, the better conversion results obtained with the $C_{27}ClC_{15}$ catalyst suggest that isolated, well-dispersed chromium species are highly active in the oxidation reaction of cyclohexane.

Table 4.6. Cyclohexane oxidation reaction over small-pore chromium catalysts using *non-aqueous* TBHP as an oxidant [a]

Catalyst	Cr (%)	Cy-ane Conv. (mol.%)	K/A	TON	Metal Leaching (%)
$C_{27}ClC_{15}$	2.3	9.5	5.5	2.0	10
$C_{27}ClC_{30}$	1.9	10.3	5.7	2.7	n.d
$C_{27}ClC_{50}$	1.7	9.6	4.8	2.8	n.d
$C_{27}ViC_{15}$	2.4	7.3	6.1	1.4	8
$C_{27}MeC_{15}$	2.4	6.6	5.5	1.3	22
CRC	2.5	4.0	6.8	0.8	26
Si-MCM-41	-	-	-	-	-

Reaction Conditions: catalyst (g), 0.1; T (°C), 70; cyclohexane : TBHP (mol/mol), 1; solvent (~5 mL), $(CH_3)_2CO$; time (h), 5.

[a] K/A, cyclohexanone/cyclohexanol ratio; TON, Turn over number, moles of cyclohexane converted per mole of chromium; percentage of metal leaching was determined by ICP-OES analysis; n.d, not determined.

At the beginning of the reaction, the K/A ratios for all the samples were close to one and this ratio increased with time showing that cyclohexanol (A) is the primary product formed which is later oxidized to cyclohexanone (K). Moreover, it is attractive to note the major formation of oxidized product cyclohexanone and the K/A ratios reached a value of >5, after 5 h reaction time (Table 4.6). Since CHHP is also formed as a product, it is reasonable that the peroxide species formed may also enhance the conversion of cyclohexane. However, kinetic measurements showed that its percentage gets increased with cyclohexane conversion in the initial stages of the reaction (up to 3 h). This indicates that CHHP does not act as an oxidizing agent and thus the increased formation of cyclohexanone may possibly arise from the mixed Russell termination (Scheme 4.1).[55]

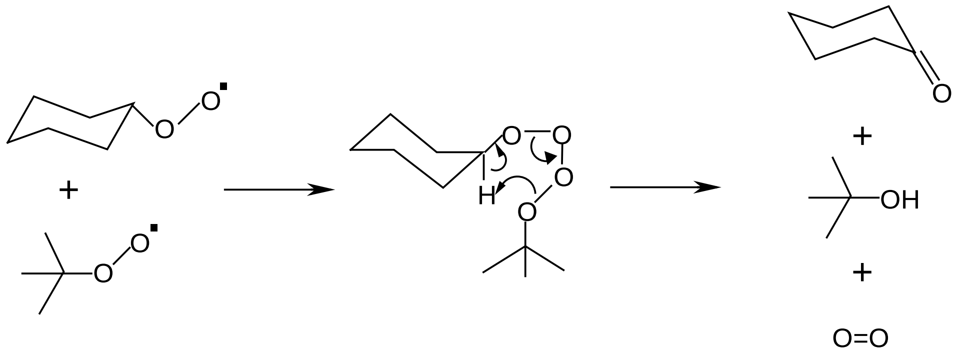

Scheme 4.1. Mixed Russell termination step between *c*-$C_6H_{11}OO^{\cdot}$ and *t*-$BuOO^{\cdot}$

Chromium-containing porous materials often exhibit leaching of chromium species during liquid phase reactions. Since, after calcination, chromium in molecular sieves is presumed to contain two extra framework Cr=O bonds, chromium can be anchored to the framework through only two Si-O bonds and so the leaching is facile in chromium-substituted porous materials (Scheme 4.2).[38,58] Hence, to confirm that the catalysts are heterogeneous and chromium was not leached out during reactions, ICP analysis of the reaction mixture was done. Results show that the catalysts are heterogeneous and shows limited leaching than the chromium-containing catalysts prepared without the addition of any organosilanes (Table 4.6). These results suggest that the organic groups introduced not only helps to tailor the pore sizes but also helps to disperse the active catalytic sites and the hydrophobic features are maintained akin to the recently reported periodic mesoporous organosilicas.[59] Remarkably, the leaching of chromium was found least for the $C_{27}ViC_{15}$ catalyst than the other chromium-containing small pore catalysts. This effect can be attributed to the better wall thickness of the $C_{27}ViC_{15}$ sample, due to the polymerization of the vinyl groups, which may helps in the stabilization of chromium than the other chromium catalysts.

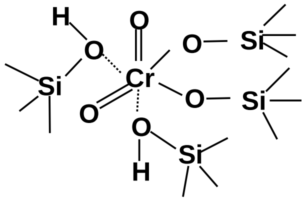

Scheme 4.2. Possible binding state of chromium inside the mesoporous support after calcination

4.4.3. Catalytic Results in Presence of Air as an Oxidant

As mentioned in Section 4.4.2, the catalytic activation, especially partial oxidation of alkanes constitutes one of the major challenges of present-day chemistry and among them the conversion of cyclohexane to cyclohexanone and cyclohexanol is the principal targets since the products were used as the feed stock in several industrial process including the production of nylon. The present commercial process for cyclohexane oxidation is carried out around 150 ^{o}C and 1-2 MPa pressure affording ~4% conversion and 70-85% selectivity to mono-oxygenated products (a mixture of cyclohexanone (K), cyclohexanol (A) and the intermediate cyclohexylhydroperoixde (CHHP)) over metal cobalt salt or metal-boric acid. The CHHP is decomposed either directly or in a separate step to yield additional ketone and alcohol.[60] However, during these chemical engineering processes, serious pollutions, low conversion and higher operating cost are growing more and more outstanding. Consequently, a heterogeneous catalyst system might offer several advantages such as ease of separation, recycling of catalyst and solvent-free reaction conditions. Hence, the selective aerial oxidation of cyclohexane under mild conditions using heterogeneous solid catalysts continues a challenge to the chemists.[61]

The catalytic activity results of all the small pore chromium samples in the aerial oxidation reaction of cyclohexane at 120 ^{o}C and 2.7 MPa air pressure are given in Table 4.7. The blank reaction carried out without any catalyst or with Si-MCM-41 shows no oxidative products. Hence, the excellent cyclohexane conversion observed with the chromium catalysts arise from the presence of active chromium sites in the small pore catalysts. Earlier, many heterogeneous solid catalysts were used for cyclohexane oxidation reaction in presence of H_2O_2, TBHP and air as oxidants. However, the activity of most of the catalysts depends on the nature of solvents used. Moreover, in order to accelerate the initiation step of the auto oxidation process using oxygen as oxidant, addition of H_2O_2 or TBHP as co-catalysts is essential.[62] However, the present catalysts show their catalytic activity only in presence of air oxidant, and no other solvents or co-catalyst systems are needed for their catalytic performance.

A comparison between the cyclohexane conversion and selectivity to cyclohexanol and cyclohexanone over the different calcined chromium catalysts are given in Table 4.7. Among the chromium catalysts, the samples prepared with the chloro propyl pendant group, $C_{27}ClC_{15}$, show higher conversion rates. The enhanced activity of the $C_{27}ClC_{15}$ catalyst may arise due to the absence of Cr_2O_3 clusters, which create all the chromium sites available for the substrate molecules. Thus, the better conversion results obtained with the $C_{27}ClC_{15}$ catalyst reasonably suggest that isolated, well-dispersed chromium species are highly active and be the active sites in the aerial oxidation of cyclohexane. Further, in accordance with the earlier observations over M-AlPO molecular sieve catalysts, the oxidation of cyclohexane with the present small pore chromium catalysts also proceed by free-radical mechanism.[63] This suggestion arise from two independent experiments: (i) the addition of free radical initiator like *tert*-butylhydroperoxide (TBHP) helps to increase the cyclohexane conversion while the selectivity towards the primary oxidized products is retained, (ii) the addition of a free radical scavenger like hydroquinone (HQ) retards the oxidation reaction and also affects the product distribution, that cyclohexylhydroperoxide (CHHP) formation is predominant and (iii) the presence of cyclohexylhydroperoxide during the initial stages of the reaction, which subsequently decomposed to the primary products like cyclohexanol and cyclohexanone (Table 4.7).

Table 4.7. Cyclohexane oxidation reaction over small-pore chromium catalysts in presence of air

Catalyst	Cy-ane Conv. (mol%)	TON [a]	Product distribution / mol% [b]			
			Cy-ol (A)	Cy-one (K)	K/A	Others
$C_{27}ClC_{15}$	8.0	43	29	63	2.1	8
$C_{27}ClC_{15}$ [c]	10.2	55	27	68	2.5	5
$C_{27}ClC_{15}$ [d]	3.3	29	34	53	1.5	13
$C_{27}ClC_{30}$	7.1	47	30	65	2.1	5
$C_{27}ClC_{50}$	5	36	30	66	2.3	4
$C_{50}ClC_{15}$	6.2	51	30	65	2.1	5
$C_{100}ClC_{15}$	3.4	46	31	66	2.1	3
$C_{27}ViC_{15}$	7	36	29	64	2.2	7
$C_{27}MeC_{15}$	6.1	31	30	65	2.1	5
CRC	6.3	31	26	66	2.5	8
Si-MCM-41	No reaction	-	-	-	-	-

Reaction Conditions: cyclohexane (mL), 20; T (°C), 120, t (h), 6; air pressure (MPa), 2.7.

[a] TON, Turn over number, moles of cyclohexane converted per mole of chromium.

[b] Cy-ol = Cyclohexanol; Cy-one = Cyclohexanone; others, mainly CHHP and adipic acid.

[c] Reactions carried out in presence of small amounts (2% of cyclohexane) of free radical initiator, *tert*-butylhydroperoxide (TBHP).

[d] Reactions carried out in presence of small amounts (2% of cyclohexane) of free radical scavenger, hydroquinone (HQ).

Figure 4.13 shows the kinetic results of the $C_{27}ClC_{15}$ catalyst. It is observed that the chromium catalyst show an increase in cyclohexane conversion in the initial stages and after 9 h the conversion remains almost constant. Moreover, the selectivity of cyclohexanol decreases with time, with the concomitant formation of cyclohexanone. These results suggest that the primary product formed is cyclohexanol and the decreased conversion of cyclohexanol at longer time durations attributes to their oxidation to cyclohexanone, as cyclohexanol was more reactive than cyclohexane. The formation of other products relates to the presence of CHHP in the initial stages while after 9 h dicarboxylic acids like adipic acid are also noted due to the excess oxidation of cyclohexanone.

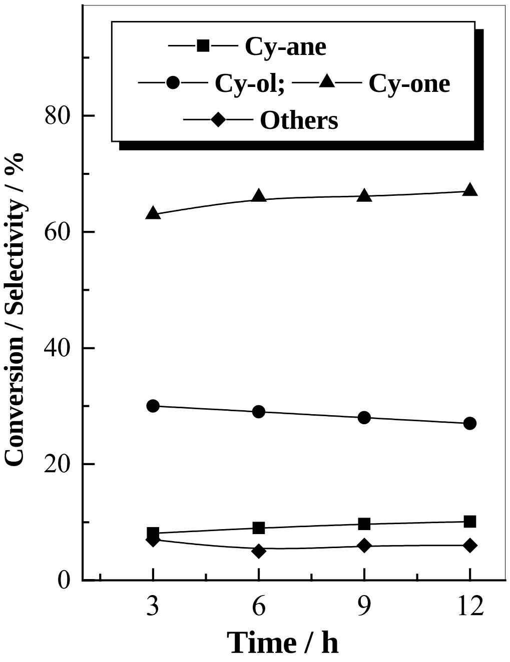

Figure 4.13. Kinetic results for the oxidation of cyclohexane using $C_{27}ClC_{15}$ catalyst.

Figure 4.14A&B illustrates the influence of reaction temperature and air pressure in the oxidation reaction of cyclohexane over $C_{27}ClC_{15}$ catalyst. With an increase in reaction temperature, cyclohexane conversion increases up to 140 ^{o}C, whereafter the conversion remains the same. The selectivity of cyclohexanone also increases with reaction time at the expense of cyclohexanol. Thus an increase in reaction temperature helps to improve the selectivity of cyclohexanone and more oxidized products like adipic acid. Similarly, an increase in air pressure also helps to increase the cyclohexane conversion up to 4.1 MPa whereafter the conversion is more or less constant. Meanwhile, the selectivity of cyclohexanol decreases and at 5.7 MPa an increased formation of adipic acid is also noted (~9%).

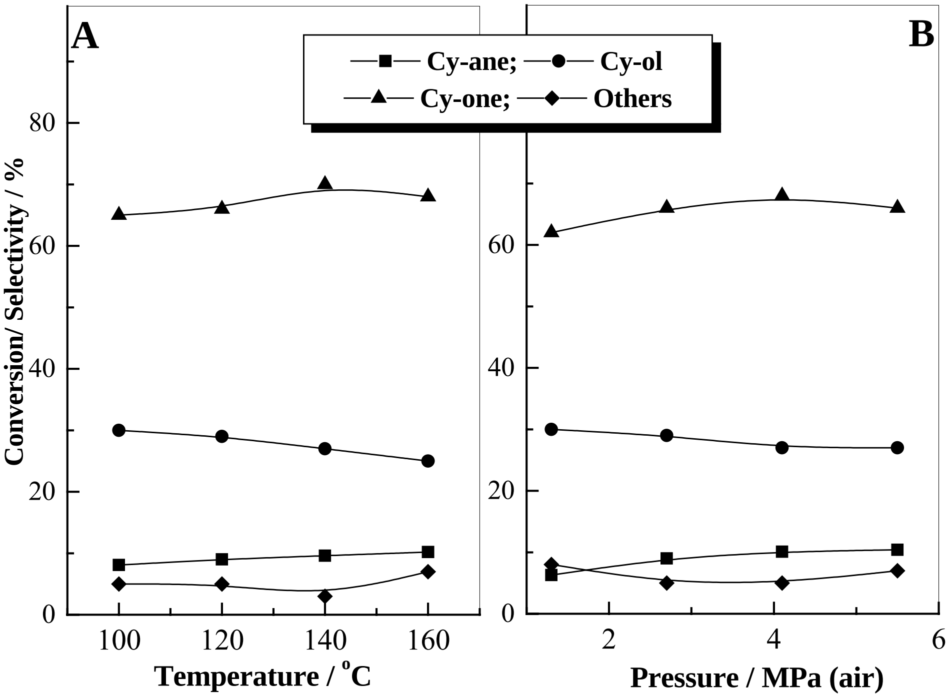

Figure 4.14. Influence of (A) temperature and (B) air pressure in the oxidation reaction of cyclohexane using $C_{27}ClC_{15}$ catalyst.

4.4.4. Recycle Studies

To confirm that the catalysts are heterogeneous and chromium was not leached out during reactions, recycling studies were carried out. As a first experiment, the catalyst was separated from the reaction mixture, washed, dried and activated at 400 °C for 5 h and was used in a fresh run. Results up to three runs shows that the catalyst retains an almost similar conversion and selectivity revealing that the catalyst is recyclable (Fig. 4.15). Thus recycling studies shows that the oxidation of cyclohexane by free or dissolved chromium ions is negligible in case of small pore mesoporous chromium catalysts.

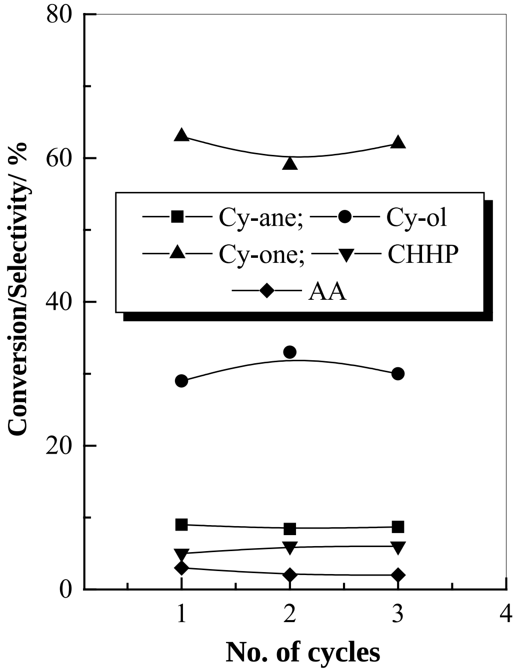

Figure 4.15. Recycling studies performed over $C_{27}ClC_{15}$ catalyst.

Thus heterogenity tests proved that the small pore chromium catalysts are heterogeneous and shows limited leaching than the chromium-containing catalysts prepared without the addition of any organosilanes (Table 4.6). These results suggest that the organic groups introduced not only helps to tailor the pore sizes but also helps to disperse the active catalytic sites and resist the leaching of chromium during liquid phase reactions. Thus the small pore chromium-silica catalysts are efficient, recyclable heterogeneous catalysts for the oxidation reaction of cyclohexane using air as an oxidant.

4.5. REFERENCES

1 C. T. Kresge, M. E. Leonowicz, W. J. Roth, J. C. Vartuli, J. S. Beck, *Nature* **1992**, *359*, 710.

2 J. H. Clark, D. J. Macquarrie, *Chem. Commun*. **1998**, 853.

3 K. Moller, T. Bein, *Chem. Mater*. **1998**, *10*, 2950.

4 T. Asefa, M. J. MacLachlan, N. Coombs, G. A. Ozin, *Nature* **1999**, *402*, 867.

5 B. J. Melde, B. T. Holland, C. F. Blanford, A. Stein, *Chem. Mater*. **1999**, *11*, 3302.

6 S. Inagaki, S. Guan, Y. Fukushima, T. Ohsuna, O. Terasaki, *J. Am. Chem. Soc*. **1999**, *121*, 9611.

7 A. Stein, B. J. Melde, R. C. Schroden, *Adv. Mater*. **2000**, *12*, 1403.

8 M. H. Lim, A. Stein, *Chem. Mater*. **1999**, *11*, 3285.

9 A. Sayari, S. Hamoudi, *Chem. Mater*. **2001**, *13*, 3151.

10 D. J. Macquarrie, *Green. Chem*. **1999**, 195.

11 X. Feng, G. E. Fryxell, L. Q. Wang, A. Y. Kim, J. Liu, K. M. Kemner, *Science* **1997**, *276*, 923.

12 T. Yokoi, H. Yoshitake, T. Tatsumi, *J. Mater. Chem*. **2004**, *14*, 951.

13 K. A. Koyano, T. Tatsumi, S. Nakata, *J. Phys. Chem. B* **1997**, *101* 9436.

14 T. Asefa, M. Kruk, M. J. MacLachlan, N. Coombs, H. Grondey, M. Jaroniec, G. A. Ozin, *J. Am. Chem. Soc*. **2001**, *123*, 8520.

15 L. Mercier, T. J. Pinnavaia, *Chem. Mater*. **2000**, *12*, 188.

16 Y. Mori, T. J. Pinnavaia, *Chem. Mater*. **2001**, *13*, 2173.

17 A. Sayari, *Chem. Mater*. **1996**, *8*, 1840.

18 A. Taguchi, F. Schuth, *Microporous Mesoporous Mater*. **2004**, *77*, 1.

19 W. H. Zhang, X-B. Lu, J-H. Xiu, Z-L. Hua, L-X. Zhang, M. Robertson, J-L. Shi, D-S. Yan, J. D. Holmer, *Adv. Funct. Mater*. **2004**, *14*, 544.

20 S. R. Hall, C. E. Fowler, B. Lebeau, S. Mann, *Chem. Commun*. **1999**, 201.

21 A. Bhaumik, T. Tatsumi, *J. Catal*. **2000**, *189*, 31.

22 N. Igarashi, S. Kidani, R. Ahemaito, K. Hashimoto, T. Tatsumi, *Microporous Mesoporous Mater*. **2005**, *81*, 97.

23 Q. Huo, D. I. Margolese, G. D. Stucky, *Chem. Mater*. **1996**, *8*, 1147.

24 M. Kruk, M. Jaroniec, Y. Sakamoto, O. Terasaki, R. Ryoo, C. H. Ko, *J. Phys. Chem. B* **2000**, *104*, 292.

25 J. Aguado, D. P. Serano, J. Escola, *Microporous Mesoporous Mater*. **2000**, *34*, 43.

26 T. Sun, M. S. Wong, J. Y. Ying, *Chem. Commun*. **2000**, 2057.

27 M. Ogawa, N. Yamamoto, *J. Porous Mater*. **1999**, *6*, 19.

28 M. Kruk, T. Asefa, M. Jaroniec, G. A. Ozin, *J. Am. Chem. Soc.* **2002**, *124*, 6383.

29 M. J. Kim, R. Ryoo, *Chem. Mater*. **1999**, *11*, 487.

30 S. A. Bagshaw, A. R. Hayman, *Adv. Mater*. **2001**, *13*, 1011.

31 T. Sun, J. Y. Ying, *Nature* **1997**, *389*, 704.

32 R. Ryoo, I-S. Park, S. Jun, C. W. Lee, M. Kruk, M. Jaroniec, *J. Am. Chem. Soc*. **2001**, *123*, 1650.

33 C. G. Sonwane, S. K. Bhatia, N. Calos, *Ind. Eng. Chem. Res.* **1998**, *37*, 2271.

34 M. Ogawa, *Chem. Commun*. **1996**, 1149.

35 M. Ogawa, T. Kikuchi, *Adv. Mater*. **1998**, *10*, 1077.

36 H. Naono, M. Hakuman, T. Shiono, *J. Colloid Interface Sci*. **1997**, *186*, 360.

37 S. Shylesh, S. P. Mirajkar, A. P. Singh, *J. Mol. Catal. A. Chem.* **2005**, *239*, 57.

38 B. M. Weckhuysen, I. E. Wachs, R. A. Schoonheydt, *Chem. Rev*. **1996**, *96*, 3327.

39 S. Huh, J. W. Wiench, M. Pruski, V. S-Y. Lin, *Chem. Mater*. **2003**, *15*, 4247.

40 M. Kruk, M. Jaroniec, *Chem. Mater*. **2001**, *13*, 3169.

41 M. C. Burleigh, M. A. Markowitz, M. S. Spector, B. P. Gaber, *J. Phys. Chem. B* **2001**, *105*, 9935.

42 S. L. Burkett, S. D. Sims, S. Mann, *Chem. Commun.* **1996**, 1367.

43 H. Yang, G. Zhang, Y. Zhu, *Microporous Mesoporous Mater*. **2004**, *68*, 119.

44 E. J. Sullivan, D. B. Hunter, R. S. Bowman, *Environ. Sci. Technol.* **1998**, *32*, 1948.

45 K. J. Chao, C. N. Wu, H. Chang, L. J. Lee, S. Hu, *J. Phys. Chem*. **1997**, *101*, 6341.

46 O. Dag, G. A. Ozin, *Adv. Mater*. **2001**, *13*, 1182.

47 Z. Zhu, Z. Chang, L. Kevan, *J. Phys. Chem. B* **1999**, *103*, 2680.

48 Y. Wang, Y. Ohishi, T. Shishido, Q. Zhang, W. Yang, Q. Guo, H. Wan, K. Takehira, *J. Catal*. **2003**, *220*, 347.

49 Y-S. Li, P. B. Wright, R. Puritt, T. Tran, *Spectrochim. Acta A* **2004**, *60*, 2759.

50 Y. K. Kun'ko, T. S. Perova, S. Balakrishnan, D. A. Potapova, R. A. Moore, E. V. Astrova, *Phys. Stat. Sol. A* **2003**, 492.

51 Z. Zhu, M. Hartmann, E. M. Maes, R. S. Czenuszewicz, L. Kevan, *J. Phys. Chem. B* **2000**, *104*, 4690.

52 E. P. Reddy, L. Davydov, P. G. Smirniotis, *J. Phys. Chem. B* **2002**, *106*, 3394.

53 G. C. Allen, P. M. Tucker, *Inorg. Chim. Acta.* **1976**, *16*, 41.

54 P. C. Thune, C. P. J. Verhagen, M. J. G. Van den Boer, J. W. Niemantsverdriet, *J. Phys. Chem. B* **1997**, *101*, 8559.

55 N. Nowotny, Y. L. N. Pedersen, U. Hanefeld, T. Maschmayer, *Chem. Eur. J.* **2002**, *8*, 3724.

56 R. Raja, P. Ratnasamy, *Catal. Lett*. **1997**, *48*, 1.

57 R. A. Sheldon, J. K. Kochi, *Metal Catalyzed Oxidation of Organic Compounds*, Academic Press, New York, **1981**.

58 R. A. Sheldon, M. Wallau, I. W. C. E. Arends, U. Schuchardt, *Acc. Chem. Res*. **1998**, *31*, 485.

59 A. Bhaumik, M. P. Kapoor, S. Inagaki, *Chem. Commun*. **2003**, 470.

60 P. A. MacFaul, I. W. C. E. Arends, K. U. Ingold, D. D. M. Wayner, *JCS., Perkin Trans*, **1997**, *2*, 135.

61 U. Schuchardt, D. Cardoso, R. Sercheli, R. Pereira, R. S. da Cruz, M. C. Guerreiro, D. Mandelli, E. V. Spinace, E. L. Pires, *Appl. Catal. A. Gen*. **2001**, *211*, 1.

62 G. Lu, R. Zhao, G. Qian, Y. Qi, X. Wang, J. Suo, *Catal. Lett*. **2004**, *97*, 115.

63 R. Raja, G. Sankar, J. M. Thomas, *J. Am. Chem. Soc*. **1999**, *121*, 11926.

5.1. INTRODUCTION

The design and synthesis of mesoporous organic-inorganic hybrid materials having high surface area and variable pore diameters had attracted considerable research attention in the field of material science, enantioselective separations and in heterogeneous catalysis.[1-4] Although, many synthetic methods have been pursued and significant advances have been made in the synthesis of organic-inorganic hybrid nanocomposites, the current state-of-the-art methods have serious limitations in the control of surface properties as well as morphologies. In this sense, the exciting discovery of periodic mesoporous organosilicas (PMO) represents a new class of organic-inorganic hybrid material as they combine the characteristics of ordered mesoporous material with organic groups in the channel walls.[5-7] This discovery led to the development of a new family of mesoporous organosilica nanocomposites.

Introduction of organic groups in the silica framework usually modifies the physical and chemical properties of the mesoporous materials, as the attached organic groups enhance the flexibility of the framework while the inorganic part makes the material thermally and structurally more stable.[8-10] The synthesis procedure utilizes the polymerization of organosilane monomer containing two trialkoxy silyl groups, which allows a homogeneous distribution of organic and inorganic groups within the framework. A highlight of these novel materials is that they exhibit entirely different pore wall structures than the conventional organic-tethered inorganic mesoporous materials. These organic-inorganic hybrid mesoporous solids possessing organic species bonded between the inorganic silica species also helps to overcome the limitations of functionalized organic pendant groups prepared *via.,* direct co-condensation method or post-synthesis method.[11] To date, a variety of organo-bridged hybrid mesoporous materials having organic groups such as methylene, ethane, phenyl and biphenyl have been synthesized.[12,13] Among these, considerable research interest had been focused on ethane-bridged organic groups due to their high rigidity and good ordering.

Selective oxidation reactions of relatively inert C-H bond of hydrocarbons is one of the most desirable and challenging reactions, since the products obtained are themselves important or act as valuable intermediates for industrial organic chemicals.[14] Among them, as mentioned in Chapter 4, the oxidation of cyclohexane to cyclohexanol (A) and cyclohexanone (K) is important because they are the key intermediates in the production of adipic acid (Nylon-66) and caprolactum (Nylon-6). Earlier, these organic transformations were carried out with stoichiometric amounts of various homogenous reagents.[14] It is known that solid catalysts, in which the active sites are fixed on solid supports, can reduce or eliminate the difficulties due to separation and handling. Chromium-containing solid materials like CrS-1, Cr-AlPO, Cr-MCM-41 and Cr-MCM-48 are reported as new heterogeneous catalysts and are widely used as catalysts in the oxidation reaction of cyclohexane.[15-17] The activity of chromium catalysts is related to the variable oxidation states, coordination environment as well as its different degrees of polymerization. However, many of these materials show low activity and thus extreme reaction conditions are usually needed to improve the catalytic performance. Under these conditions leaching of active metal sites makes the process highly undesirable. Therefore, the development of novel chromium-containing mesoporous materials having better stability and activity is of particular relevance in various oxidation reactions.

This chapter describes the synthesis, characterization and catalytic application of chromium-containing periodic mesoporous organosilica materials (Cr-PMO) prepared using C_{18}- and C_{16}-TAB surfactants and the further possibility of incorporation of chromium over a mixed silica source, under basic conditions. Structural characterizations of these materials was performed with XRD, N_2 physisorption analysis, thermal analysis and TEM while the nature of chromium inside the hybrid catalyst matrix was analyzed by various spectroscopic techniques including *in situ* FT-Raman, UV-Vis and XPS.

5.2. EXPERIMENTAL

5.2.1. Materials

Tetraethyl orthosilicate (TEOS, Aldrich), 1,2-bis(triethoxysilyl)ethane (BTEE, Aldrich), octadecyl trimethyl ammonium bromide (C_{18}-TAB, Aldrich), cetyl trimethyl ammonium bromide (C_{16}-TAB, Aldrich), sodium hydroxide (NaOH, Loba Chemie), tetramethyl ammonium hydroxide (TMAOH, Aldrich) and chromium nitrate ($Cr(NO_3)_3.6H_2O$, Loba Chemie). All chemicals were used as received without further purification.

5.2.2. Chromium-containing Periodic Mesoporous Organosilicas Synthesized Using BTEE-C_n-TAB-NaOH-H_2O system (Method I)

Chromium-containing organo-modified hybrid periodic mesoporous organosilica samples were synthesized using a mixture of 1,2-bis(triethoxysilyl)ethane as the silica precursor and octadecyl trimethyl ammonium bromide or cetyl trimethyl ammonium bromide as surfactants. In a typical synthesis procedure, 5 g of BTEE was added with constant stirring to a mixture of 3.7 g of surfactant in an aqueous NaOH solution (1.8 g). After stirring for a predefined time, required amount of chromium nitrate (Si/Cr = 25), was slowly added with vigorous stirring to ensure homogeneity. Stirring was continued overnight. The mixture was then refluxed for an additional 48 h at 100 ^oC. The green colored precipitate obtained was then collected by filtration, washed well with water and vacuum-dried (CHA). The surfactant occluded inside the pores was removed by stirring the as-synthesized material (1 g) with an HCl-EtOH mixture (0.5 g/100 mL) at 50 ^oC for 6 h. The extraction process was repeated twice and the material was finally washed with copious amounts of ethanol and vacuum dried (CHE). The material was also calcined at 550 ^oC for 5 h to remove the organic groups and to further convert the Cr (III) species to Cr (VI) species (CHC). A support hybrid organosilica sample was also prepared under similar experimental conditions using a gel ratio of 1BTEE-0.6C_{18}-TAB-3.2NaOH-450H_2O, but without the addition of chromium source. The as-synthesized hybrid organosilica was designated as BTA, while the surfactant-extracted sample was designated as BTE.

5.2.3. Chromium-containing Periodic Mesoporous Organosilicas Synthesized Using TEOS-BTEE-C_{18}-TAB-TMAOH-H_2O system (Method II)

Chromium-containing organo-modified hybrid periodic mesoporous organosilica samples were also synthesized under alkaline conditions using a mixture of tetraethyl orthosilicate and 1,2-bis(triethoxysilyl)ethane as the silica sources and octadecyl trimethyl ammonium bromide (C_{18}-TAB) as the surfactant. In a typical synthesis procedure, 4.1 g of C_{18}-TAB surfactant was dissolved in 40 mL of water. Required amounts of TEOS and BTEE (TEOS: BTEE ratio, 90:10) was then added to the aqueous surfactant solution. After stirring for 30 min, chromium nitrate (Si/Cr = 25) dissolved in water was slowly added with vigorous stirring. This was followed by the slow addition of TMAOH. The final gel having the molar composition of 1TEOS-0.1BTEE-0.27C_{18}-TAB-2.4TMAOH-60H_2O was then stirred at ambient conditions for 24 h and then refluxed at 100 ^{o}C for 48 h. The green colored precipitate obtained was then collected by filtration, washed well with water and vacuum dried (TBA). The surfactant occluded inside the pores was removed by stirring the as-synthesized material (1 g) with an HCl-EtOH mixture (0.5 g/100 mL) at 50 ^{o}C for 6 h and the surfactant-extracted chromium sample is denoted as TBE. The material was also calcined at 550 ^{o}C for 5 h to remove the organic groups and to further convert the Cr (III) species to Cr (VI) species and is denoted as TBC. An organosilica sample was also prepared under similar experimental conditions without the addition of chromium source. The as-synthesized hybrid organosilica sample was designated as TEA while the surfactant-extracted sample was designated as TEE.

5.2.4. Instruments for Characterization

Powder X-ray diffractograms of the materials were recorded on a Rigaku D MAX III VC Ni-filtered Cu K_{α} radiation, λ=1.5404 Å, between 1.5 to 80° (2θ) with a step size of 0.02^{o}.

N_2 adsorption-desorption isotherms, pore size distributions as well as the textural properties of the hybrid materials were determined at -196 °C by a NOVA 1200 (Quanta chrome) instrument. Before analysis, the samples were activated at 200 °C for 6 h under vacuum and then the adsorption-desorption was conducted by passing nitrogen into the sample, which was kept under liquid nitrogen. Pore size distribution (PSD) and average pore size of the hybrid samples were obtained from the adsorption branch of the isotherms using the Barrer-Joyner-Halenda (BJH) method.

TEM images were obtained on a JEOL JEM-1200 EX instrument at an acceleration voltage of 120 kV. Samples were prepared by sonicating the powdered samples for 30 min in isopropanol, followed by depositing two drops on a holey carbon film supported by a copper grid.

FT-IR spectra of the solid samples were taken in the range of 4000 to 400 cm^{-1} on a Shimadzu FTIR 8201 instrument by diffuse reflectance scanning disc technique. FT-Raman spectra were measured using a Bruker RFS 100/S spectrometer equipped with a Nd:YAG laser (1064 nm) and an InGaAs detector. Powdered samples were pressed into a stainless steel sample holder and run in the open atmosphere. A laser power of 75 mW was used. Spectra were acquired from 4000 to 250 cm^{-1} at a resolution of 4 cm^{-1}. In order to increase the signal-to-noise ratio 2000 scans were coadded. Temperature studies were performed by placing the powdered sample into a Specac Environmental Chamber™ DRIFTS cell modified with a near-infrared transparent quartz window. In order to enable quantitative measurement of intensity changes boron nitride powder was physically mixed (1 wt %) with the powdered sample. Boron nitride is stable to high temperatures and its Raman spectrum contains a single, intense band at 1365 cm^{-1} (no band overlap with the samples measured here). After measuring the Raman spectrum at room temperature the sample was heated *in situ* in flowing artificial air (20 mL/min) to 100 °C, held for 1 h, and then cooled to room temperature where the Raman spectrum was remeasured. This process was then repeated at 200 °C, 300 °C and 400 °C for each sample.

Solid-state ^{13}C CP MAS NMR and ^{29}Si MAS NMR spectra were recorded on a Bruker MSL 300 NMR spectrometer with a resonance frequency of 75.5 MHz and 59.6 MHz for ^{13}C and ^{29}Si using 4 mm zirconia rotors and a sample spinning frequency of 3 kHz. ^{13}C NMR spectra were collected with 70^o rf pulses, 5 s delay while ^{29}Si NMR spectra were collected with 70^o rf pulses, 30 s delay and in both cases with ~6000 scans. The chemical shifts were referenced to glycine and TMS, respectively, for ^{13}C and ^{29}Si.

Diffuse reflectance UV-Vis spectra were recorded in the range 200-600 nm with a Shimadzu UV-2101 PC spectrometer equipped with a diffuse reflectance attachment, using $BaSO_4$ as the reference. XPS measurements were performed on a VG Microtech ESCA 3000 instrument, using non-monochromatized Mg K_α radiation at pass energy of 50 eV and an electron takeoff angle of 60^o. Base pressure in the analysis chamber was 4×10^{-10} Torr. The overall energy resolution of the instrument is better than 0.7 eV, determined from the full width at half maximum (FWHM) of the $4f_{7/2}$ core level of the gold surface. The correction of binding energy was performed by using the C 1s peak of carbon at 284.9 eV as reference.

5.3. CHARACTERIZATION

5.3.1. Powder X-Ray Diffraction

The structural ordering of the ethane-bridged organosilicas and chromium-containing organosilicas was determined from the XRD patterns. Figure 5.1A shows the XRD patterns of the as-synthesized (BTA) and surfactant-extracted (BTE) hybrid organosilica samples prepared using Method I. Compared to the as-synthesized sample, the surfactant-extracted sample shows high intense XRD reflections and the peaks are well distinguished. This difference is attributed to the density contrast between the framework and the open pores (surfactant-extracted samples) relative to that of the framework-surfactant composite of the as-synthesized sample.[18]

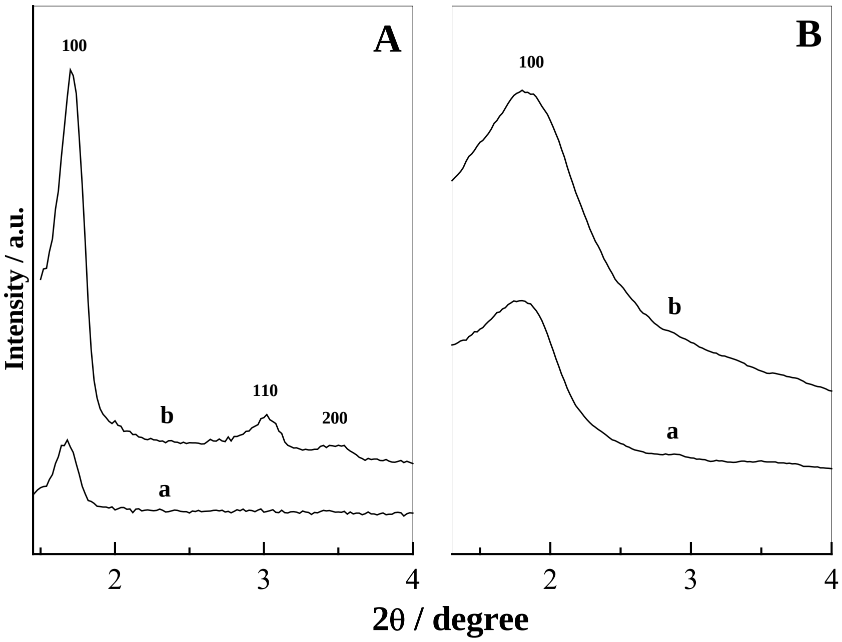

Figure 5.1. XRD patterns of hybrid samples prepared by (A) Method I: (a) BTA, (b) BTE and (B) Method II: (a) TEA, (b) TEE.

Figure 5.2A shows the XRD results of chromium-containing as-synthesized (CHA), surfactant-extracted (CHE) and calcined (CHC) hybrid samples prepared under Method I. The as-synthesized chromium-containing hybrid material prepared by Method I show the characteristic (100), (110) and (200) Bragg reflections. These patterns are similar to the earlier literature reports over periodic mesoporous organosilicas (Fig. 5.2A (a)).[5] Compared to the pristine hybrid support samples, the decrease in the peak intensity after chromium introduction is attributed to the interference of chromium ions in the structure directing action of template, resulting from a change in the ionic strength of the medium.[19] The changes in the unit cell values after chromium substitution suggest that the hybrid materials incorporated chromium and that the organic constituents are molecularly dispersed in the channel walls (Table 5.1). Similar results were observed earlier for Cr-MCM-41 materials and were assigned to the incorporation of chromium on the frame wall positions, as the ionic radius of Cr^{3+} (0.76 Å) is larger than that of Si^{4+} (0.40 Å).[17] However, since the radius of Cr^{3+} is much greater than that of Si^{4+}, a large increase in the unit cell parameter was expected. In fact, only a small increase in the lattice value is noted after metal introduction. This would suggest that a greater part of chromium exists on the wall surface than gets truly incorporated inside the framework.

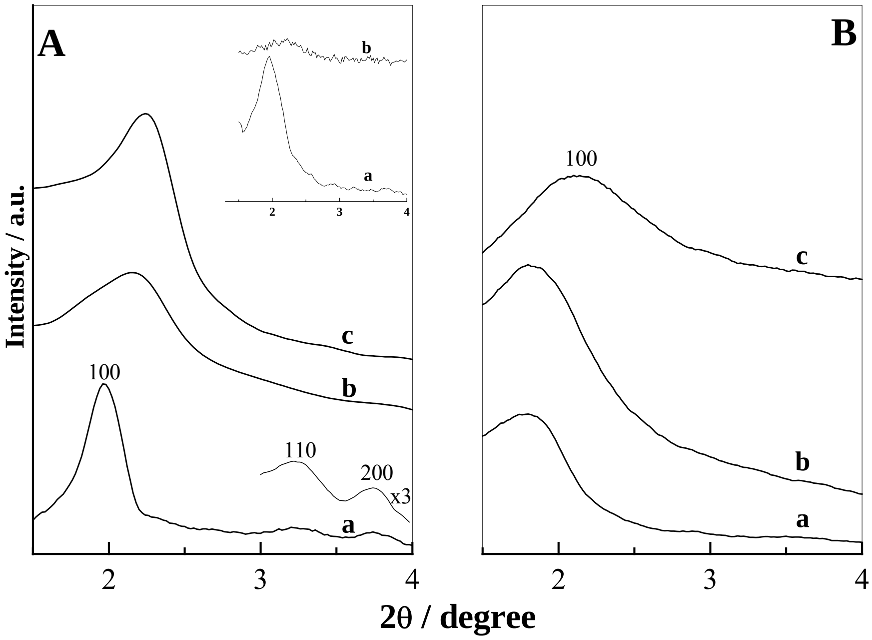

Figure 5.2. XRD patterns of chromium-containing PMO samples prepared by (A) Method I: (a) CHA, (b) CHE, (c) CHC and (B) Method II: (a) TBA, (b) TBE, (c) TBC. Insert in Figure A shows the XRD patterns of hybrid chromium samples prepared by C_{16}-TAB surfactant; where (a) as-synthesized sample and (b) calcined sample.

For the hybrid material synthesized with different chain length surfactants (C_{18}- and C_{16}-TAB) it appears that the material made with the C_{18}- chain length surfactant produced a better resolved and distinct XRD pattern than did the material prepared using the C_{16}- chain length surfactant (Fig. 5.2A). This improved result may arise that if the chain length of the surfactant is long it can form a large pore channel. Thus the introduced heteroatoms can be better arranged in the pore channel more easily than in the small pore channels produced by the shorter chain surfactants.[20] However, after surfactant removal a decrease in the intensity of the characteristic peak, degree of long-range ordering and a lattice contraction are observed, indicating a partial structural collapse and these changes are more pronounced after the calcination. Indeed, the significant lattice contraction, after calcination is not surprising, as thermal treatments removes the organic groups from the frame wall positions and thereby modifying the structural and textural properties of the materials. However, it is noteworthy that after calcination, no peaks attributable to the formation of a crystalline Cr_2O_3 phase were detected. This points to a lack of accumulated chromium species on the surfaces and thus indicates that the metal ions were highly dispersed in the support matrix.

Interestingly, it was observed that when a mixed silica source (TEOS-BTEE, Method II) was used during the synthesis of chromium-containing hybrid materials, the results were dependant upon the nature of alkaline medium used. When NaOH was used as the alkaline medium, no material precipitated from solution, even after stirring for long durations or after hydrothermal treatments. However, upon changing the alkaline medium from NaOH to TMAOH in the TEOS-BTEE-surfactant mixture, precipitation of the hybrid material occurred. The XRD patterns of as-synthesized (TEA) and surfactant-extracted pristine organosilica sample (TEE) prepared by Method II are shown in Figure 5.1B, while the as-synthesized (TBA), surfactant-extracted (TBE) and calcined (TBC) chromium-containing hybrid samples are given in Figure 5.2B. Contrary to the BTEE-C_{18}-TAB-NaOH system, the XRD patterns of organosilicas prepared by Method II and its chromium analog shows only a single, broad band in the low angle and are devoid of higher-ordered reflections. This result shows that the pore walls are either amorphous or lack structural ordering between adjacent pores in the mixed silica synthesis. Hence the well-resolved and intense XRD pattern obtained for the BTEE-C_{18}-TAB-NaOH system can be related to the complete hydrolysis and condensation of the silica precursor favoring a smooth interaction with the preformed surfactant species. However, in the mixed silica source, since BTEE hydrolyze and condense much faster than TEOS, due to the inductive effect of the ethylene bridges, an increase in the density of the negative charges of the silicon and oxygen atoms may occur.[21] Hence, the difference in the rate of hydrolysis and condensation between the two different silica sources, *viz.*, BTEE and TEOS, and its different interaction with the charged template species resulted in the single reflection under Method II.

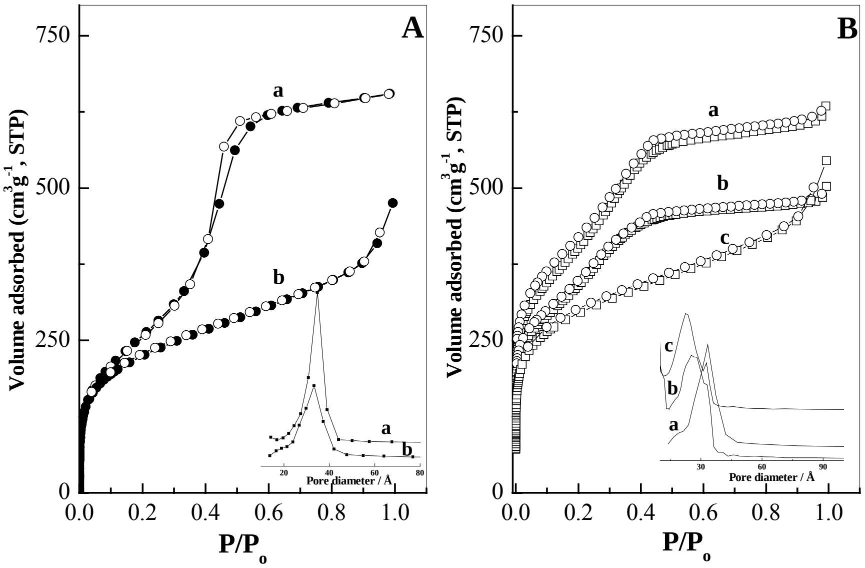

Figure 5.3. N_2 adsorption-desorption isotherms of: (A) pristine organosilica samples; (a) BTE, (b) TEE and (B) chromium-containing mesoporous samples; (a) CHE, (b) CHC, (c) TBE. Insert in Figure A and B shows the corresponding pore size distribution curves.

5.3.2. N_2 Adsorption and Desorption

N_2 adsorption-desorption isotherms as well as the pore size distribution (PSD) plots of surfactant removed organosilica and organo chromiumsilica samples are depicted in Figure 5.3. All samples show type IV adsorption isotherms, according to the IUPAC classification, indicating the uniformity of the mesopores due to capillary condensation of N_2 within the mesopores.[5] A comparison in the adsorption step for the materials prepared from Method I and II shows that Method I produces a material capable of high nitrogen uptake, suggesting a more ordered pore array, while the materials prepared under Method II lacks the steepness in the adsorption step. Hence, the usage of mixed silica source alters the pore assembly leading to materials having disordered structural as well as textural features. Moreover, compared to the support hybrid material, the capillary condensation step for hybrid chromium samples is shifted to slightly lower partial pressures, showing a possible reduction in the pore size and a partial distortion in pore arrangement, consistent with the XRD results.

Table 5.1. Pore structural parameters of Chromium-containing PMO samples [a]

Sample	Unit cell Parameter (Å) [b]	Surface Area (m^2g^{-1})	Pore Volume (cm^3g^{-1})	Pore Diameter (Å)	Wall Thickness (Å)
BTE	51.5	933	0.94	35.1	16.4
CHE	52.8	877 (753)	0.85 (0.53)	34.5 (28.2)	19.7 (20.6)
CHE (C_{16}-) [c]	47.6	734 (646)	0.78 (n.d)	33.6 (n.d)	15.4 (n.d)
TEE	52.8	727	0.76	33.2	19.6
TBE	54.1	702 (631)	0.73 (0.48)	31.8 (23.2)	15.9 (16.2)

[a] Values in parentheses show the results of calcined samples. [b] Unit cell parameter = $2d_{100}/\sqrt{3}$, [c] prepared from C_{16}-TAB surfactant, n.d = not determined.

The specific surface area, pore volume, pore diameter and wall thickness of the organosilica and Cr-PMO samples are tabulated in Table 5.1. The surface area of surfactant-extracted hybrid chromium samples shows a high surface area of 877 m^2g^{-1} (Method I) and 702 m^2g^{-1} (Method II), respectively, and the calcined materials shows only ~10-15% surface area decrease. Hence, even after calcination, the hybrid samples retain the characteristic textural properties of the mesoporous materials. However, compared to organosilica, the chromium-containing organosilica samples show a reduction in pore size with a concomitant increase in the wall thickness. In view of the reduction in pore size of the chromium-containing hybrid samples and from the unit cell parameter values (from XRD) it is anticipated that a greater percentage of chromium resides in the wall channels rather than incorporated in the thick frame wall positions.[20]

5.3.3. Transmission Electron Microscopy

The structural ordering and morphology of the hybrid catalysts were further investigated *via*., TEM. TEM images show interesting structural differences between the different silica-templated mesoporous materials and their chromium analogs (Fig. 5.4). It was noted that the pore array of the material changed with the silica source and with the presence of chromium ions. The support material prepared from BTEE-C_{18}-TAB-NaOH system produced spherical structures while hexagonal pore channels were noted in case of chromium-containing BTEE-C_{18}-TAB-NaOH system (Method I). In sharp contrast, the TEOS-BTEE-C_{18}-TAB-TMAOH system produced wormhole-like or spongy structures while its chromium analog contains small particles with poorly ordered mesopore channels (Method II).[21,22] These results indicate that different silica sources and the presence of chromium in the pore channels affects the structural morphology of the mesoporous organosilica hosts.

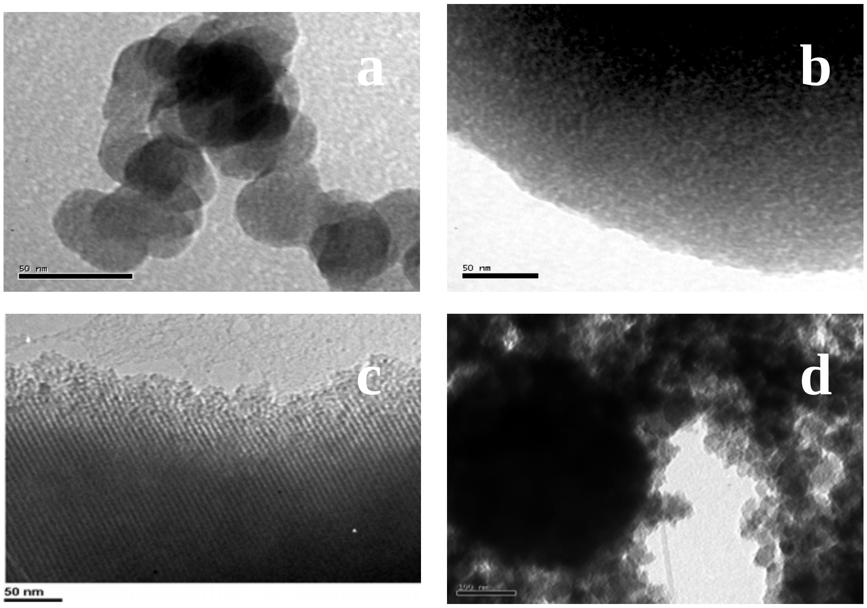

Figure 5.4. TEM images of surfactant-removed mesoporous organosilicas and chromiumsilicas: (a) BTE, (b) TEE, (c) CHC and (d) TBC.

The typical framework structures obtained under different silica sources results from the lower anionic charge density of the oligomerized organosilica species than the silica species formed from TEOS. This may possibly enlarge the effective head group of the cationic surfactant in accordance with the charge density matching relationships ($g = V/a_o l$), which in turn may induce distinct morphologies as well as framework structures in BTEE- containing mesoporous materials.[23] Moreover, in the TEOS-BTEE mixed silica source, because of the inductive effect of the ethane bridges, BTEE hydrolyzes and condenses much faster than TEOS and the difference in the co-operative assembly process of the hydrolyzed organosilica/silica with template lead to the wormhole-like structural motif. Hence, the differences in the ionic strength as well as hydrolysis and condensation rates of the different silica sources used in the synthesis of hybrid materials lead to the different framework structures. This result confirms that slight changes in the gel conditions of periodic mesoporous organosilica (PMO) materials can lead to materials having interesting morphologies. The developed materials may finds applications in catalysis because the regular particle size and mesoporous structure, observed under Method I, allow an easy modeling of mass transfer reactions inside the hybrid materials while the peculiar wormlike channel morphology facilitates an enhanced access for the diffused reactant species to the reactive sites in the wall positions.[24,25]

5.3.4. FT-IR Spectra

Removal of surfactant groups from the pore channels of the hybrid materials as well as the presence of ethane fragments in the framework were analyzed by FT-IR studies. Figure 5.5a&b shows the infrared spectra of the as-synthesized and surfactant-extracted organosilica samples. In Figure 5.5a strong bands are present at 2939, 2854 and 1410 cm^{-1}. The first two bands correspond to ν(C-H) of the surfactant C_{18}-TAB as well as ethane groups of the BTEE.[21] The band at 1410 cm^{-1} is due to δ(C-H). Following solvent extraction, there is a sharp decrease in peak intensities at 2939 and 2854 cm^{-1} (Fig. 5.5b), while the presence of bands at 1405, 1270 and 1165 cm^{-1} suggests the retention of organic fragments related to the $-CH_2-CH_2-$ unit in the framework positions.[22] In addition, the presence of bands at 1275 cm^{-1} and 690 cm^{-1}, assigned to the CH_2-Si stretching vibrations (*v*(C-Si)), indicates that the organic bridge had not cleaved during the extraction procedures. The asymmetric and symmetric stretching vibrations of the Si-O bands were also observed at 1089 cm^{-1} and at 805 cm^{-1} and the band at 930 cm^{-1} indicate the presence of residual silanol, *v*(Si-OH) stretching vibrations. Compared to the support hybrid material, the hybrid mesoporous chromium sample shows a decrease in the symmetric and asymmetric Si-O vibration, which may arise due to the presence of chromium in the frame wall positions (Fig. 5.5c). Further, the band at 930 cm^{-1} shifts to lower wave numbers for the chromium sample. This shift can be related to a perturbation of the vibration of the silica structure after the substitution of chromium into the organosilica framework. Similar results have been noted for metal-containing periodic mesoporous silica materials.[17,26]

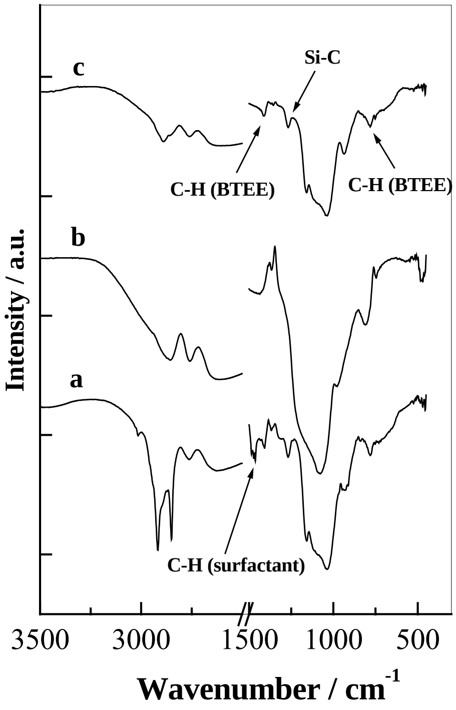

Figure 5.5. FT-IR spectra of: (a) BTA, (b) BTE and (c) CHE.

5.3.5. FT-Raman Spectra

Figure 5.6 shows the FT-Raman spectra of the hybrid mesoporous material before and after removal of the C_{18}-TAB surfactant by solvent extraction (BTA and BTE). The peaks assignments are listed in Table 5.2. Except for the obvious increase in intensity in the C-H stretching region the bands present with and without surfactant are similar although more intense and broader with C_{18}-TAB remaining in the sample.[27,28] The bands at 1000 and 795 cm^{-1} are similar in position to those previously reported in these mesoporous materials and are assigned to the stretching modes of surface silanols (υ O_3Si-OH) and siloxane bridges (Si-O-Si).[29,30] The band at 1600 cm^{-1} has also been observed; assigned to the deformation mode of water (δ H_2O). The band at 522 cm^{-1} was previously reported by Dag *et al*. and was assigned to the Si-C stretching mode of organic groups '*frozen inside the channel walls'* during synthesis using 1,2-bis(triethoxysilyl)ethane, as was used here.[29] These authors also observed bands in the region 1400-1600 cm^{-1} and at 1410 cm^{-1}, which they assigned to these groups. Again similar bands were observed in this study. These authors however made no attempt to assign vibrational modes in the C-H stretching region to these species. As shown in Figure 5.6, after removal of the surfactant by solvent extraction, peaks at 3066 cm^{-1}, 2890 cm^{-1} and 2803(w) cm^{-1} remain. Measurements made after calcinations at temperatures up to and including 400 °C showed no significant decrease in the intensity of these bands. The peak at 2890 cm^{-1} overlaps the υ_{as} CH_2 mode of the surfactant and is properly due to the asymmetric stretching mode of (υ_s CH_3) of the trapped ethyl species. The frequency of the band at 3066 cm^{-1} is rather high for the asymmetric stretch (υ_{as} CH_3), which would normally come at *circa*. 2960 cm^{-1} and the high intensity is attributed to its interaction with the framework.

Raman spectra of chromium-containing samples did not show any distinct peaks due to chromium oxide species indicating that the transition metal is well dispersed. Close inspection of the peak at 1000 cm^{-1} showed a shoulder at 980 cm^{-1} when chromium was in the sample. This could be due to the asymmetric stretching mode of dehydrated monochromate (CrO_4^{2-}), however the spectra were not conclusive. For comparison, the mesoporous organosilica sample (BTE) was impregnated with chromium (2%) and calcined at 500 °C. A weak but discernible peak at *circa.* 870 cm^{-1} appeared (assigned to either hydrated monochromate or hydrated polychromate species).[15,28,31] Thus, chromium added during synthesis was clearly stabilized in a manner absent in post-synthesis impregnation.

Table 5.2. Assignment of peaks for Raman spectra of Cr-PMO samples

Assignment	Literature (cm^{-1})	This study (cm^{-1})
ν_{as} (CH_3)	-	3066
ν_{as} $(CH_3\text{-}N)^+$ (surfactant)	3038 [27]	3032
ν_s $(CH_3\text{-}N)^+$ (surfactant)	2971 [27]	2964 (w)
ν_s (CH_3-R) (surfactant)	2893 (sh) [27]	2922 (sh)
ν_{as} (CH_2) (surfactant)	2899 [27]	2890
ν_s (CH_3)	-	2890
ν_s (CH_2) (surfactant)	2853 [27]	2854
δ (H_2O)	1620 [27]	1600
δ_{as} (CH_3) (surfactant)	1446 [27]	1450
δ_{as} (CH_3)	1410 [29]	1410
δ_s (CH_3) (surfactant)	1306 [27]	1300
δ_s (CH_3)	-	1270
ν (O_3Si-OH)	971 [28], 978 [30]	1000
ν (dehydr. CrO_4^{2-})	980 [15,30,31]	980 (sh)
ν (Si-O-Si)	812 [30], 791 [31]	795
ν $(C\text{-}N)^+$ (surfactant)	761	759
ν (Si-C)	530 [27]	522
ν (4-fold siloxane rings)	484 [28]	-
δ_s (O-Si-O)	450 [28]	-

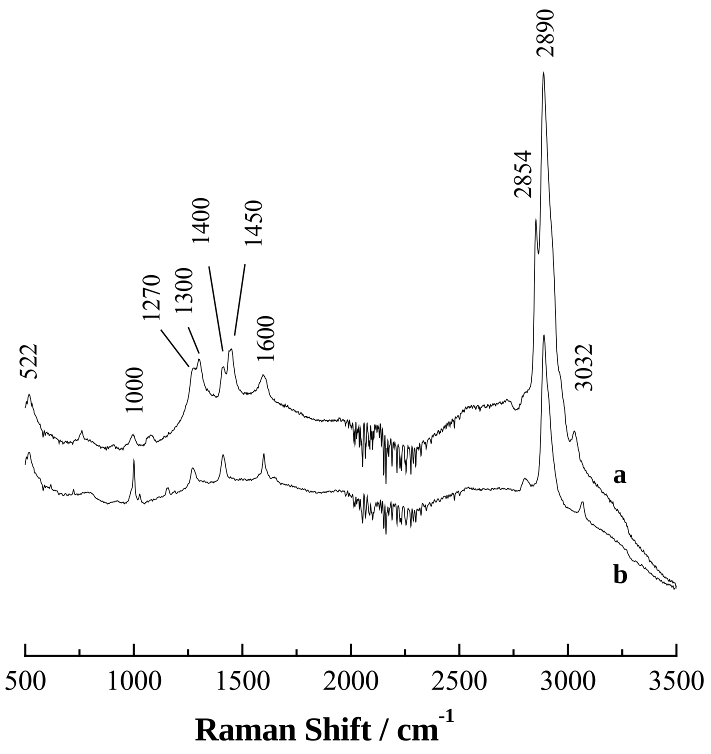

Figure 5.6. FT-Raman spectra of: (a) as-synthesized mesoporous organosilica sample (BTA) and (b) surfactant-extracted mesoporous organosilica sample (BTE).

5.3.6. ^{29}Si and ^{13}C CP MAS NMR Spectra

Silicon NMR spectra of the surfactant-extracted samples prepared by Method I shows the presence of peaks at –57 ppm, corresponding to T^2 sites [R**Si**(OSi)$_2$OH], and at –68 ppm for the T^3 sites, [R**Si**(OSi)$_3$]. No signals due to Q^n species [**Si**(OSi)$_n$(OH)$_{4-n}$] was observed showing that all silicon are covalently bonded to carbon atoms.[5] However, the materials prepared using mixed silica source, TEOS-BTEE, shows the presence of Q^3 [**Si**(OSi)$_3$(OH)] and Q^4 [**Si**(OSi)$_4$] sites along with T^2 and T^3 sites, indicating a condensation reaction between the oligomerized organosilica and silica species (Fig. 5.7A).[32] After calcination, both the chromium samples prepared by Method I and II devoids T^n sites and shows the presence of Q^n sites, which indicates that the calcination treatments had removed the organic groups from the wall positions and thereby a possible structural disordering (from PXRD). ^{13}C CP MAS NMR of surfactant-extracted hybrid sample, prepared by Method I, shows only a sharp peak at 5.6 ppm for the ethane fragments. The absence of peaks between 10-30 ppm proves a complete removal of the occluded surfactant species after solvent extraction processes while the surfactant-extracted sample, prepared by Method II, shows an additional peak at 31 ppm, which may possibly arise from the surfactant groups.[5] In addition, the absence of peaks at 15 and 58 ppm, assigned to the SiO-CH_2-CH_3 species, indicate that the hydrolysis of the organo silane monomers is complete (Fig. 5.7B). Hence, from NMR studies it can be deduced that the pore walls of surfactant-extracted samples consist of $SiO_{1.5}$-$(CH_2)_2$-$SiO_{1.5}$ network units. Meanwhile, the absence of signal at 5.6 ppm for the calcined sample indicates that the organic groups are decomposed after the high temperature calcination treatments.

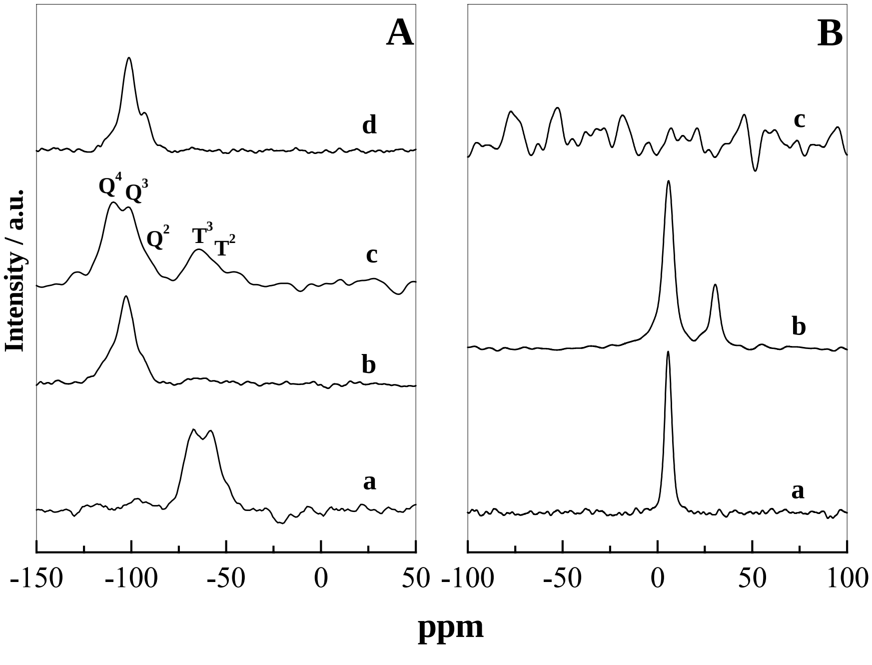

Figure 5.7. (A) ^{29}Si MAS NMR spectra of solvent-extracted (a&c) and calcined (b&d) mesoporous materials synthesized by Method I (a&b) and Method II (c&d). (B) ^{13}C CP MAS NMR spectra of: (a) solvent-extracted hybrid sample prepared by Method I, (b) solvent-extracted hybrid sample prepared by Method II and (c) calcined sample prepared by Method I.

5.3.7. UV-Vis Experiments

Diffuse reflectance UV-Vis analysis of chromium-containing hybrid samples was performed and the results were compared with chromium model compounds and a Cr-MCM-41 sample. All the as-synthesized and surfactant-extracted hybrid chromium samples were pale green in colour and following calcination changed to an intense yellow. The green colour of the materials implies the presence of trivalent chromium ions in octahedral geometry while the yellow color would imply the presence of a high-valent chromium ion *viz*., chromate/polychromate in tetrahedral coordination.[15] UV-Vis spectra of as-synthesized hybrid chromium materials and a Cr-MCM-41 sample show two sharp absorption bands at 440 and 610 nm typical of d-d transitions corresponding to the $^4A_{2g}(F)$ to $^4T_{1g}(P)$ and $^4A_{2g}(F)$ to $^4T_{2g}(F)$ transitions, for the trivalent chromium ions in octahedral coordination (Fig. 5.8A).[33] This observation suggests that Cr^{3+} ions inside the mesoporous molecular sieves are surrounded by six oxygen ligands (two from extra water ligands) in octahedral coordination and are not really substituted inside the framework positions. One of the major questions in chromium-containing molecular sieves is, whether chromium (Cr^{3+}) really substitutes into the framework because of the high crystal field stabilization energies (CFSE) of octahedral Cr^{3+} complexes. The unit cell values as well as the pore size datas observed in the present study support the observation from UV-Vis that chromium remains mainly as extra-framework metal species.

The spectra of calcined Cr-PMO samples are dominated by the presence of bands at 224, 340 and 445 nm. The bands at 224 and 340 nm are assigned to the O to Cr (VI) charge transfer transitions of chromate species while the band centered at 445 nm is assigned to the charge transfer bands associated with dichromate- or polychromate- type species (Fig. 5.8B).[15-17] These results indicate that dichromates and polychromate species are also formed over the Cr-PMO samples. However, the Cr-MCM-41 sample shows only a very weak band at 445 nm. This suggests that the primary species in Cr-MCM-41 be the mono chromate species. In fact, a close examination of the TBC sample (Method II) shows a small hump after 600 nm, which may possibly arise due to the presence of nano-sized Cr_2O_3 species. Generally, the chromate species (mono- as well as dichromates) formed during the calcination process are anchored on the surface of the support silica through an esterification reaction with the silanol groups. Earlier studies have shown that the nature of chromium species formed depends on the percentage of chromium loading, calcination temperature as well as the percentage of hydroxyl groups (here silanols) present over the support samples.[15] Thus, the formation of Cr_2O_3 species in the chromium catalyst synthesized from the mixed silica source implies that the silanol groups are not able to stabilize a part of the Cr (VI) species and these may be thermally converted in to the Cr_2O_3 species.

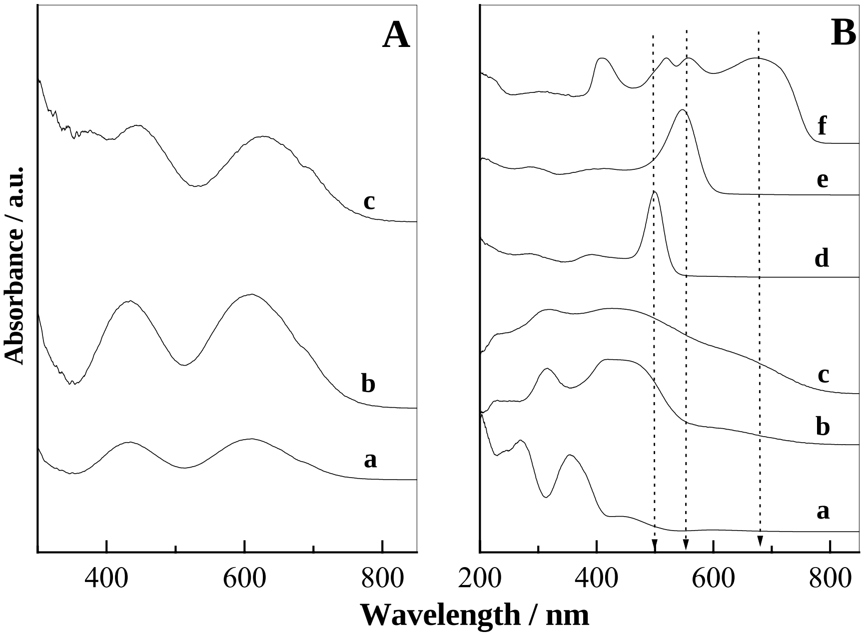

Figure 5.8. UV-Vis spectra of: (A) as-synthesized chromium-containing mesoporous samples, (a) Cr-MCM-41, (b) CHA, (c) TBA and (B) calcined chromium-containing samples, (a) Cr-MCM-41, (b) CHC, (c) TBC, (d) $NaCrO_4$, (e) $K_2Cr_2O_7$, (f) Cr_2O_3.

5.3.8. X-Ray Photoelectron Spectroscopy

The Cr $2p_{3/2}$ binding energy (B.E) region of chromium in as-synthesized samples shows a value of ~577.5 eV. However, for the calcined hybrid chromium samples the value shifted to a higher energy of 578.3 eV, characteristic of Cr (IV) species, and hence it is reasonable that the calcination treatments had changed the Cr (III) ions to Cr (VI) (Fig. 5.9).[34] The slight discrepancy in the B.E values from those of the pure compounds may originate from the different chemical environments or be due to the systematic errors in the measurements (Table 5.3).[35] For the TBC sample, an intensity decrease as well as a broadening of the Cr $2p_{3/2}$ peak to lower value was also noted. This may arise due to the existence of Cr_2O_3 species in the samples, as determined by the UV-Vis studies. However, since the Cr (VI) species can be easily reduced to the Cr (III) species under the high vacuum in the ESCA chamber or under the influence of X-ray beams used during XPS measurements, an accurate estimation of different oxidation states is not further explored.[15]

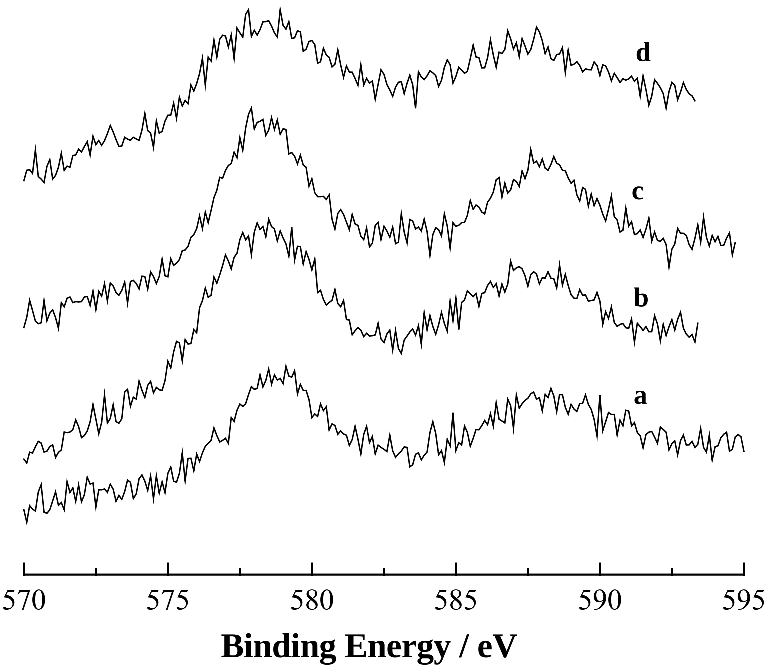

Figure 5.9. XPS plots of: (a) CHA, (b) CHC, (c) TBA and (d) TBC.

The relative dispersion of chromium ions on the surface of PMO catalysts was estimated from the XPS techniques (Table 5.3). Generally, the metal-to-silicon atomic ratio can be considered as the relative dispersion of transition metal ions on the framework of porous supports and hence the bulk Cr/Si ratio was compared with the Cr/ Si ratio determined from the XPS analysis. In accordance with the ICP metal analysis, it is observed that the surface Cr/Si molar ratio increases with an increase in the percentage of chromium in the hybrid catalysts. Comparison of these results with the XRD unit cell values, confirms that a greater percentage of chromium species reside as extra framework species. This verifies that the chromium atoms are not truly incorporated inside the framework since a large part of the species is detected in the surface and the surface and bulk ratios are more or less the same.

Table 5.3. XPS Binding Energy values and Surface atomic concentration of Chromium-containing solvent-extracted and calcined PMO samples

Samples	Cr content (%)	Si 2p	O 1s	Cr/Si (ICP)	Surface Cr/Si atomic ratio	Cr $2p_{3/2}$ B.E. (eV)
CHA	2.69	103.4	533.3	0.026	0.016	577.5
CHC	2.30	103.3	532.8	0.023	0.020	578.3
TBA	1.83	103.2	533.0	0.018	0.010	577.3
TBC	2.32	103.2	532.9	0.023	0.014	578.4
Cr-MCM-41	2.53	103.4	532.8	0.025	0.018	578.4
Cr_2O_3	-	-	530.4	-	-	576.8
Na_2CrO_4	-	-	529.9	-	-	579.8
$K_2Cr_2O_7$	-	-	530.1	-	-	579.4
CrO_3	-	-	530.0	-	-	580.0

Interesting supporting results about the characteristic nature of the Cr-PMO samples were further obtained from the O 1s and Si 2p core level XP spectra (Fig. 5.10). The O 1s XP spectra of the MO/SiO_2 samples usually arise from the contribution of oxygen from the support and the oxygen from the introduced metal oxide systems.[36] Hence in the present case, the contributions may arise from the oxygen of the support silica surface (O 1s of SiO_2) and from the oxygen of chromia species (O 1s of Cr_2O_3). Accordingly, the XP spectra of the as-synthesized and calcined chromium sample from Method I (CHC) show only a main peak at 532.9 eV characteristic for the O 1s, arising entirely from the framework oxygen species while in addition to the peak at 532.9 eV, the calcined hybrid chromium sample prepared by Method II (TBC) shows a distinct tailing of this band to a lower energy of ~530 eV (Fig. 5.10A). This peak may arise from the oxygen of the dispersed chromia species. Furthermore, it was also observed that the intensity of the O 1s peak increased after calcination showing the removal of the organic fragments from the framework and the complete formation and exposure of silica wall surfaces. Figure 5.10B compares the Si 2p core levels and shows a peak around 103.2 eV characteristic of silicon. As observed with the changes over O 1s, the intensity of the Si 2p is very strong and sharp for all the calcined samples than the as-synthesized samples, which contained the framework organic groups (Table 5.3).

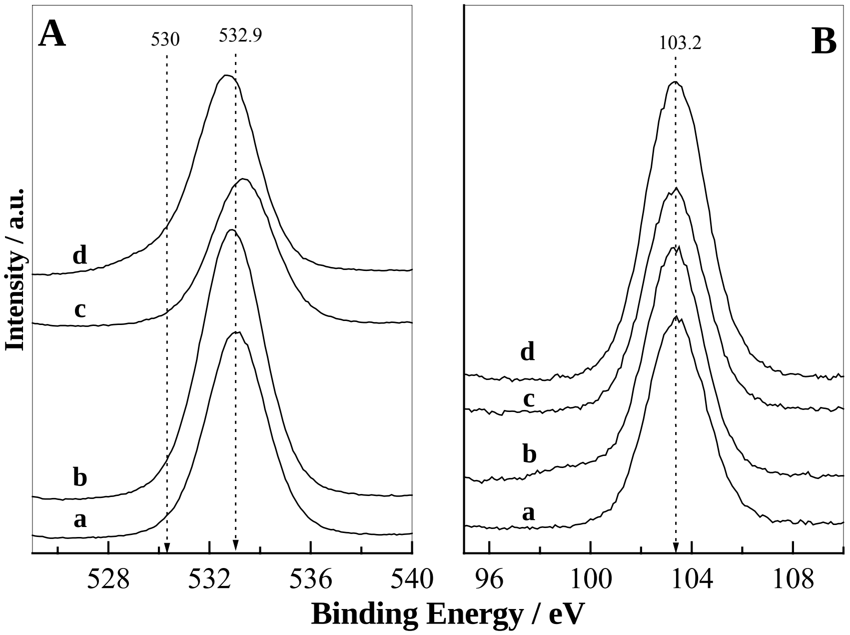

Figure 5.10. XPS plots of: (A) O 1s and (B) Si 2p; (a) CHA, (b) CHC, (c) TBA and (d) TBC.

5.4. CATALYTIC OXIDATION OF CYCLOHEXANE

5.4.1. Reaction Procedure

Cyclohexane oxidation reactions were carried out in a 10 mL round bottom flask fitted with a water-cooled condenser using *aqueous* H_2O_2 (30%) and TBHP (70%) as oxidants. In addition, stock solutions of TBHP in cyclohexane were also prepared by extraction of TBHP (70%) in equal volumes of cyclohexane. Phase separation was promoted by the addition of NaCl, in the aqueous layer and finally the organic part was dried over $MgSO_4$.[37] The reactant mixtures of cyclohexane (10 mmol, E-Merck, 99%, dried over 4 Å molecular sieves), oxidant (10 mmol, E-Merck) and acetone solvent (5 mL, E-Merck, 99%, dried over 4 Å molecular sieves) was added to 0.1 g of catalyst and was heated at a constant temperature of 70 ^{o}C under magnetic stirring (*ca*. 800 rpm).

The aerial oxidation of cyclohexane was carried out in a high pressure autoclave (Parr 4843) using 20 mL (185 mmol) of cyclohexane in presence of 0.2 g of catalyst, under solvent free condition at different temperature (100-160 ^{o}C) and pressures (1.3-5.5 MPa).

After reactions, the reaction mixture was cooled to room conditions and the catalysts were separated from the reaction mixture by centrifugation. The oxidized products were analyzed on a gas chromatograph (HP 6890) equipped with a flame ionization detector (FID) and a capillary column (5 μm cross linked methyl silicone gum, 0.2 mm × 50 m). The formation of carboxylic acid side products was determined by performing the GC analysis after conversion in to the respective methyl esters.[38]

5.4.2. Catalytic Results Using Peroxides as Oxidants

The oxidation of cyclohexane was carried out to probe the catalytic activity of chromium-containing PMO catalysts. The catalytic activity results obtained using *aqueous* H_2O_2 was shown in Table 5.4. The major products obtained were cyclohexanol (A) and cyclohexanone (K) with trace amounts of cyclohexylhydroperoxide (CHHP). First the catalyst, CHC, was screened in different solvents to probe the influence of solvents in presence of *aqueous* H_2O_2. It was observed that the cyclohexane conversion followed the order, $(CH_3)_2CO$ (38 %) > CH_3CN (30 %) > MeOH (6 %) > 1,4-Dioxane (5 %), no solvent (< 4 %), after 3 h run. Thus the conversion was negligible in the absence of solvent. This may be due to the distinct phase separation between the aqueous oxidants and the organic substrate, which in turn limits the substrate interaction with the active catalyst sites. The chromium-containing PMO catalysts are more active than the conventional Cr-MCM-41 catalyst. Even though trace amounts of Cr_2O_3 clusters are observed over TBC catalyst, the increased conversion of this catalyst over Cr-MCM-41 shows that they are not blocking the accessible active sites. This conclusion was derived that under identical conditions the Cr_2O_3 catalyst shows very low conversion (< 5%), with the formation of more cyclohexanol. Moreover, the K/A ratio was found to be ~1 for the Cr-PMO catalysts and Cr-MCM-41 (after 3 h reaction) and increased to > 2 after a 6 h catalytic run. This result indicates that the primary product obtained in cyclohexane oxidation reaction is cyclohexanol, which is further oxidized to cyclohexanone as time progresses. Notably, the selectivity to cyclohexanone was also more over the CHC catalyst than over the other chromium catalysts. Thus in terms of conversion, turn-over number and selectivity to cyclohexanone, the chromium-containing PMO catalyst prepared by Method I is a better catalyst than the other chromium-containing catalysts.

In order to probe the role of oxidants in cyclohexane oxidation reaction, the catalytic activity of the chromium-containing catalysts was evaluated in presence of *non-aqueous tert*-butylhydroperoxide (TBHP) oxidant (Table 5.5). The conversion of cyclohexane was observed less over *tert*-butylhydroperoxide oxidant than *aqueous* H_2O_2. The main products obtained with TBHP are cyclohexanol and cyclohexanone with trace amounts of cyclohexylhydroperoxide (CHHP) as well as cyclohexyl-*tert*-butylperether (CHTB). Influence of solvents shows that the conversion of cyclohexane was ~2 % in the absence of solvent and in presence of solvents such as 1,4-Dioxane and methanol, after a 5 h run. However, acetone showed a higher conversion of 12 % for CHC, 7 % for TBC and 6 % for Cr-MCM-41, after 5 h run. Further, it is attractive that the K/A ratios are very high in presence of TBHP, and after 5 h, the ratio reached a significant value of > 5.

Since CHHP is also formed as a product, it is reasonable that the peroxide species formed can also enhance the conversion of cyclohexane. However, kinetic measurements showed that its percentage increased from 1 h to 5 h and thereafter decreased with time. Thus, the increased formation of cyclohexanone may possibly arise from the mixed Russell termination (refer Scheme 4.1).[35] Thus the excellent catalytic activity obtained with *non-aqueous* TBHP suggests that the chromium catalysts are active in presence of organic peroxides. The decreased conversion obtained with TBC catalyst than CHC catalyst confirms that isolated metal species are the active catalytic sites than the aggregated metal sites, in the oxidation reaction of cyclohexane.

Table 5.4. Cyclohexane oxidation with *aqueous* H_2O_2 over Cr-PMO catalysts

Catalyst	Cy-ane Conv. (mol%)	TON [a]	Product distribution / mol% [b]			
			Cy-ol (A)	Cy-one (K)	K/A	Others
PMO	4	-	60	40	0.6	-
CHC	38	8.1	32	63	1.9	5
C-C_{16}-C	35	8.1	35	61	1.7	4
TBC	35	7.3	34	59	1.7	7
Cr-MCM-41	31	6.0	46	49	1.0	5

Reaction Conditions: catalyst (g), 0.1; T (°C), 70; substrate : oxidant (mol/mol), 1; solvent (5 mL), $(CH_3)_2CO$; time (h), 3.

[a] Turn over number, moles of cyclohexane converted per mole of chromium.

[b] Cy-ol = cyclohexanol, Cy-one = cyclohexanone, others, mainly CHHP.

Although Cr-MCM-41 lacks Cr_2O_3 sites, the conversion were less than the Cr-PMO catalysts and more importantly than the TBC catalyst, containing trace amounts of Cr_2O_3 species. This interesting result, observed over both the oxidants, suggests that the textural as well as the morphological features of the support material also influences the conversion rates as suggested by Pinnavaia *et al.* for hexagonal mesoporous silica (HMS) materials.[39] Thus, the wormhole-like or spongy channel morphology obtained for TBC catalyst facilitates an enhanced access for cyclohexane molecules to the active chromium sites and thereby enhances the conversion rates, than the one-dimensional channel structured Cr-MCM-41 catalyst. These results also suggest that even though the ethane fragments are decomposed after calcination, the hydrophobic environment remained in the material and lead to an improved catalytic activity over the conventional Cr-MCM-41 catalyst, similar to earlier observations over titanium-containing PMO samples.[32,40]

Table 5.5. Cyclohexane oxidation with *non-aqueous tert*-butylhydroperoxide over Cr-PMO catalysts

Catalyst	Cy-ane Conv. (mol%)	TON [a]	Product distribution / mol% [b]				Metal Leaching [c]
			Cy-ol (A)	Cy-one (K)	K/A	Others	
PMO	0	-	0	0	0	0	-
CHC	12	2.5	22	70	3.1	8	9
CHC [d]	15	3.2	13	77	5.9	10	16
C-C_{16}-C	5	1.2	12	80	6.6	8	n.d
TBC	6	1.3	20	64	3.2	16	19
Cr-MCM-41	2.5	0.5	13	78	6.0	9	26

Reaction Conditions: catalyst (g), 0.1; T (^{o}C), 70; substrate : oxidant (mol/mol), 1; solvent (~5 mL), $(CH_3)_2CO$; time (h), 5.

[a] Turn over number, moles of cyclohexane converted per mole of chromium.

[b] Cy-ol = cyclohexanol, Cy-one = cyclohexanone, others, mainly CHHP and CHTB.

[c] Determined by ICP-OES analysis.

[d] with 70% TBHP oxidant. n.d = not determined.

5.4.3. Heterogenity Studies

Chromium-containing porous materials often exhibit leaching of active metal species during liquid phase reactions. Thus the catalytic activity may arise from the presence of homogeneous leached metal species.[17,33,41] Since, after calcination, chromium in molecular sieves is presumed to contain two extra framework Cr=O bonds, chromium can be anchored to the framework through only two Si-O bonds and so the leaching is facile in chromium-substituted porous materials.[15] Hence, in order to confirm that the present catalysts are heterogeneous and chromium is not leached out, hot filtration experiments and ICP-OES analysis of reaction mixture was carried out.

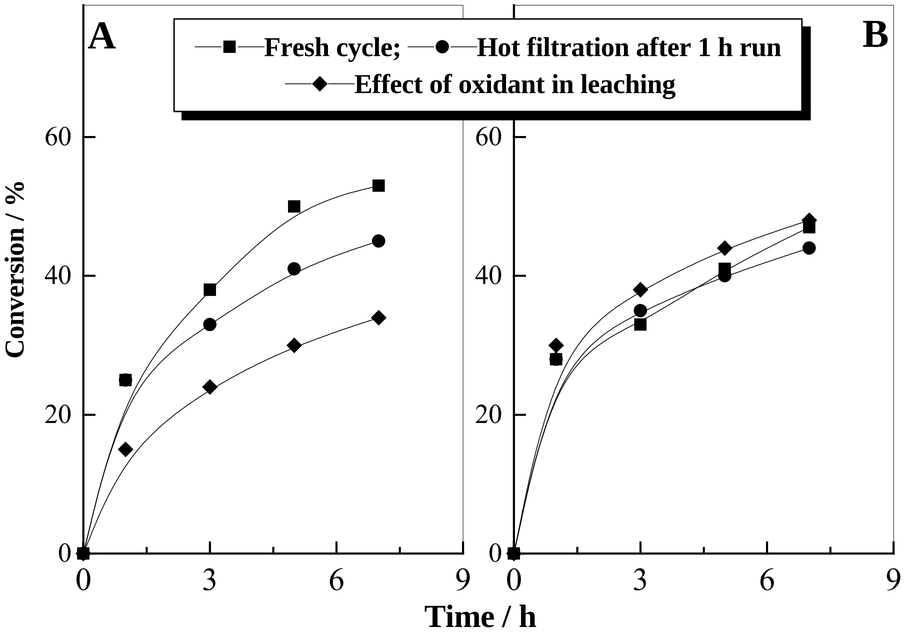

Figure 5.11. Leaching studies performed over: (A) CHC and (B) Cr-MCM-41, in presence of *aqueous* H_2O_2 oxidant.

Following 1 h reaction, the catalyst was removed from the hot reaction mixture and the reaction was continued with the filtrate (Fig. 5.11). The result showed that, the conversion increased even after the removal of the catalyst confirming chromium leaching, in presence of *aqueous* H_2O_2. This result was supported by another experiment in which the catalyst was first stirred for 2 h in H_2O_2 solution. The catalyst removed filtrate shows an almost equal percentage of cyclohexane conversion to that obtained with the fresh catalyst. These results imply that chromium-containing mesoporous materials are not appropriate catalysts for oxidation reactions, in presence of oxidants like *aqueous* H_2O_2 (30%). However, compared to the Cr-MCM-41 catalyst the hybrid catalyst, CHC, is more resistant towards leaching (Fig. 5.11).

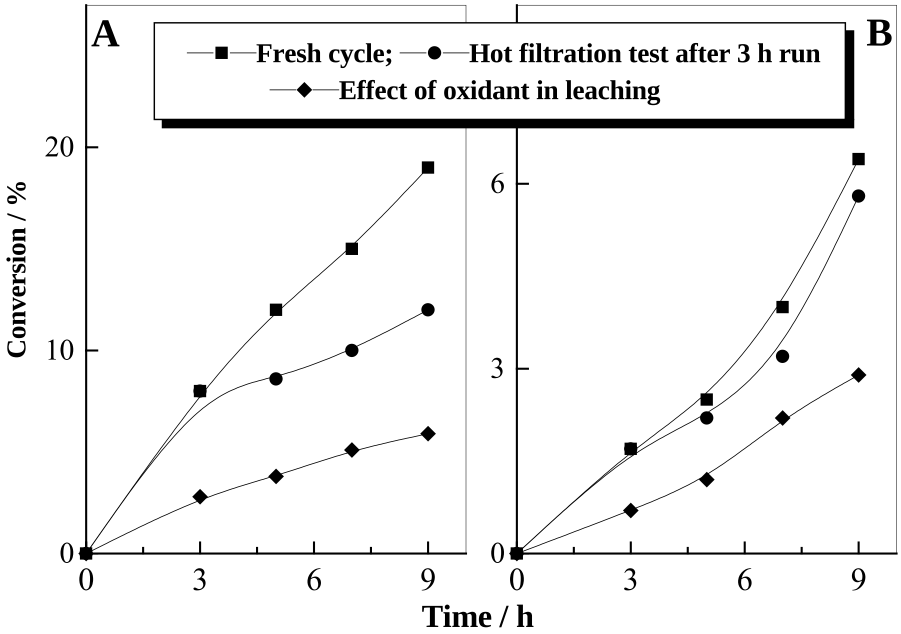

Figure 5.12. Leaching studies performed over: (A) CHC and (B) Cr-MCM-41, in presence of *non-aqueous tert*-butylhydroperoxide oxidant.

By contrast, to the results observed with H_2O_2, the catalysts were stable in presence of *non-aqueous* TBHP oxidant, showing no serious leaching as determined by hot filtration experiments and by the secondary leaching experiment as described above (Fig. 5.12). However, Cr-MCM-41 showed the leaching of active sites, even in presence of *non-aqueous* TBHP. Further the percentage of chromium leached out into the reaction mixture during reactions, determined by ICP-OES analysis, also shows that the Cr-PMO catalysts are more heterogeneous than the conventional Cr-MCM-41 catalyst (Table 5.5).

The present results thus suggest that the absence of water, from oxidants or from solvents, in the oxidation reaction mixture and hydrophobic catalyst supports helps to develop reusable chromium-containing mesoporous catalysts of better catalytic activity.

5.4.4. Catalytic Results Using Air as an Oxidant

The catalytic activity results of Cr-PMO and Cr-MCM-41 catalysts in the aerial oxidation reaction of cyclohexane at 120 ^{o}C and 2.7 MPa are given in Table 5.6. The blank reaction carried out without any catalyst or with pristine support sample shows no oxidative products and among the chromium catalysts the CHC catalyst shows higher conversion than the TBC catalyst and their catalytic activity exceeds the Cr-MCM-41 catalyst. The excellent cyclohexane conversion observed with the CHC catalyst arise due to its better structural ordering and/or due to the presence of highly dispersed active chromium sites which create all the active chromium sites available for the substrate molecules.[19,33] Hence, the decreased catalytic activity observed with TBC catalyst can be related to the presence of aggregated chromium species present in the catalysts, as noted from the characterization techniques. Furthermore, a comparison with other metal-containing mesoporous catalysts (M-MCM-41, M = Ti, V, Co) shows that the conversion was more over the chromium-containing mesoporous catalysts (Table 5.6).

Figure 5.13 shows the effect of reaction time over the CHC catalyst. It is observed that the catalyst show an increase in cyclohexane conversion in the initial stages and after 6 h the conversion remains almost constant. Moreover, figure shows that the selectivity to cyclohexanol decreases with time while the percentage of cyclohexanone gets increased. This result suggest that the primary product formed is cyclohexanol and the decreased percentage of cyclohexanol with time attributes to their oxidation to cyclohexanone, as cyclohexanol was more reactive than the cyclohexane. The other products mentioned in Figure 5.13 mainly relates to the presence of cyclohexyl hydroperoxide (CHHP) in the initial stages while after 9 h traces of dicarboxylic acids like adipic acid (AA) are also noted, due to the excess oxidation of cyclohexanone.

Table 5.6. Oxidation of cyclohexane in air: Comparison of catalysts

Catalyst	Cy-ane Conv. (mol%)	TON	Product distribution / mol% [a]			
			Cy-ol (A)	Cy-one (K)	Others	
					CHHP	AA
BTE	-	-	-	-	-	-
CHC	7.1	38	39	55	4	2
CHC	6.6	-	41	55	4	-
C-C_{16}-C	4.7	27	36	56	6	2
TBC	4.9	26	30	65	5	-
Cr-MCM-41	6.3	31	26	66	5	3
Cr-MCM-48	7.1	36	24	69	4	3
Ti-MCM-41	1.6	25	38	48	14	-
V-MCM-41	2.3	28	35	49	16	-
Co-MCM-41	5.4	31	35	59	6	-
Cr/SiO_2	4.4	25	30	66	2	2

Reaction Conditions: cyclohexane (mL), 20; catalyst (g), 0.2; air pressure (MPa), 2.7; T (°C), 120; time (h), 6.

[a] Cy-ol = cyclohexanol, Cy-one = cyclohexanone, CHHP = cyclohexylhydroperoxide, AA = adipic acid.

Figure 5.14A&B illustrates the influence of reaction temperature and air pressure in the oxidation reaction of cyclohexane. With an increase in reaction temperature the conversion increases up to 140 °C, whereafter the conversion remains the same. The selectivity of cyclohexanone also increases with reaction time, at the expense of cyclohexanol. Like wise, an increase in the air pressure also shows an increase in the cyclohexane conversion up to 2.7 MPa, whereafter the conversion is constant. The selectivity of cyclohexanol decreases with the formation of cyclohexanone and adipic acid at higher pressures (~5% at 5.7 MPa).

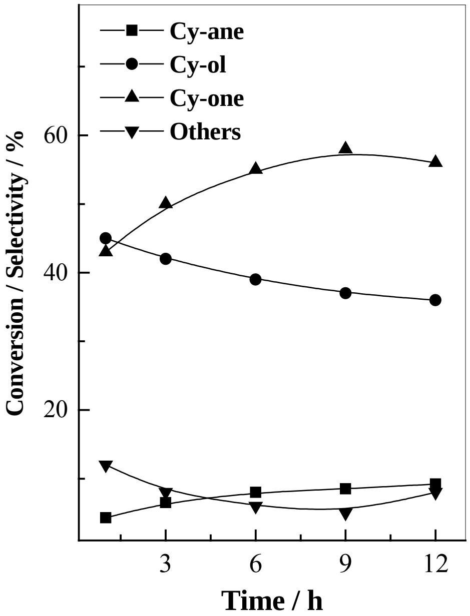

Figure 5.13. Effect of reaction time in the conversion and selectivity of cyclohexane over chromium catalyst prepared by Method I (CHC).

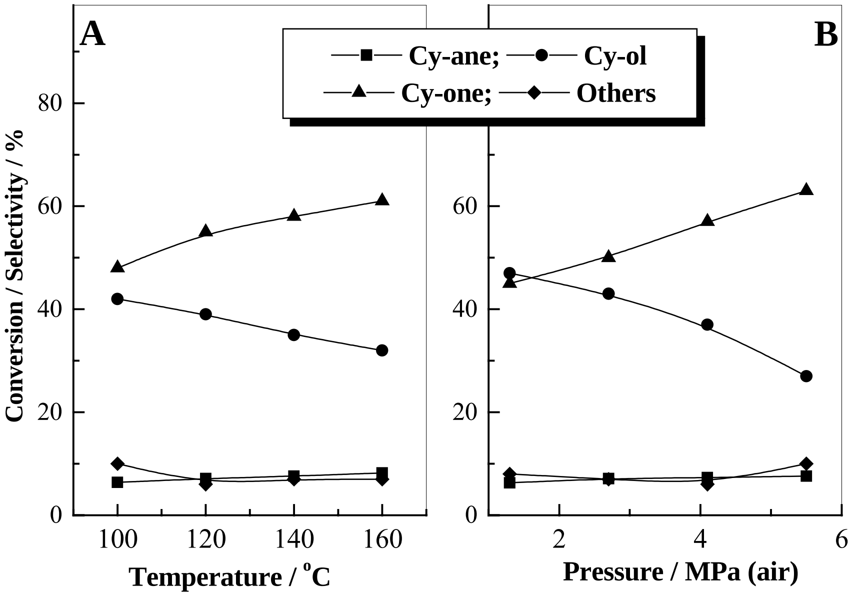

Figure 5.14. Effect of (A) reaction temperature and (B) air pressure in the conversion and selectivity of cyclohexane over chromium catalyst prepared by Method I (CHC)

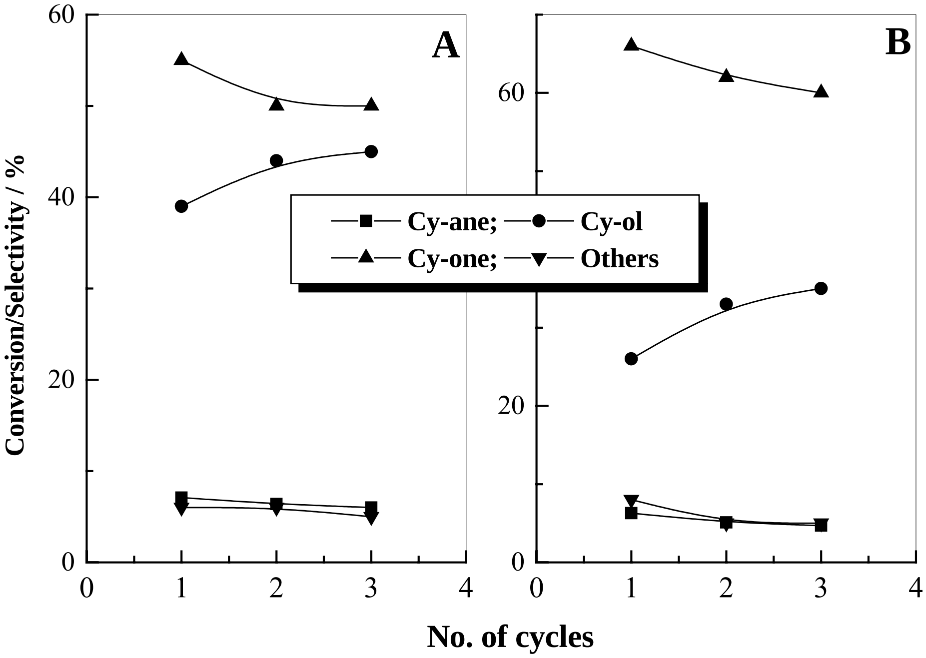

Figure 5.15. Recycling studies carried out over: (A) CHC and (B) Cr-MCM-41 catalysts.

To confirm that the Cr-PMO catalysts are heterogeneous and chromium was not leached out during reactions, recycling studies were carried out and are compared with a Cr-MCM-41 catalyst. For that, the catalyst was separated from the reaction mixture, washed with acetone, activated at 400 °C for 3 h and was used in a fresh run. Results up to three run shows that the CHC catalyst retains an almost similar conversion and selectivity revealing that the catalyst is recyclable (Fig. 5.15A). However, the Cr-MCM-41 catalyst shows slight decrease in conversion during reuse, revealing the leaching of chromium from the frame wall positions (Fig. 5.15B). This indicates that the leaching of chromium is not facile in Cr-PMO samples and hence are robust catalysts in the aerial oxidation of cyclohexane and the optimum reaction conditions for better cyclohexane conversion and cyclohexanone selectivity for the CHC catalyst is 120 °C reaction temperature and 2.7 MPa air pressure.

5.5. REFERENCES

1 C. W. Jones, K. Tsuji, M. E. Davis, *Nature* **1998**, *393*, 52.

2 J. Y. Ying, C. P. Mehnert, M. S. Wong, *Angew. Chem. Int. Ed.* **1999**, *38*, 57.

3 A. Sayari, *Chem. Mater.* **1996**, *8*, 1840.

4 A. Stein, B. J. Melde, R. C. Schroden, *Adv. Mater.* **2000**, *12*, 1403.

5 S. Inagaki, S. Guan, Y. Fukushima, T. Ohsuna, O. Terasaki, *J. Am. Chem. Soc.* **1999**, *121*, 9611.

6 T. Asefa, M. J. MacLachlan, N. Coombs, G. A. Ozin, *Nature* **1999**, *402*, 867.

7 B. J. Melde, B. T. Holland, C. F. Blanford, A. Stein, *Chem. Mater.* **1999**, *11*, 3302.

8 Y. Lu, H. Fan, N. Doke, D. A. Loy, R. A. Assink, D. A. LaVan, C. J. Brinker, *J. Am. Chem. Soc.* **2000**, *122*, 5258.

9 W. Guo, X. Li, X. S. Zhao, *Microporous Mesoporous Mater.* **2006**, *233*, 285.

10 W. Guo, J. Y. Park, M. O. Oh, H. W. Jeong, W. J. Cho, I. Kim, C-S. Ha, *Chem. Mater.* **2003**, *15*, 2295.

11 F. Hoffmann, M. Cornelius, J. Morell, M. Froba, *Angew. Chem. Int. Ed.* **2006**, *45*, 3216.

12 T. Asefa, M. J. MacLachlan, H. Grondey, N. Coombs, G. A. Ozin, *Angew. Chem. Int. Ed.* **2000**, *39*, 1808.

13 C-Y. Ishii, T. Asefa, N. Coombs, M. J. MacLachlan, G. A. Ozin, *Chem. Commun.* **1999**, 2539.

14 R. A. Sheldon, J. K. Kochi, *Metal-Catalyzed Oxidation of Organic Compounds*, Academic Press, New York, **1981**.

15 B. M. Weckhuysen, I. E. Wachs, R. A. Schoonheydt, *Chem. Rev.* **1996**, *96*, 3327.

16 J. D. Chen, R. A. Sheldon, *J. Catal.* **1995**, *153*, 1.

17 S. E. Dapurkar, A. Sakthivel, P. Selvam, *New J. Chem.* **2003**, *27*, 1184.

18 Y. Liang, R. Anwander, *Microporous Mesoporous Mater.* **2004**, *72*, 153.

19 V. Parvulescu, C. Anastasescu, B. L. Su, *J. Mol. Catal. A. Chem.* **2003**, *3919*, 1.

20 D. Wei, H. Wang, X. Feng, W. T. Chueh, P. Ravikovitch, M. Lyubovsky, C. Li, T. Takeguchi, G. L. Haller, *J. Phys. Chem. B* **1999**, *103*, 2113.

21 V. Rebbin, M. Jakubowski, S. Potz, M. Froba, *Microporous Mesoporous Mater*. **2004**, *72*, 99.

22 M. A. Wahab, II. Kim, C-S. Ha, *Microporous Mesoporous Mater*. **2004**, *69*, 19.

23 M. P. Kapoor, S. Inagaki, *Chem. Mater*. **2002**, *14*, 3509.

24 M. Etienne, B. Lebeau, A. Walcarius, *New. J. Chem*. **2002**, *26*, 384.

25 (a) W. Zhang, M. Froba, J. Wang, P. T. Tanev, J. Wong, T. J. Pinnavaia, *J. Am. Chem. Soc*. **1996**, *118*, 9164. (b) Y. Mori, T. J. Pinnavaia, *Chem. Mater*. **2001**, *13*, 2173.

26 S. Shylesh, A. P. Singh, *J. Catal*. **2005**, *233*, 359.

27 E. J. Sullivan, D. B. Hunter, R. S. Bowman, *Environ. Sci. Technol*. **1998**, *32*, 1948.

28 K. J. Chao, C. N. Wu, H. Chang, L. J. Lee, S. Hu, *J. Phys. Chem*. **1997**, *101*, 6341.

29 O. Dag, G. A. Ozin, *Adv. Mater*. **2001**, *13*, 1182.

30 Z. Zhu, Z. Chang, L. Kevan, *J. Phys. Chem. B* **1999**, *103*, 2680.

31 Y. Wang, Y. Ohishi, T. Shishido, Q. Zhang, W. Yang, Q. Guo, H. Wan, K. Takehira, *J. Catal*. **2003**, *220*, 347.

32 M. P. Kapoor, A. Bhaumik, S. Inagaki, K. Kuraoka, T. Yazawa, *J. Mater. Chem*. **2002**, *12*, 3078.

33 A. Sakthivel, P. Selvam, *J. Catal*. **2002**, *211*, 134.

34 (a) P. C. Thune, C. P. J. Varhagen, M. J. G. van den Boer, J. W. Niemantsverdriet, *J. Phys. Chem. B* **1997**, *101*, 8559. (b) P. C. Thune, R. Linke, W. J. H. Van Gennip, A. M. De Jong, J. W. Niemantsverdriet, *J. Phys. Chem. B* **2001**, *105*, 3073.

35 G. C. Allen, P. M. Tucker, *Inorg. Chim. Acta*. **1976**, *16*, 41.

36 E. P. Reddy, L. Davydov, P. C. Smirniotis, *J. Phys. Chem. B* **2002**, *106*, 3394.

37 M. Nowotny, Y. L. N. Pedersen, U. Hanefeld, T. Maschmayer, *Chem. Eur. J.* **2002**, *8*, 3724.

38 R. Raja, P. Ratnasamy, *Catal. Lett*. **1997**, *48*, 1.

39 W. Zhang, M. Froba, J. Wang, P. T. Tanev, J. Wong, T. J. Pinnavaia, *J. Am. Chem. Soc*. **1996**, *118*, 9164.

40 A. Bhaumik, M. P. Kapoor, S. Inagaki, *Chem. Commun*. **2003**, 470.

41 H. E. B. Lempers, R. A. Sheldon, *J. Catal*. **1998**, *175*, 62.

42 U. Schuchardt, D. Cardoso, R. Sercheli, R. Pereira, R. S. da Cruz, M. C. Guerreiro, D. Mandelli, E. V. Spinace, E. L. Pires, *Appl. Catal. A. Gen*. **2001**, *211*, 1.

6.1 SUMMARY

The present thesis gives an account of: (i) the syntheses of vanadium and chromium-containing periodic mesoporous silicas, organic-inorganic hybrid mesoporous materials and periodic mesoporous organosilicas having ethane groups in the frame wall positions, (ii) in-depth characterization of these metal-containing mesoporous materials, and (iii) application of these materials as catalyst in selective oxidation and epoxidation reactions.

Chapter 1 presents a general introduction about various physicochemical aspects of periodic mesoporous silica and periodic mesoporous organosilica materials. The different characteristic properties of these materials, their synthesis parameters, formation mechanisms, different approaches for surface-functionalization, characterization techniques and application as supports for different catalytically active transformations are discussed in brief. Based on the literature survey, the scope and objectives of the present work have been outlined at the end of this chapter.

Chapter 2 describes the synthesis of vanadium-containing mesoporous MCM-41 samples by the direct substitution method, grafting method and by the immobilization method. The synthesis procedures of the V-MCM-41 catalysts are probed in detail by using different silica sources in order to account the role of silica sources in the mesoporous structural ordering, stabilization of vanadium sites, catalytic activity and stability. The immobilization of vanadium was carried out over different amino propyl modified mesoporous supports like SBA-15, MCM-41 and a silica gel, in order to probe the role of surface hydroxyl groups in the anchoring of organic groups as well as to attain information about the nature and coordination of vanadium over different supports, having reactive functional sites. All the catalysts are characterized by XRD, N_2 adsorption, TEM, FT-IR spectroscopy, FT-Raman spectroscopy, ^{29}Si MAS NMR, ^{13}C CP MAS NMR, ^{51}V MAS NMR, UV-Vis, TPR and EPR. The catalytic potential of these heterogeneous catalysts in the oxidation reaction of naphthalene and cyclohexane and in the epoxidation reaction of cyclooctene under various reaction conditions have been demonstrated. The recycle studies of the catalysts have also been presented to emphasize the heterogeneous nature of the catalysts.

Chapter 3 describes the synthesis of vanadium-containing periodic mesoporous organosilica samples, having ethane groups in the frame wall positions, prepared using cationic surfactants of different chain lengths *viz.*, C18-, C16- and C14-. All the synthesized catalysts are characterized in detail by XRD, N_2 adsorption, SEM, TEM, TG-DTG analysis, solid-state ^{13}C CP MAS NMR, ^{29}Si and ^{51}V MAS NMR, UV-Vis and FT-Raman spectroscopy. The catalytic activity and stability of these hybrid vanadium catalysts were compared with V-MCM-41 catalyst in the epoxidation reaction of styrene, using *aqueous* hydrogen peroxide (H_2O_2) as well as *tert*-butylhydrogenperoxide (TBHP) as oxidants and are discussed in detail.

Chapter 4 focuses a novel method for the synthesis of bifunctional chromium-containing mesoporous materials using various organo modifiers like chloro propyl, methyl and vinyl units and their further transformation to chromium-containing small pore silicas. The effect of different chain length organosilanes in the percentage of chromium loading, structural shrinkage and dispersion of chromium and the controlled transformation of these bifunctional mesoporous materials to small pore chromium silicas having pore size in the super microporous region have been demonstrated. The catalytic activity and stability of these chromium catalysts in the oxidation reaction of cyclohexane to cyclohexanol and cyclohexanone using *non-aqueous tert*-butylhydrogenperoxide as well as air as oxidants under different reaction conditions have been discussed in detail.

Chapter 5 deals with the synthesis of chromium-containing periodic mesoporous organosilicas, having ethane groups in the frame wall positions, by two different synthesis routes using 1,2-bis(triethoxysilyl)ethane as the silica source and 1,2-bis (triethoxysilyl)ethane and tetraethyl orthosilicate as a mixed silica source. The newly developed organo-modified mesoporous chromium materials are characterized by XRD, N_2 adsorption, TEM, TG-DTA, solid-state ^{13}C CP MAS NMR, ^{29}Si MAS NMR, FT-IR spectroscopy, FT-Raman spectroscopy, UV-Vis and XPS. The catalytic activity of these chromium catalysts was assessed in the oxidation reaction of cyclohexane to cyclohexanol and cyclohexanone using *aqueous* hydrogen peroxide, *non-aqueous tert*-butylhydrogenperoxide as well as air as oxidants under different reaction conditions. The stability and reusability of the catalysts were also carried out and are discussed in detail.

6.2. CONCLUSIONS

6.2.1. Synthesis and Characterization

- Vanadium-containing mesoporous MCM-41 samples prepared by the direct hydrothermal method and by the post-synthesis grafting and immobilization methods show that the hexagonal channel ordering of MCM-41 support get seriously damaged after the post synthesis methods.
- Influence of silica source in the synthesis of Si-MCM-41 and V-MCM-41 materials reveals that the mesoporous materials prepared from fumed silica source show better thermal and hydrothermal stability than the materials prepared from tetraethyl orthosilicate source.
- In the post synthesis grafting of 3-aminopropyl triethoxysilane over SBA-15, MCM-41 and an amorphous silica gel, toluene was found the best solvent for functionalization than the low boiling solvents like dichloromethane. However, mesoporous structural disordering was more over toluene than the dichloro methane solvent.
- The extent of 3-APTS functionalization was found more over MCM-41 solids than the large pore SBA-15 and amorphous silica gel samples, due to the abundant silanols prevailing in the MCM-41 pore channels than the other supports, as envisaged from the elemental analysis and ^{29}Si MAS NMR studies.
- Compared to the periodic mesoporous silica materials like Si-MCM-41, periodic mesoporous organosilicas having ethane groups in the frame wall positions possess better hydrothermal stability.

- Vanadium-containing periodic mesoporous organosilica samples prepared with different cationic surfactants having carbon numbers of C18-, C16- and C14- revealed that better structural ordering and vanadium incorporation were more over the long chain C18- surfactant.
- Bifunctional periodic mesoporous silica materials having chromium in the frame wall positions and high content of organic groups like chloro propyl, vinyl and methyl groups in the inner pore channels of MCM-41 can be prepared by a one-pot synthesis method.
- Chromium-silica samples having pore size in the super microporous region can be prepared from the bifunctional periodic mesoporous silicas by high temperature calcinations and thus porous materials that effectively bridge the gap between the conventional zeolites and mesoporous materials can be produced from the mesopore region.
- Chromium-containing periodic mesoporous organosilica samples prepared by 1,2-bis(ethoxysilyl)ethane and TEOS silica source show that the mixed silica source synthesized organosilica samples exhibit disordered pore channels. Infact, structures resembling hexagonal mesoporous silica (HMS) were obtained, as envisaged from XRD, SEM and TEM analysis.

6.2.2. Catalysis

- Vanadium-containing mesoporous material prepared by the immobilization of vanadyl sulfate over an amino propyl modified MCM-41 sample shows better catalytic activity and stability in the oxidation reaction of naphthalene than a hydrothermally synthesized V-MCM-41 and grafted V/MCM-41 catalyst.
- Vanadium-substituted mesoporous V-MCM-41 sample prepared from fumed silica source exhibit higher catalytic activity in the epoxidation reaction of cyclooctene than the material prepared from tetraethyl orthosilicate source.

- Vanadium-immobilized NH_2-SBA-15 and NH_2-MCM-41 catalysts show better conversion and stability than a NH_2-silica gel immobilized vanadium sample and a V-MCM-41 sample, in the oxidation reaction of cyclohexane. The better catalytic activity and stability obtained over amine-functionalized mesoporous vanadium catalysts are due to active site isolation, more hydrophobic environments and the pore confinement effect than the V-MCM-41 and NH_2-silica gel immobilized vanadium catalysts.
- Vanadium-containing periodic mesoporous organosilica (V-PMO) samples exhibit promising catalytic activity and stability in the liquid phase epoxidation reaction of styrene using *aqueous* H_2O_2 and TBHP as oxidants. The improved catalytic activity and stability of the V-PMO samples are due to the hydrophobic environment imparted inside the pore channels of the mesoporous organosilica samples.
- Chromium-containing small-pore silicas show promising catalytic activity, selectivity and stability in the liquid phase oxidation reaction of cyclohexane using peroxides and air as oxidants. Among the porous chromium catalysts, the samples prepared using chloro propyl silane show higher cyclohexane conversion, cyclohexanone selectivity and behaves as a true heterogeneous catalyst.
- Chromium-containing periodic mesoporous organosilica (Cr-PMO) samples exhibited better catalytic activity than the conventional mesoporous Cr-MCM-41 catalyst in the oxidation reaction of cyclohexane, using peroxides and air as oxidants. The higher catalytic activity of the Cr-PMO samples is due to the increased hydrophobicity of the materials and to the complementary structural features that facilitates the accessibility of cyclohexane to the active framework chromium sites. The Cr-PMO catalysts are heterogeneous and are efficient ketone selective catalysts in the oxidation reaction of cyclohexane.

List of Publications

1 Synthesis, characterization and catalytic activity of vanadium -incorporated, -grafted and –immobilized mesoporous MCM-41 in the oxidation of aromatics
S. Shylesh and A. P. Singh
Journal of Catalysis **2004**, *228*, 333

2 Silica functionalized sulphonic acid groups: Synthesis, characterization and catalytic activity in acetalization and acetylation reactions
S. Shylesh, S. Sharma, S. P. Mirajkar and A. P. Singh
Journal of Molecular Catalysis A. Chemical **2004**, *212*, 219

3 Vanadium-containing ordered mesoporous silicates: Does the silica source really affect the catalytic activity, structural stability and nature of vanadium sites in V-MCM-41?
S. Shylesh and A. P. Singh
Journal of Catalysis **2005**, *233*, 359

4 Influence of silica source in the catalytic activity and heterogenity of mesoporous vanadosilicates
S. Shylesh, S. P. Mirajkar and A. P. Singh
Journal of Molecular Catalysis A. Chemical **2005**, *239*, 57

5 Vanadium-containing ordered mesoporous silicas: Synthesis, characterization and catalytic activity in the hydroxylation of biphenyl
J. George, **S. Shylesh** and A. P. Singh
Applied Catalysis A. General **2005**, *290*, 148

6 Designing isolated vanadium sites over mesoporous MCM-41: Characterization and catalytic applications
S. Shylesh, S. Parambadath and A. P. Singh
Bulletin of Catalysis Society of India **2005**, *4*, 45

7 Synthesis, characterization and catalytic activity of Mn (III)- and Co (II)- salen complexes immobilized mesoporous alumina
V. D. Chaube, **S. Shylesh** and A. P. Singh

Journal of Molecular Catalysis A. Chemical **2005**, *241*, 79

8 Cobalt-containing hexagonal mesoporous molecular sieves (Co-HMS): Synthesis, characterization and catalytic activity in the oxidation reaction of ethyl benzene

S. S. Bhoware, **S. Shylesh**, K. R. Kamble and A. P. Singh

Journal of Molecular Catalysis A. Chemical **2006**, *255*, 123

9 Vanadium-containing ethane-silica hybrid periodic mesoporous organosilicas: Synthesis, structural characterization and catalytic applications

S. Shylesh and A. P. Singh

Microporous and Mesoporous Materials (in press)

10 Oxidation of ethyl benzene and diphenyl methane over M-MCM-41 catalysts (M = Ti, V, Cr): Synthesis, characterization and structure-activity correlations

R. K. Jha, **S. Shylesh**, S. S. Bhoware and A. P. Singh

Microporous and Mesoporous Materials (in press)

11 Assembly of hydrothermally stable periodic mesoporous organosilicas having spherical and wormlike framework structures

S. Shylesh, R. K. Jha and A. P. Singh

Microporous and Mesoporous Materials (in press)

List of Manuscripts Communicated

1 Bridging the gap between micropores and mesopores by the controlled transformation of bifunctional periodic mesoporous silicas

S. Shylesh, Ch. Srilakshmi, A. P. Singh and B. G. Anderson

Journal of Physical Chemistry B. Materials (communicated)

2 Synthesis of hydrothermally stable aluminium-containing ethane-silica hybrid mesoporous materials using different aluminium sources.

S. Shylesh, Prinson P. Samuel and A. P. Singh

Microporous and Mesoporous Materials (communicated)

3 Heterogenized vanadyl cations over modified silica surfaces: A comprehensive understanding towards the structural property and catalytic activity difference over mesoporous and amorphous silica support
S. Shylesh and A. P. Singh
Journal of Catalysis (communicated)

4 One step synthesis of chromium-containing hybrid periodic mesoporous organosilicas and their catalytic activity in the oxidation reaction of cyclohexane
S. Shylesh, Ch. Srilakshmi, A. P. Singh and B. G. Anderson
Journal of Catalysis (communicated)

5 Cyclooctene epoxidation over mesoporous vanadosilicates having $-CH_2-CH_2-$ units in the frame wall positions.
S. Shylesh, Prinson P. Samuel and A. P. Singh
Catalysis Communications (communicated)

Awards

1 **Best Poster Award**, National Science Day celebrations, National Chemical Laboratory, Pune, February 28, **2004**.
Poster Title: Synthesis of silica functionalised sulphonic acid groups for acid catalyzed reactions

2 **Best Poster Award**, National Science Day celebrations, National Chemical Laboratory, Pune, February 28, **2005**.
Poster Title: Heterogenization of vanadyl cations over mesoporous MCM-41: Why immobilized catalysts are more active and stable than isomorphous substituted V-MCM-41 catalysts?

Contributions to National/International Symposia/Conferences

1. Synthesis and Characterization of an Alumino Silsesquioxane
   S. Shylesh and A. P. Singh
   16th National Symposium in Catalysis and Ist Indo-German Conference on Catalysis, Indian Institute of Chemical Technology, Hyderabad, February **2003** (***Poster Presentation***)
2. Synthesis of silica functionalized sulphonic acid groups for acid catalyzed reactions
   S. Shylesh, S. Parambadath, S. S. Bhoware and A. P. Singh
   6th National Symposium in Chemistry, Indian Institute of Technology, Kanpur, February **2004** (***Poster Presentation***)
3. Hydrothermal synthesis of metal substituted mesoporous M-MCM-41: Comparative study over Ti-MCM-41, V-MCM-41 and Cr-MCM-41
   S. S. Bhoware, **S. Shylesh**, K. R. Kamble and A. P. Singh
   17th National Symposium in Catalysis, Central Salt and Marine Chemical Research Institute, Bhavnagar, India, January **2005** (***Oral presentation***)
4. Periodic Mesoporous Silicas vs Periodic Mesoporous Organosilicas
   S. Shylesh, Prinson P. Samuel, S. Parambadath and A. P. Singh
   National Science Day Celebrations, National Chemical Laboratory, Pune, February **2006** (***Poster Presentation***)
5. Synthesis, characterization and catalytic applications of vanadium-containing ethane-bridged hybrid periodic mesoporous organosilicas
   S. Shylesh, Prinson P. Samuel and A. P. Singh
   5th Tokyo Conference on Advanced Catalytic Science and Technology, TOCAT-5, Japan, **2006** (***Oral Presentation***)